DESIGN, CHARACTERISATION AND APPLICATION OF MOLECULAR MAGNETS: A THEORETICAL STUDY

Thesis Submitted for the Degree of Doctor of Philosophy in Science (Chemistry) of the University of North Bengal

By

Debojit Bhattacharya (M.Sc.)

Supervisor

Dr. Anirban Misra

Associate Professor in Chemistry

Department of Chemistry
University of North Bengal
Darjeeling 734013
India

2012

Th 541.378
B571sd

252141

31 MAY 2013

Dedicated to The Memory of My Father,

Biswajit Bhattacharya

DECLARATION

I declare that the thesis entitled "**DESIGN, CHARACTERISATION AND APPLICATION OF MOLECULAR MAGNETS: A THEORETICAL STUDY**" has been prepared by me under the guidance of Dr. Anirban Misra, Associate Professor of Chemistry, University of North Bengal, Siliguri, Dist- Darjeeling, Pin-734013. No part of this thesis has formed the basis for the award of any degree or fellowship previously.

Debojit Bhattacharya.

(DEBOJIT BHATTACHARYA)
Department of Chemistry,
University of North Bengal,
Siliguri, Dist- Darjeeling,
Pin-734013.

Date: 17.09.2012

CERTIFICATE

I certify that DEBOJIT BHATTACHARYA has prepared the thesis entitled **"DESIGN, CHARACTERISATION AND APPLICATION OF MOLECULAR MAGNETS: A THEORETICAL STUDY"**, for the award of Ph.D. degree of the University of North Bengal, under my guidance. He has carried out the work at the Department of Chemistry, University of North Bengal, Siliguri, Dist- Darjeeling, Pin-734013.

(Dr. ANIRBAN MISRA)
Associate professor
Department of Chemistry,
University of North Bengal,
Siliguri, Dist- Darjeeling,
Pin-734013.

Date: 17.09.2012

ABSTRACT

A substantial amount of work has already been done on molecule based magnetism as evident from the existing literature. The main objective of this thesis is to study the properties as well as the applications of the designed molecular magnets particularly of organic domain. Transparency, photo activity, low toxicity and biocompatibility are the properties which make the field of molecule based magnetism to rise over traditional magnetism. The studies described in the thesis are divided into eight chapters.

The **Chapter 1** describes the general introduction of this work based on magnetic molecules. The background of this thesis is clearly described. This chapter also categorically portrays the different objectives of this thesis.

The **Chapter 2** depicts the theoretical background of how the magnetic exchange coupling constant (J) is evaluated by broken symmetry (BS) approach in the unrestricted density functional theory (UDFT) framework. The theoretical background of estimation of axial spin-spin zero field splitting (ZFS) parameter (D), the rhombic ZFS parameter (E) and ZFS magnitude (a_2) are also discussed here.

The **Chapter 3** describes our investigation on different linkage specific oxoverdazyl diradicals. Here, we have used *meta*- and *para*-connected aromatic cyclic ring couplers in between two oxoverdazyl moieties to form the desired diradicals. Their J values are then evaluated at UB3LYP/6-311++G(d,p) level of theory. A correlation between sign and magnitude of J with respect to their connectivity is also made. The ferromagnetic and antiferromagnetic interactions are observed for *meta*-connected and *para*-connected diradicals respectively. After that, the estimated J values are clarified using spin polarization maps and magnetic orbitals. The hyperfine coupling constant values are also computed to support the intramolecular magnetic interactions. Figure 1 is the representative of two such *meta*- and corresponding *para*-connected systems.

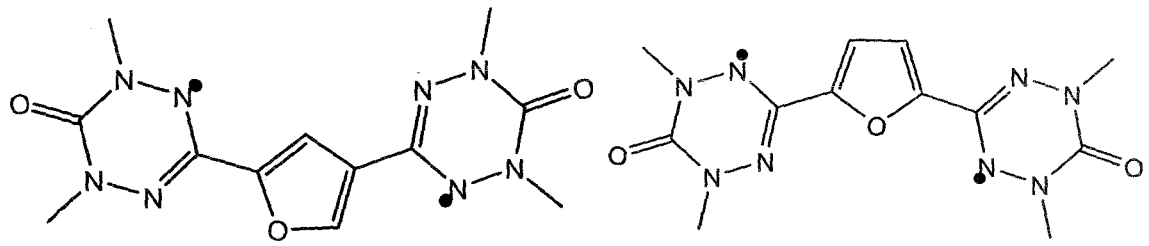

Figure 1. Bis-oxoverdazyl diradicals where *meta-* and *para*-connected furan is used as couplers.

The **Chapter 4** encompasses the intramolecular magnetic exchange coupling constant for different high spin diradicals using BS-UDFT treatment. The role of linear polyacenes of varying length which are used as couplers in these bis-oxo- and bis-thioxo-verdazyl diradicals is discussed. The spin density distribution as well as an analysis made by "magnetic" orbitals is used to explain their magnetic character. The Nuclear Independent Chemical Shift (NICS) values have been correlated with *J* values. Figure 2 shows a general schematic representation of the diradicals investigated in **Chapter 4**.

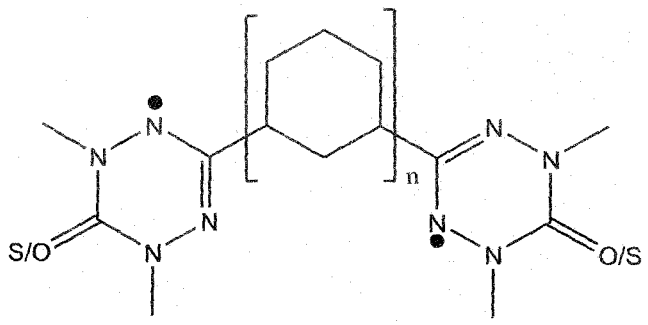

Figure 2. Bis-oxo- and bis-thioxo-verdazyl diradicals where *meta* connected linear polyacenes are used as couplers, where n is the number of benzenoid rings.

In **Chapter 5** geometry based aromaticity index harmonic oscillator model of aromaticity (HOMA) along with magnetic aromaticity index NICS has been evaluated. Here we have taken so called heteroverdazyl diradicals where *meta-* and *para*-phenylene coupled high spin and the corresponding low spin diradicals (Figure 3) are used. The result of the spin leakage phenomena on *J* and that on HOMA and NICS values of certain phosphaverdazyl systems has been unequivocally argued. However, the main novelty of this work stands upon

the consideration of the aromatic behavior by means of the geometrical global and local aromaticity index HOMA.

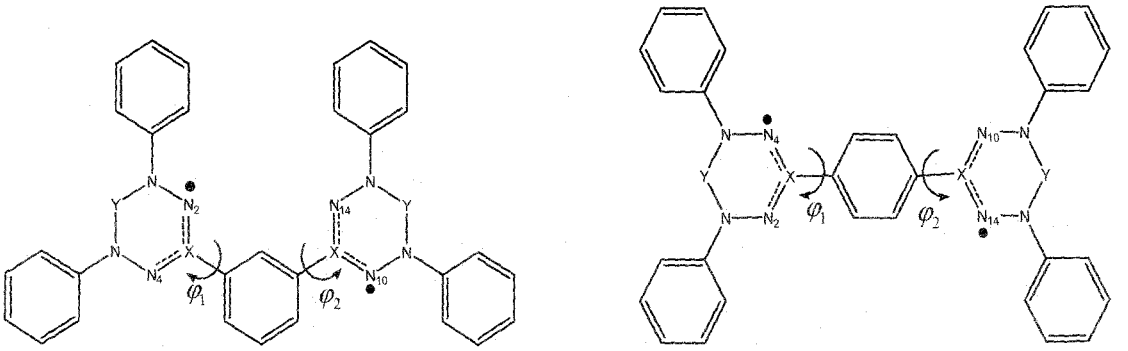

Figure 3. Substitution at X and Y position gives rise to different "so called" *meta-* and corresponding *para*-phenylene coupled heteroverdazyl diradicals. The φ_1 and φ_2 denote two different relevant dihedral angles.

The **Chapter 6** has embodied the study of different variants of green fluorescent

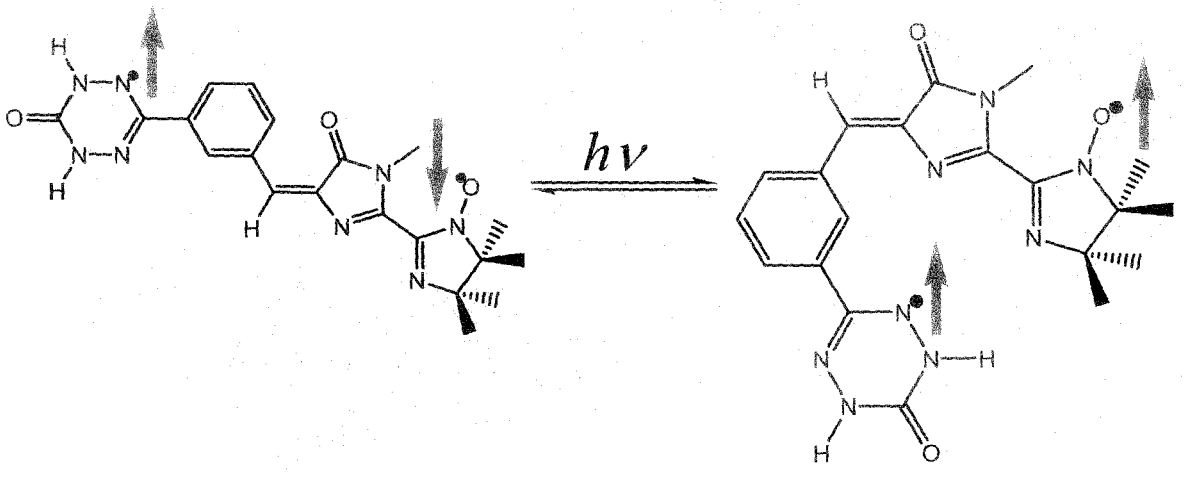

Dark, antiferromagnetic and trans

Blue fluorescent, ferromagnetic and cis

Figure 4. The trans (antiferromagnetic) and the respective photoconverted cis (ferromagnetic) diradicals, where the blue variant of GFP chromophore (BFPF) is used as coupler. Here, IN and oxo-verdazyl radicals are used as mixed magnetic sites. The up and down arrows show α and β spin respectively.

protein (GFP) chromophore coupled diradicals where imino nitroxide (IN) and IN or oxo- or phospha-verdazyl radical moieties are used as magnetic centers. A spin crossover from antiferromagnetic to ferromagnetic state is observed as the trans diradicals are converted into their cis state by the irradiation of appropriate wave length of light, which is estimated by the time dependent DFT calculation. The most novel property observed here is that the dark trans diradicals turn into their fluorescent cis isomers upon irradiation of appropriate light. As a result, only visual inspection is required to know the magnetic status of these diradicals (Figure 4).

The **Chapter 7** describes biomedical applications of different analogues of GFP chromophores coupled diradicals where we have introduced bis-IN as radical sites. To confirm their biomedical uses we have optimized them not only in gas phase but also in water and *blood plasma medium* by adopting 2-layer our own N-layer integrated

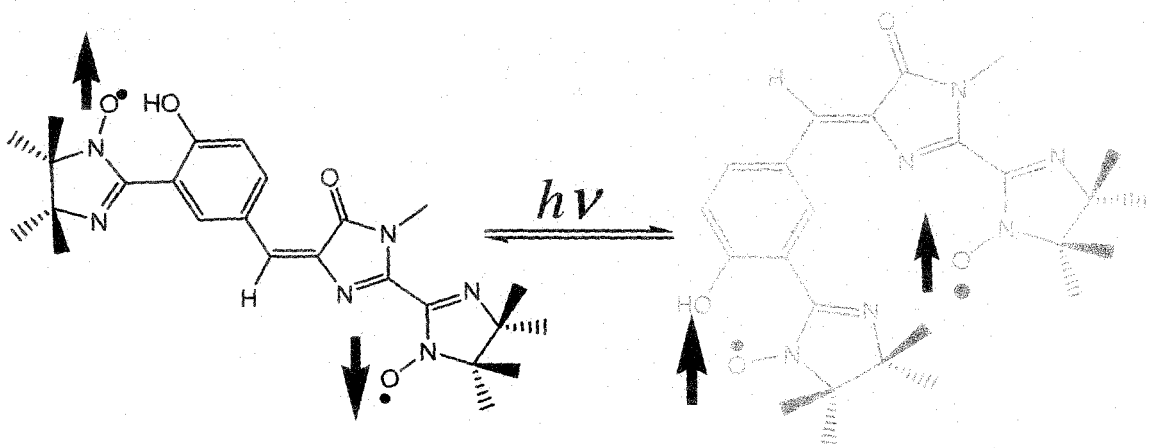

Antiferromagnetic, trans and dark Ferromagnetic, cis and green fluorescent

Figure 5. The antiferromagnetic planar trans (dark) and corresponding photoconverted puckered cis fluorescent (green) bis-IN diradicals where GFP chromophore is used as couplers. These diradicals are used as contrast agents in MRI experiment. The α and β spins are represented by the up and down arrows.

molecular orbital and molecular mechanics (ONIOM) method and polarized continuum model (PCM) method respectively. In ONIOM method the water molecules are treated as

low level layer whereas the diradicals are treated as high level layer. The magnetic nature of these diradicals is estimated by ONIOM-BS [where BS calculations are done for inner high level layer (diradical system) keeping the outer water layer at low level] and in PCM-BS methodology. Their suitability to be used as magnetic resonance imaging contrast agent (MRICA) has been quantified by the estimation of the axial zero field splitting (ZFS) parameter (D), rhombic ZFS parameter (E) and ZFS magnitude (a_2) for each ferromagnetic species in three different media. One can ambitiously expect from our calculations that if these diradicals are synthesized then they can be used as successful, non-hazardous MRICA in place of other metal based contrast agents. Figure 5 shows the photoconversion of antiferromagnetic dark planar trans and their corresponding fluorescent (green) puckered cis diradicals where GFP chromophore is used as couplers between two IN moieties.

A comprehensive conclusion of the total thesis work is given at the end in **Chapter 8.**

List of Publications

I. Published in Journals:

(1) **Bhattacharya, D.**; Misra, A. "Density functional theory based study of magnetic interactions in bis-oxoverdazyl diradicals connected by different aromatic couplers" *J. Phys. Chem. A.* **2009**, *113*, 5470-5475.

(2) **Bhattacharya, D.**; Shil, S.; Misra, A. Klein, D. J. "Intramolecular ferromagnetic coupling in bis-oxoverdazyl and bis-thioxoverdazyl diradicals with polyacene spacers" *Theor. Chem. Acc.* **2010**, *127*, 57-67.

(3) **Bhattacharya, D.**; Shil, S.; Panda, A.; Misra, A. "A DFT study on the magneto-structural property of ferromagnetic heteroverdazyl diradicals with phenylene coupler" *J. Phys. Chem. A.* **2010**, *114*, 11833-11841.

(4) **Bhattacharya, D.**; Shil, S.; Misra, A. "Photoresponsive Magnetization Reversal in Green Fluorescent Protein Chromophore Based Diradicals" *J. Photochem. Photobiol. A: Chem.* **2011**, *217*, 402-410.

(5) **Bhattacharya, D.**; Panda, A.; Shil, S.; Goswami, T.; Misra, A. "A Theoretical Study on Photomagnetic Fluorescent Protein Chromophore Coupled Diradicals and Their Possible Applications" *Phys. Chem. Chem. Phys.* **2012**, *14*, 6509-6913.

II. Published Book Chapter:

(1) **Bhattacharya, D.**; Panda, A.; Misra, A. "Diradical Based Organic Molecular Magnetism: Theory and Applications" Eds.; Wythers, M. C. Nova Science Publishers, Inc.; *Advances in Materials Science Research*, Vol. 11, Chapter 4, pp. 291-318, 2011.

III. Submitted/in preparation:

(1) **Bhattacharya, D.**; Misra, A.; Panda, A.; Klein, D. J. "Clar Theory for Linear Polyacenes"

(2) **Bhattacharya, D.**; Shil, S.; Goswami, T.; Panda, A.; Misra, A.; Klein, D. J. "On Fluoro Protein Chromophore Coupled Bis-TEMPO Based MRI Contrast Agents and Their Other Applications: A DFT Investigation"

(3) Shil, S.; **Bhattacharya, D.**; Sarkar, S.; Misra, A. "Heat of Formations, Ionization Potentials and Ground States of Different Transition Metal Complexes: The Performance of M0X Suite"

Table of Contents

Chapter 1

Molecules Manifesting Magnetic Behavior

A general introduction of molecules manifesting magnetic behavior is presented in this chapter. A detailed literature survey along with the objectives of this thesis is systematically stated in this chapter.

1.1. Introduction

In recent years, research work on magnetism and magnetic materials has gained a tremendous momentum. Particularly synthetic magnetic molecules both of organic and inorganic origin have drawn a huge attention of researchers worldwide. One can have an idea of the volume of work that has already been done on this subject by the result of a Google search. Such a search in September 2012 gives around 18,100,000 http links in just 0.34 seconds with a keyword "magnetic molecules". Searching with a keyword "synthetic magnetic molecules" gave around 19,900,000 links on the subject. Several books have also been written on this topic.[1] A closer look on these articles reveals that the materials containing magnetic molecules with inorganic origin have some historical importance as many of the early magnetic materials is basically inorganic in nature. Nevertheless, in past few decades organic magnetic molecules have emerged as one of the most interesting topics in this line of research.[2] This field of study has numerous technological and biological applications. In a broader perspective the present thesis deals with the design, characterisation and application of molecular magnets of organic origin and in particular, of organic diradical systems. This chapter includes the background, objective and justification of the present research work.

1.2. Types of Magnetism

Although the initial discovery of magnetic phenomenon is not known; however, the word magnet is derived from the name of Magnesia province of Thessalia, where magnetite was found abundantly.[3] Depending on magnetic behavior, solids can be classified in different categories; say, diamagnetic, paramagnetic, ferromagnetic (FM), antiferromagnetic (AFM), ferrimagnetic, metamagnetic and so on. The genesis of these different types is due to the diverse coupling arrangements of electronic spin angular momentum in molecular and supramolecular arrays. So far, the most precious and rare class of materials from both theoretical and experimental point of view are ferromagnets. According to the first principle of magnetism, if spontaneous coupling between two equal spin moments occurs in parallel fashion then ferromagnetism arises leading to permanent magnetization. On the other hand,

when two unpaired but equal spin moments are coupled in antiparallel fashion avoiding spin pairing then antiferromagnetism arises, leading to the lowering of magnetism. Both ferromagnetic and antiferromagnetic substances behave like paramagnetic substances beyond a certain temperature called Curie temperature (for FM) or Neel Temperature (for AFM) respectively. Paramagnetic substances show spontaneous magnetization under an external magnetic field but they loose that property in absence of such field. Diamagnetic substances contain spin paired electrons and do not show spontaneous magnetization under an external magnetic field. In ferrimagnetism unequal spin moments couple to give net magnetization. All these things are nicely discussed in different articles.[4]

1.3. Design, Characterisation and Application

Molecular designing is a creative process or strategy of finding new tailor made molecules having requisite characteristics. This is frequently done either by scratching or by creating intended variations in the known structures. Since 1960s the synthetic chemists are having continuous interest for designing of high spin magnetic molecules such as organic ferromagnets,[5] as ferromagnetic interactions are preconditioned to most attractive magnetic properties.[6] Thus the capability to design molecules or crystals with ferromagnetic exchanges in a balanced manner is significant and equally intellectually challenging.[7]

To design a molecule with desired magnetic properties it is essential to characterise the molecule with available theoretical tools. In characterising the magnetic molecules one must reveal its magnetic nature (ferro or antiferro) and its extent of magnetism. Magnetic systems are best characterised by magnetic exchange coupling constant (J) values. A positive sign of J, in which a situation of parallel spin is essential, is used to indicate a ferromagnetic interaction, whereas an antiferromagnetic interaction is indicated by a negative value, where a state of antiparallel spin is favored.[1] The high positive value of J indicates that the magnetic molecule is strongly ferromagnetic whereas less ferromagnetic character is observed for its low positive value.

It's being extremely essential to observe the applicability either in technologies or in biomedical sciences of the magnetic molecules after their design and characterisation.

Molecule based magnets are a class of compounds capable of showing interesting magnetic behavior. The first synthesis and characterisation of molecule-based magnet, a diethyldithiocarbamate-Fe(III) chloride complex, was credited to Wickman and co-workers.[8] Low density, mechanical flexibility, low-temperature processability, solubility, low environmental contamination, biocompatibility, high remanent magnetizations, low magnetic anisotropy, transparency, semiconducting properties and so on make these molecules suitable for the uses in different purpose.[4(b)] On the other hand, in biomedical field of research magnetic molecules can provide new opportunities including the improvement of magnetic resonance imaging, magnetic hyperthermia for cancerous cell and also in site specific drug delivery.[9]

1.4. Background: The Essence of Interest

Magnetism in molecules has given rise to newer aspects of various interesting research areas both in the filed of Physics and Chemistry. In numerous studies the results are radiating. In the following subsections few gems are collected from the sea of knowledge which suit best to the present thesis work.

1.4.1. Molecule Based Magnetism

To be an effective building block of a synthetic magnetic molecule, the constituting magnetic sites must be stable enough. They can be prepared, isolated, and characterised with ease. It is known that stable organic radicals in pure state are the most suitable candidates for the building of various magnetically active substances. More specifically, stable diradical based organic ferromagnets are of primary interest to study the molecule based magnetism.[2] According to Borden and Davidson a diradical is "a molecule in which two electrons occupy a degenerate or nearly degenerate pair of orbitals".[10] In a more lucid version, diradical is a molecular species with two radical centers. One point should be noted here that there are two types of non-kekule diradical molecules, *disjoint* and *non-disjoint* type. This classification is based on the shape of their two non-bonding molecular orbitals (NBMOs). In case of non-disjoint molecules both NBMOs have electron density at the same atom; whereas, in the dis-

-joint molecules electron density resides on different atoms. Following Hund's rule, unpaired electrons in non-disjoint molecules are preferred to be in parallel orientation resulting in a triplet ground state. However, in case of disjoint molecules, the relative stability of the singlet ground state to the triplet ground state will be nearly equal even electrons can have anti parallel orientation resulting in a singlet ground state. The simplest examples of diradical is methylene $(CH_2)^{\cdot\cdot}$, but methylene **(1)** (Figure 1.1) is very reactive and unstable in nature.[11]

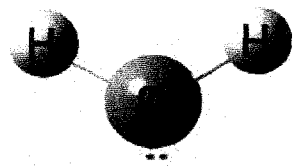

(1)

Figure 1.1. The simplest methylene diradical (**1**) (ref. 11).

1.4.2. Searching of Stable Radicals as Building Blocks for Magnetic Molecules

In molecular magnetochemistry nitroxide radical family is playing a prime role since long.[12] The first reported stable organic nitroxyl based ferromagnetic species was β-crystal phase of *para*-nitrophenyl nitronyl nitroxide (Figure 1.2). After its discovery by Kinosita and co-workers[13] in 1991, nitronyl nitroxide based diradicals with different couplers have been experimentally investigated and characterised by many group of researchers.[12] Zeissel *et al.* have extensively studied nitronyl nitroxide diradicals with ethylene coupler.[14]

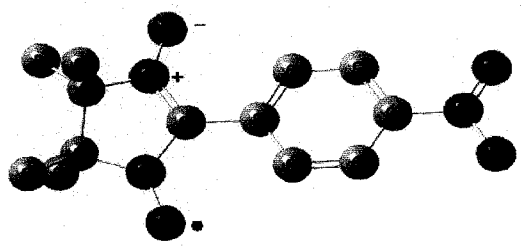

Figure 1.2. The *para*-nitrophenyl nitronyl nitroxide (ref. 13). Hydrogens are excluded for clarity.

The excellent stability of nitronyl nitroxides (NN), imino nitroxides (IN), (2,2,6,6-Tetramethylpiperidin-1-yl)oxyl (TEMPO) (Figure 1.3) has made them mesmerizing to both synthetic and theoretical chemists.[13-19] The presence of strongly delocalized unpaired electrons in NN and IN make them perfect ferromagnetic precursor. Nonetheless, their excellent stability, lucid method of preparation, flexibility in coordination, and capacity to generate tailor made magnetic properties are the reasons for their wide study.[13-17] On the other hand, diradicals containing TEMPO as one of the radical centers have been synthesized and characterised.[18] TEMPO is well known class of stable organic radical which can be used in preparing molecule based magnetic materials, organomagnetic systems and so on. Charge transfer complexes, photo responsive devices can also be developed from TEMPO radicals.[19] Nonetheless; besides nitroxide family of radicals only few radical classes are used in preparing diradical based magnetic molecules due to their suitability in preparation, isolation, and characterisation. Following the trend, investigations were carried out to synthesize other radical species such as verdazyl, tetrathiafulvalene (TTF) etc. (Figure 1.4) which are suitable candidates for preparing organic diradical based ferromagnets at relatively higher temperature.[20-24]

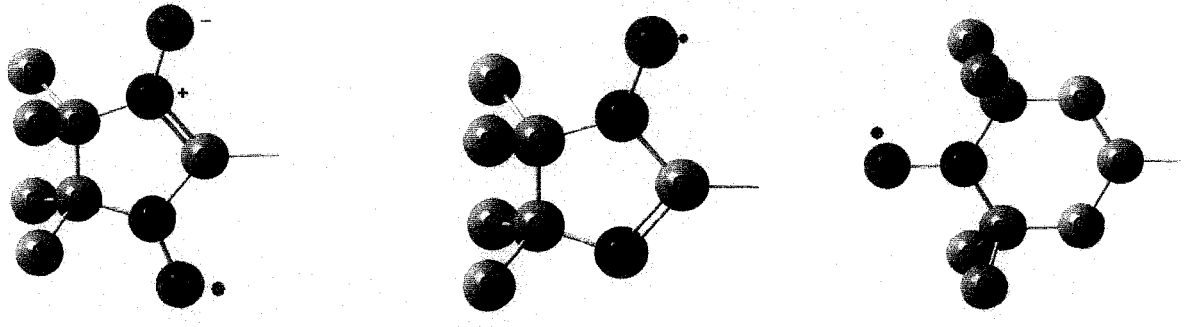

(NN-radical) (IN-radical) (TEMPO-radical)

Figure 1.3. NN, IN and TEMPO radicals, the building blocks of diradicals based magnetic molecules (ref. 28). Hydrogens are omitted for picture clarity.

The Verdazyl radical was discovered by Kuhn and Trischmann in early 1960s.[20] In recent years, a lot of effort is given to synthesize and characterise the "so-called" heteroverdazyl radicals incorporating different hetero atoms in place of nitrogen and carbon

ring atoms at X or Y position or the both.[25] The most common heteroverdazyls are oxoverdazyl (OV), thioverdazyl (TV) and phosphaverdazyl (PV) and the last one is generally considered as the inorganic analogue of verdazyl radical (Figure 1.4). In the later case, spin leakage is prominent due to mixing of σ- and π-systems.[26] Spin leakage is the phenomena where the spin density of a particular atom at a definite site becomes lower than the expected spin density value. The spin leakage has an insightful effect on magnetic behavior of the concerned diradical. Different research groups have established the method of synthesis of the above mentioned different types of verdazyl radicals.[25–28]

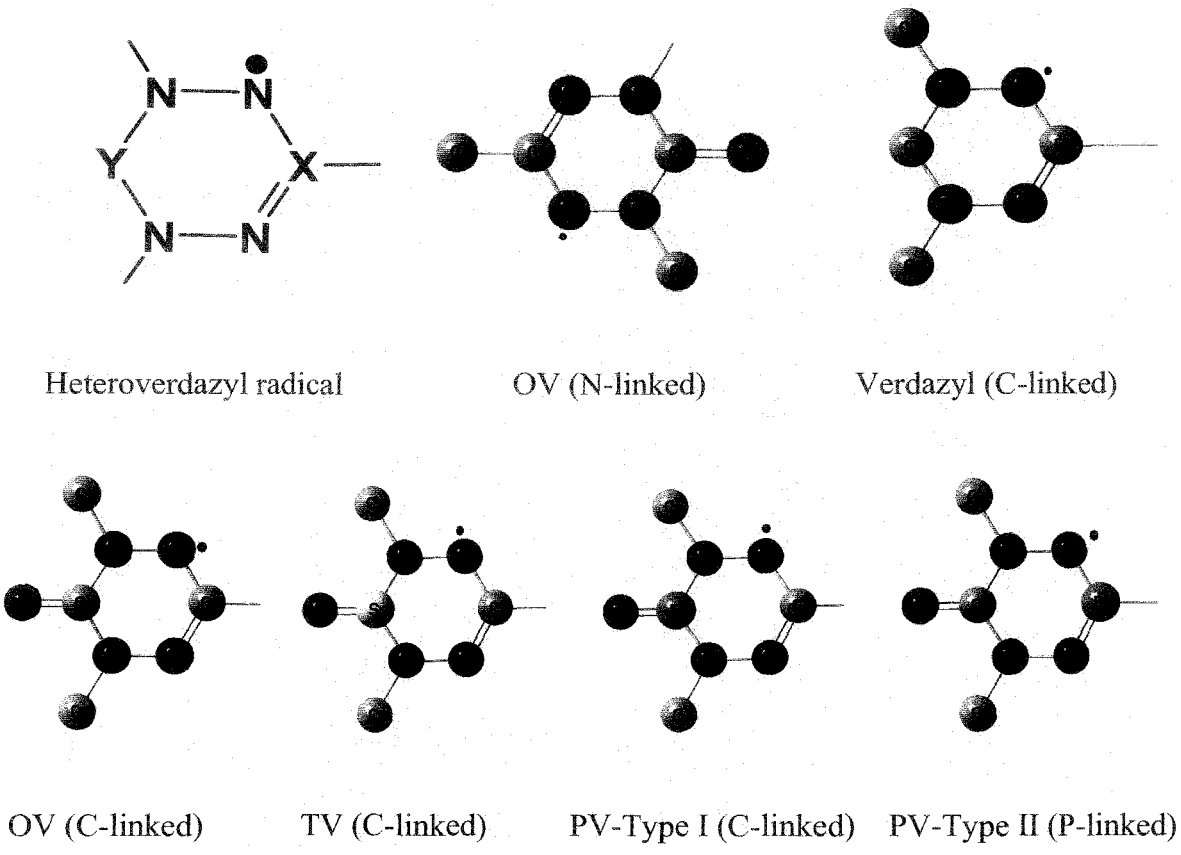

Figure 1.4. General schematic representation of heteroverdazyl radical, upon substitution of different atoms on X and Y positions yields different verdazyl analogues, such as OV (N-linked), Verdazyl (C-linked), OV (C-linked), TV (C-linked), PV-Type-I (C-linked), PV-Type-II (P-linked) which act as radical centers in different diradicals (ref. 28). Hydrogens are excluded for clarity.

Lahti and his co-workers have prepared azide substituted verdazyles.[29] Synthesis of carboxyl substituted verdazyl complexes of Ni(II) and Co(II) have been carried out in aqueous system as carboxyl substituted verdazyl radicals are highly soluble in water.[30] On the other hand, TTF has shown through bond and through space intramolecular ferromagnetic exchange interactions (Figure 1.5). TTF has also been used as building blocks for magnetic molecules having been used as supramolecular chemistry, molecular memories, organic conductors and so on.[31]

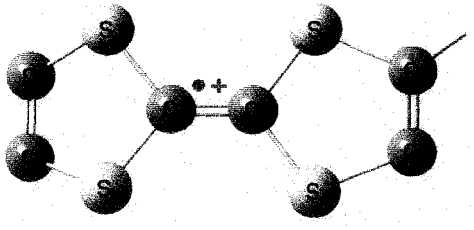

(TTF-radical cation)

Figure 1.5. TTF radical moieties used to develop different magnetic molecules (ref. 31). Hydrogens are excluded for simplicity.

1.5. Qualitative Methods: Ground State of the Diradical Based Magnetic Molecules

Qualitative prediction of the ground state of a magnetic molecule is a state of the art technique. Several methods are available for qualitative prediction of the ground spin state of diradicals. The first successful method of predicting the ground state of magnetic molecules was made by Longuet-Higgins.[32(a)] The method says, if there are total X number of carbon atoms with total Y maximum number of possible double bond then the number NBMOs can be calculated as $n = (X - 2Y)$. As an example, we predict the ground spin state of *para*-benzoquinodimethan (**2**). In case of *para*-benzoquinodimethan maximum four double bonds are possible. Hence the number of NBMOs is zero resulting in an antiferromagnetic interaction. Similarly for *meta*-benzoquinodimethan (**3**), there are two NBMOs and from Hund's rule, a triplet (S=1) ground state is estimated[32(b)] (Figure 1.6).

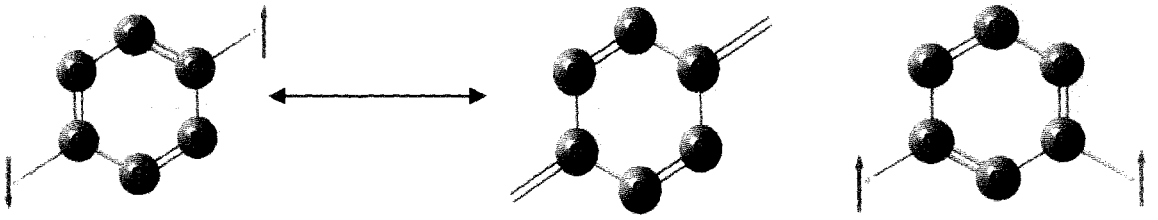

(2) **(3)**

para- benzoquinodimethan (S= 0) *meta*-benzoquinodimethan (S = 1)

Figure 1.6. Demonstration of ground spins state of *para-* (**2**) and *meta*-benzoquinodimethan (**3**) [ref 32(a)]. Hydrogen atoms are not shown in the picture for simplicity.

Another simple method was proposed by Ovchinnikov considering valence-bond formalism for planar alternate hydrocarbons.[32(c)] The method suggests that if the number of starred (K) and unstarred (K*) carbon atoms are not equal then the ground state spin S=|K*–K|/2 and the value is always nonzero. Applying the rule to previous examples of *meta-* (**4**) and *para-* (**5**) benzoquinodimethan one concludes that *meta* and *para* isomers have triplet and singlet ground spin states respectively (Figure 1.7). This model was further applied for the simplest case of trimethylenemethane (TMM) diradical, and triplet ground state was predicted and in addition confirmed by the experiment.[33]

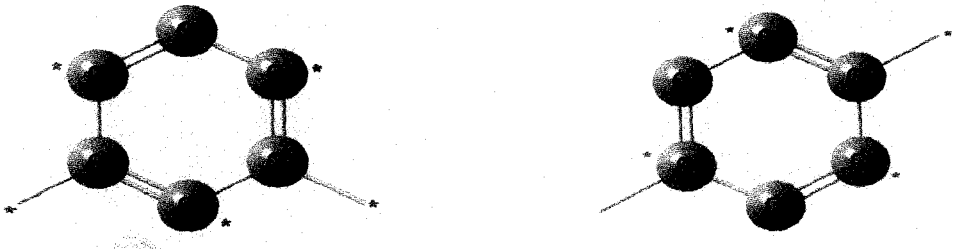

(4) **(5)**

Figure 1.7. Determination of the ground spins state of *meta-* (**4**) and *para-* (**5**) benzoquinodimethan using starred/unstarred model by Ovchinnikov [ref. 32(c)]. Hydrogen atoms are not shown in the picture for simplicity.

The rule of spin alternation has been successfully explained and demonstrated in UHF treatment by Trindle et al.[32(h,i)] Heuristically, in a planar π-conjugated system the spin densities of a particular atom prefers opposite signs to that of its adjacent atoms. That is, the polarization of spins will follow an alternate $\alpha\beta\alpha\beta\alpha\beta$ pattern. The spin density alternation rule efficiently predicts the nature of exchange coupling interaction in almost every case (Figure 1.8). This rule states that, if the number of bonds through the coupler is odd in the coupling path, the exchange pattern is antiferromagnetic, whereas, exchange pattern is ferromagnetic if the number of bonds in the coupler is even between two π-conjugated magnetic sites. In the following figure, by using the rule, one can easily find the proper ground state of these diradicals with butadiene (**6**), *para*-phenylene (**7**), *ortho*-phenylene (**8**), and *meta*-phenylene (**9**) as couplers. They have antiferromagnetic ground state as the spin-spin coupling is transmitted through odd number of bonds. However, for the *meta*-phenylene (**9**) coupled diradicals ferromagnetic ground state is observed as the spin coupling is propagated through even number of bonds.

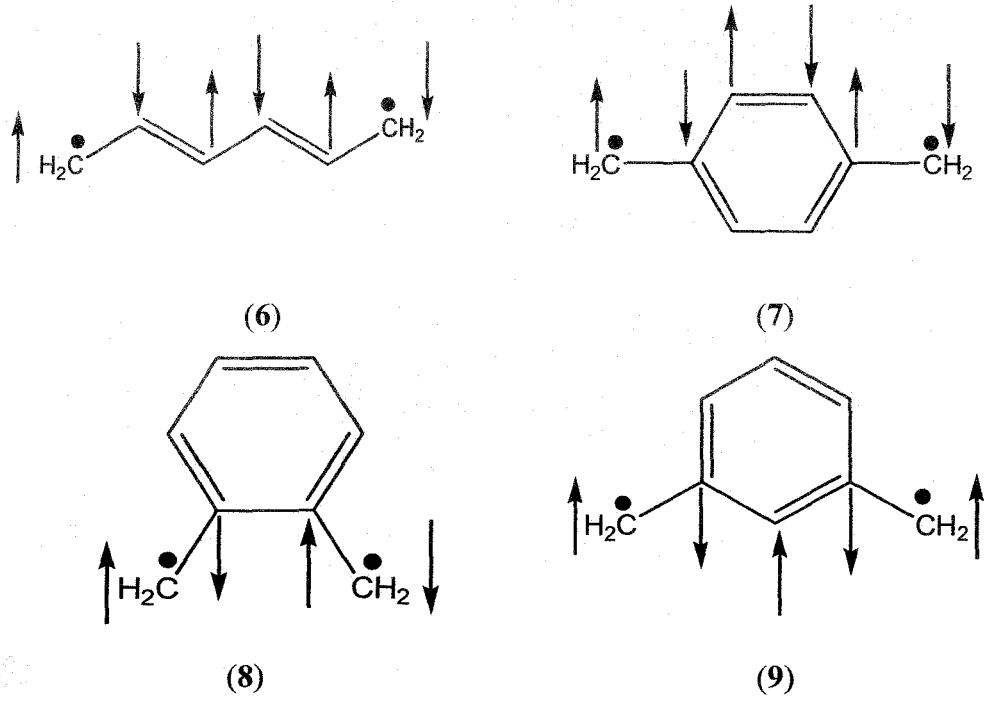

Figure 1.8. Spin alternation rule demonstrating the ground state ferromagnetic nature of *meta*-phenylene (**9**) coupled diradical with net two up spins in two magnetic centers; whereas the linear conjugated π-polyene (**6**), *para*-phenylene (**7**) and *ortho*-phenylene (**8**) coupled diradicals are antiferromagnetic in nature [ref. 32(h,i)].

1.6. Different Diradicals

In diradicals the magnetism arises mainly due to intramolecular interactions between two magnetic sites. The credit to synthesize and characterise the first stable ferromagnetic diradical (**10**) was accounted for Schlenk (Figure 1.9) in 1915.[34] In a diradical generally the spin polarization and spin delocalization play the major role for determining the magnetic coupling. A large number of works have been executed on this issue.[35,36] On the other hand, a great deal of theoretical works have also been done on organic molecule based magnetism. It must be noted that the first theoretical work to predict the high spin ground state had been attributed to McConnell.[5(a)]

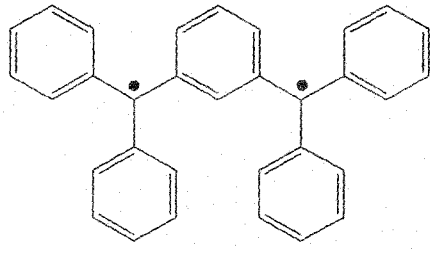

(**10**)

Figure 1.9. The Schlenk diradical (**10**) which is stable and remain in triplet ground state (ref. 34).

1.6.1. Simple Hydrocarbon Diradicals

Molecular topology and spin alignment in some simple hydrocarbon diradicals are interesting to understand their nature of magnetism in their ground state. Dowd[33] have first reported one of the most simple π-conjugated hydrocarbon diradical named trimethylenemethane diradical (**11**). This diradical has triplet ground state which can be proved both theoretically and experimentally. However, when two methyl radicals are attached in two different ends of ethylene (**12**), which is essentially a butadiene moiety, antiferromagnetism is observed. Benzene containing diradical *meta*-benzoquinodimethane (**13**) is strongly ferromagnetically coupled, whereas its *para* and *ortho* isomers (**14**,**15**) are

antiferromagnetically coupled. It is to be noted here that ferromagnetic coupling is observed in non-kekulé molecules having non-disjoint nature,[37] that is, these MO's would be non-orthogonal and have overlapped at one or two atomic sites. There are other molecular structures where the simple hydrocarbon diradicals are disjoint in nature. Tetramethylene ethane (TME) (**16**), 2,3-bis(methylene)-1,3-cyclohexadiene (**17**), 2,2-dimethyl-4,5-bis(methylene)-1,3-cyclopentadiene (**18**), and 2-(1-methyleneethenly)cyclopentenyl (**19**) are such disjoint diradicals having triplet ground state (Figure 1.10). This fact has been attributed to the zero overlap between perpendicular π-systems. This phenomenon suggests that high spin ground state is also obtained in *para*-phenylene system when doped.[33]

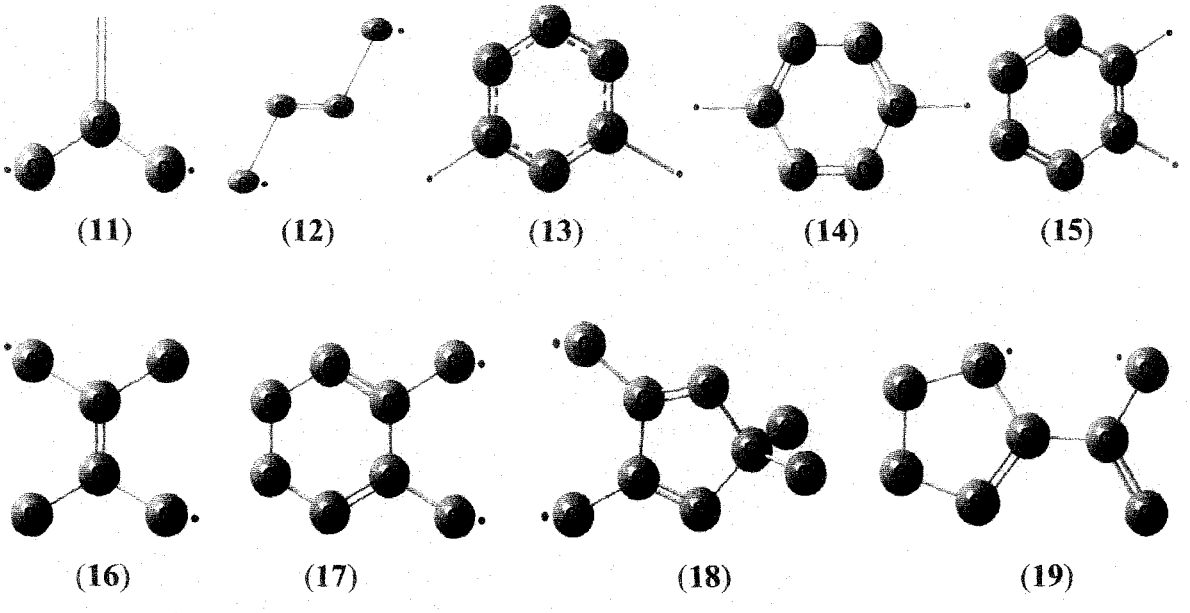

Figure 1.10. Molecular topology and spin coupling of some hydrocarbon diradicals (**11-19**). Hydrogen atoms are not shown in the picture for simplicity (ref. 33,37).

1.6.2. Biphenyl and Tetraphenyl Diradicals

Biphenyls have important uses in chemical synthesis and these are the potential linkers used as couplers for designing high spin organic molecules. Diradical species has been prepared and studied in frozen solutions with 3,3' and 3,4' biphenyl as spin coupling units.[38] Diradical (**20**) possessing 3,3'-biphenyl in its coupling unit, has antiferromagnetic

ground state, whereas, its other isomer (**21**) has ferromagnetic ground state with 3,4'-biphenyl as coupling unit. This isomer (**21**) can be easily handled in low temperature in laboratory. However, there are examples where two different exchange coupling pathways (ECPs) are possible depending upon the structure of the coupler. A molecule having one ECP with 3,3'-biphenyl units (**22**) has the half exchange coupling constants in magnitude than the molecules with two ECPs with 3,3'-biphenyl units (**23**)[39] (Figure 1.11). If there are multiple parallel ECPs in a ferromagnetic coupled diradicals the magnetic exchange can be controlled with the increase or decrease of ECPs.

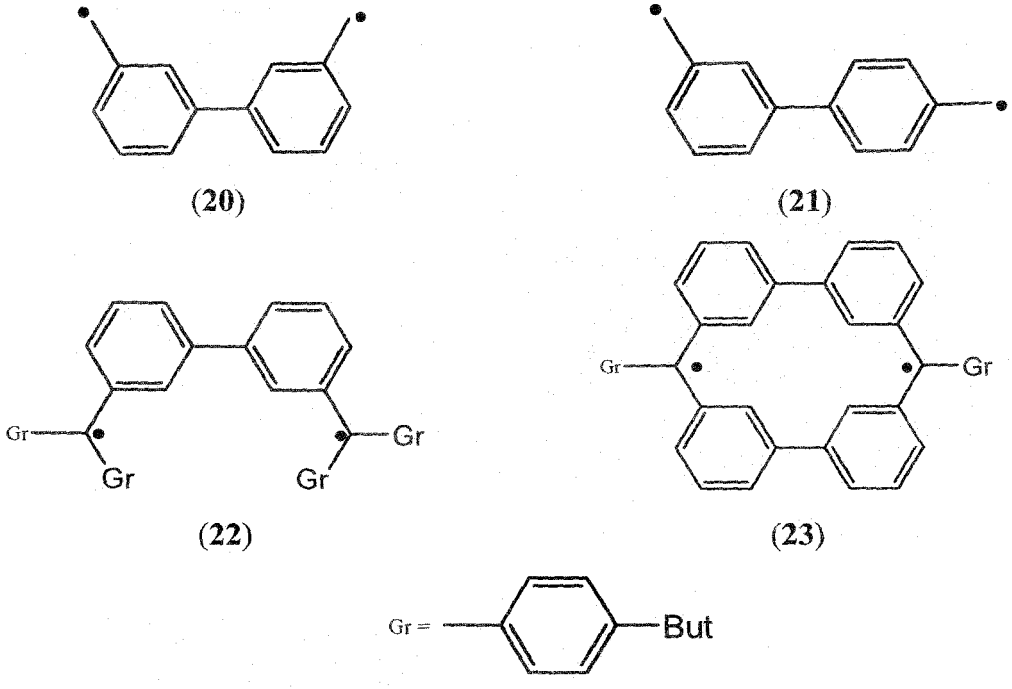

Figure 1.11. Synthesized biphenyl hydrocarbon diradicals with one ECP (**20**,**21**,**22**) and two parallel biphenyl units containing diradical (**23**) with two different ECPs (ref. 38,39).

1.6.3. Theoretically Designed Diradicals

Many researchers have studied theoretically intermolecular and intramolecular interactions, on which magnetic properties of diradical based systems depend. The degree of magnetism in magnetic molecules is best represented through intramolecular magnetic

exchange coupling constant which depends on the structure and spin orientation of such systems. Previous knowledge about the magnetic characteristics of the designed diradicals is essential before synthesizing possible organic magnetic systems with desired magnetic nature. This has been successfully proven in many cases resulting in the discovery of several ferromagnetic molecules.[1] A development in this direction is discussed chronologically in the following:

Diradical based magnetic molecules have been studied both with *ab-initio* or density functional theory (DFT) approach.[17,40] The spin states of some fused ring diradical systems[40(a)] along with some other diradical derivatives of IN and NN[40(b)] radicals have been investigated by *ab-initio* quantum chemical approach to calculate their singlet-triplet energy gap. At higher basis set it has been found that the calculated gas phase values are in excellent agreement with the solid state results.[17] Although, the *ab-initio* methods can give us accurate J value in principle but in actual practice it needs high level of computational resources. On the other hand, spin polarized DFT based broken symmetry (BS) approach in unrestricted formalism (BS-UDFT) is very suitable for evaluating J with less computational cost. Datta and co-workers have predicted the J values in different nitronyl nitroxide based diradicals (**24**) (Figure 1.12) using BS-UDFT approach.[40(c,d)] They have found that the ferromagnetic interactions prevail where *meta*-coupler is used, and for diradicals with linear couplers the antiferromagnetic interaction decreases as the length of the chain increases.[40(c)] In another work, molecular tailoring is executed to obtain the planarity of the molecules of trimethylenemethane-based nitroxide diradicals with the prediction of high positive J values due to larger delocalization of π–electrons.[40(d)]

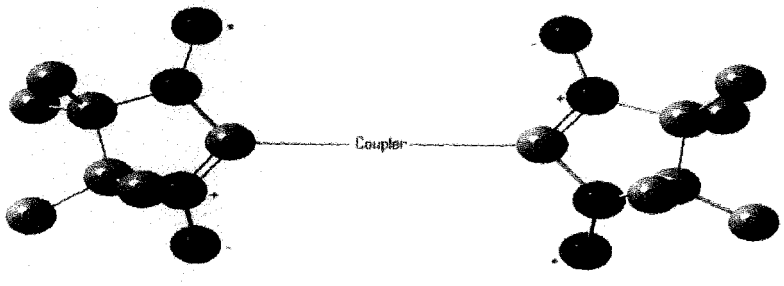

(24)

Figure 1.12. Bis-IN diradical (**24**) with coupler. Hydrogens are omitted for clarity (ref. 40).

So far, we are confined in diradical based organic magnets with one particular monoradical in two different ends of the coupler; however, the diradicals with neutral OV radical and TTF radical cation as mixed magnetic sites (**25**) having different aromatic and nonaromatic linkers (Figure 1.13) have also been studied in the spin polarized BS-UDFT frame work by Polo and coworkers.[41] The OV and TTF are used as radical centers to prepare the cationic diradical based magnetic molecules. The obtained J values for the diradicals without coupler have been found to be very weak antiferromagnetic which is in good harmony with previous experimental work by Sugawara and coworkers.[42] Yamaguchi et al.[43] also have inspected mixed diradicals assembled from TTF and verdazyl with high positive magnetic exchange coupling constants. Nonetheless, in the work of Polo and coworkers,[41] the J values are explained in the light of planarity of the π–system, and in the presence of heteroatom in the spinning pathway as well as in the existence of different spin polarization paths instead of one. The novelty of this work is that, if these ferromagnetic materials are used in columnar staking one would get molecule based conducting ferromagnets.

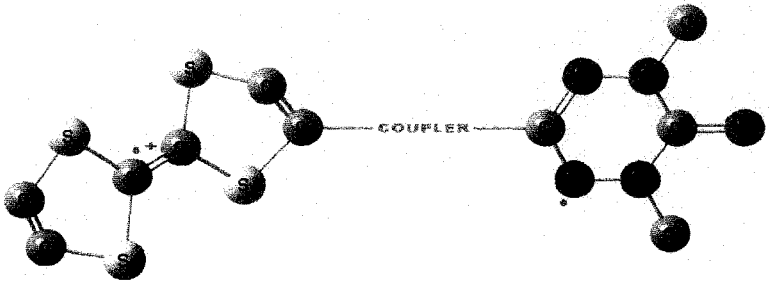

(**25**)

Figure 1.13. OV and TTF cationic radicals based diradicals (**25**) with the couplers investigated by Polo and coworkers (ref. 41). Hydrogens are not shown in picture for simplicity.

Recently, magnetic interactions of some dinitrene systems (Figure 1.14) have also been investigated.[44] The J values for few unconjugated and their corresponding conjugated systems have been evaluated to compare the role of π-conjugation in such systems. A strong antiferromagnetic interaction is observed in investigated conjugated dinitrene systems [44(a)] (**26-28**). With the increase of chain length the magnetic interactions decrease for such systems. The corresponding unconjugated dinitrenes have weakly antiferromagnetic

interactions (**28**). In another work, [44(a)] using the spin flip DFT, the positive J values in alkyl substituted cyclohexane diradicals (**29-30**) (Figure 1.15) have been evaluated. The dramatic change of J value is explained with positive inductive effect of the alkyl substituents.

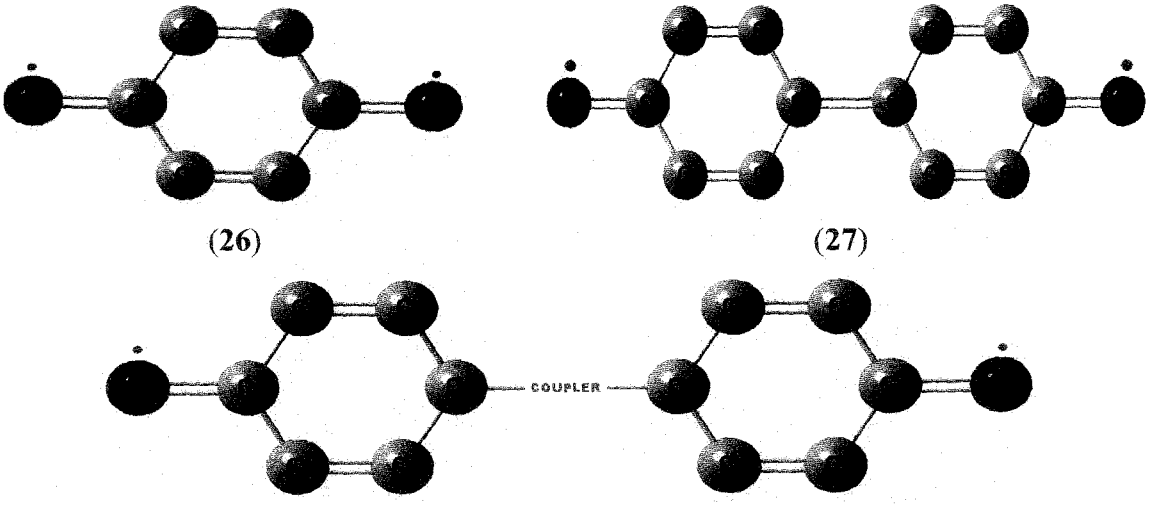

(**26**) (**27**)

(**28**)

Figure 1.14. Investigated dinitrene systems (**26-28**) [ref. 44(a)]. Hydrogens are omitted for lucidity.

(**29**) (**30**)

Figure 1.15. Alkyl substituted cyclohexane-1,4- (**29**) and -1,3-diyls (**30**) [ref. 44(b)]. Hydrogens are excluded for lucidity.

1.7. Organic Polyradicals and Polymer Magnets

Iwamura and co-workers have designed and characterised nitroxyl group containing triradical with ferromagnetic interactions having quartet ground state (**31**).[45] Rajca and co-workers have made significant progress in design and preparation of organic branched chain

π-conjugated potential ferromagnets with strong intermolecular exchange coupling,[46] such as heptaradical (S=7/2) (**32**) and decaradical (S=5) (**33**) based on star branched topology.[46(a)] They have prepared magnetic polymer with large magnetic moment and magnetic order even at 10K.[46(b)] The credit of preparation and characterisation of dendritic polyradicals (**34**) and polymer magnets (**35**) with triplet ground state goes to the same group of researchers.[46(c-d)] Nonetheless, the presence of spin deficiencies in large systems is known as spin defects which has happened on a potential spinning site due to the non-generation of spins on the required site, and it causes the hindrance of spin propagation through the exchange coupling pathway. This problem can be overcome by designing multiple exchange coupling pathways in a single entity. One of such example is Calix[3]arene (**36**).[46(e)] Nonetheless, recently a computationally less rigorous technique has been developed so that one can estimate magnetic exchange between each two sites of the polyradicals following the Heisenberg model.[47] All the molecules are sketched in Figure 1.16.

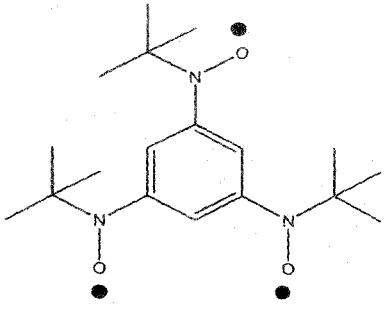

(31)

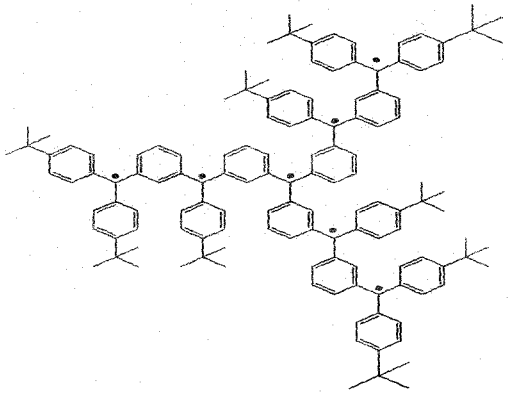

(32)

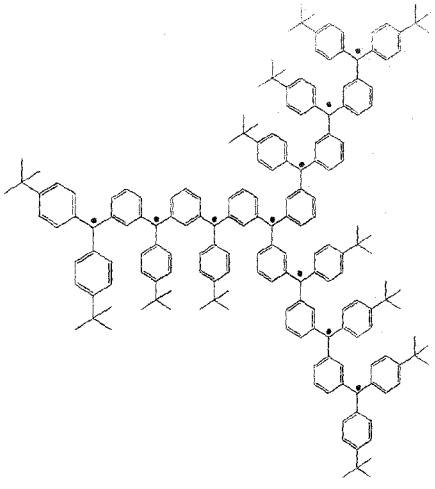

(33)

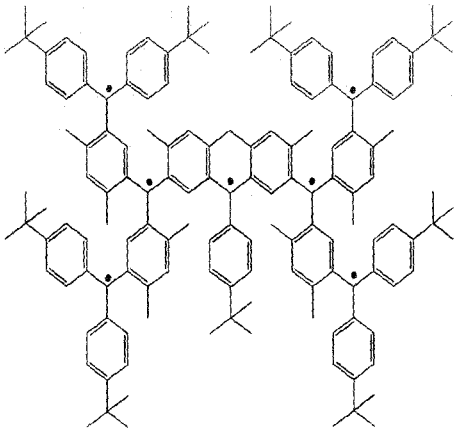

(34)

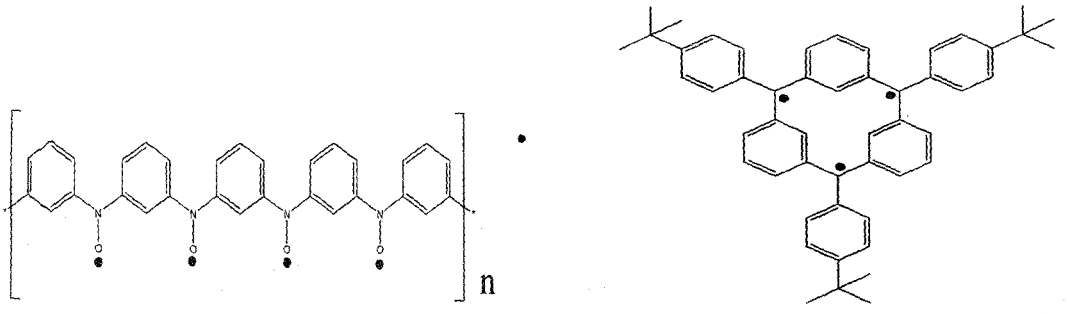

(35) (36)

Figure 1.16. Different types of synthesized polyradicals (ref. 45, 46).

1.8. Application of Diradical Based Magnetism

There are many uses of diradical based magnetic molecules. In technological applications[48] or in bio- medicines[9] they are in use. The organic diradicals are used as molecular junctions in spintronics.[48(a)] Apart from this role, they also serve as common intermediate in numerous chemical reactions and this is why they are very significant in chemical synthesis. However, the phenomena of magnetization reversal is important in the field of magnetic data storage, hard disk drives, and also in spintronic materials.[48(b)] The field induced magnetization reversal is difficult to execute,[48(c)] however, the photoinduced magnetic crossover is easy to accomplish and find wide applications in high density information storage devices, in superior resolution etc. [48(d)]

1.8.1. Earlier Photomagnetic Diradical Systems

If a photochromic moiety is used as a coupler between two magnetic sites then the nature of magnetic interaction of the resulting magnetic material can change upon photoirradiation of appropriate wavelength. In organic systems, electron spins can be conserved for longer time and distance than in conventional inorganic materials. In recent years, photomagnetism in organic compounds has engrossed generous attentiveness. Various photochromic spin couplers like diarylethene, azobenzene etc. have been synthesized and characterised with their magnetic properties by Matsuda and coworkers.[49]

31 MAY 2013 252141

Theoretically the photomagnetic behavior of nitronyl nitroxide, imino nitroxide and verdazyl derivatives of substituted dihydropyrene has been investigated.[50] The change of structural pattern from cyclophanediene to dihydropyrene can be obtained by the application of appropriate wavelength of electromagnetic radiation (Figure 1.17). When bis-IN or bis-NN are used as radical sites with these photochromic couplers the observed J values are very low.[50(a)] However, the J values are drastically increased when N-linked OV and NN are used as radicals with these couplers.[50(b)]

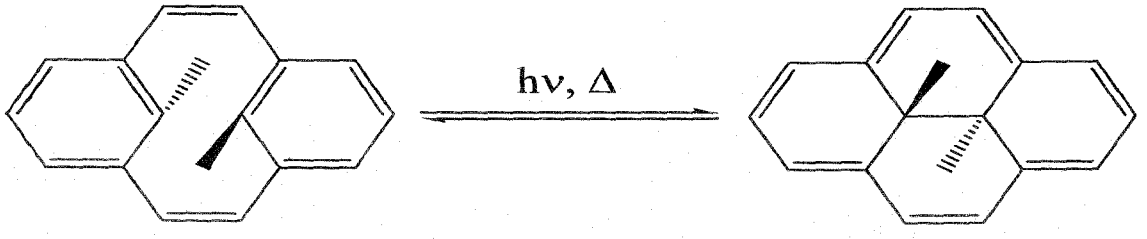

Cyclophanediene Dihydropyrene

Figure 1.17. Photoconversion of cyclophanediene to dihydropyrene upon irradiation of appropriate wave length of light.

1.8.2. Photoinduced Antiferromagnetic to Ferromagnetic Crossover

The most interesting point of these previous systems is that only the change of magnitude of coupling constants is found yet the sign of coupling does not change. This leads to theoretical design and explore photomagnetic switch systems of organic origin, where magnetic crossover takes place when exposed to the light of a particular wave length,[51] (Figure 1.18) although different systems of inorganic origin, where such magnetic crossover takes place are already known.[52] Trans (a) and cis (b) azobenzene with bis-IN, bis-NN and bis-OV as radical sites (Figure 1.18) is used to design photomagnetic molecules which would likely to attract immediate attention of the experimentalists for their potential applications. It is needless to say that, in suitably crafted azobenzene molecules light can perform the magnetic crossover at nano second time scale which is more applicable in modern technology.

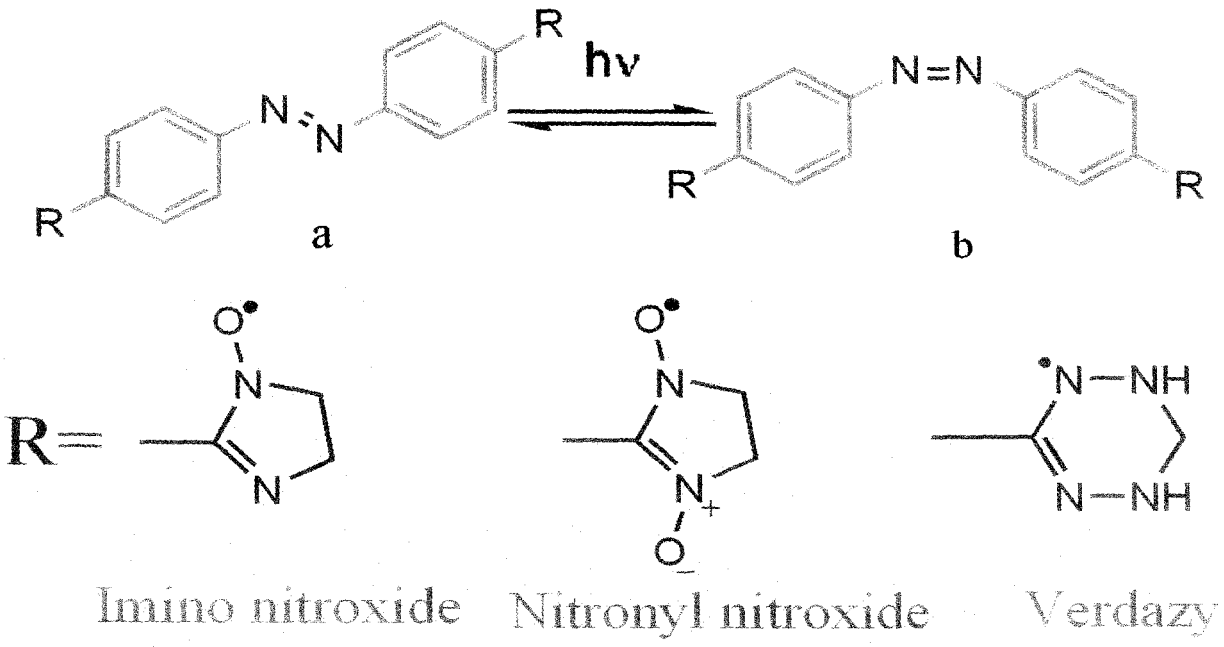

Figure 1.18. Conversion of trans azo-benzene diradicals to cis azo-benzene diradicals with the application of proper wave length of electromagnetic radiation (ref. 51).

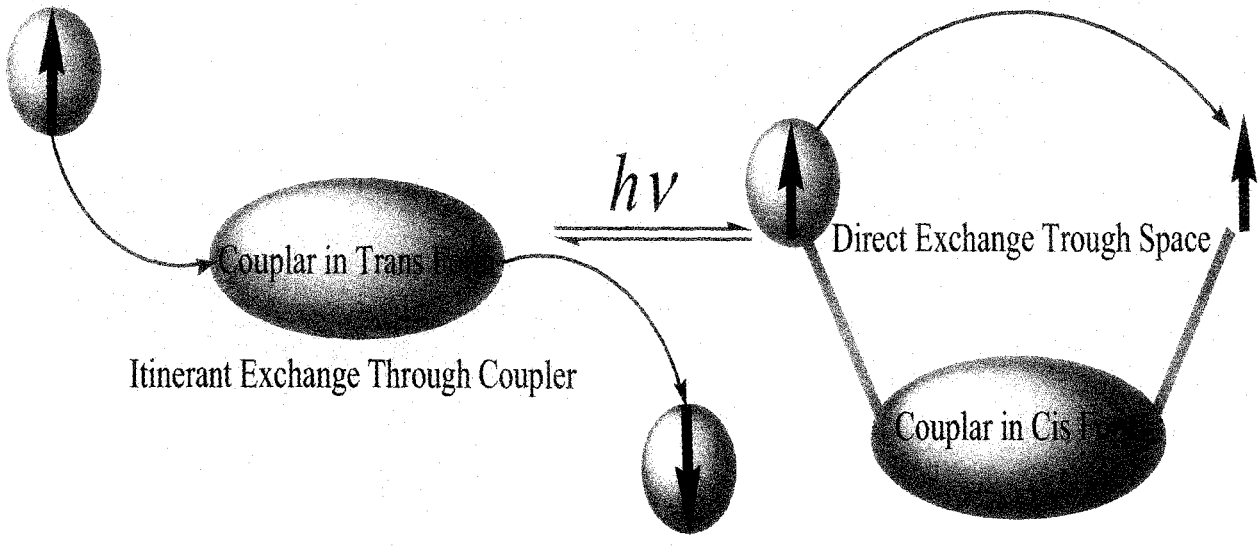

Figure 1.19. Pictorial representation of itinerant (through coupler) exchange and direct (through space) exchange in trans and cis geometric isomeric azobenzene (ref. 51) based diradicals showing anti parallel and parallel spin alignment respectively upon irradiation of light of appropriate wavelength.

In the azobenzene based work,[51] the J values of all three species in the trans forms are negative, but in the case of cis forms, J values are positive. Hence, from the basic principles of magnetism one may note that all trans forms have spins with opposite orientation (antiferromagnetic) in two spin sites and similarly all cis forms have spins with same alignment (ferromagnetic) in two radical centers (Figure 1.19). Accordingly, a magnetic crossover from antiferro (trans) to ferro (cis) would be noticed in all cases when the trans isomers undergo photoisomerization by the application of range 340–380 nm wavelength of light[51] (Figure 1.18).

1.8.3. Biologically Active Diradicals

Huge attention has been paid for the designing of tailor made biomedicines attached with magnetically active molecules for their site specific uses at the pathologic sites. Biocompatible multifunctional magnetic micro- and nano-particles are used to release specific drugs in the target by external or local control.[53] These magnetic particles find diverse biological applications such as in magnetic resonance imaging (MRI) contrast agents, hyperthermia treatment for malignant tumors, conveying medicines, gene delivery, fluorescent biological leveler, discovery of proteins, inquiring DNA structures, and so on, as discussed comprehensively in the review of Salata.[9] The use of target specific magnetic biodegradable materials reduces the inherent side effects through the local distribution of drugs. In MRI, the aminoxyl radicals are known as contrast agents.[54] Rajca and co-workers have made various attempts to synthesize many aminoxyl radicals with S=1 ground state.[55] Generally, gadolinium (Gd) complexes are used as MRI contrast agents, however they are nonspecific and the toxic nature of Gd^{+3} complexes causes renal failure in many cases. On the other hand, nitroxyls and aminoxyls are water soluble and can do the renal excretion with ease. Oppeneer and co-workers have theoretically investigated the effect of hydrogen (aminoxyl-water hydrogen) bonding ($NO^{\bullet}\cdots\cdots H_2O$) on J for different synthesized biologically active ferromagnetically coupled bis-aminoxyl diradicals.[56] However, the searching for biocompatible, easily renal excreable organic less toxic MRI contrast agents are still encouraging.

1.8.4. Molecular Spintronics

So far as the technological applications are concern the organic magnetic molecules are promising in the field of spintronic materials.[48(a)] Literally spintronics means spin based electronics, which is also called magneto electronics. One of the major advantages of the spintronic materials is that the nature of spin orientation makes them suitable candidate for making devices like memory storage, quantum computing, magnetic sensors etc.[57] Several experimental groups have reported the quantification of the current-voltage (*I-V*) characteristics of different organic molecules.[58] These developments have expanded the immense curiosity in modeling and understanding the capabilities of the molecular conductors from the basic scientific and applied point of view.[59] Recently, Sen and Chakrabarti have reported the smallest molecular spin filter which is essentially a ferromagnetically coupled cobalt-benzene-cobalt (CBC) system adsorbed on Au(III) surface with extraordinary spin injection coefficient.[60] In another work, it has been shown that the chemical and magnetic interactions of metalloporphyrenes and metallic substrates can be modified through the tuning of magnetic interactions between manganese porphyrenes and ferromagnetic Co substrates. The objective of the work was to tune the properties of molecular spintronic materials, that is, the adsorption of nano-magnetic molecules on metal surfaces by means of dedicated control of the molecule-surface interaction.[61] However, the field is in early stage, and the scientists are very keen to develop numerous spintronic nano- or micro-devices. Photoinduced spin valve effect has also been predicted in case of organic systems,[51] in azobenzene based diradicals examining density of states at Fermi level.

1.9. On Molecular Magnetism

The field of research where the magnetic properties of an isolated molecule as well as their assemblies are taken into consideration is the area of molecular magnetism. The molecules may have one or more magnetic centers. In case of assemblies of molecules residing in the solid state, the intramolecular magnetic interactions occur in between different magnetic entities. The similar type of interactions is observed among a single isolated magnetic entity where intermolecular magnetic interactions prevail. At this point it is really

informative to mention that, in an extended isolated magnetic system strong magnetic interactions may be found which is responsible for bulk magnetic properties.

Over the time, as the science related to molecular magnetism is developing, the discovery of new magnetic building blocks as well as the way to assemble them in the solid state is increasing rapidly. It is to be noted that, the spin bearing entity is called as building block in such cases. There are different strategies by which one can assemble these unpaired spins in the molecular magnetic materials. The fundamental efforts are necessary to understand the structural and physicochemical features of these magnetic species to get the newly created molecular magnets.

In organic domain of molecular magnetism the organic radicals are used as spin active components. However, these radicals must be stable in air and moisture, isolated and characterised at room temperature. This limitation makes only a few organic radical classes to be useful for this purpose. It is found that the most active spin bearing site to be used as building block does not have much steric bulk. Hence, the radical approach to realize molecular magnet pays attention to nitroxides, verdazyls, heterocyclic thiazyl radicals etc.

As far as the applications of these materials are concerned their uses in domestic as well as high tech appliances are not overlooked. The increasing necessity of microelectronic devices with decreasing size finally reaches the molecular dimension. On the other hand, in biomolecular field of research molecule based magnetic materials can also find diverse uses. However, reaching the ultimate goal in the field of molecular magnetism in organic domain is still intellectually challenging.[27,62]

1.10. Objectives of the Thesis

The essence of magnetism is well known, however the design, characterisation and applications of molecular magnets are still fascinating. The main objective of my thesis is to examine molecular magnetic systems of organic origin. The magnetic character of a molecule is best quantified by the intramolecular magnetic exchange coupling constant (J).

Hence, the objectives of this thesis are to understand the magnetic features and applicability of different magnetic substances through quantification. These are systematically indentified in the following:

(1) To design different bis-oxoverdazyl based diradicals connected by various linkage specific aromatic ring couplers and to quantify their magnetic properties (**Chapter 3: Magnetism in Bis-Oxoverdazyl Diradicals Coupled with Different Linkage Specific Aromatic Ring Spacers**).

(2) To understand the magnetic nature and aromaticity of different high spin bis-oxo- and -thioxo-verdazyl based diradicals with linear polyacenes with varying length as couplers (**Chapter 4: Role of Linear Polyacene Spacers in Intramolecular Magnetic Exchange Coupling**).

(3) To find out a relation between the magnetic exchange coupling constant and different aromaticity index among different high spin and their corresponding low spin bis-heteroverdazyl diradicals having meta- and para-phenylene as couplers (**Chapter 5: Influence of Aromaticity on the Magneto Structural Property of Heteroverdazyl Diradicals**).

(4) To briefly investigate the antiferromagnetic to ferromagnetic crossover upon irradiation of appropriate wavelength of electromagnetic radiation in green fluorescent protein (GFP) chromophore coupled diradicals (**Chapter 6: Photoresponsive Magnetic Crossover**).

(5) To study computationally the possible biomedical uses, particularly as a potent candidates of magnetic resonance imaging contrast agents, of our designed different variants of GFP chromophore coupled diradicals (**Chapter 7: Possible Applications of Fluoro Protein Chromophore Coupled Photomagnetic Diradicals**).

1.11. References and Notes

(1) (a) Coronado, E.; Delhaè, P.; Gatteschi, D.; Miller, J. S. *Molecular Magnetism*: *From Molecular Assemblies to the Devices*, Eds.; Nato ASI Series E, Applied Sciences, Kluwer Academic Publisher: Dordrecht, Netherland, 1996, Vol. 321. (b) Kahn, O. *Molecular Magnetism*, New York, VCH, 1993. (c) Blundell, S. J. *Magnetism in Condensed Matter*; Oxford University Press: New York, 2001.

(2) (a) Kahn, O.; Gatteschi, D.; Miller, J. S.; Palacio, F. Eds.; *Magnetic Molecular Materials*; Kluwer: London, 1991. (b) Miller, J. S.; Epstein, A. J. *Angew. Chem., Int. Ed. Engl.* **1994**, *33*, 385. (c) Gatteschi, D. *Adv. Mater.* **1994**, *9*, 635.

(3) Hellemans, A.; Bunch, B. Timetables of *Science*, Simon and Schuster: New York, 1988, p 19.

(4) (a) Crayston, J. A.; Devine, J. N.; Walton, J. C. *Tetrahedron*, **2000**, *56*, 7829. (b) Miller, J. S.; Epstein, A. J. *MRS Bull.* November 2000, p 21.

(5) (a) McConnell, *J. Chem. Phys.* **1963**, *39*, 1910. (b) Itoh, K. *Chem. Phys. Lett.* **1967**, *1*, 235. (c) Mataga, N. *Theor. Chim. Acta.* **1968**, *10*, 372.

(6) Carlin, R. L. *Magnetochemistry*; Springer-Verlag: Berlin, 1968.

(7) Mason, J. *J. Am. Chem. Soc.* **1991**, *113*, 24.

(8) (a) Wickman, H. H.; Trozzolo, A. M.; Williams, H. J.; Hull, G. W.; Merritt, F. R. *Phys. Rev.* **1967**, *155*, 563. (b) Wickman, H. H. *J. Chem. Phys.* **1972**, *56*, 976.

(9) Salata, O. V. *J. Nanobiotechnol.*, **2004**, *2*, 3.

(10) Borden, W. T.; Davidson, E. R. *Ann. Rev. Phys. Chem.* **1979**, *30*, 125.

(11) March, J. *Advanced Organic Chemistry*, 4th edition, 1992.

(12) (a) Takui, T.; Sato, K.; Shiomi, D.; Ito, K.; Nishizawa, M.; Itoh, K. *Syn. Metals* **1999**, *103*, 2271. (b) Romero, F. M.; Ziessel, R.; Bonnet, M.; Pontillon, Y.; Ressouche, E.; Schweizer, J.; Delley, B.; Grand, A.; Paulsen, C. *J. Am. Chem. Soc.* **2000**, *122*, 1298. (c) Nagashima, H.; Irisawa, M.; Yoshioka, N.; Inoue, H. *Mol. Cryst. Liq. Cryst. Sci. Technol. Sect. A* **2002**, *376*, 371. (d) Rajadurai, C.; Ivanova, A.; Enkelmann, V.; Baumgarten, M. *J. Org. Chem.* **2003**, *68*, 9907. (e) Wautelet, P.; Le Moigne, J.; Videva, V.; Turek, P. *J. Org. Chem.* **2003**, *68*, 8025. (f) Deumal, M.; Robb, M. A.; Novoa, J. J. *Polyhedron* **2003**, *22*, 1935.

(13) Tamura, M.; Nakazawa, Y.; Shiomi, D.; Nozawa, K.; Hosokoshi, Y.; Ishikawa, M.; Takahashi, M.; Kinoshita, M. *Chem. Phys. Lett.* **1991**, *186*, 401.

(14) Ziessel, R.; Stroh, C.; Heise, H.; Khler, F. H.; Turek, P.; Claiser, N.; Souhassou, M.; Lecomte, C. *J. Am. Chem. Soc.* **2004**, *126*, 12604.

(15) (a) Caneschi, A.; Ferraro, F.; Gatteschi, D.; Lirzin, A. L.; Rentschler, E. *Inorg. Chim. Acta* **1995**, *235*, 159. (b) Oshio, H.; Watanabe, T.; Ohto, A.; Ito, T. *Inorg. Chem.* **1997**, *36*, 1608. (c) Lescope, C.; Luneau, D.; Rey, P.; Bussiere, G.; Reber, C. *Inorg. Chem.* **2002**, *41*, 5566.

(16) Wautelet, P.; Catala, L.; Bieber, A; Turek, P.; Andre′, J.-J. *Polyhedron* **2001**, *20*, 1571.

(17) Vyas, S.; Ali, Md. E.; Hossain, E.; Patwardhan, S.; Datta, S. N. *J. Phys. Chem. A* **2005**, *109*, 4213.

(18) Dane, E. L.; Maly, T.; Debelouchina, G. T.; Griffin, R. G.; Swager, T. M. *Org. Lett.* **2009**, *11*, 1871.

(19) Nakatsuji, S.; Takai, A.; Nishikawa, K.; Morimoto, Y.; Yasuoka, N.; Suzuki, K.; Enokid, T.; Anzaia, H. *J. Mater. Chem.* **1999**, *9*, 1747.

(20) Kuhn, R.; Trischmann, H. *Angew. Chem. Int. Ed. Engl.* **1963**, *2*, 155.

(21) Nesterenko, A. M.; Polumbrik, O. M.; Markovskii, L. M. *J. Struct. Chem.* **1984**, *25*, 209.

(22) Kornuta, P. P.; Bobkov, V. N.; Polumbrik, O. M.; Markovskii, L. N. *Zh. Obshch. Khim.* **1978**, *48*, 697.

(23) Barclay, T. M.; Hicks, R. G.; Ichimura, A. S.; Patenaude, G. W. *Can. J. Chem.* **2002**, *80*, 1501.

(24) Neugebauer, F. A.; Fischer, H.; Siegel, R. *Chem. Ber.* **1988**, *121*, 815.

(25) Hicks, R. G.; Hooper, R. *Inorg. Chem.* **1999**, *38*, 284.

(26) Hicks, R. G.; Ohrstrom, L.; Patenaude, G. W. *Inorg. Chem.* **2001**, *40*, 1865.

(27) Koivisto, B. D.; Ichimura, A. S.; McDonald, R.; Lemaire, M. T.; Thompson, L. K.; Hicks, R. G. *J. Am. Chem. Soc.* **2006**, *128*, 690.

(28) Koivisto, B. D.; Hicks, R. G. *Coord. Chem. Rev.* **2005**, *249*, 2612.

(29) Serwinski, P. R.; Esat, B.; Lahti, P.M.; Liao, Y.; Walton, R.; Lan, J. *J. Org. Chem.* **2004**, *69*, 5247.

(30) Barclay, T. M.; Hicks, R. G.; Lemaire, M. T.; Thompson L. K.; Xu, Z. *Chem. Commun.* **2002**, 1688.

(31) (a) Otsubo, T.; Aso, Y.; Takimiya, K. *Adv. Mater.* **1996**, *8*, 203. (b) Iyoda, M;. Hasegawa, M.; Miyake, Y. *Chem. Rev.* **2004**, *104*, 5085.

(32) (a) Longuet-Higgins, H. C. *J. Chem. Phys.* **1950**, *18*, 265. (b) Woodgate, G. K. *Elementary Atomic Structure, physics*, McGraw-Hill, 1970. (c) Ovchinikov, A. A. *Theor. Chim. Acta* **1978**, *47*, 297. (d) Dougherty, D. A. *Acc. Chem. Res.* **1991**, *24*, 88. (e) Lahti, P. M.; Ichimura, A. S. *J. Org. Chem.* **1991**, *56*, 3030. (f) Ling, C.; Minato, M.; Lahti, P. M.; van Willigen, H. *J. Am. Chem. Soc.* **1992**, *114*, 9959. (g) Trindle, C.; Datta, S. N. *Int. J. Quantum Chem.* **1996**, *57*, 781. (h) Trindle, C.; Datta, S. N.; Mallik, B. *J. Am. Chem. Soc.* **1997**, *119*, 12947. (i) Minato, M.; Lahti, P. M. *J. Am. Chem. Soc.* **1997**, *119*, 2187.

(33) (a) Dowd, P. A. *J. Am. Chem. Soc.* **1966**, *88*, 2587. (b) Dowd, P. *Acc. Chem. Res.* **1970**, *5*, 242.

(34) Schlenk, W.; Brauns, M. *Chem. Ber.* **1915**, *48*, 661.

(35) (a) Nachtigall, P.; Jordan, K. D. *J. Am. Chem. Soc.* **1992**, *114*, 4743. (b) Nachtigall, P.; Jordan, K. D. *J. Am. Chem. Soc.* **1993**, *115*, 270.

(36) (a) Klein, D. *J. Pure Appl. Chem.* **1983**, *55*, 299. (b) Klein, D. J.; Alexander, S. A. *In Graph Theory and Topology in Chemistry*; King, R. B., Rouvay, D. H., Eds.; Elsevier: Amsterdam, The Netherlands, 1987; vol. 51, p 404. (c) Davidson, E. R.; Clark, A. E. *J. Phys. Chem. A.* **2002**, *106*, 7456. (d) Shen, M.; Sinanõglu, O. *In Graph Theory and Topology in Chemistry*; King, R. B., Rouvay, D. H., Eds.; Elsevier: Amsterdam, The Netherlands, 1987; vol. 51, p 373.

(37) (a) Borden, W. T.; Davidson, E. R. *J. Am. Chem. Soc.* **1977**, *99*, 4587. (b) Borden, W. T.; Davidson, E. R.; Feller, D. *Tetrahedron* **1982**, *38*, 737.

(38) Rajca, A.; Rajca, S. *J. Am. Chem. Soc.* **1996**, *118*, 8121.

(39) Rajca, A.; Rajca, S.; Wongsriratanakul, J. *Chem. Comm.* **2000**, 1021.

(40) (a) Datta, S. N.; Jha, P. P.; Ali, Md. E. *J. Phys. Chem. A* **2004**, *108*, 4087. (b) Datta, S. N.; Mukherjee, P.; Jha, P. P. *J. Phys. Chem. A* **2003**, *107*, 5049. (c) Ali, Md. E.; Datta, S. N. *J. Phys. Chem. A* **2006**, *110*, 2776. (d) Ali, Md. E.; Datta, S. N. *J. Phys. Chem. A* **2006**, *110*, 13232.

(41) Polo, V.; Alberola, A.; Andres, J.; Anthony, J.; Pilkington, M. *Phys. Chem. Chem. Phys.* **2008**, *10*, 857.

(42) (a) Kumai, R.; Matsushita, M. M.; Izuoka, A.; Sugawara, T. *J. Am. Chem. Soc.*, **1994**, *116*, 4523. (b) Nakazaki, J.; Matsushita, M. M.; Izuoka, A.; Sugawara, T. *Tetrahedron Lett.* **1999**, *40*, 5027.

(43) (a) Matsuoka, F.; Yamashita, Y.; Kawakami, T.; Kitagawa, Y.; Yoshioka, Y.; Yamaguchi, K. *Polyhedron*, **2001**, *20*, 1169. (b) Morita, Y.; Kawai, J.; Haneda, N.; Nishida, S.; Fukui, K.; Nakazawa, S.; Shiomi, D.; Sato, K.; Takui, T.; Kawakami, T.; Yamaguchi, K.; Nakasuji, K. *Tetrahedron Lett.* **2001**, *42*, 7991.

(44) (a) Ghosh, R.; Seal, P.; Chakrabarti, S. *J. Phys. Chem. A* **2010**, *114*, 93. (b) Seal, P.; Chakrabarti, S. *J. Phys. Chem. A* **2008**, *112*, 3409.

(45) Kanno, F.; Inoue, K.; Koga, N.; Iwamura, H. *J. Phys. Chem.* **1993**, *97*, 13267.

(46) (a) Rajca, A.; Utamapanya, S.; Thayumanavam, D. *J. Am. Chem. Soc.* **1992**, *14*, 1884. (b) Rajca, A.; Wongsriratanakul, J.; Rajca, S. *Science* **2001**, 294. (c) Rajca, A.; Utamapanya, S. *J. Am. Chem. Soc.* **1993**, *115*, 10688. (d) Rajca, A.; Utamapanya, S. *Liq. Cryst. Mol. Cryst.* **1993**, *232*, 305. (e) Rajca, A.; Lu. K.; Rajca, S. *J. Am. Chem. Soc.* **1997**, *119*, 10335.

(47) Paul. S.; Misra, A. *J. Phys. Chem. A* **2010**, *114*, 6641.

(48) (a) Herrmann, C.; Solomon, G. C.; Ratner, M. A. *J. Am. Chem. Soc.* **2010**, *132*, 3682. (b) Stohr, J.; Siegmann, H. C.; *Magnetism: From fundamentals to Nanoscale Dynamics*, Springer-Verlag, Berlin, 2006. (c) Thirion, C.; Wernsdorfer, W.; Mailly, D. *Nat. Mater.* **2003**, *2*, 524. (d) Sato, O.; Iyoda, T.; Fujishima, A.; Hashimoto, K. *Science* **1996**, *272*, 704.

(49) (a) Matsuda, K.; Matsuo, M.; Irie, M. *J. Org. Chem.* **2001**, *66*, 8799. (b) Matsuda, K.; Irie, M. *J. Photochem. Photobiol. C: Photochem. Res.* **2004**, *5*, 69. (c)Tanifuji, N.; Matsuda, K.; Irie, M. *Polyhedron* **2005**, *24*, 2484. (d) Matsuda, K.; Irie, M. *Polyhedron* **2005**, *24*, 2477. (e) Matsuda, K. Bull. *Chem. Soc. Jpn.* **2005**, *78*, 383.

(50) (a) Ali, Md. E.; Datta, S. N. *J. Phys. Chem. A Lett.* **2006**, *110*, 10525. (b) Bhattacharjee, U.; Latif, I. A.; Panda, A.; Datta S. N. *J. Phys. Chem. A* **2010**, *114*, 6701.

(51) Shil, S.; Misra, A. *J. Phys. Chem. A* **2010**, *114*, 2022.

(52) Hamachi, K.; Matsuda, K.; Itoh, T.; Iwamura, H. *Bull. Chem. Soc. Jpn.* **1998**, *71*, 2937.

(53) (a) Pankhurst, Q. A.; Connolly, J.; Jones, S. K.; Dobson, J. *J. Phys. D: Appl. Phys.* **2003**, *36*, R167. (b) Tartaj, P.; Morales, M. P.; Veintemillas-Verdaguer, S.; González-

Carreño, T.; Serna, C. J. *J. Phys. D: Appl. Phys.* **2003**, *36*, R182. (c) Pankhurst, Q. A.; Thanh, N. K. T.; Jones, S. K.; Dobson, J. *J. Phys. D: Appl. Phys.* **2009**, *42*, 224001.

(54) (a) Rajca, A. *Chem. Rev.* **1994**, *94*, 871. (b) Matsumoto, K.; Hyodo, F.; Matsumoto, A.; Koretsky, A. P.; Sowers, A. L.; Mitchell, J. B.; Krishna, M. C. *Clin. Cancer Res.* **2006**, *12*, 2455.

(55) (a) Spagnol, G.; Shiraishi, K.; Rajca, S.; Rajca, A. *Chem. Commun.* **2005**, 5047. (b) Rajca, A.; Takahashi, M.; Pink, M.; Spagnol, G.; Rajca, S. *J. Am. Chem. Soc.* **2007**, *129*, 10159.

(56) Ali, Md. E.; Oppeneer, P. M.; Datta, S. N. *J. Phys. Chem. B* **2009**, *113*, 5545.

(57) Pati, R.; Senapati, L.; Ajayan, P. M.; Nayak, S. K. *Phys. Rev. B* **2003**, *68*, 100407(R).

(58) (a) Reed, M. A.; Zhou, C.; Muller,C. J.; Burgin, T. P.; Tour, J. M. *Science* **1997**, *278*, 252. (b) Chen, J.; Reed, M. A.; Rawlett, A. M.; Tour, J. M. *Science* **1999**, *286*, 1550. (c) Gittins, D. I.; Bethell, D.; Schriffrin, D. J.; Nichols, R. J. *Nature* **2000**, *408*, 67. (d) Liang, W.; Shores, M. P.; Bockrath, M.; Long, J. R.; Park, H. *Nature* **2002**, *417*, 725.

(59) (a) Tian, W.; Datta, S.; Hong, S. H.; Reifenberger, R.; Henderson, J. I.; Kubiak, C. P. *J. Chem. Phys.* **1998**, *109*, 2874. (b) Evers, F.; Weigend, F.; Koentopp, M. *Phys. Rev. B* **2004**, *69*, 235411. (c) Taylor, J.; Guo, H.; Wang, J. *Phys. Rev.* B **2001**, *63*, 245407. (d) Damle, P. S.; Ghosh, A. W.; Datta, S. *Phys. Rev. B* **2001**, *64*, 201403(R).

(60) Sen, S.; Chakrabarti, S. *J. Am. Chem. Soc.* **2010**, *132*, 15334.

(61) Ali, Md. E.; Sanyal, B.; Oppeneer, P. M. *J. Phys. Chem. C* **2009**, *113*, 14381.

(62) (a) Miller, J. S.; Epstein, A. J.; William, M. R. *Acc. Chem. Res.* **1988**, *21*, 114. (b) Caneschi, A.; Gatteschi, D.; Sessoli, R.; Rey, P. *Acc. Chem. Res.* **1989**, *22*, 392.

Chapter 2

Theoretical Background

The theoretical background for the determination of the magnetic exchange coupling constants from the first principle of magnetism has been discussed here. Theory for zero field splitting parameters and magnitude are also described in this chapter.

2.1. Introduction

In the previous chapter we have discussed the background of the different qualitative methods of how the ground state of a diradical based magnetic species can be estimated. Although these qualitative methods can estimate the ground state of a diradical very effectively; however, the quantification is necessary. Theoretically the quantification of the magnetic nature of a diradical species have been done by estimating the magnetic exchange coupling constant (J). In diradical species J is mainly the energy difference between the triplet and the singlet states. Positive and negative values of J indicate the ferromagnetism and antiferromagnetism respectively. Nonetheless, as far as the applications of the organic diradical based magnetic species are concerned, after evaluating their magnetic characters, one needs to quantify their biological activity such as applicability as magnetic resonance imaging contrast agent (MRICA), as hyperthermic agent, applicability in optoelectronic devices, in spintronic applications and so on. A point to be mentioned here is that, the quantification of a diradical to be applicable as MRICA can be done by the quantitative estimation of spin spin axial and rhombic zero field splitting (ZFS) parameters D, E and also with the static ZFS magnitude a_2.

2.2. Quantitative Methods: The Hamiltonian

It is known that the magnetic interaction is electronic spin related phenomenon. In organic ferromagnetic diradicals, electronic spins at two different radical centers are aligned parallel to each other whereas in antiferromagnetic substances spins are aligned in antiparallel fashion.[1] Hence, ferromagnetic substances have high spin ground state. For example, organic ferromagnetic diradicals have triplet ground state in contrary antiferromagnetic diradicals have singlet ground state. This indicates that for a moiety to be ferromagnetic it must have singly occupied molecular orbitals as their HOMO and HOMO-1. We now discuss how this interaction energy can be quantified.

Let us consider a diradical with two unpaired electrons at sites 1 and 2. The isotropic interaction between two spin sites, say S_1 and S_2, can be best described by Heisenberg effective spin exchange Hamiltonian

$$\hat{H} = -2J\hat{S}_1 \cdot \hat{S}_2 . \tag{2.1}$$

The eigenfunctions of the Heisenberg Hamiltonian are eigenfunction of $\hat{S}^2$ and $\hat{S}_z$ where S is the total spin angular momentum and is directly related to the energy difference between the spin eigenstates.

Let the two electrons are in $\Psi_a(r_1)$ and $\Psi_b(r_2)$ where r is the spatial coordinate. For a singlet system, the spin part χ_S will be antisymmetric and for triplet χ_T is symmetric. Electrons being fermionic the total wave function must be antisymmetric under the exchange of coordinates which is written as:

$$\Psi_S = \frac{1}{\sqrt{2}}[\Psi_a(r_1)\Psi_b(r_2) + \Psi_a(r_2)\Psi_b(r_1)]\chi_S$$

$$\Psi_T = \frac{1}{\sqrt{2}}[\Psi_a(r_1)\Psi_b(r_2) - \Psi_a(r_2)\Psi_b(r_1)]\chi_T . \tag{2.2}$$

The singlet and triplet energies are given by

$$E_S = \int \Psi_S^* \hat{H} \Psi_S dr_1 dr_2$$

$$E_T = \int \Psi_T^* \hat{H} \Psi_T dr_1 dr_2 . \tag{2.3}$$

The quantity $(E_S - E_T)$ can be estimated assuming χ_S and χ_T to be normalized,

$$E_S - E_T = 2\int \Psi_a^*(r_1)\Psi_b^*(r_2)\hat{H}\Psi_a(r_2)\Psi_b(r_1)dr_1 dr_2 . \tag{2.4}$$

Now, we define exchange integral J as

$$J = \int \Psi_a^*(r_1)\Psi_b^*(r_2)\hat{H}\Psi_a(r_2)\Psi_b(r_1)dr_1dr_2. \quad (2.5)$$

Here the quantity J is called isotropic interaction parameter or magnetic exchange coupling constant. For diradical systems, when J is negative, $S = 0$ is the ground state with anti-parallel spins resulting an antiferromagnetic interaction. In contrast, when J is positive, $S = 1$ is the ground state with parallel orientation of the electronic spins resulting in a ferromagnetic interaction.

In summary, if the two centers interact with each other then the total spin of the diradical system will be S=0 and 1, i.e., singlet and triplet respectively. Due to the electrostatic reason, energy of the singlet and triplet states are separated by a $2J$ energy gap which is defined as

$$2J = E_{S=0} - E_{S=1}. \quad (2.6)$$

An explanation of eq 2.6 is required here. Considering electronic correlation, one can describe the limiting behavior of a diradical molecule in a weak coupling limit. We note that for a ferromagnetic system in weak coupling limit, the spin polarized description of the lowest energy electronic configuration corresponds to all spin up with $S = 1$ and lowest energy configuration with half spin up and half spin down corresponds to $S = 0$. But for an S value in between 0 and 1, more than one configuration can be written. Therefore, $S = 1$ correctly describes a state with all radical centers with spin up condition. However, $S = 0$ corresponds to a state in which radical moieties have their magnetic electrons equally distributed among localized spin up and spin down orbitals. Hence $E_{S=1}$ gives correct energy for triplet whereas $E_{S=0}$ gives a poor approximation to energy of singlet state. The magnetic exchange coupling constant can be evaluated by determining the proper singlet and triplet energy values from a multiconfigurational approach. However, quantitative description of spin exchange interaction is a difficult task and computationally very expensive.

Nevertheless, many groups have done theoretical research using multiconfigurational techniques.

2.3. Methodology: The Density Functional Theory (DFT) Based Methods

DFT is the powerful methodology for chemical simulation where the energy of the systems can be defined in terms of its electron probability density (ρ), that is, in DFT formalism the electronic energy E is treated as the functional of the electron density $E(\rho)$, so that one to one correspondence between the total electron density of a system and its electronic energy is made. Notable point is that, compared to the *ab initio* methodology the density functional theory based treatments are easy to use in respect of their time consumption and flexibility. The simplicity of DFT based methods over other pure methods can be understood by considering a system with n electrons. In such systems the wavefunctions have 3 coordinates for each electron and there must be one extra coordinate where spin is included. However, the electron density actually depends on the 3 coordinates and independent of the number of total electrons of the system. As a matter of fact, if complexity in the wavefunction is increased for the large systems the electron density keeps up the same number of variables, irrespective of the size of the system.

The density functional concept for the first time was emerged from the work of Fermi and Thomas in late 1920s,[2] where the energy of a system is expressed as a function of total electron density. In early 1950s, Slater has made the development of Hartree-Fock method to form Hartree-Fock-Slater[3] method which is treated today as an ancestor theory of DFT. However, it is the mid 1960s, when Kohn and Sham[4] have developed a formalism with the introduction of atomic orbitals then the application of DFT in the field of computational chemistry really sets in motion. The difficulties in the representation of the kinetic energy (KE) of a system are the main problem in earlier DFT formalism. The main essence of Kohn-Sham approach to overcome this problem is that they have splitted the KE functional into two different parts. The first part considered electrons are non-interacting particles and this part is calculated exactly, and in the other part the electron-electron interactions are considered by the introduction of a small correction term.

According to the Kohn-Sham formalism the ground state electronic energy of a system having n electrons and N nuclei is written as

$$E(\rho) = -\frac{1}{2}\sum_{i=1}^{n}\int \Psi_i^*(r_1)\nabla_i^2\Psi_i(r_1)dr_1 - \sum_{X=1}^{N}\int\frac{Z_X}{r_{X_i}}\rho(r_1)dr_1 + \frac{1}{2}\iint\frac{\rho(r_1)\rho(r_1)}{r_{12}}dr_1dr_2 + E^{XC}[\rho], \qquad (2.7)$$

where, Ψ_i's (i=1.....n) are called Kohn-Sham orbitals, KE of the noninteracting electrons are represented by the first term, second term accounts for the nuclear-electron repulsion, whereas the last two terms represent the Coulombic repulsion and exchange correlation term which leads to correction to total kinetic energy of the system respectively.

Within the Kohn-Sham orbital formulations the ground state electron density $\rho(r)$ at a point r can be written as

$$\rho(r) = \sum_{i=1}^{n} |\Psi_i(r)|^2. \qquad (2.8)$$

The importance of Kohn-Sham orbitals lies in the fact that the electron density of the total electronic system is calculated from the above equation. To obtain the Kohn-Sham orbital one needs to solve the Kohn-Sham equation for which the application of variational principle to the electronic energy $E(\rho)$ with the charge density (eq 2.8) is required.

$$\hat{h}_i\Psi_i(r_i) = \varepsilon_i\Psi_i(r_1). \qquad (2.9)$$

In the above equation $\hat{h}_i$ and ε_i represent the Kohn-Sham Hamiltonian and respective orbital energy. The Kohn-Sham Hamiltonian has the form

$$\hat{h}_i = -\frac{1}{2}\nabla_1^2 - \sum_{X=1}^{N}\int\frac{Z_X}{r_{X_i}} + \int\frac{\rho(r_2)}{r_{12}}dr_2 + V^{XC}(r_1), \qquad (2.10)$$

where V^{XC} is the functional derivative of the exchange correlation energy and the description of this term causes the major challenge of DFT methodology, which is given by

$$V^{XC}[\rho] = \frac{\delta E^{XC}[\rho]}{\delta \rho}. \tag{2.11}$$

Hence, having known the E^{XC}, the term V^{XC} can be obtained readily. In Kohn-Sham density functional theory starting from the tentative charge density ρ the dependence of E^{XC} on electron density is used to calculate V^{XC}. Once the initial set of Kohn-Sham orbitals is obtained, these orbitals are used to obtain the superior electron density from eq (2.8). Until the density and the E^{XC} meet the certain convergence criteria the process is repeated again and again. At last, from eq (2.7) the electronic energy is calculated.

One point to be noted here is that, the exchange correlation energy (E^{XC}) is separated in two terms, namely the exchange term (E^{X}), the interactions between the electrons having same spin and the correlation term (E^{C}), the interactions between the electrons having opposite spins. The respective functionals are known as exchange functional and correlation functional correspondingly

$$E^{XC}[\rho] = E^{X}[\rho] + E^{C}[\rho]. \tag{2.12}$$

Today, one can find different functionals depending on the variation of different values of exchange and correlation functional. However, Perdew and Schmidt[5] have successfully represented their vision of the progress of DFT functionals in the form of Jacob's ladder, the famous allusion from the book of *Genesis* (*28, 10-12*), in a DFT symposium in Menton, France. The ladder has five different rungs depicting the five different generations of DFT functionals (Scheme 2.1). One gets local density approximation (LDA) in the first rung, generalized gradient approximation (GGA) stands in the second rung, meta generalized gradient approximation (M-GGA) remains in the third rung, whereas the hybrid generalized gradient approximation (H-GGA) and hybrid meta generalized gradient approximation (HM-GGA) stand in the fourth rung and the fully nonlocal

approximation remains in the last rung when moving from the lower to the higher steps in the Jacob's ladder. If one climbs up with the ladder one needs to assume more and more sophisticated and complicated approximation and reach the heaven of chemical accuracy. A point to be mentioned here is that, each rung has its own drawbacks and advantages. Although the better rung gives better results than its lower one, however, the choice of functionals somehow depends on the problems in hand.

Scheme 2.1. The vision of Perdew for Jacob's ladder of five generation DFT functionals from the world of Hartree to the heaven of chemical accuracy, with the indication of most popular density functional B3LYP at the fourth rung of the ladder.

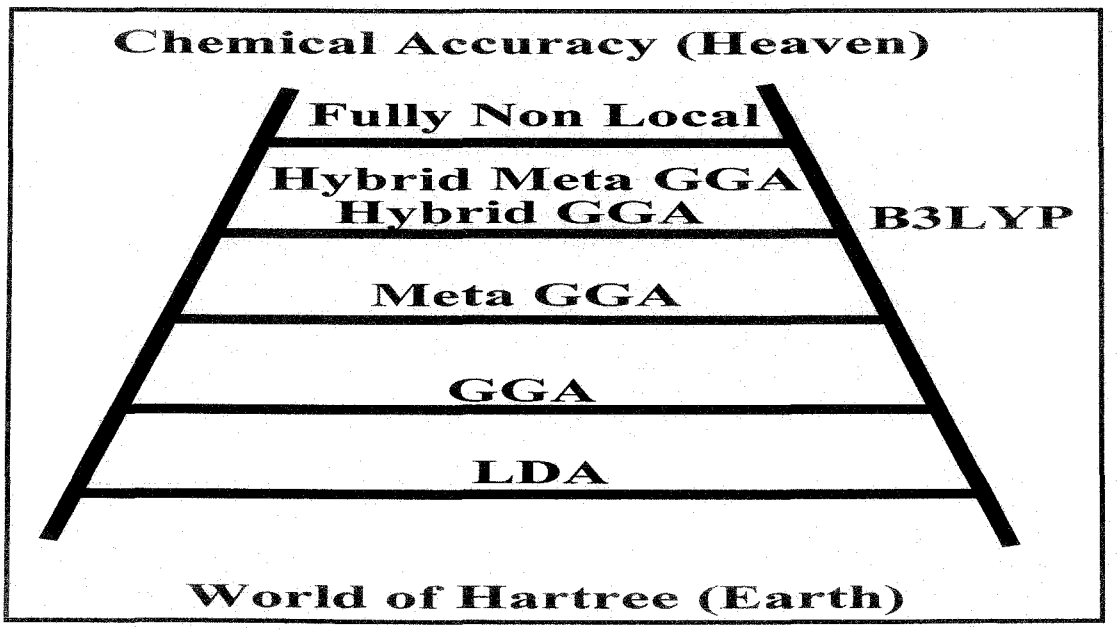

The H-GGA functional has possessed a new dimension in the field of density functional study especially after the birth of B3LYP having 20% Hartree-Fock exchange in 1994. The most popular and widely used B3LYP functional contains Becke 3 parameter exchange in addition to Lee-Yang-Parr correlation functional.[6] There are very few alternatives of B3LYP functional for average quantum chemical problems. If publication is a criterion then from its birth to 2005, the B3LYP is the most accepted one. Many competitive functionals of B3LYP, like M0X suite[7] of functionals are still mounting. However, it is

expected that the supremacy of popular B3LYP may continue for another 4-5 years or more. At last, the property and obviously the type of the systems under study is the key factor of choosing accurate functionals. All these discussions are nicely portrayed in a nice review of Ramos and coworkers.[8]

2.4. Broken Symmetry: Noodleman's Approach

A reliable and computationally less expensive solution to estimate the exchange coupling constant (J) is provided by Density Functional Theory (DFT) based methodologies. To date, the best technique to calculate the S-T energy gap is the well known broken symmetry (BS) method. This method was developed by Noodleman and coworkers.[9] In this method, the spin-polarized, triplet state from unrestricted formalism ($\langle S^2 \rangle = 2$ for diradical) and a broken-symmetry (BS) solution is needed. According to Noodleman "when the magnetic orbitals, i.e., the singly occupied orbital of two spin bearing monomers are allowed to interact by overlapping in self-consistent field procedure, a state of mixed spin symmetry and lowered space symmetry is obtained. This is referred to as the mixed spin or broken symmetry state." The BS state is not an eigenstate of $\hat{H}$. It has the expectation value of $\langle S^2 \rangle$ equal to 1 for a diradical. It is assumed to be an equal admixture of a singlet and a triplet state. States of pure spin symmetry can be retrieved from the BS state using projection operator method. A detailed theoretical description of the BS state is given below.

Following the description of the BS state given by Caballol et al.,[10] we write broken symmetry triplet state in unrestricted formalism as $|T'\rangle = |....\phi_A\phi_B\rangle$, where φ_A and φ_B are the open shell localized spin up orbitals. If one assumes that the spin contamination is small enough to neglect its effect, then one can easily approximate that $|T'\rangle = |T\rangle$ where $|T\rangle$ represents pure triplet. In case of broken symmetry solutions, two types of solutions are possible. These are

$$|BS_1\rangle = |.....\bar{m}n\rangle$$
$$|BS_2\rangle = |.....m\bar{n}\rangle. \qquad (2.13)$$

The two magnetic orbitals m and n are expressed as

$$m = c_1\varphi_A + c_2\varphi_B$$
$$n = c_2\varphi_A + c_1\varphi_B\ , \tag{2.14}$$

where $(c_1^2 + c_2^2) = 1$. Using these BS solutions one can write the spin adopted singlet function S' (not the pure singlet, S) as

$$\left|S'\right\rangle = \frac{\left|BS_1\right\rangle + \left|BS_2\right\rangle}{\sqrt{2(1+\left\langle BS_1 \middle| BS_2\right\rangle)}}, \tag{2.15}$$

where $\left\langle BS_1 \middle| BS_2\right\rangle$ is the overlap integral between the two non-orthogonal BS Slater determinant. Similarly one can write the triplet with $S_z = 0$ as

$$\left|T'\right\rangle = \frac{\left|BS_1\right\rangle - \left|BS_2\right\rangle}{\sqrt{2(1-\left\langle BS_1 \middle| BS_2\right\rangle)}}. \tag{2.16}$$

From the energy expectation values of S' and T' one can express that the intramolecular exchange coupling constant J as

$$J = E_{S'} - E_{T'} = \frac{2(E_{BS} - E_{T'})}{1+\left\langle BS_1 \middle| BS_2\right\rangle}. \tag{2.17}$$

Assuming that the spin polarization of the closed shells can be neglected, the quantity $\left\langle BS_1 \middle| BS_2\right\rangle$ can be approximated as the square of simple overlap integral between the magnetic orbitals $S_{ab} = \langle m|n\rangle$. Hence the J value can be written as

$$J = \frac{(E_{BS} - E_{T'})}{1+S_{ab}^2}\ . \tag{2.18}$$

As discussed earlier, in a single determinantal approach, because of the much less spin contamination in the high-spin state, $E_{T'}$ can be approximated by the energy of the triplet state that is achieved from a direct computation i.e., $E_{T'} \approx E_T$. In contrast, the BS state is often found as spin-contaminated. Therefore, to eliminate the effect of spin contamination from the energy of the BS state, spin-projected methods have been applied. Eq (2.18) is valid when there is only one pair of magnetic orbitals.

The BS method was further investigated for various systems with different degrees of overlap between the magnetic orbitals. The following three spin-projected equations are the results obtained from the same basic methodology and valid for different general cases depending on the degrees of overlap between the magnetic orbitals:

$$J^{GND} = \frac{({}^{DFT}E_{BS} - {}^{DFT}E_T)}{S^2_{\max}}, \tag{2.19}$$

$$J^{BR} = \frac{({}^{DFT}E_{BS} - {}^{DFT}E_T)}{S_{\max}(S_{\max}+1)}, \tag{2.20}$$

$$J^{Y} = \frac{({}^{DFT}E_{BS} - {}^{DFT}E_T)}{\langle S^2 \rangle_T - \langle S^2 \rangle_{BS}}. \tag{2.21}$$

These three relations differ in their applicability. For a sufficiently small overlap between the magnetic orbitals, eq (2.18) reduces to eq (2.19).[9,11] This expression is given by Giensberg, Noodleman and Davidson. In another work, Bencini et al.[12] and Ruiz et al.[13] have proposed an expression for evaluation of J which was further modified by Illas et al.[14,10] (eq 2.20) for the systems with sufficiently large overlap integral, that generally happens for binuclear transition metal complexes. On the other hand, eq (2.21), can be reduced to eq (2.19) and eq (2.20) in the weak and strong overlap limits respectively, has been derived by Yamaguchi et al.[15] One notable point to be mentioned here is that, in my entire thesis work I

have used eq (2.21), the expression given by Yamaguchi and coworkers[15] for the quantification of magnetic exchange coupling constant (J) values.

2.5. Zero Field Splitting (ZFS) Parameters

The direction dependent magnetic properties of a material are known as magnetic anisotropy. Magnetically isotropic material, in absence of magnetic field has no preferential direction of their magnetic moments; however, in absence of such field magnetically anisotropic materials align their magnetic moments with one of the easy axes. The easy axis means an energetically favorable direction of spontaneous magnetization. The magnetic anisotropy may lead to the splitting of 2S+1 magnetic sublevels in absence of external magnetic field. This phenomenon is called zero field splitting (ZFS). The magnetic anisotropy also known as ZFS can characterize the geometric and electronic environment of a radical having spin > 1/2.[16] The reason for the quantification of the ZFS data, that is, its utility in the biomedical applications (D, E and a_2 the axial and rhombic parameters and magnitude of ZFS respectively) and the theoretical background of ZFS are discussed below.

Rajca and co-workers have synthesized and characterized various nitroxide diradicals and polyradicals. Nonetheless, the most interesting bio-features of these radicals are that they can be used as magnetic resonance contrast agents (MRICAs).[17] To design MRICAs in a rational manner, one needs to know the ZFS parameters. The electron spin correlation time is a leading factor for clearer MRI scans with enhanced contrast. The easy estimation of the electron spin correlation time is possible by the ZFS data.[18] The sign and magnitude of axial ZFS parameter D is crucial in determining different magnetic properties of a system. Rajca and co-workers have established that the diradical and polyradical systems of organic origin can be successfully used as MRICAs.[17] The ZFS arises from two contributions, namely the direct electron-electron magnetic-dipole spin-spin (SS) (to first order in perturbation theory) interaction and the spin-orbit coupling (SOC) (to second order in perturbation theory) of the electronically excited state with the ground state.[16] The second order correction to the total energy, originating entirely from the spin orbit coupling interactions in molecular systems, is estimated with the help of the following expression

$$\Delta_2 = \sum_{\sigma\sigma'} \sum_{ij} M_{ij}^{\sigma\sigma'} S_i^{\sigma\sigma'} S_j^{\sigma'\sigma} \tag{2.22}$$

where different spin degrees of freedoms are represented by σ, and i, j denote coordinate levels x, y and z. However, spin-orbit interaction happens to be dominant in case of heavy metal ion systems; in case of organic systems containing lighter elements, this part contributes a negligible amount to the total magnetic anisotropy of the system.

On the other hand, the SS coupling contribution is the main source of ZFS in case of organic radicals.[19] The ZFS value arising from the SS interactions can be estimated through effective spin Hamiltonian

$$\hat{H}_{ZFS} = \sum_{ij} \boldsymbol{D}_{ij} \hat{S}_i \hat{S}_j , \tag{2.23}$$

where $\boldsymbol{D}_{ij}$ is the ZFS tensor, $\hat{S}_k$ is the k'th Cartesian component of the total electron spin operator. Rearrangement of the $\boldsymbol{D}_{ij}$ leads to

$$\hat{H}_{ZFS} = D\left(\hat{S}_z^2 - \frac{1}{3}\hat{S}^2\right) + E\left(\hat{S}_x^2 - \hat{S}_y^2\right), \tag{2.24}$$

where D and E are axial and rhombic ZFS parameters respectively.[20] The spin spin coupling interaction appears as a dipole dipole interaction[21]

$$\hat{H}_{SS} = \frac{\alpha^2}{2} \sum_{i,j} \left[\frac{\vec{s}_i \cdot \vec{s}_j}{r_{ij}^3} - \frac{3(\vec{s}_i \cdot \vec{r}_{ij})(\vec{s}_j \cdot \vec{r}_{ij})}{r_{ij}^5} \right]. \tag{2.25}$$

The single ground-state Kohn-Sham determinant approximates the result of the SS coupling part of the ZFS tensor as the expectation over the single determinant, thereby[22]

$$D_{kl}^{(SS)} = \frac{g_e}{4} \frac{\alpha^2}{S(2S-1)} \left\langle 0SM_S \left| \sum_i \sum_{j \neq i} \frac{r_{ij}^2 \delta_{kl} - 3(r_{ij})_k (r_{ij})_l}{r_{ij}^5} \times \left\{ 2\hat{S}_{iz}\hat{S}_{jz} - \hat{S}_{ix}\hat{S}_{jx} - \hat{S}_{iy}\hat{S}_{jy} \right\} \right| 0SM_S \right\rangle, \tag{2.26}$$

where α is the fine structure constant, g_e is the gyromagnetic ratio. The operators $\hat{S}_{mn}$ signify n'th component of m'th spin vector and r_{ij} is the distance between spins i and j; k and l run over x, y, and z coordinates. McWeeny and Mizuno expressed the above equation using the spin density matrix as[23]

$$D_{kl}^{(SS)} = \frac{g_e}{4}\frac{\alpha^2}{S(2S-1)}\sum_{\mu\nu}\sum_{\kappa\lambda}\left\{P_{\mu\nu}^{\alpha-\beta}P_{\kappa\lambda}^{\alpha-\beta} - P_{\mu\kappa}^{\alpha-\beta}P_{\nu\lambda}^{\alpha-\beta}\right\}\times\left\langle\mu\nu\left|r_{12}^{-5}\left\{\left\{3r_{12,k}r_{12,l}\right\}-\delta_{kl}r_{12}^2\right\}\right|\kappa\lambda\right\rangle. \quad (2.27)$$

Here $P^{\alpha\text{-}\beta} = P^{\alpha} - P^{\beta}$ is the spin density matrix in the atomic-orbital basis, and $\mu, \nu, \kappa, \lambda$ are the basis functions.[18] The ZFS parameters D and E are determined from the tensor components $D_{kl}^{(SS)}$, in the following way[24]

$$D = D_{ZZ} - \frac{1}{2}(D_{XX} + D_{YY}) \quad (2.28)$$

$$E = \frac{1}{2}(D_{XX} - D_{YY}). \quad (2.29)$$

The D and E values are utilized to determine the static ZFS magnitude (a_2) using the formula

$$a_2 = \sqrt{\left(\frac{2}{3}D^2 + 2E^2\right)}. \quad (2.30)$$

From this a_2, the longitudinal electron spin relaxation rate $\frac{1}{T_{1e}}$ can be estimated via[25]

$$\frac{1}{T_{1e}(B_0)} = \frac{2}{5}a_2^2\tau_R\left[\frac{1}{1+\omega_0^2\tau_2^2} + \frac{4}{1+4\omega_0^2\tau_2^2}\right] + \frac{12}{5}a_{2T}^2\tau'\left[\frac{1}{1+\omega_0^2\tau'^2} + \frac{4}{1+4\omega_0^2\tau'^2}\right], \quad (2.31)$$

where B_0 is the external magnetic field, ω_0 is the Larmor frequency, τ_2 and τ' are the reduced spectral densities and a_{2T} is the transient ZFS magnitude.[26] Larger a_2 corresponds to a faster relaxation rate $\frac{1}{T_{1e}}$.[25]

2.6. Conclusions

In this chapter we have discussed the theoretical background for the quantification of the ground state of a diradical based magnetic species. A brief discussion on Hamiltonian relevant to magnetic molecules such as Heisenberg effective spin exchange Hamiltonian is given. We also discuss different studies on this subject density functional theory (DFT) based methods. A brief focus on the development of DFT from Fermi and Thomas (1920) to Kohn and Sham (1965) is also discussed. In recent years broken symmetry (BS) approach in DFT framework has gained much attention for its effectiveness in handling very critical problems with less computational effort. A section of this chapter has been attributed to the BS formalism. Computational methodology on different contemporary research articles is also given. At last, a systematic theoretical discussion on the magnetic anisotropy which is also called zero field splitting (ZFS) as well as the need of its quantification for design a magnetic resonance imaging contrast agents is made. These theoretical methodologies would be followed systematically in this thesis.

2.7. References and Notes

(1) (a) Coronado, E.; Delhaè, P.; Gatteschi, D.; Miller, J. S. *Molecular Magnetism: From Molecular Assemblies to the Devices*, Eds.; Nato ASI Series E, Applied Sciences, Kluwer Academic Publisher: Dordrecht, Netherland, 1996, Vol. 321. (b) Kahn, O. *Molecular Magnetism*, New York, VCH, 1993. (c) Blundell, S. J. *Magnetism in Condensed Matter;* Oxford University Press: New York, 2001.

(2) Fermi, E. *Rend. Accad. Naz. Lincei* **1927**, *6*, 602. (b) Thomas, L. H. *Proc. Cambridge Philos. Soc.* **1927**, *23*, 542.

(3) Hohenberg, P.; Kohn, W. *Phys. Rev. B* **1964**, *136*, 864.

(4) Kohn, W.; Sham, L. J. *Phys. Rev. A* **1965**, *140*, 1133.

(5) Perdew, J. P.; Schmidt, K. Jacob's ladder of density functional approximations for the exchange-correlation energy. *In Density Functional Theory and Its applications to Materials*; Van Doren, V. E.; Van Alseoy, K.; Geerlings, P. Eds.; AIP Press: New York, 2001.

(6) (a) Becke, A. D. *J. Chem. Phys.* **1993**, *98*, 5648. (b) Becke, A. D. *Phys. Rev. A* **1988**, *38*, 3098. (c) Lee, C. T.; Yang, W. T.; Parr, R. G. *Phys. Rev. B* **1988**, *37*, 785.

(7) (a) Zhao, Y.; Schultz, N. E.; Truhlar, D. G. *J. Chem. Phys.* **2005**, *123*, 161103. (b) Zhao, Y.; Schultz, N. E.; Truhlar, D. G. *J. Chem. Theory Comput.* **2006**, *2*, 364. (c) Zhao, Y.; Schultz, N. E.; Truhlar, D. G. *Theor. Chem. Acc.* **2008**, *120*, 215. (d) Zhao, Y.; Truhlar, D. G. *J. Chem. Phys.* **2006**, *125*, 194101. (e) Zhao, Y.; Truhlar, D. G. *Acc. Chem. Res.* **2008**, *41*, 157.

(8) Sausa, S. F.; Fernandes, P. A.; Ramos, M. J. *J. Phys. Chem. A* **2007**, *111*, 10439.

(9) (a) Noodleman, L. *J. Chem. Phys.* **1981**, *74*, 5737. (b) Noodleman, L.; Baerends, E. J. *J. Am. Chem.* Soc. **1984**, *106*, 2316. (c) Noodleman, L.; Davidson, E. R. *Chem. Phys.* **1986**, *109*, 131. (d) Noodleman, L.; Peng, C. Y.; Case, D. A.; Mouesca, J.-M. *Coord. Chem. Rev.* **1995**, *144*, 199.

(10) Caballol, R.; Castell, O.; Illas, F.; Moreira I. de P. R.; Malrieu, J. P. *J. Phys. Chem. A,* 1997, *101*, 7860.

(11) Ginsberg, A. P. *J. Am. Chem. Soc.* **1980**, *102*, 111.

(12) (a) Bencini, A.; Totti, F.; Daul, C. A.; Doclo, K.; Fantucci, P.; Barone, V. *Inorg. Chem.* **1997**, *36*, 5022. (b) Bencini, A.; Gatteschi, D.; Totti, F.; Sanz, D. N.; McClevrty, J. A.; Ward, M. D. *J. Phys. Chem. A* **1998**, *102*, 10545.

(13) Ruiz, E.; Cano. J.; Alvarez, S.; Alemany, P. *J. Comput. Chem.* **1999**, *20*, 1391.

(14) (a) Martin, R. L.; Illas, F. *Phys. Rev. Lett.* **1997**, *79*, 1539. (b) Caballol, R.; Castell, O.; Illas, F.; Moreira, I. de P. R.; Malrieu, J. P. *J. Phys. Chem. A* **1997**, *101*, 7860. (c) Barone, V.; di Matteo, A.; Mele, F.; Moreira, I. de P. R.; Illas, F. *Chem. Phys. Lett.* **1999**, *302*, 240. (d) Illas, F.; Moreira, I. de P. R.; de Graaf, C.; Barone, V. *Theor. Chem. Acc.* **2000**, *104*, 265. (e) de Graaf, C.; Sousa, C.; Moreira, I. de P. R.; Illas, F. *J. Phys. Chem. A* **2001**, *105*, 11371. (f) Illas, F.; Moreira, I. de P. R.; Bofill, J. M.; Filatov, M. *Phys. Rev. B* **2004**, *70*, 132414.

(15) (a) Yamaguchi, K.; Takahara, Y.; Fueno, T.; Nasu, K. *Jpn. J. Appl. Phys.* **1987**, *26*, L1362. (b) Yamaguchi, K.; Jensen, F.; Dorigo, A.; Houk, K. N. *Chem. Phys. Lett.* **1988**, *149*, 537. (c) Yamaguchi, K.; Takahara, Y.; Fueno, T.; Houk, K. N. *Theo. Chim. Acta* **1988**, *73*, 337.

(16) Duboc, C.; Ganyushin, D.; Sivalingam, K.; Collomband, M.; Neese, F. *J. Phys. Chem. A* **2010**, *114*, 10750.

(17) (a) Olankitwanit, A.; Kathirvelu, V.; Rajca, S.; Eaton, G. R.; Eaton, S. S.; Rajca, A. *Chem. Commun.* **2011**, *47*, 6443. (b) Spagnol, G.; Shiraishi, K.; Rajca, S.; Rajca, A. *Chem. Commun.* **2005**, 5047.

(18) Tucker, B. J. *Dissertation in Chemistry in the Graduate College of the University of Illinois at Urbana-Champaign*, 2010.

(19) Zein, S.; Duboc, C.; Lubitz, W.; Neese, F. *Inorg. Chem.* **2008**, *47*, 134.

(20) Loboda, O.; Minaev, B.; Vahtras, O.; Schimmelpfennig, B.; Ågren, H.; Ruud, K.; Jonsson, D. *Chem. Phys.* **2003**, *286*, 127.

(21) McGlynn, S. P.; Azumi, T.; Kinoshita, M. *Molecular Spectroscopy of the Triplet State*, Prentice Hall, Engelwood Clins, NJ, 1969.

(22) Harriman, J. E. *Theoretical Foundations of Electron Spin Resonance*, Academic Press, New York, 1987.

(23) McWeeny, R.; Mizuno, Y. *Proc. R. Soc.*, London, **1961**, *A259*, 554.

(24) Boča, R. *Theoretical Foundations on Molecular Magnetism*, Elsevier, Netherlands, 1999.

(25) Benmelouka, M.; Borel, A.; Moriggi, L.; Helm, L.; Merbach, A. E. *J. Phys. Chem. B* **2007**, *111*, 832.

(26) Belorizkya, E.; Fries, P. H. *Phys. Chem. Chem. Phys.* **2004**, *6*, 2341.

Chapter 3

Magnetism in Bis-Oxoverdazyl Diradicals Coupled with Different Linkage Specific Aromatic Ring Spacers

In this chapter the design and investigation of 11 different bis-oxoverdazyl diradicals connected by various aromatic couplers for their magnetic properties are given. The intramolecular magnetic exchange coupling constants (J) have been calculated using broken symmetry approach in DFT framework. The J values are explained using spin polarization maps and magnetic orbitals. Isotropic hyperfine coupling constants (hfccs) have been calculated for all the species in vacuum. The computed hfcc values also support intramolecular magnetic interactions. It has been found that some of these diradicals have ferromagnetic character while the others are antiferromagnetic in nature.

3.1. Introduction

A global interest has recently been emerged in the field of materials science to search for new magnetic materials where a permanent magnetization and magnetic hysterisis can be achieved not through a three dimensional magnetic ordering but as a purely one-molecule phenomenon. Diverse possibilities for the development of some novel properties such as photo-magnetic behavior,[1] superconductivity,[2] spintronic property[3] and so on make molecular magnetism an interesting field to probe theoretically. Biocompatibility of magnetic materials may lead to several prospective therapeutic applications like in the field of magnetic imaging,[4] in hyperthermic oncology[5] etc. Stable organic radicals, which can be separated and handled in pure state, are most suitable for the study of molecular magnetism. The search for ferromagnetic organic systems leads to the invention of β-crystal phase *p*-nitrophenyl nitronyl nitroxide by Kinosita and co-workers in 1991.[6] Nitronyl nitroxide diradical with ethylene coupler has been extensively studied by Ziessel et al.,[7] which shows a very high exchange coupling constant. Nitronyl nitroxide based molecular ferromagnets with different π-conjugated couplers were comprehensively studied in DFT frame work by Ali and Datta.[8,9] Verdazyl radical was first synthesized by Kuhn and Trischmann in early 1960s,[10] nevertheless, its potential as a precursor of molecular magnets remained unnoticed for long.[11] To design molecular magnets, active verdazyl moiety, which is essentially resonance stabilized hydrazyl radical, is a viable alternative to nitronyl nitroxide. Non-Kekulé bis-oxoverdazyl diradical remains in *singlet* ground state with a small amount of thermally populated *triplet*.[12] Brook et al.[13] have extensively studied its electronic properties and found strong antiferromagnetic coupling among unpaired spins. It is stable due to its chemical resistance and becomes attractive as a prospective building block for magnetic materials. Azidophenyl substituded verdazyls have also been prepared by Serwinski et al.[14]

The extent of magnetism in molecular magnets is best represented through intramolecular magnetic exchange coupling constant and found to be dependent on the structure and spin orientation of such systems. Prior knowledge about the magnetic characteristics of designed molecular magnets is useful in the synthesis of such materials. This has been successfully proved in many cases resulting in the discovery of several

ferromagnetic molecules.[15] Present theoretical study and computational technique lead us to predict magnetic properties of eleven different bis-oxoverdazyl diradicals connected with different linkage-specific aromatic ring couplers, while some of them are already synthesized.[13]

Normally, the magnetic interaction between two radical centers depends on the distance and the nature of the coupler[8,9]. Verdazyl molecule and its various derivatives have been synthesized by Gilroy et al.,[16] they have found fascinating values of magnetic exchange coupling constant for verdazyl molecules connected with a variety of organic couplers. Applying unrestricted density functional methodology the intramolecular magnetic exchange coupling constants have been studied for a series of tetrathiafulvalene (TTF) and verdazyl diradical cations bridged with some aromatic and linear π-couplers by Polo et al.[17] Ali and Datta[8] also have investigated bis-nitronyl nitroxide diradicals in DFT framework having same couplers as used by Polo et al.[17] They have found that the magnetic interaction is mainly transmitted via π-conjugation. They have also established that the magnitude of the coupling constant depends strongly on the planarity of the molecular structure, length of the couplers and spin polarization paths. As a logical consequence, these schemes form the background of this very chapter. In this chapter, we have considered two linkage-specific sets, Set-I and Set-II of different bis-oxoverdazyl diradical derivatives and noticed that the magnetic exchange coupling constant enormously depends on the spin polarization path. The couplers (i) 2, 4 furan, (ii) 2, 4 pyrrole, (iii) 2, 4 thiophene, (iv) 2, 6 pyridine, and (v) *m*-phenylene are used in Set-I. On the other hand, in Set-II (vi) 2, 5 furan coupler, (vii) 2, 5 pyrrole coupler, (viii) 2, 5 thiophene coupler, (ix) 2, 5 pyridine coupler, (x) *p*-phenylene coupler, and (xi) no coupler are used (Figure 3.1). All the couplers are π-conjugated aromatic molecules.

In this chapter, the spin-polarized DFT methodology is used to evaluate magnetic exchange coupling constants. Broken-symmetry (BS) approach, described in the next section, has been adopted here to quantify ferromagnetic coupling constants for all the systems described above.

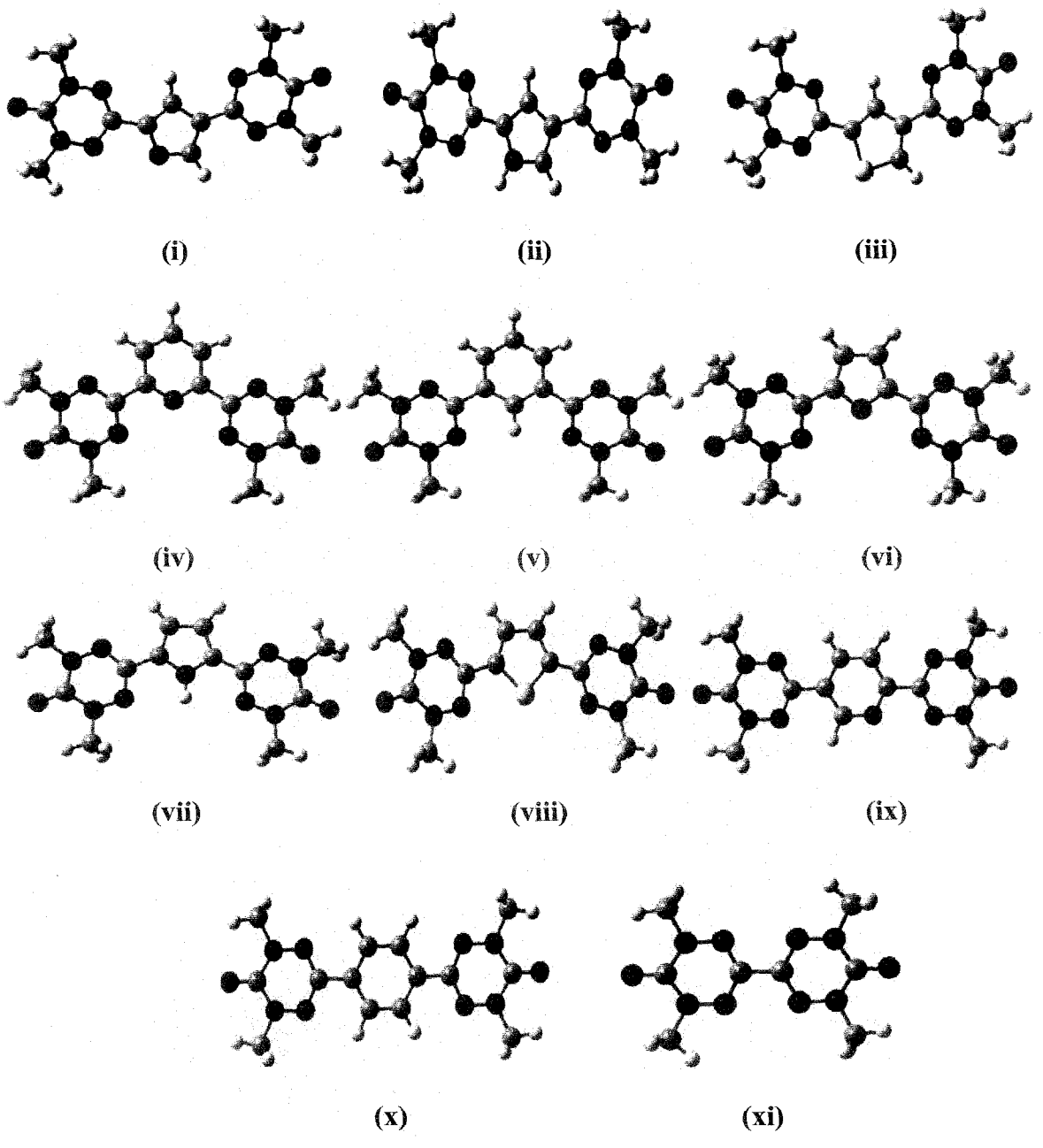

Figure 3.1. Investigated coupler added bis-oxoverdazyl diradical sytems (i-xi), where the couplers are (i) 2, 4 furan coupler, (ii) 2, 4 pyrrole coupler, (iii) 2, 4 thiophene coupler, (iv) 2, 6 pyridine coupler, (v) *m*-phenylene coupler, (vi) 2, 5 furan coupler, (vii) 2, 5 pyrrole coupler, (viii) 2, 5 thiophene coupler, (ix) 2, 5 pyridine coupler, and (x) *p*-phenylene coupler and (xi) no coupler. Atoms having red, blue, black, yellow and white colors represent oxygen, nitrogen, carbon, sulphur and hydrogen respectively.

3.2. Theoretical Background

The Heisenberg spin Hamiltonian is normally used to express the magnetic exchange interaction between two magnetic sites 1 and 2

$$\hat{H} = -2J\hat{S}_1 \bullet \hat{S}_2 , \tag{3.1}$$

where J is the exchange coupling constant between two magnetic centers of a diradical, $\hat{S}_1$ and $\hat{S}_2$ are the respective spin angular momentum operators. The square of the total spin operator $\hat{S}^2$ has eigen value $S(S+1)$ in unit of $\hbar^2$. A ferromagnetic interaction is indicated by a positive sign of J in which a situation of parallel spin is essential, whereas the negative value indicates an antiferromagnetic interaction, where a state of antiparallel spin is favored. For a diradical with single unpaired electron on each site, J can be written as

$$E_{(S=1)} - E_{(S=0)} = -2J . \tag{3.2}$$

The singlet state of a diradical can not be truly represented by a single determinant (SD) wave function in the unrestricted formalism and this leads to spin contamination in such calculations. Multiconfigurational methods are useful to describe pure spin states in an appropriate way; however, they are resource intensive and not being employed in this chapter. Broken symmetry formalism proposed by Noodleman[18] in DFT framework is an alternative approach to evaluate J with less computational effort. The BS state is a weighted average of a singlet and a triplet state and not an eigenstate of the Hamiltonian. BS solution is often found to be spin contaminated, using spin projection technique reliable estimate of magnetic exchange coupling constant can be obtained. Depending upon the extent of overlap between magnetic orbitals, different expressions for J have been given by many researchers,[18-26] using unrestricted spin polarized BS solution for lower spin state. The expression for J given by Ginsberg,[19] Noodleman,[20] and Davidson[21] is more useful when overlap of the magnetic orbitals is very small. Expression given by Bencini and coworkers,[22]

Ruiz et al.,[23] has been further justified by Illas and coworkers[24] and Dual,[25] is applicable when the overlap is sufficiently large. Nevertheless, expression given by Yamaguchi and coworkers[26] is a balance between above two extremes.

In this chapter, we have calculated magnetic exchange coupling constant by using the elegant expression given by Yamaguchi and coworkers[26] which can be reduced to the expressions given for weak[19-21] and strong[22-25] coupling strength. The expression is

$$J = \frac{(E_{BS} - E_T)}{\langle S^2 \rangle_T - \langle S^2 \rangle_{BS}}, \qquad (3.3)$$

where E_{BS} and E_T denote the energy of the broken symmetry singlet and triplet state where as $\langle S^2 \rangle_T$ and $\langle S^2 \rangle_{BS}$ represent average spin square values in triplet and BS state respectively.

Commonly used DFT exchange correlation potentials yield an overestimation of J values due to the presence of high self interaction error (SIE). Polo et al. have concluded that the presence of SIE in commonly used functionals in DFT is related to nondynamic correlation energy.[27] Hybrid functionals perform better than pure DFT functionals in BS-UDFT calculations because the former reduce the SIE of DFT exchange functionals.[28] In a recent work, Ruiz et al.[29] have shown that B3LYP functionals in the unrestricted framework produces low SIE, this makes the use of such functionals more suitable when spin projected techniques are used to evaluate J. In this chapter the molecular geometries of all the compounds (i-xi) have been fully optimized with the UB3LYP[30] exchange correlation potential using 6-311+G(d,p) basis set. To obtain open shell BS singlet solution "guess =mix" key word is used within unrestricted formalism. The BS states for all diradicals are stable. The J values for all eleven diradicals have been calculated on the optimized geometry of all the species at the UB3LYP level with 6-311+G(d,p) and 6-311++G(d,p) basis sets. All the calculations have been carried out using GAUSSIAN 03W[31] quantum chemical package. The visualization softwares, Hyperchem 7.5[32] and Molekel 4.0[33] have also been used.

3.3. Results and Discussion

Radicals of verdazyl family are well known for their stability and ferromagnetic characteristics which has already been theoretically and magnetically established.[24e,34] The optimized structures of the systems under investigation are planar. As a result, according to spin polarization rule better spin polarization along the π-conjugated system stabilizes the triplet states.[35] The linker between two same or different organic radicals plays a major role in determining the sign and magnitude of magnetic exchange coupling constant.[8,9,17] We have estimated the value of J for two sets of compounds, some of them are already known and the others are newly designed as given in Figure 3.1. In each set five different linkage-specific aromatic ring couplers connect two oxoverdazyl monomers, hence forming bis-oxoverdazyl diradicals. In addition to five systems with different aromatic couplers, in Set-II oxoverdazyl diradical with no coupler has also been included. It is established that the unpaired spins are largely delocalized on the four nitrogen atoms of a verdazyl radical.[36] The $\langle S^2 \rangle$ and energy values for both triplet and BS states are obtained by using eq (3.3). Numerical values of the coupling constant for all eleven species are reported in Table 3.1.

Normally, the sign and magnitude of J does not largely depend on basis set. The observation made by us that the *m*-phenylene and *p*-phenylene coupled bis-oxoverdazyl diradicals are ferromagnetic and antiferromagnetic respectively, are in good agreement with the work of Ali and Datta[8] where they have used the same couplers grafted among two nitronyl nitroxide moieties. In our computational results, J value (Table 3.1) for direct coupling between two oxoverdazyl units (xi) leads to a very strong antiferromagnetic coupling (J = −589 cm^{-1}). This result is in good agreement with previous experimental studies made by Brook et al.[13] in frozen chloroform solution where they reported singlet-triplet energy separation J of −760 cm^{-1}, that is, the two radicals are strongly antiferromagnetically coupled.

For a diradical, spin alternation rule[35] indicates that six membered aromatic ring couplers result antiferromagnetic coupling for *o*-phenylene and *p*-phenylene couplers, and a ferromagnetic coupling arises in case of *m*-phenylene coupler. For five membered

Table 3.1. UB3LYP level absolute energies in *au*, $\langle S^2 \rangle$ and intramolecular magnetic exchange coupling constant (J/cm^{-1}) using 6-311+G(d,p) and 6-311++G(d,p) basis sets, for bis-oxoverdazyl diradicals (i-xi).

Diradicals		At UB3LYP/6-311+G(d,p) level			At UB3LYP/6-311++G(d,p) level		
		BS	Triplet	J/cm^{-1}	BS	Triplet	J/cm^{-1}
(i)	E	−1129.57169	−1129.57187	39	−1129.57190	−1129.57211	46
	$\langle S^2 \rangle$	1.044	2.051		1.042	2.050	
(ii)	E	−1109.72118	−1109.72135	37	−1109.72138	−1109.72145	15
	$\langle S^2 \rangle$	1.043	2.048		1.041	2.043	
(iii)	E	−1452.55688	−1452.55742	117	−1452.55734	−1452.55756	48
	$\langle S^2 \rangle$	1.035	2.051		1.039	2.044	
(iv)	E	−1147.82754	−1147.82773	41	−1147.82770	−1147.82787	37
	$\langle S^2 \rangle$	1.042	2.048		1.040	2.043	
(v)	E	−1131.79327	−1131.79360	72	−1131.79363	−1131.79388	54
	$\langle S^2 \rangle$	1.040	2.049		1.039	2.046	
(vi)	E	−1129.57101	−1129.57072	−64	−1129.57110	−1129.57085	−55
	$\langle S^2 \rangle$	1.053	2.043		1.049	2.040	
(vii)	E	−1109.72406	−1109.72379	−60	−1109.72432	−1109.72390	−93
	$\langle S^2 \rangle$	1.051	2.043		1.051	2.038	
(viii)	E	−1452.55732	−1452.55693	−86	−1452.55728	−1452.55705	−51
	$\langle S^2 \rangle$	1.054	2.044		1.045	2.039	
(ix)	E	−1147.83100	−1147.83070	−66	−1147.83122	−1147.83094	−62
	$\langle S^2 \rangle$	1.051	2.042		1.049	2.040	
(x)	E	−1131.79440	−1131.79410	−67	−1131.79443	−1131.79431	−26
	$\langle S^2 \rangle$	1.053	2.042		1.042	2.039	
(xi)	E	−900.67135	−900.66865	−579	−900.67156	−900.66882	−589
	$\langle S^2 \rangle$	1.010	2.033		1.010	2.031	

heteronuclear aromatic ring couplers 2,3 and 3,4 species are treated as *o*-couplers, the 2,5 species are *p*-coupler and the 2,4 one as *m*-couplers because the heteroatom at 1 provides two π-electrons. The diradicals belong to Set-I (*m*-coupled diradicals) yield strong ferromagnetic interaction whereas Set-II diradicals (*p*-coupled diradicals) are antiferromagnetic in nature. This trend indicates triplet ground state for Set-I diradicals and for Set-II diradicals singlet ground state results. These are also the preferred ground states according to spin alternation rule.[35] Compounds (v), (viii), (x) and (xi) have been synthesized by Fox and co-workers.[12] They have found from spectral evidence that 36nm and 66 nm red shift is observed for diradicals (x) and (viii) correspondingly with respect to the parent compound (xi), indicating an increase in conjugation. It can also be noticed from their experimental studies that bis-oxoverdazyl diradical (xi) without bearing heavy substituents are planar and exists in a singlet ground state which have also been established by our investigation. In six membered m-coupled diradicals (iv) and (v), we find (v) has larger *J* value (Table 3.1) as a consequence of increase in aromatic character in the coupler in the later case.[8] On the other hand, decrease in aromaticity increases antiferromagnetic character (Table 3.1). Further, in diradical (ix) the presence of pyridyl nitrogen atom instead of phenyl C-H fragment reduces its steric hindrance compared to diradical (x), hence the magnitude of *J* increases.[17]

3.3.1. Spin Density Distribution

Exchange coupling constant is largely dependent on the delocalization of π-electron densities. Hund's rule based spin alternation rule,[35] for a diradical coupled with different aromatic systems, are very helpful to predict the state of magnetism. When the coupling pathway through the coupler propagates through even number of bonds, ferromagnetism arises, but antiferromagnetism occurs in case of odd number of bonds. The existence of apparently two different spin polarization paths, presence of heteroatom in the coupling pathway and non-planarity of the system makes it tricky to predict the magnetic characteristics of molecular systems.[17] However, Ali and Datta demonstrate the spin density alternation in the case of such systems satisfactorily with examples of bis-

nitronyl nitroxide diradicals connected by different heterocyclic aromatic couplers. At a first glance, one would think that there is a competition between the two pathways. In

Scheme 3.1. General schematic representation of diradicals (i-xi) with different couplers, where there are two unpaired electrons at N_4 and N_{10} atoms.

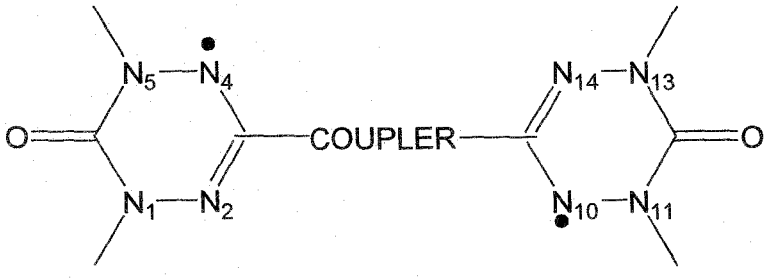

reality, the odd route is supported by the even path through the heteroatom as the latter contributes two π-electrons.[8] The unpaired electron in the verdazyl radical is delocalized over four nitrogen atoms,[36] so the linker carbon atoms with two oxoverdazyl moieties suffer strong spin polarization to make the bonds stronger in nature. Moreover, the linkage position of the π-donar unit to an aromatic ring coupler determines the sign of *J*. As a result, five and six membered aromatic ring coupled *para* substitution as in Set-II, *meta* substitution as found in Set-I lead to antiferromagnetic and ferromagnetic coupling respectively. In compound (ix) the C-H fragment is replaced by N-atom which restores the planarity thus favoring delocalization of π-electrons.[17] The sign of *J* also largely depends on the number of bonds and nature of atoms in the spin polarization paths through the coupler. In this chapter, in Set-I, the diradicals with six membered aromatic couplers are (iv) and (v) (Figure 3.1). There are two even (four- and six-bond) coupling pathways through the couplers for above two diradicals, as a result, the *J* values are positive. The Set-I diradicals having five membered heteronuclear aromatic couplers are (iii), (iv) and (v), where there are one even (four-bond) and one odd (five-bond) coupling pathways, nevertheless, all of them are ferromagnetic in nature. The number of bonds in the coupling pathway is even through carbon chain, though with hetero atom it is odd, with the contribution of two π-electrons by the heteroatom (the count increases by one and becomes even), the odd path also supports the spin density alternation rule.[35] As a

result we get positive J value which makes it clear that the path through carbon chain and the alternate route through heteroatom actually complement each other and spin density alternation is followed by both the ways (Figure 3.2). The parent diradical (xi) has C_2

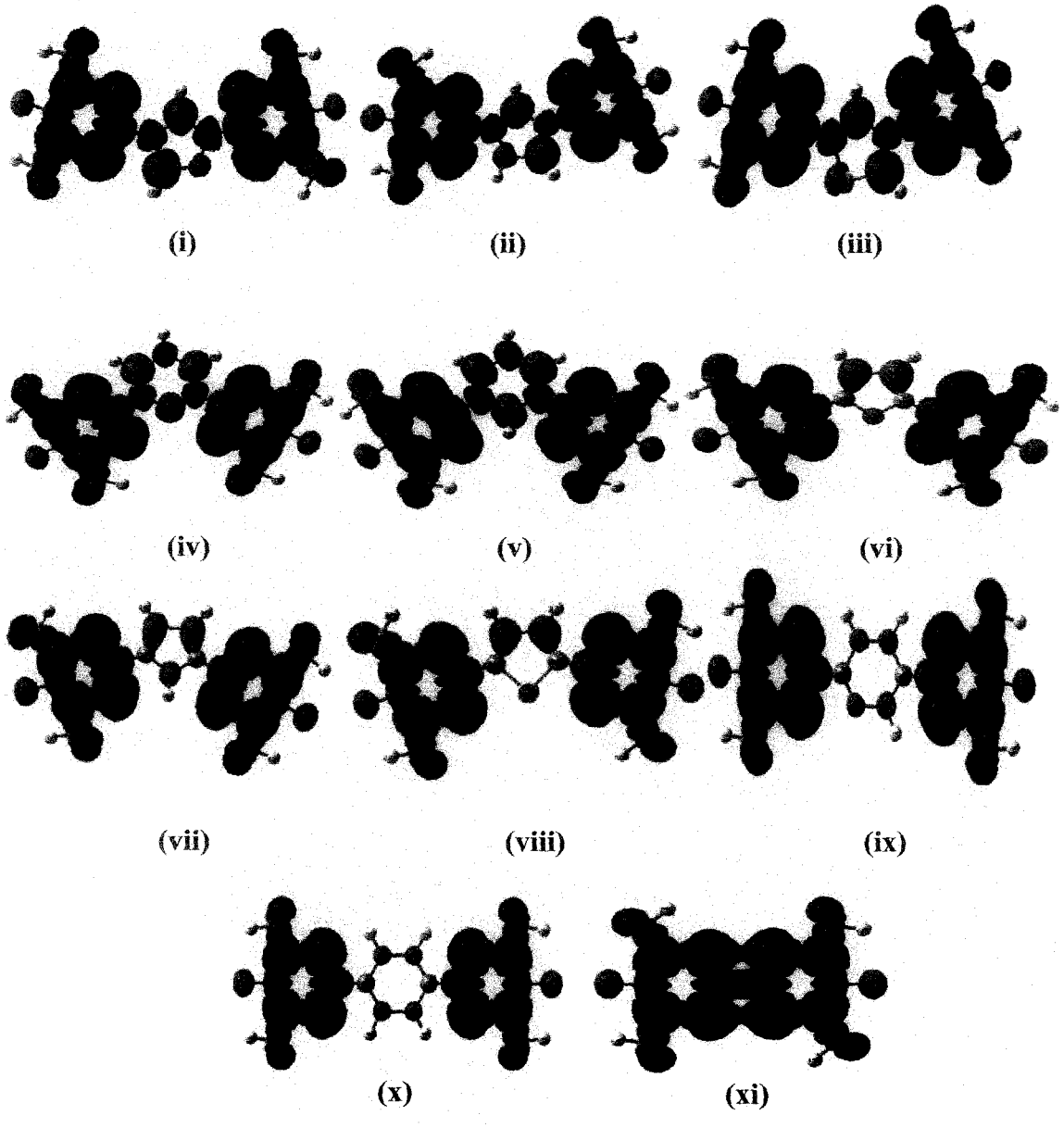

Figure 3.2. Spin density distribution plots for Set-I and Set II diradicals (i–xi), blue color indicates α spin and green color indicates β spin respectively.

point group with a nodal plane passing through the linkage bond (Scheme 3.1 and Figure 3.1) between the two monoradicals so spin distribution is subdued and as a result antiferromagnetism arises.[36] On the other hand, for the systems of Set –II, J value is negative which can be easily rationalized by spin density alternation in a similar fashion. In Set-II diradicals, the magnitude of J values for diradicals (vi), (vii), (viii) (Table 3.1) are larger than that of diradical (x) which can be viewed as an extension of spin alternation rule in case of heteronuclear aromatic ring couplers.[8]

3.3.2. Analysis of Singly Occupied Molecular Orbitals (SOMOs)

Based on extended Hückel theory (ETH), that is, all valence-electron independent particle model on benzyne and diradicals, Hoffmann[37] suggested that if the energy difference between two consecutive SOMOs is less than 1.5 eV so as to maximize the

Table 3.2. The energy of SOMOs in *au* and their differences in eV at UB3LYP level using 6-311+G(d, p) basis set for diradicals (i-xi).

Diradicals	$E_S(1)au$	$E_S(2)au$	$\Delta E_{SS}eV$
(i)	–0.20642	–0.20420	0.0604
(ii)	–0.20473	–0.19705	0.2090
(iii)	–0.20620	–0.20440	0.0490
(iv)	–0.20204	–0.20044	0.0435
(v)	–0.20445	–0.20279	0.0452
(vi)	–0.20496	–0.20343	0.0416
(vii)	–0.20536	–0.20368	0.0457
(viii)	–0.20507	–0.20360	0.0400
(ix)	–0.20928	–0.20162	0.2085
(x)	–0.20482	–0.20335	0.0400
(xi)	–0.20866	–0.19551	0.3578

electrostatic repulsion between two different degenerate orbitals, then parallel orientation of spins occurs. On the other hand, at B3LYP level with 6-31G(d,p) basis set, $4n\pi$ antiaromatic linear and angular polyheteroacenes have been investigated by Constantinides et al.[38] where they found that when $\Delta E_{SS} > 1.3\ eV$ singlet ground state results with antiparallel orientation of spins. Zhang et al.[39] using DFT calculations have shown that critical value of ΔE_{SS} is different in different cases, however, increasing values of ΔE_{SS} indicates spin pairing as evident from compounds (xi) in our present chapter, where we found largest ΔE_{SS} values among the eleven diradicals and consequently singlet ground state with antiferromagnetic character is observed. However, in Set-I, diradical (ii) has highest value of ΔE_{SS} (Table 3.2) with a low J value. For compounds (i), (iii) and (v) the ΔE_{SS} value (Table 3.2) decreases as J value increases. The above observations made it clear that our calculation is in good agreement with Hay-Thibeault-Hoffmann (HTH) formula for the singlet-triplet energy gap[40] in weakly coupled dinuclear metal complexes and as well as the work of Paul and Misra[41] where they have found gradual increase of ΔE_{SS} values with a net effect of decreased magnitudes of ferromagnetic coupling constant through the Cr_2O_n cluster series.

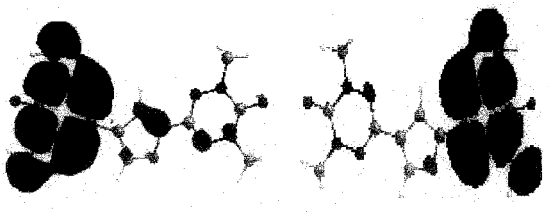

[i] Disjoint

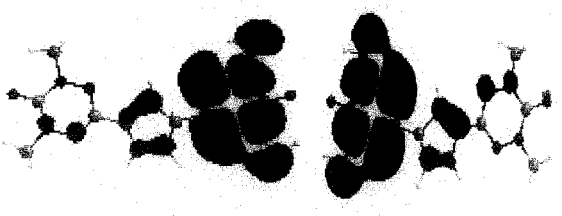

[ii] Disjoint

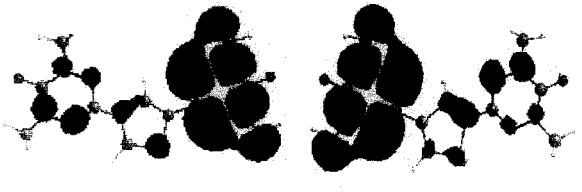

[iii] Disjoint

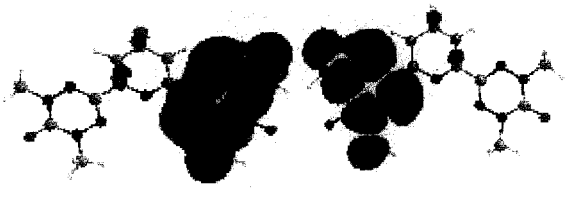

[iv] Disjoint

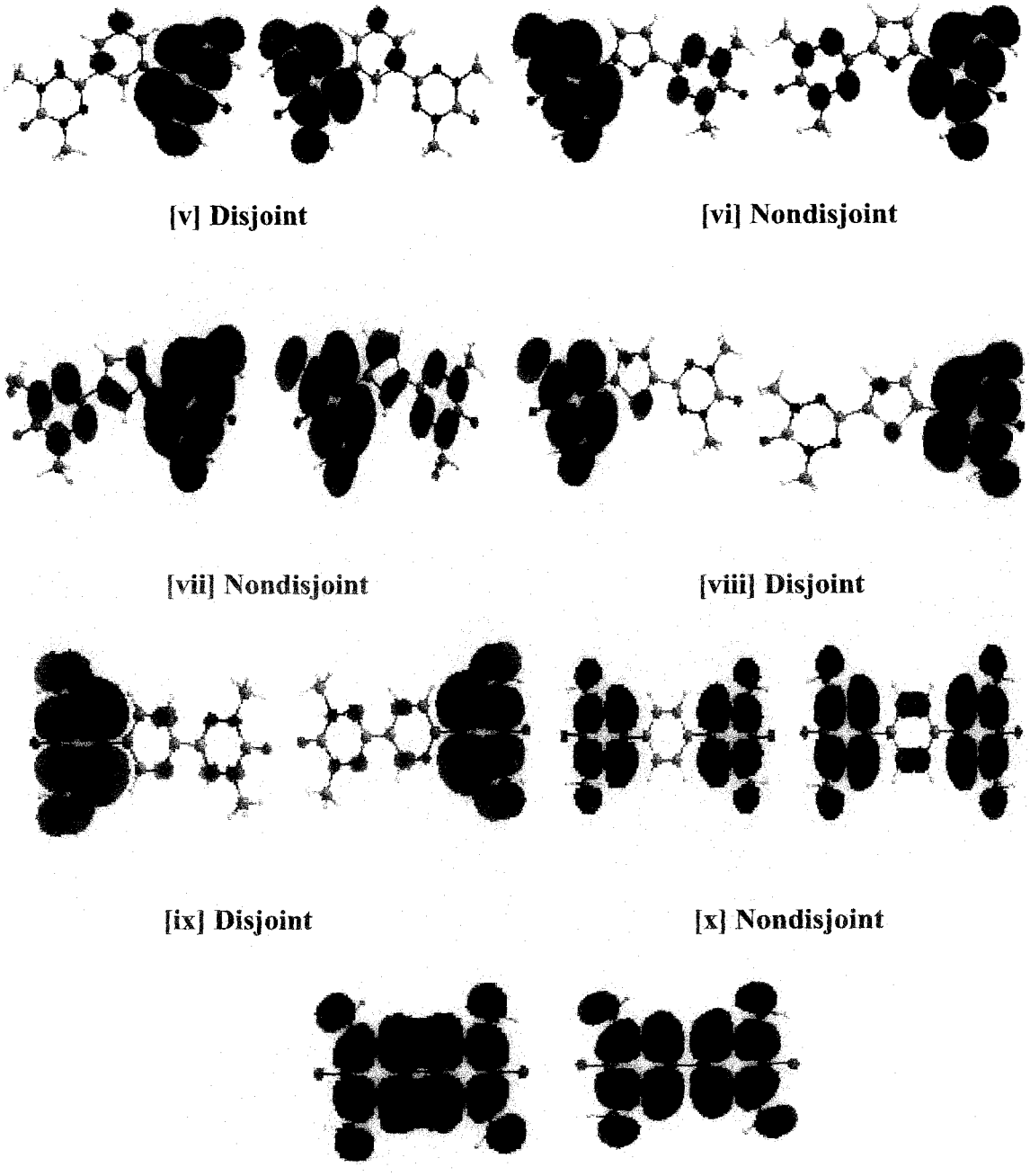

Figure 3.3. Triplet SOMOs for diradicals (i-xi), plotted at UB3LYP level using 6-311+G(d,p) basis set.

The shapes of the SOMOs (Figure 3.3) play a major role in determining the magnetic properties of the diradicals. In this chapter, we have found that in Set-I

diradicals, the SOMOs are disjoint (atoms are not common) in nature and accordingly ferromagnetic.[8] Set-II diradicals are antiferromagnetic, and the SOMOs are mostly nondisjoint (atoms are common).

3.3.3. Isotropic Hyperfine Coupling Constants (HFCCs)

The interaction between nuclear and electronic magnetic moment is characterized by hfcc. It depends on the spin density of the related nuclei. Due to electron correlation and basis set effects hfccs are difficult to calculate. Solvent also plays an effective role in evaluating the hfcc values. In this chapter, hfccs are calculated under DFT framework by using EPR-II basis set at UB3LYP level in vacuum. As "S" atoms are not considered in EPR-II basis set in the quantum chemical package used for computations,[31] so we have used 6-311+G(d, p) basis set for "S" atom.

Fox and co-workers[12] have shown that if there is an aromatic coupler (Scheme 3.1) between two monomers then a red shift is observed compared to that of parent diradical (xi), suggesting an increase in conjugation. In oxoverdazyl monoradical, two sets of two equivalent nitrogen atoms (N_1-N_5 and N_2-N_4) (Scheme 3.1) are found. Plater et al.[42] have observed that hfcc for $a(N_2\text{-}N_4)$ = 6.5 G and $a(N_1\text{-}N_5)$ = 5.3 G (depending upon nature of substitution), which are nearly similar to that observed by Neugebauer et al.[43,44] They have also found that larger hfcc values are obtained at N_2, N_4 and N_{10}, N_{14} which means that the spins are localized along N=C-N group rather than over the Me-N-CO-N-Me group (Scheme 3.1). Nitronyl nitroxide diradical with different couplers[8,9] have been studied and the hfcc values for conjugated coupler added diradicals reduces to half of the values for corresponding monoradical.

In this chapter, we have computed (Table 3.3) the hfcc values for all the eight N-atoms present in each bis-oxoverdazyl diradical. We have found that the calculated gas phase hfcc values for N_2-N_4 and N_{10}-N_{14} are larger than that of N_1-N_5 and N_{11}-N_{13} which are in good agreement with different experimental results.[43,44] However, we can not get any perfect relationship of hfcc values with magnetic exchange coupling constant.

Table 3.3. Evaluated hyperfine coupling constants (HFCCs) in *Gauss* at UB3LYP level using EPR-II basis set for diradicals (i-xi).

Diradicals	a_{N1}	a_{N2}	a_{N4}	a_{N5}	a_{N10}	a_{N11}	a_{N13}	a_{N14}
(i)	1.85832	2.38518	2.67110	1.87494	2.62724	1.86688	1.79370	2.36602
(ii)	1.82520	2.59019	2.41342	1.75696	2.35668	1.74092	1.96261	2.59318
(iii)	1.61759	2.95559	2.13403	1.69148	2.83684	1.15914	1.26903	2.44571
(iv)	1.88313	2.45098	2.57799	1.80510	2.46730	1.80827	1.80789	2.54126
(v)	1.87546	2.45333	2.50391	1.81105	2.45941	1.80140	1.80758	2.47663
(vi)	1.86201	2.35111	2.64272	1.87390	2.35061	1.77835	1.88444	2.61720
(vii)	1.73190	2.25968	2.58498	1.88905	2.29739	1.73734	1.96681	2.59163
(viii)	1.10544	2.82310	2.78463	1.15423	2.16139	1.15535	1.22148	2.78933
(ix)	1.85434	2.48057	2.45545	1.85264	2.45197	1.82553	1.81063	2.52009
(x)	1.83863	2.49922	2.50999	1.82895	2.50999	1.82895	1.83863	2.49922
(xi)	1.92324	2.42065	2.46129	1.84293	2.46129	1.84293	1.92324	2.42065

3.4. Conclusions

. Oxoverdazyl radicals are promising groups for the development of new molecular materials with magnetic properties due to its better stability than other simpler groups. Bis-oxoverdazyl diradical (xi) is known to be one of the stable organic diradicals due to its chemical resistance but antiferromagnetic species.[12,13] In this chapter, we have studied intramolecular magnetic exchange coupling constants for two different linkage-specific sets of bis-oxoverdazyl diradicals with different aromatic couplers. The purpose of this investigation lies in the fact that they are straight-forward to prepare and are air and moisture stable. All the eleven diradicals in two different sets have been optimized at UB3LYP level and J values were calculated using BS approach under DFT framework. It is found that members of Set-I diradicals which are essentially *m*-coupled oxoverdazyl diradicals are ferromagnetic with high magnetic exchange coupling constant, whereas the p-coupled oxoverdazyl diradicals belong to Set-II are antiferromagnetic. As the aromaticity of the spacer increases, the ferromagnetic character also increases and vice

versa. These observations strictly follow the spin density alternation rule.[35] Here, we find that the magnetic interactions are primarily transmitted through π–electron conjugation as observed by other authors.[8,9,17] This is justified through MO analysis and spin density alternations as obvious from Figure 3.2. The shape of SOMOs (Figure 3.3) also helps to predict the magnetic characteristics of the diradicals.

This work has been published in The Journal of Physical Chemistry A (Ref. 45).

3.5. References and Notes

(1) (a) Matsuda, K.; Matsuo, M.; Irie, M. *J. Org. Chem.* **2001**, *66*, 8799. (b) Matsuda, K.; Irie, M. *J. Photochem. Photobiol. C: Photochem. Res.* **2004**, *5*, 69.

(2) (a) Kobayashi, H.; Kobayashi, A.; Cassoux, P. *Chem. Soc. Rev.* **2000**, *29*, 325. (b) Uji, S.; Shinagawa, H.; Terashima, T.; Yakabe, T.; Terai, Y.; Tokumoto, M.; Kobayashi, A.; Tanaka, H; Kobayashi, H. *Nature* **2001**, *410*, 908.

(3) (a) Prinz, G. A. *Science* **1998**, *282*, 1660. (b) Emberly, E. G.; Kirczenow, G. *Chem. Phys.* **2002**, *281*, 311.

(4) (a) Miller, J. S.; Epstein, A. J. *Angew. Chem. Int. Ed. Engl.* **1994**, *33*, 385. (b) Berry, C. C.; Curtis, A. S. G. *J. Phys. D: Appl. Phys.* **2003**, *36*, 198.

(5) (a) Hilger, I.; Hergt, R.; Kaiser, W. A. *J. Magn. Magn. Mater.* **2005**, *293*, 314. (b) Atsumi, T.; Jeyadevan, B.; Sato, Y.; Tohji, K. *J. Magn. Magn. Mater.* **2007**, *310*, 2841.

(6) Tamura, M.; Nakazawa, Y.; Shiomi, D.; Nozawa, K.; Hosokoshi, Y.; Ishikawa, M.; Takahashi, M.; Kinosita, M. *Chem. Phys. Lett.* **1991**, *186*, 401.

(7) Ziessel, R.; Stroh, C.; Heise, H.; Khler, F. H.; Turek, P.; Claiser, N.; Souhassou, M.; Lecomte, C. *J. Am. Chem. Soc.* **2004**, *126*, 12604.

(8) Ali, Md. E.; Datta, S. N. *J. Phys. Chem. A* **2006**, *110*, 2776.

(9) Ali, Md. E.; Datta, S. N. *J. Phys. Chem. A* **2006**, *110*, 13232.

(10) Kuhn, R.; Trischmann, H. *Angew. Chem. Int. Ed. Engl.* **1963**, *2*, 155.

(11) (a) Takeda, K.; Hamano, T.; Kawae, T.; Hidaka, M.; Takahashi, M.; Kawasaki, S.; Mukai, K. *J. Phys. Soc. Jpn.* **1995**, *64*, 2343. (b) Mukai, K.; Konishi, K.; Nedachi, K.; Takeda, K. *J. Phys. Chem.* **1996**, *100*, 9658.

(12) Fico, R. M. Jr.; Hay, M. F.; Reese, S.; Hammond, S.; Lambert, E.; Fox, M. A. *J. Org. Chem.* **1999**, *64*, 9386.

(13) Brook, D. J. R.; Fox, H. H.; Lynch, V.; Fox, M. A. *J. Phys. Chem.* **1996**, *100*, 2066.

(14) Serwinski, P. R.; Esat, B.; Lahti, P. M.; Liao, Y.; Walton, R.; Lan, J. *J. Org. Chem.* **2004**, *69*, 5247.

(15) Kahn, O. *Molecular Magnetism*, VCH: New York, 1993.

(16) Gilroy, J. B.; McKinnon, S. D. J.; Kennepohl, P.; Zsombor, M. S.; Ferguson, M. J.; Thompson, L. K.; Hicks, R. G. *J. Org. Chem.* **2007**, *72*, 8062.

(17) Polo, V.; Alberola, A.; Andres, J.; Anthony, J.; Pilkington, M. *Phys. Chem. Chem. Phys.* **2008**, *10*, 857.

(18) (a) Noodleman, L. *J. Chem. Phys.* **1981**, *74*, 5737. (b) Noodleman, L.; Baerends, E. J. *J. Am. Chem. Soc.* **1984**, *106*, 2316.

(19) Ginsberg, A. P. *J. Am. Chem. Soc.* **1980**, *102*, 111.

(20) Noodleman, L.; Peng, C. Y.; Case, D. A.; Mouesca, J.-M. *Coord. Chem. Rev.* **1995**, *144*, 199.

(21) Noodleman, L.; Davidson, E. R. *Chem. Phys.* **1986**, *109*, 131.

(22) (a) Bencini, A.; Totti, F.; Daul, C. A.; Doclo, K.; Fantucci, P.; Barone, V. *Inorg. Chem.* **1997**, *36*, 5022. (b) Bencini, A.; Gatteschi, D.; Totti, F.; Sanz, D. N.; McClevrty, J. A.; Ward, M. D. *J. Phys. Chem. A* **1998**, *102*, 10545.

(23) Ruiz, E.; Cano, J.; Alvarez, S.; Alemany, P. *J. Comput. Chem.* **1999**, *20*, 1391.

(24) (a) Martin, R. L.; Illas, F. *Phys. Rev. Lett.* **1997**, *79*, 1539. (b) Caballol, R.; Castell, O.; Illas, F.; Moreira, I. de P. R.; Malrieu, J. P. *J. Phys. Chem. A* **1997**, *101*, 7860. (c) Barone, V.; di Matteo, A.; Mele, F.; Moreira, I. de P. R.; Illas, F. *Chem. Phys. Lett.* **1999**, *302*, 240. (d) Illas, F.; Moreira, I. de P. R.; de Graaf, C.; Barone, V. *Theor. Chem. Acc.* **2000**, *104*, 265. (e) de Graaf, C.; Sousa, C.; Moreira, I. de P. R.; Illas, F. *J. Phys. Chem. A* **2001**, *105*, 11371. (f) Illas, F.; Moreira, I. de P. R.; Bofill, J. M.; Filatov, M. *Phys. Rev. B* **2004**, *70*, 132414.

(25) Ciofini, I.; Daul, C. A. *Coord. Chem. Rev.* **2003**, *238*, 187.

(26) (a) Yamaguchi, K.; Takahara, Y.; Fueno, T.; Nasu, K. *Jpn. J. Appl. Phys* **1987**, *26*, L1362. (b) Yamaguchi, K.; Jensen, F.; Dorigo, A.; Houk, K. N. *Chem. Phys. Lett.* **1988**, *149*, 537. (c) Yamaguchi, K.; Takahara, Y.; Fueno, T.; Houk, K. N. *Theor. Chim. Acta* **1988**, *73*, 337.

(27) Polo, V.; Gräfenstein, J.; Kraka, E.; Cremer, D. *Theor. Chem. Acc.* **2003**, *109*, 22.

(28) Gräfenstein, J.; Kraka, E.; Filatov, M.; Cremer, D. *Int. J. Mol. Sci.* **2002**, *3*, 360.

(29) Ruiz, E.; Alvarez, S.; Cano, J.; Polo, V. *J. Chem. Phys.* **2005**, *123*, 164110.

(30) (a) Becke, A. D. *Phys. Rev. A* **1988**, *38*, 3098. (b) Lee, C. T.; Yang, W. T.; Parr, R. G. *Phys. Rev. B* **1988**, *37*, 785. (c) Becke, A. D. *J. Chem. Phys.* **1993**, *98*, 5648.

(31) Frisch, M. J.; Trucks, G. W.; Schlegel, H. B.; Scuseria, G. E.; Robb, M. A.; Cheeseman, J. R.; Montgomery, J. A. Jr.; Vreven, T.; Kudin, K. N.; Burant, J. C.; Millam, J. M.; Iyengar, S. S.; Tomasi, J. J.; Barone, V.; Mennucci, B.; Cossi, M.; Scalmani, G.; Rega, N.; Petersson, G. A.; Nakatsuji, H.; Hada, M.; Ehara, M.;

Toyota, K.; Fukuda, R.; Hasegawa, J ; Ishida, M.; Nakajima, T.; Honda, Y.; Kitao, O.; Nakai, H.; Klene, M.; Li, X.; Knox, J. E.; Hratchian, H. P.; Cross, J. B.; Bakken, V.; Adamo, C.; Jaramillo, J.; Gomperts, R.; Stratmann, R. E.; Yazyev, O.; Austin, A. J.; Cammi, R.; Pomelli, C.; Ochterski, J.; Ayala, P. Y.; Morokuma, K.; Voth, A.; Salvador, P.; Dannenberg, J. J.; Zakrzewski, V. G.; Dapprich, S.; Daniels, A. D.; Strain, M. C.; Farkas, O.; Malick, D. K.; Rabuck, A. D.; Raghavachari, K.; Foresman, J. B.; Ortiz, J. V.; Cui, Q.; Baboul, A. G.; Clifford. S.; Cioslowski, J.; Stefanov, B. B.; Liu, G.; Liashenko, A.; Piskorz, P.; Komaromi, I.; Martin, R. L.; Fox, D. J.; Keith, T.; Al-Laham, M. A.; Peng, C. Y.; Nanayakkara, A ; Challacombe, M.; Gill, P. M. W.; Johnson, B.; Chen, W.; Wong, M. W.; Gonzalez, C.; Pople, J. A. GAUSSIAN 03W (Revision D.01), Gaussian, Inc.: Wallingford, CT, (2004).

(32) Hyperchem Professional Release 7.5 for Windows; Hypercube Inc., Gainesville, 2002.

(33) Flükiger, P.; Lüthi, H. P.; Portmann, S.; Weber, J. MOLEKEL 4.0, J. Swiss Center for Scientific Computing, Manno, Switzerland, 2000.

(34) Brook, D. J. R.; Yee, G. T. *J. Org. Chem.* **2006**, *71*, 4889.

(35) (a) Trindle, C.; Datta, S. N. *Int. J. Quantum Chem.* **1996**, *57*, 781. (b)Trindle, C.; Datta, S. N.; Mallik, B. *J. Am. Chem. Soc.* **1997**, *119*, 12947.

(36) Koivisto, B. D.; Hicks, R. G. *Coord. Chem. Rev.* **2005**, *249*, 2612.

(37) Hoffmann, R.; Zeiss, G. D.; Van Dine, G.W. *J. Am. Chem. Soc.* **1968**, *90*, 1485.

(38) Constantinides, C. P.; Koutentis, P. A.; Schatz, J. *J. Am. Chem. Soc.* **2004**, *126*, 16232.

(39) Zhang, G.; Li, S.; Jiang, Y. *J. Phys. Chem. A* **2003**, *107*, 5373.

(40) Hay, P. J.; Thibeault, C. J.; Hoffmann, R. *J. Am. Chem. Soc.* **1975**, *97*, 4884.

(41) Paul, S.; Misra, A. *J. Mol. Struct. (THEOCHEM)* **2009**, *895*, 156.

(42) Plater, M. J.; Kemp, S.; Coronado, E.; Gómez-García, C. J.; Harrington, R. W.; Clegg, W. *Polyhedron* **2006**, *25*, 2433.

(43) Neugebauer, F. A.; Fischer, H.; Siegel, R. *Chem. Ber.* **1988**, *121*, 815.

(44) Neugebauer, F. A.; Fischer, H. *Angew. Chem. Int. Ed. Engl.* **1980**, *19*, 724.

(45) Bhattacharya, D.; Misra, A. *J. Phys. Chem. A.* **2009**, *113*, 5470.

Chapter 4

Role of Linear Polyacene Spacers in Intramolecular Magnetic Exchange Coupling

The estimation of intramolecular exchange coupling constant (J) for 10 different oxo- and thioxo-verdazyl based high spin ground state diradicals with linear polyacene couplers of varying length using the broken symmetry approach in an unrestricted DFT framework is described in this chapter. The magnetic characteristics of these systems are explained using the spin-density distribution, and an analysis is made by "magnetic" orbitals. The Nuclear Independent Chemical Shift (NICS) values have been calculated for these diradicals. The average NICS(1) (1Å above the ring surface) value per benzenoid ring increases as the size of the coupler increases. So-called ΔNICS(1) values [the difference among average NICS(1) per benzenoid ring in the coupler and the NICS(1) of the linear polyacene molecule] are correlated with J values. Bond orders and hyperfine coupling constant values have also been evaluated and analyzed for these diradicals.

4.1. Introduction

In the last few decades, experimentalists as well as theoreticians have paid special attention to the design, characterization and application of ferromagnetic materials based on organic diradicals.[1-3] The first purely organic magnetic material, based on the β-crystal phase of *p*-nitrophenyl nitronyl nitroxide radical, was discovered by Kinoshita and co-workers,[4] and has thrust the work nearer to the target of an organic ferromagnet. It is often important to have proper apprehension about the intramolecular magnetic exchange coupling constants before synthesizing organic diradicals intended as prospective ferromagnets.[1] As the aromatic linear fused-ring couplers of varying length can be synthesized easily, an interest has grown up concerning diradicals coupled with polyacene spacers.

Only a few organic paramagnetic species have reasonable stability to be suitable for the design of organic molecular ferromagnets.[5,6] Organic radicals such as nitronyl nitroxide, verdazyl, tetrathiafulvalene are appropriate for this purpose. The advantage of working with such systems is that they do not have any bulky substituent.[7] Nitronyl nitroxide diradical with ethylene coupler, isolated and studied by Ziessel et al.,[8] shows a very high exchange coupling constant. In the DFT framework, Ali and Datta[9,10] have comprehensively studied nitronyl-nitroxide-based molecular ferromagnets with different π-conjugated couplers. The potentiality of verdazyl radical as a precursor of molecular magnets remained unnoticed for a long time,[11,12] although it was first synthesized by Kuhn and Trischmann.[13] The spin-active verdazyl moiety is a good option for the design of molecular magnets. Non-Kekulé bis-oxoverdazyl diradical remains in the singlet ground state with small amount of thermally populated "triplet".[14] Brook et al.[15] have also extensively studied its electronic properties and found that it is strongly antiferromagnetically coupled. The HOMO and LUMO of bis-oxoverdazyl diradicals are similar to those of tetramethylene ethane (TME).[15,16] Substitution of both of the oxygen atoms in bis-oxoverdazyl diradical by sulfur atoms (bis-thioxoverdazyl diradical) gives a red shift.[17] Fico et al.[14] have reported that the room-temperature EPR spectrum of bis-thioxoverdazyl diradical is similar to that of the bis-oxoverdazyl diradical. They also have found that there is a notable variation in electron density between the oxo and thioxo derivatives. The magnetic properties of different derivatives of verdazyl radicals have

been studied extensively.[11,12,18-26] The radicals, 6-oxo- and 6-thioxo-verdazyl are also known to be chemically stable. They can be isolated in solvent-free pure forms in the crystalline state.[17,27] Azidophenyl substituted verdazyls have also been prepared by Lathi and co-workers.[28] Hicks et al.[29] have studied the supra-molecular chemistry of verdazyl molecules. Phosphaverdazyl radicals are also synthesized and characterized by Hicks and Hooper.[30]

The intramolecular magnetic exchange-coupling constant (J) as described by Heisenberg Hamiltonian is the best known descriptor of magnetism. The value of J depends on the molecular geometry of the diradicals and the unpaired-electron structures. Prior knowledge of the magnetic exchange-coupling constant characteristics becomes useful before synthesizing molecular ferromagnets.[1] In a diradical, the exchange-coupling constant depends crucially on the distance between two radical centers and the nature of the couplers. Gilroy et al.[31] have synthesized various verdazyl based compounds and characterized their magnetic properties. Applying unrestricted density functional methodology, intramolecular magnetic exchange-coupling constants have been studied for a series of bis-nitronyl nitroxide diradicals bridged with different π-couplers by Ali and Datta.[9] Polo et al.[32] have investigated tetrathiafulvalene (TTF) and verdazyl diradical cations with similar couplers. Although, in that work they have criticized the use of spin projected techniques and decided not to use it, but they finally end up using one such method. In a recent work, Latif et al.[33] investigated polyene spacers with mixed radical systems, in which they have established that the magnitude of the coupling constant depends strongly on the planarity of the molecular structure, spin polarization paths, length of the couplers, etc. In some recent work, we have designed and investigated 11 bis-oxoverdazyl diradicals connected by different linkage-specific aromatic couplers and found that *meta*-coupled diradicals are ferromagnetic whereas *para*-coupled diradicals are antiferromagnetic in nature.[34] Logically, our present chapter follows these investigations, where the objective is to design and characterize oxoverdazyl and thioxoverdazyl based molecular ferromagnets coupled with different polyacene spacers. We have designed two sets of diradicals, (set A with 5 bis-oxoverdazyl diradicals and set B with 5 bis-thioxoverdazyl diradicals) coupled by different *meta*-connected linear polyacene

Scheme 4.1. General schematic representation of diradicals (i-x) with five different polyacene couplers, where formally there are two unpaired electrons at N_4 and N_{10} atoms and the benzenoid rings are denoted as A, B, C, D and E . The polyacene couplers (X=1 to 5) are used in both sets of diradicals.

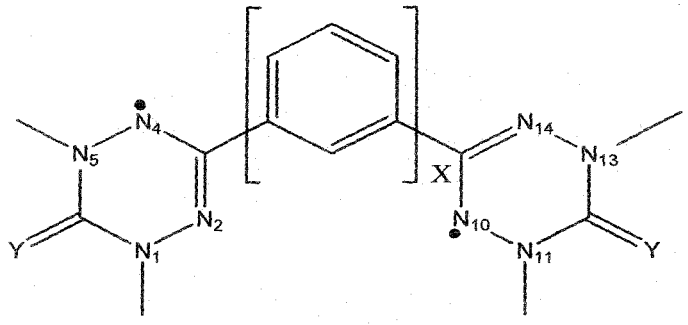

where Y=O (Set A) and S (Set B) and X=1-5

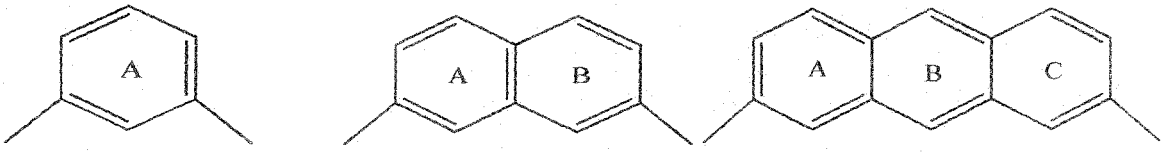

Diradical (i), X=1, Y=O Diradical (ii), X=2, Y=O Diradical (iii), X=3, Y=O

Diradical (vi), X=1, Y=S Diradical (vii), X=2, Y=S Diradical (viii), X=3, Y=S

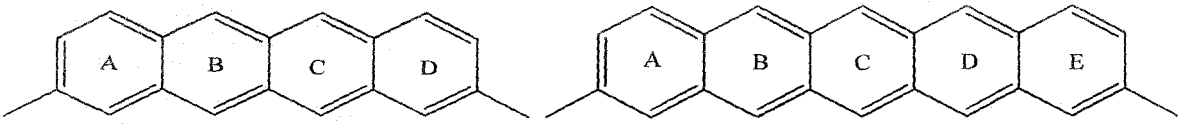

Diradical (iv), X=4, Y=O Diradical (v), X=5, Y=O

Diradical (ix), X=4, Y=S Diradical (x), X=5, Y=S

spacers of varying length. The designed systems are depicted in Scheme 4.1. Some of the systems under investigation are already synthesized and characterized.[14,31] It is noticed that the magnetic exchange coupling constant depends on the length of the coupler and spin polarization path. The polyacenes are aromatic hydrocarbons with linearly fused benzene rings.[35] Experimentalists as well as theoreticians have been attracted by these substances for a long time.[36] Pentacenes are known to have semiconducting property[35,37] hence; it can be used in spintronic materials. It is established that the polyacenes are predicted to have smaller band gaps than the corresponding polyenes.[38] The polyacenes become less stable with increasing numbers of benzene rings.[35,36] In this chapter, we find, linear polyacene coupled bis-oxo- and bis-thioxo-verdazyl diradicals have moderate ferromagnetically signed exchange-coupling constants. The exchange coupling constants are evaluated through the spin-polarized unrestricted DFT methodology. The broken-symmetry (BS) approach, described in the next section, has been adopted here to quantify ferromagnetic coupling constants for all the systems described above.

4.2. Theoretical Background and Computational Details

The Heisenberg spin Hamiltonian is normally used to express the magnetic exchange interaction between two magnetic sites 1 and 2,

$$\hat{H} = -2J\hat{S}_1 \bullet \hat{S}_2, \tag{4.1}$$

where J is the exchange coupling constant between two magnetic centers of a diradical, with $\hat{S}_1$ and $\hat{S}_2$ being the respective spin angular momentum operators. The square of the total spin operator $\hat{S}^2$ has eigenvalue $S(S+1)$. A positive sign of J, in which a situation of parallel spin is essential, is used to indicate a ferromagnetically signed interaction, whereas an antiferromagnetically signed interaction is indicated by a negative value, where a state of antiparallel spins is favored. For a diradical with a single unpaired electron on each site, J can be written as

$$E_{(S=1)} - E_{(S=0)} = -2J. \tag{4.2}$$

A single determinantal wave function in the unrestricted Hartree Fock formalism cannot truly represent the singlet state of a diradical. Moreover, this introduces spin contamination in such calculations. Therefore, this method cannot directly yield reliable J values. However, one can evaluate J by determining the exact singlet and "triplet" energy values from a multiconfigurational approach and MCSCF calculations on bis-verdazyl systems have been carried out.[39] The performance of the complete active space second-order perturbation theory (CASPT2) and accurate Difference Dedicated Configuration Interaction (DDCI) calculations for α-4-dehydrotoluene and 1,1',5,5'-tetramethyl-6,6'-dioxo-3,3'-bis-verdazyl and other diradicals have also been reported by Illas and coworkers[40] and the authors found that CASPT2 provides a clean alternatives to the use of BS-UDFT based methods. However, these methods are resource intensive and are not employed in this chapter. On the other hand, the broken-symmetry (BS) formalism proposed by Noodleman[41,42] in a DFT framework is an alternative approach to evaluate J with less computational effort. The BS state, which is a weighted average of low- and high-spin states, is often found to be spin contaminated. But with the use of a "spin-projection" technique, reliable estimates of the exchange-coupling constant can be obtained via this BS approach. Depending upon the extent of overlap between magnetic orbitals, different expressions for J have been proposed by many researchers,[40-57] using the unrestricted spin-polarized BS solution for the lower-spin state. The expression for J given by Ginsberg,[43] Noodleman,[44] and Davidson[45] is more useful when overlap of the magnetic orbitals is very small. The expression put forward by Bencini and coworkers,[46,47] Ruiz et al.[48] uses the energy of the BS state as that of the open-shell singlet without spin projection and attempt to justify their choice (later on) by the hypothesis of the large overlap limit between magnetic orbitals. However, this approach has been shown to be unphysical by Caballol et al.,[50] where the overlap is explicitly calculated and found to be small. In a more recent work, Moreria and Illas[52] have shown that there exists a common physical background in the magnetic interactions in organic diradicals, inorganic complexes or ionic solids, where the magnetic interactions occur between localized spins. Further, Illas and coworkers[51-53] have shown that Spin Unrestricted Broken Symmetry (SUBS) and Spin-Restricted-Ensemble-referenced Kohn-Sham (REKS) lead to similar estimate of J value. However, exchange correlation

functional used in REKS approach is under development and performance of each functional is yet to be explored.

Nevertheless, in this chapter, the Yamaguchi model[54-57] is employed to get the J values, and this is the proper choice, especially if one is uncertain of the magnitude of J beforehand. The expression is

$$J = \frac{(E_{BS} - E_T)}{\langle S^2 \rangle_T - \langle S^2 \rangle_{BS}}, \tag{4.3}$$

where E_{BS} and E_T denote the energy of the broken symmetry singlet and "triplet" state, and where $\langle S^2 \rangle_T$ and $\langle S^2 \rangle_{BS}$ represent respective average spin-square values in "triplet" and BS states. It should be noted here that E_T is the approximate form of $E_{T'}$, the energy of the "triplet" state in the unrestricted formalism using the BS orbital. The approximation is valid because of the very less spin contamination in the high spin state.[9,10] However, even for this high symmetry states the spin unrestricted calculations converge to a state which has not spin well defined. As $\langle S^2 \rangle_T$ is near 2 and $\langle S^2 \rangle_{BS}$ is near 1, eq (4.3) reduces essentially to the case with small overlap and the denominator is just a very small correction.

The energy differences in B3LYP calculations are accurate to ± 2-5 kcal/mole. In this chapter, the computed energy difference is less than 0.1 kcal/mole. As a result, this is not surprising that the J values may be little overestimated. Nevertheless, in this chapter we get the sign of exchange coupling right and therefore correctly predict the nature of coupling. Ruiz et al. [58] related the overestimation of J values with the presence of high self interaction error (SIE) in commonly used DFT exchange correlation potentials. However, this has been severely questioned by a comment co-authored by a large list of specialists in this field.[59] Polo and coworkers[60] have concluded that the presence of SIE in commonly used DFT approximations is related to "nondynamic" correlation energy. Hybrid functionals are more suitable than pure DFT functionals in BS-UDFT calculations because the former reduces the self interaction error (SIE) of DFT exchange functionals.[61] The suitability of B3LYP over LSDA and GGA approach has also been justified by Martin and Illas.[62] Thus, one can

surmise that as B3LYP functional is parameterized mainly to molecules composed of light atoms, it likely to give superior energy differences in such molecules. In this chapter, the molecular geometries of a sequence of compounds (i-x) have been fully optimized with the UB3LYP[63-65] exchange correlation potential using a 6-31G(d,p) basis set.[66-68] At the optimized geometries energy calculations of each of the species are then done with a larger basis set i.e., 6-311++G(d,p), and these are used to calculate the *J* values. To obtain the open-shell BS singlet solution, "guess =mix" keyword is used within the unrestricted formalism. The BS states are stable for all 10 diradicals. All the calculations have been carried out using the GAUSSIAN 03W[69] quantum chemical package. Hyperchem 7.5[70] and Molekel 4.0[71] softwares have also been used for visualization. All computations of this chapter have been carried out in a HP xw4600 workstation, processor Intel® Core (TM) 2 Duo CPU @ 2.33 GHz, 3,072 MB of RAM with 64-bit operating system.

4.3. Results and Discussion

The main characteristic of the radicals of the verdazyl family is their stability as well as their ferromagnetic nature in suitably designed diradicals.[40,72] The optimized structures of the systems under investigation are planar (Figure 4.1). As a result, better spin polarization along the π-conjugated network stabilizes the "triplet" states.[73,74] The linker between two same or different organic radicals plays a major role in determining the sign and magnitude of exchange coupling constants.[9,10,32-34] We examine spin coupling between radical centers separated by polyaromatics, using density functional theory to calculate values of the exchange coupling constants (Table 4.1) from the differences in high-spin and low-spin broken symmetry energies for two sets (set A and set B) of compounds, some of which are already known,[14,31] and the others are newly designed as given in Scheme 4.1 (also see Figure 4.1). In set A, we have considered *meta*-coupled diradicals with general formula OV-*X*-OV, where X [when *X*=1 (benzene coupler), 2 (naphthalene coupler), 3 (anthracene coupler), 4 (tetracene coupler), 5 (pentacene coupler)] is the number of aceneic benzene ring(s) used as couplers and OV is oxo-verdazyl monoradical, whereas for set B diradicals, –OV radicals are replaced by –TV (thioxo-verdazyl) radicals. It is established that the unpaired spins are equally distributed among the specified atoms of the diradicals (N_2, N_4,

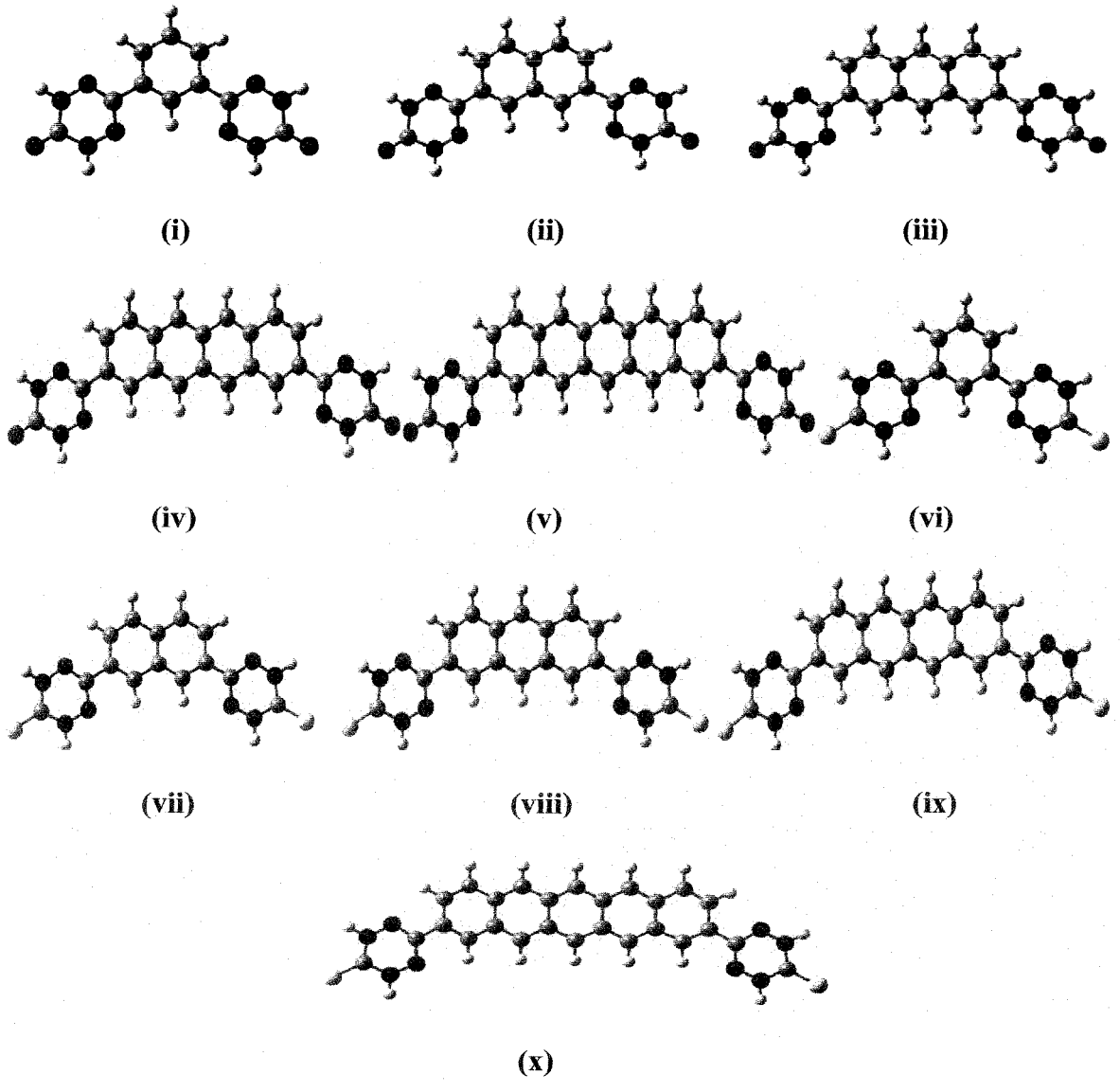

Figure 4.1. The optimized images of polyacene coupled bis-oxoverdazyl (i-v) and bis-thioxoverdazyl (vi-x) diradical systems at UB3LYP/6-31G(d,p) level. Atoms having red, blue, black, yellow and white colors represent O, N, C, S, and H, respectively.

N_{10} and N_{14} in Scheme 4.1).[7] Numerical values of J are obtained by use of eq (4.3) for all 10 species, and are reported in Table 4.1. Normally, the sign of J does not depend on the basis set employed;[32] hence the nature of predicted magnetic behavior in this chapter is reliable. Through close inspection of Table 4.1, it can be inferred that consistent results have been obtained with different basis sets and all 10 diradicals are ferromagnetic in nature. The methyl groups linked with verdazyl N atoms are replaced by hydrogen atoms to save the

Table 4.1. UB3LYP level absolute energies in *au*, $\langle S^2 \rangle$ and intramolecular exchange-coupling constant (J cm^{-1}) using 6-31G(d,p) and 6-311++G(d,p) basis sets, for bis-oxoverdazyl diradicals (i-v) and bis-thioxoverdazyl diradicals (vi-x).

		At UB3LYP/6-31G(d,p) level			At UB3LYP/6-311++G(d,p) level		
Di radicals		BS	"Triplet"	J(cm^{-1})	BS	"Triplet"	J(cm^{-1})
(i)	E	–974.25460	–974.25491	67	–974.50782	–974.50816	74
	$\langle S^2 \rangle$	1.049	2.059		1.048	2.055	
(ii)	E	–1127.90269	–1127.90284	33	–1128.18659	–1128.18673	31
	$\langle S^2 \rangle$	1.050	2.060		1.052	2.056	
(iii)	E	–1281.54431	–1281.54432	02	–1281.85856	–1281.85858	04
	$\langle S^2 \rangle$	1.056	2.065		1.052	2.054	
(iv)	E	–1435.18313	–1435.18315	04	–1435.52783	–1435.52801	39
	$\langle S^2 \rangle$	1.058	2.078		1.052	2.057	
(v)	E	–1588.82059	–1588.82080	44	–1589.19595	–1589.19614	41
	$\langle S^2 \rangle$	1.079	2.138		1.059	2.068	
(vi)	E	–1620.17104	–1620.17131	59	–1620.42061	–1620.42081	44
	$\langle S^2 \rangle$	1.047	2.054		1.047	2.051	
(vii)	E	–1773.81940	–1773.81944	09	–1774.09948	–1774.09965	37
	$\langle S^2 \rangle$	1.049	2.055		1.048	2.053	
(viii)	E	–1927.46107	–1927.46110	07	–1927.77164	–1927.77178	31
	$\langle S^2 \rangle$	1.050	2.060		1.048	2.053	
(ix)	E	–2081.09999	–2081.10004	11	–2081.44114	–2081.44120	13
	$\langle S^2 \rangle$	1.054	2.072		1.051	2.054	
(x)	E	–2234.73756	–2234.73776	42	–2235.10927	–2235.10941	31
	$\langle S^2 \rangle$	1.072	2.128		1.055	2.061	

computation time.[32] In other recent work,[34] the bis-oxoverdazyl diradical with no coupler has been found to generate a strong antiferromagnetically signed interaction according to DFT computations, as is in good agreement with previous experimental studies.[15] In this chapter, we find that the *meta*-aceneic coupled bis-oxoverdazyl and bis-thioxoverdazyl diradicals manifest a ferromagnetically signed interaction, which is also in good agreement with other works.[9,10,31,34] The decreasing order of calculated J values from (i)-(iii) in set A and (vi)-(viii) in set B are also in good agreement with the work of Ali and Datta.[10] The change in J values from (iii)-(v) in set A and (viii)-(x) in set B can be attributed to the fact that the larger polyacenes possess open-shell singlet ground states.[35] However, with our larger basis set, the J value obtained for diradical (viii) is marginally higher than expected.

4.3.1. Bond Order

Using natural bond-order (NBO) analysis we have calculated the Wiberg bond order[75] at the UB3LYP/6-31G(d,p) level. The calculated average Wiberg bond orders between the

Table 4.2. The calculated average Wiberg bond order for the linkage bond between the monoradical and the coupler on both sides, for all the diradicals (i-x) at the UB3LYP level using a 6-31G(d, p) basis set.

Diradicals	Wiberg bond order
(i)	1.042
(ii)	1.045
(iii)	1.048
(iv)	1.050
(v)	1.051
(vi)	1.048
(vii)	1.053
(viii)	1.056
(ix)	1.059
(x)	1.061

coupler and the monoradical moieties on both sides for each of the 10 diradicals are given in Table 4.2. With the increase in the number of benzenoid rings in the coupler, the number of delocalizable π-electrons increases and small increment in Wiberg bond order is noted. It can also be observed that as the average bond order increases, the average Mulliken atomic spin densities decrease modestly on the radical centers (Table 4.3) for the first three diradicals of each set. As a consequence, the magnitude of J value also decreases for the first three diradicals in both sets. On the other hand, for the last two diradicals in every set, with the increase of the diradical character of the coupler, the average Mulliken atomic spin density on the radical centers increases and hence the J value.[10]

Table 4.3. The calculated Mulliken atomic spin densities for all the diradicals (i-x) with the couplers at UB3LYP level using 6-31G(d,p) basis set [N_2, N_4 and N_{10}, N_{14} (Scheme 4.1) are the respective atoms in the verdazyl moiety where the unpaired spins are delocalized (Ref. 7)].

Diradicals	N_2	N_4	Average	N_{10}	N_{14}	Average
(i)	0.4307	0.4326	0.4317	0.4318	0.4316	0.4317
(ii)	0.4435	0.4191	0.4313	0.4199	0.4426	0.4313
(iii)	0.4109	0.4489	0.4299	0.4110	0.4489	0.4300
(iv)	0.4533	0.4121	0.4327	0.4128	0.4527	0.4328
(v)	0.4566	0.4136	0.4351	0.4136	0.4566	0.4351
(vi)	0.4292	0.4283	0.4289	0.4285	0.4291	0.4288
(vii)	0.4406	0.4168	0.4287	0.4168	0.4406	0.4287
(viii)	0.4067	0.4451	0.4259	0.4066	0.4451	0.4259
(ix)	0.4512	0.4096	0.4304	0.4097	0.4511	0.4304
(x)	0.4546	0.4111	0.4329	0.4105	0.4501	0.4303

4.3.2. Spin Density Distribution

Hund's rule based spin alternation rule,[73,74] is very helpful to predict the ground state magnetism for diradicals coupled with different couplers. This rule states that when the pathway through the coupler propagates through an even number of bonds, ferromagnetism arises. Kiovisto and Hicks[7] have discussed the fact that bis-oxoverdazyl diradical possess a

plane of symmetry through the linkage bond between two monoradicals, as a result, the spin distribution is subdued and antiferromagnetism arises. However, the linkage position of the π-donor unit to an aromatic ring coupler determines the sign of J. It is widely recognized that *meta*-phenylene coupled diradicals exhibit a high ferromagnetically signed interaction.[9,10,31-34] In our present chapter, we have used "*meta*"-coupled linear polyacene spacers of varying length between two oxo-verdazyl and two thio-verdazyl monoradicals and found that all the diradicals strictly follow the spin alternation rule (Figure 4.2). Indeed, the consequences of

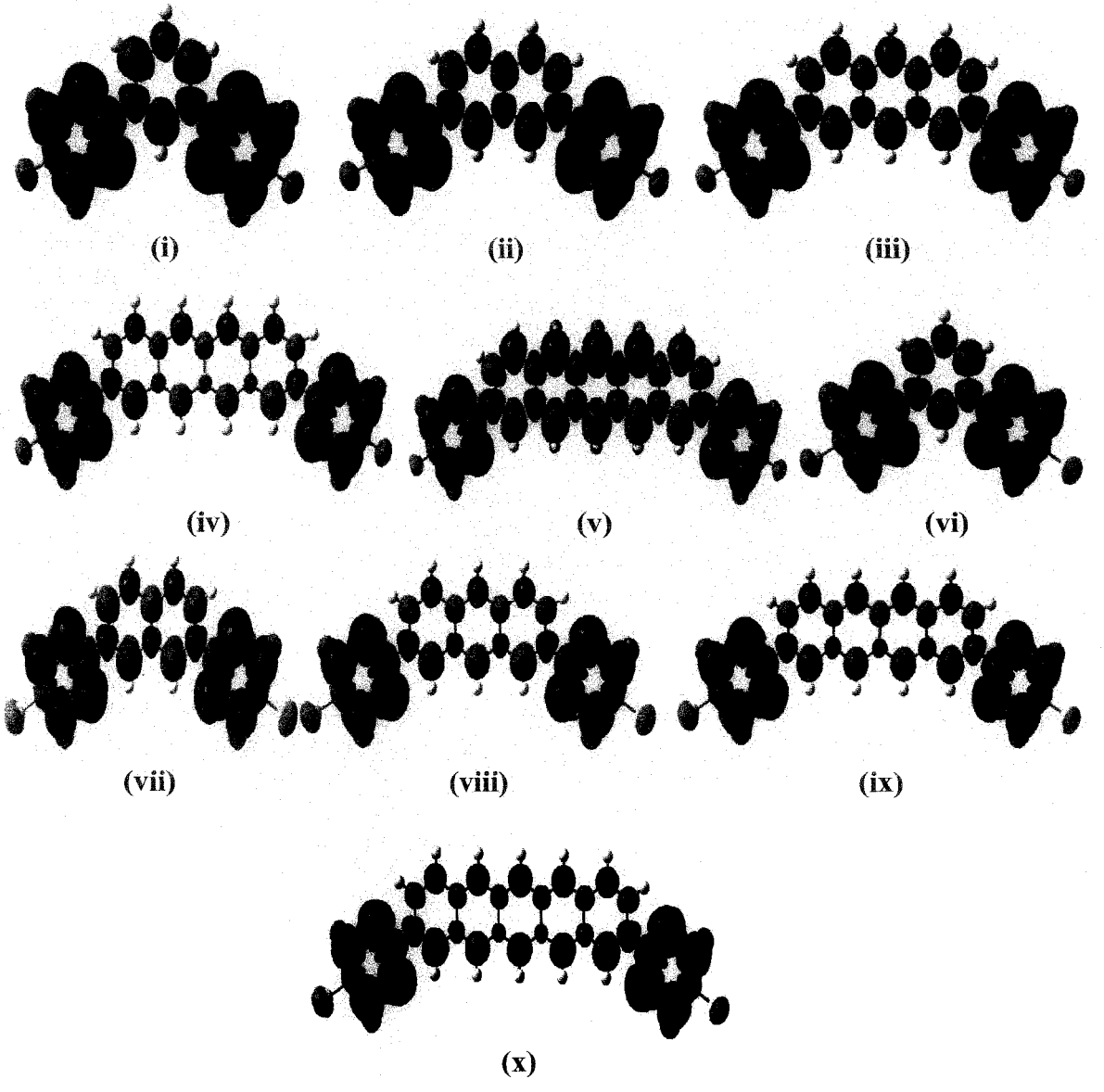

Figure 4.2. Spin-density distribution plots for each of the diradicals (i–x); blue color indicates α spin, and green color indicates β spin respectively.

this spin-alternation rule follows directly from the results[76-78] for alternant conjugated π-networks that the total ground-state spin is half of the difference between the number of spins on "starred" and "unstarred" sites. An alternant network is such that the sites can be partitioned into the starred and unstarred sites with every neighboring pair of sites of different types. That is, in a diradical species, the two unpaired electrons are, predicted to give a "triplet" or a "singlet" ground state as the two electrons are respectively on like (i.e., both "starred" and both "unstarred") or unlike (i.e., one is "starred" and the other "unstarred"). It is also to be noted that two like sites are separated by an even number of bonds, while unlike sites are separated by odd number of bonds, which is essentially the same as that given by Trindle et al.[73,74] This general result arises in the context of the nearest neighbor Heisenberg spin model, which is equivalent to the covalent-space Pauling-Wheland VB model. This theorematic result is a consequence of a general symmetry feature of the no des of the many-electron wave-function.[76] However, these theorematic results apply when the average formal number of π-electrons per site in the π-network is 1.[79] If one includes in the π-network a different number of π-electrons, that is, when one introduces a formally neutral N atom with 3 σ-bonds and a net contribution of 2 π-electrons, then a different situation arises. To understand this, when two N atoms are neighbors, as that in verdazyl, with one N atom formally contributing 1 π-electron and the other 2, there is a major ground-state contribution with spin$\uparrow$ on the first site and spin$\uparrow\downarrow$ on the second site. This configuration also interacts with another configuration via electron transfer, with spin$\uparrow\downarrow$ on the first site and spin$\uparrow$ on the second site. Thus one finds parallel spins on these two neighboring N-atom sites which are in agreement with our computational results, as illustrated in Figure 4.2.

4.3.3. Analysis of Singly Occupied Molecular Orbitals (SOMOs)

With the help of extended Hückel theory (ETH), Hoffmann[80] suggested that if the energy difference is less than 1.5 eV between two consecutive SOMOs, then parallel orientation of spins occurs. However, the theorem concerning the number of sites of the two different types ("starred" and "unstarred"), indicates the situation which is generally more nuanced. Within the MO framework, one also needs to figure out the overlap between the

SOMOs, for which the argumentation leading to Hund's rule is severely weakened.[16,81] At the B3LYP level with 6-31G(d,p) basis set, $4n\pi$ anti-aromatic linear and angular polyheteroacenes have been investigated by Constantinides et al.;[82] where they found that for a SOMO splitting ΔE_{SS}>1.3 eV, a singlet ground state results with antiparallel orientation of spins. The critical value of ΔE_{SS} is different in different cases.[34] In this chapter, we calculate the SOMO-SOMO energy gap for the "triplet" ground state of all 10 diradicals. It is observed that, diradicals (i) in set A and (vi) in set B have the lowest ΔE_{SS} (Table 4.4) value with the highest J value in their respective sets. Among the diradicals (i), (ii), (iii) (in set A) and (vi), (vii), (viii) (in set B) the ΔE_{SS} value increases as the J value decreases. This observation makes it clear that our calculations are consistent with the Hay-Thibeault-Hoffmann[83] (HTH) formula for the singlet-triplet energy gap in weakly coupled dinuclear metal complexes.

Table 4.4. The energy of SOMOs in *au* and their differences in eV at UB3LYP level using a 6-31G(d, p) basis set for diradicals (i-x).

Diradicals	$E_S(1)au$	$E_S(2)au$	$\Delta E_{SS}eV$
(i)	–0.20778	–0.20771	0.0019
(ii)	–0.20774	–0.20681	0.0253
(iii)	–0.20744	–0.19874	0.2367
(iv)	–0.20706	–0.18565	0.5826
(v)	–0.20665	–0.17576	0.8406
(vi)	–0.21952	–0.21941	0.0030
(vii)	–0.21878	–0.21739	0.0378
(viii)	–0.21778	–0.20625	0.3137
(ix)	–0.21698	–0.19244	0.6678
(x)	–0.21587	–0.18212	0.9184

However, for last two diradicals in each set, the ΔE_{SS} values are higher; despite they show high values of J. This is due to the fact that larger polyacenes possess within themselves a significant radicaloid character, with a "triplet" state approaching toward the singlet ground state, which then may be better viewed as an open-shell singlet. This observation is also found in recent computations,[35,84,85] but this is also conceivable from reasonable extensions of "classical" arguments of Clar.[86] If one imagines that as the length of an N-acene increases, the N+1 ordinary single Clar-sextet structures become of ever lesser importance

than the diradicaloid two-Clar-sextet structures, for which there is a much greater number $=\frac{1}{12}N(N-1)^2(N-2)$. In fact, Clar paid little attention to radicals, though recent extensions[87,88] to deal with radicaloid species reflect favorably on his ideas, and such natural extensions follow. The point is that with an extended diradicaloid nature for the spacer, its spin-polarization is eased, and the communication (as mediated by J) is enhanced. In any event in this present chapter, all 10 diradicals under investigation have ΔE_{SS}<1.5 eV and show manifestly ferromagnetic coupling. Thus, even if it is not conclusively proved that the Kohn-Sham orbital energies have a relationship with the magnetic coupling constants, this analysis provides justification of such a connection, albeit empirically.

4.3.4. Nuclear Independent Chemical Shift (NICS)

The quintessence of aromaticity can be straightforwardly documented with ease, yet it is

Table 4.5. The calculated NICS values at the centre of the aromatic rings at UB3LYP level using a 6-311+G(d, p) basis set for diradicals (i-x).

Diradical	NICS	A	B	C	D	E
(i)	NICS(0)	–6.62				
	NICS(1)	–8.96				
(ii)	NICS(0)	–8.77	–8.77			
	NICS(1)	–9.46	–9.46			
(iii)	NICS(0)	–6.62	–9.90	–6.62		
	NICS(1)	–8.81	–11.71	–8.81		
(iv)	NICS(0)	–5.81	–10.25	–10.24	–5.80	
	NICS(1)	–8.12	–11.95	–11.95	–8.11	
(v)	NICS(0)	–5.10	–9.64	–11.20	–9.64	–5.10
	NICS(1)	–7.49	–1.43	–12.65	–11.43	–7.49
(vi)	NICS(0)	–6.56				
	NICS(1)	–8.99				
(vii)	NICS(0)	–7.21	–7.27			
	NICS(1)	–9.55	–9.51			
(viii)	NICS(0)	–6.42	–10.00	–6.29		
	NICS(1)	–8.87	–11.80	–8.82		
(ix)	NICS(0)	–5.63	–10.25	–10.25	–5.75	
	NICS(1)	–8.14	–11.99	–11.99	–8.18	
(x)	NICS(0)	–4.88	–9.60	–11.24	–9.63	–5.02
	NICS(1)	–7.50	–1.46	–12.70	–11.45	–7.55

tricky to categorize quantitatively because of its multidimensional[89-92] or partially-ordered[93,94] nature. In some interesting work, Illas and co-workers[95] and Feixas et al.[96] have shown that different measures of aromaticity exhibit some discrepancies. There are many descriptors to study aromaticity, but NICS, which is a local aromaticity index, has many advantages over others. The NICS values depend on the methodology used and the basis set employed.[90-92] In our present chapter, the NICS values for all aromatic rings in 10 different diradicals are calculated by using GIAO-UB3LYP methodology with a 6-311+G(d,p) basis set. The NICS values are calculated at the centre of the ring [NICS (0)] and 1Å above the ring surface [NICS (1)], where, π-orbital density is maximum. Schleyer and coworkers[90-92]

Table 4.6. The calculated NICS(1) values for the all the diradicals (i-x) and corresponding acene molecules, ΔNICS(1), at UB3LYP level using 6-311+G(d,p) basis set, where (*) sign represents the NICS(1) values in bis-oxo- and bis-thioxo-verdazyl diradicals (Table 4.5), on the other hand, (**) sign represents the NICS(1) values in acene molecules without bis-oxo- and bis-thioxo-verdazyl diradicals as given in ref. 92.

	Average NICS(1)		
Diradicals	Couplers*	Acenes**	ΔNICS(1)
(i)	–8.96	–10.60	1.64
(ii)	–9.46	–10.80	1.34
(iii)	–9.78	–11.00	1.22
(iv)	–10.03	–11.10	1.07
(v)	–10.10	–11.20	1.10
(vi)	–8.99	–10.60	1.61
(vii)	–9.53	–10.80	1.27
(viii)	–9.83	–11.00	1.17
(ix)	–10.08	–11.10	1.02
(x)	–10.13	–11.20	1.07

have studied linear polyacene molecules with B3LYP/6-311+G(d,p) level using GIAO-B3LYP methodology. Ali and Datta[10] also have used the same methodology and basis sets for nitronyl nitroxide based polyacene spacers. These authors have noticed that terminal rings in the linear polyacenes have less benzenoid character and the inner rings are more aromatic

than benzene itself. These results are in good agreement with the results obtained in this chapter (Table 4.5). It is observed from Table 4.6 that $NICS(1)_{coupler} < NICS(1)_{acenes}$. The difference between average $NICS(1)_{coupler}$ and $NICS(1)_{acene}$ is represented by ΔNICS(1). For both set of diradicals it is obvious that the average NICS(1) value per benzenoid ring increases as the size of the coupler increases. It is also observed that with the decrease of ΔNICS(1), J value decreases for the first three species in each set but the reverse trend is observed for the last two species in both sets of diradicals due to the increase of diradical character of the couplers as discussed in the previous section.

4.3.5. Isotropic Hyperfine Coupling Constants (HFCCs)

Isotropic hyperfine coupling constant (HFCC), the interaction between nuclear and electric magnetic moments depends on the spin density of the related nuclei. HFCCs are difficult to calculate because of electron correlation and basis-set effects. Solvent also often plays an effective role to influence the HFCC values. In our present chapter, we have calculated HFCCs within the DFT framework by using an EPR-II basis set at the UB3LYP level in vacuum. As it turns out, "S" atoms are not considered in the EPR-II basis set in the quantum chemical package used for computations[69] so we have used the 6-31G(d,p) basis set for "S" atoms in all set B diradicals.

In oxo-vardazyl and thioxo-verdazyl monoradicals, two sets of two equivalent nitrogen atoms (N_1-N_5 and N_2-N_4) (Scheme 4.1) are found. Plater et al.[97] in bis-verdazyl diradical have observed that hfcc for $a(N_2\text{-}N_4)$ = 6.5 G and $a(N_1\text{-}N_5)$ = 5.3 G (depending upon the nature of substitution), which are nearly similar to that observed by Neugebauer et al.[27,98] They have also found that larger hfcc values are obtained at N_2, N_4 and N_{10}, N_{14} which means that the spins are localized along the N=C–N group rather than over the Me–N–CO–N–Me group (Scheme 4.1). Nitronyl nitroxide diradical with different couplers[9,10] have been studied and the HFCC values for conjugated coupler added diradicals reduce to half of the values for corresponding monoradicals.

In our present chapter, we have computed HFCC values for all eight N-atoms present in each bis-oxo- and thioxo-verdazyl diradical (Table 4.7). From these computations we see that the calculated gas phase HFCC values for N_2-N_4 and N_{10}-N_{14} are larger than that of N_1-N_5 and N_{11}-N_{13} (Scheme 4.1) in both sets of diradicals. These results are in good agreement with many experiments.[27,98] However, we do not find a clear relationship between the HFCC values and the exchange-coupling constants.

Table 4.7. Evaluated hyperfine coupling constant (HFCC) in *Gauss* at UB3LYP level using EPR- II basis set [for "S" atom 6-31G(d,p) basis set is employed] for all diradicals.

Diradicals	a_{N1}	a_{N2}	a_{N4}	a_{N5}	a_{N10}	a_{N11}	a_{N13}	a_{N14}
(i)	1.39456	2.81214	2.81926	1.38991	2.80826	1.38999	1.39465	2.82350
(ii)	1.37680	2.84858	2.50333	1.32396	2.84127	1.38191	1.31987	2.51208
(iii)	1.21091	2.19120	2.97822	1.34377	2.75415	1.33215	1.40500	3.10998
(iv)	1.28194	2.71955	2.13397	1.17365	2.72345	1.29045	1.18250	2.16933
(v)	1.41566	3.14904	2.57570	1.30419	3.14903	1.41564	1.30422	2.57576
(vi)	1.18701	3.17927	3.26141	1.12447	3.17827	1.18679	1.12477	3.26315
(vii)	1.49530	3.19138	3.03626	1.14349	3.19407	1.46392	1.36941	3.04159
(viii)	1.88941	2.93919	3.15984	1.71353	2.94157	1.89106	1.70922	3.15784
(ix)	1.44644	3.32940	3.60754	1.83785	3.16914	1.77647	1.76401	2.87529
(x)	1.33400	3.01129	2.74187	1.27111	3.01187	1.03849	1.23550	2.73678

4.4. Conclusions

This chapter presents a theoretical study of magnetic intramolecular coupling in bis-oxoverdazyl and bis-thioxoverdazyl diradicals with polyacene spacers using a density functional theory based method within the broken symmetry approach to estimate the energy of the open shell singlet. We discuss the results in light of correlation with several qualities related to spin density. This subject is of interest for the community seeking for stable organic ferromagnets. Although we have used the unrestricted B3LYP exchange-correlation potential, recent advances have shown that other functionals, such as functionals of M06 family[99] and the range-separated functionals[100] represent a considerable improvement over B3LYP. Bis-verdazyl is one of the compounds included to study the usefulness of such

functionals; thus, these functionals are promising to study organic ferromagnets. In our study, all 10 diradicals (i)-(x), have been found to be ferromagnetic in nature (i.e., with a "triplet" ground state). A general site-type-classification given by theorematically based rule,[76,77] accurately predicts the sign of J, as well as the spin-density alternation pattern,[78] which is also consonant with an empirically designed rule[73,74] for the sign of J. The exchange-coupling interactions are mainly transmitted through conjugated π-electron network as observed by other authors.[9,10,31-34] It is emphasized that this coupling between distant diradical sites is enhanced when the coupler itself has a low-lying excited "triplet" state with spin-density spread over the intervening space, as manifested in (iv), (v) and (ix), (x). A clear signature of this effective transmission is seen in the strong spin-density alternation (Figure 4.2) pattern, as obvious from an MO analysis. The J values decrease (Table 4.1) from X=1 to X=3 (Scheme 4.1) but increase from X=3 to X=5 for both sets of diradicals. The increase in J value in the later case is due to the evident increase of diradical character of tetracene and pentacene couplers. In dimetal systems which exhibit little charge transfer from ligands to metals, predicted J values are found to be pretty accurate.[101] In the present study, our systems do not seem to be susceptible to much charge transfer onto the spin centers. Thereby, we expect that the predicted J values should be accurate in analogy with the inorganic complexes. However, this generalization needs systematic study with organic systems. To compare our results with experimental works, we find Gilroy et al.[31] have reported 1,3-benzene-bridged *N,N'*-di(isopropyl)-6-oxoverdazyl diradical from empirical method by measuring magnetic susceptibility data at different temperatures. They have found that the diradical has a high-spin ground state with J =19.3 ± 1.7 cm^{-1}. In our DFT study, we get J = 67 cm^{-1} (Table 4.1), at the optimized level for diradical (i) which is essentially a similar diradical studied by Gilroy et al.,[31] with only difference is that the isopropyl groups are substituted by the hydrogens. Thus, our results are in good agreement with experimental work. In case of bis-thioxo-verdazyl series not many experimental studies are reported. Nevertheless, from this study it is clear that bis-thioxo verdazyls are good precursors for single molecule magnets. In this study, we notice that the J values are found to increase with bond order between the coupler and the radical fragments, which is manifested in spin population analysis. The NICS values (Table 4.5) are higher for the central benzenoid ring(s) of each coupler, while it is found that terminal rings have low NICS values, that is, a loss of

benzenoid character is observed.[90-92] However, for tetracene and pentacene coupled diradicals in both sets, the J value increases due to increase in open-shell radicaloid character of the spacers. Finally, this chapter also estimates HFCC values.

This work has been published in Theoretical Chemistry Accounts (Ref. 102).

4.5. References and Notes

(1) Kahn, O. *Molecular Magnetism*, New York, VCH, 1993.

(2) Coronado, E.; Delhaè, P.; Gatteschi, D.; Miller, J. S. *Molecular Magnetism: From Molecular Assemblies to the Devices*, Eds.; Nato ASI Series E, Applied Sciences, Kluwer Academic Publisher: Dordrecht, Netherland, 1996, Vol. 321.

(3) Benelli, C.; Gatteschi, D. *Chem. Rev.* **2002**, *102*, 2369.

(4) Tamura, M.; Nakazawa, Y.; Shiomi, D.; Nozawa, K.; Hosokoshi, Y.; Ishikawa, M.; Takahashi, M.; Kinoshita, M. *Chem. Phys. Lett.* **1991**, *186*, 401.

(5) Dougherty, D. A. *Acc. Chem. Res.* **1991**, *24*, 88.

(6) Borden, W. T.; Iwamura, H.; Berson, J. A. *Acc. Chem. Res.* **1994**, *27*, 109.

(7) Koivisto, B. D.; Hicks, R. G. *Coord. Chem. Rev.* **2005**, *249*, 2612.

(8) Ziessel, R.; Stroh, C.; Heise, H.; Khler, F. H.; Turek, P.; Claiser, N.; Souhassou, M.; Lecomte, C. *J. Am. Chem. Soc.* **2004**, *126*, 12604.

(9) Ali, Md. E.; Datta, S. N. *J. Phys. Chem. A* **2006**, *110*, 2776.

(10) Ali, Md. E.; Datta, S. N. *J. Phys. Chem. A* **2006**, *110*, 13232.

(11) Takeda, K.; Hamano, T.; Kawae, T.; Hidaka, M.; Takahash, M.; Kawasaki, S.; Mukai, K. *J. Phys. Soc. Jpn.* **1995**, *64*, 2343.

(12) Mukai, K.; Konishi, K.; Nedachi, K.; Takeda, K. *J. Phys. Chem.* **1996**, *100*, 9658.

(13) Kuhn, R.; Trischmann, H. *Angew. Chem. Int. Ed. Engl.* **1963**, *2*, 155.

(14) Fico, R. M. Jr.; Hay, M. F.; Reese, S.; Hammond, S.; Lambert, E.; Fox, M. A. *J. Org. Chem.* **1999**, *64*, 9386.

(15) Brook, D. J. R.; Fox, H. H.; Lynch, V.; Fox, M. A. *J. Phys. Chem.* **1996**, *100*, 2066.

(16) Borden, W. T.; Davidson, E. R. *J. Am. Chem. Soc.* **1977**, *99*, 4587.

(17) Neugebauer, F. A.; Fischer, H.; Krieger, C. *J. Chem. Soc. Perkin. Trans.* **1993**, *2*, 535.

(18) Mukai, K.; Konishi, K.; Nedachi, K.; Takeda, K. *J. Magn. Magn. Mater.* **1995**, *140*, 1449.

(19) Mukai, K.; Nedachi, K.; Takiguchi, M.; Kobayashi, T.; Amaya, K. *Chem. Phys. Lett.* **1995**, *238*, 61.

(20) Kremer, R. K.; Kanellakopulos, B.; Bele, P.; Brunner, H.; Neugebauer, F. A. *Chem. Phys. Lett.* **1994**, *230*, 255.

(21) Mito, M.; Nakano, H.; Kawae, T.; Hitaka, M.; Takagi, S.; Deguchi, H.; Suzuki, K.; Mukai, K.; Takeda, K. *J. Phys. Soc. Jpn.* **1997**, *66*, 2147.

(22) Mukai, K.; Nuwa, M.; Morishita, T.; Muramatsu, T.; Kobayashi, T. C.; Amaya, K. *Chem. Phys. Lett.* **1997**, *272*, 501.

(23) Jamali, J. B.; Achiwa, N.; Mukai, K.; Suzuki, K.; Ajiro, Y.; Matsuda, K.; Iwamura, H. *J. Magn. Magn. Mater.* **1998**, *177*, 789.

(24) Mukai, K.; Wada, N.; Jamali, J. B.; Achiwa, N.; Narumi, Y.; Kindo, K.; Kobayashi, T.; Amaya, K. *Chem. Phys. Lett.* **1996**, *257*, 538.

(25) Jamali, J. B.; Wada, N.; Shimobe, Y.; Achiwa, N.; Kuwajima, S.; Soejima, Y.; Mukai, K. *Chem. Phys. Lett.* **1998**, *292*, 661.

(26) Hamamoto, T.; Narumi, Y.; Kindo, K.; Mukai, K.; Shimobe, Y.; Kobayashi, T. C.; Muramatsu, T.; Amaya, K. *Physica B* **1998**, *246*, 36.

(27) Neugebauer, F. A.; Fischer, H.; Siegel, R. *Chem. Ber.* **1988**, *121*, 815.

(28) Serwinski, P. R.; Esat, B.; Lahti, P. M.; Liao, Y.; Walton, R.; Lan, J. *J. Org. Chem.* **2004**, *69*, 5247.

(29) Hicks, R. G.; Koivisto, B. D.; Lemaire, M. T. *Org. Lett.* **2004**, *12*, 1887.

(30) Hicks, R. G.; Hooper, R. *Inorg. Chem.* **1999**, *38*, 284.

(31) Gilroy, J. B.; McKinnon, S. D. J.; Kennepohl, P.; Zsombor, M. S.; Ferguson, M. J.; Thompson, L. K.; Hicks, R. G. *J. Org. Chem.* **2007**, *72*, 8062.

(32) Polo, V.; Alberola, A.; Andres, J.; Anthony, J.; Pilkington, M. *Phys. Chem. Chem. Phys.* **2008**, *10*, 857.

(33) Latif, I. A.; Panda A.; Datta S. N. *J. Phys. Chem. A* **2009**, *113*, 1595.

(34) Bhattacharya, D.; Misra, A. *Phys. Chem. A* **2009**, *113*, 5470.

(35) Bendikov, M.; Duong, H. M.; Starkey, K.; Houk, K. N.; Carter, E. A.; Wudl, F. *J. Am. Chem. Soc.* **2004**, *126*, 7416.

(36) Clar, E. *Polycyclic Hydrocarbons*, Academic Press: London, 1964, Vols. 1, 2.

(37) Hegmann, F. A.; Tykwinski, R. R.; Lui, K. P. H.; Bullock, J. E.; Anthony, J. E. *Phys. Rev. Lett.* **2002**, *89*, 227403.

(38) Houk, K. N.; Lee, P. S.; Nendel, M. *J. Org. Chem.* **2001**, *66*, 5517.

(39) Chung, G.; Lee, D. *Chem. Phys. Lett.* **2001**, *350*, 339.

(40) de Graaf, C.; Sousa, C.; Moreira, I. de P. R.; Illas, F. *J. Phys. Chem. A* **2001**, *105*, 11371.

(41) Noodleman, L. *J. Chem. Phys.* **1981**, *74*, 5737.

(42) Noodleman, L.; Baerends, E. J. *J. Am. Chem. Soc.* **1984**, 106, 2316.

(43) Ginsberg A. P. *J. Am. Chem. Soc.* **1980**, *102*, 111.

(44) Noodleman, L.; Peng, C. Y.; Case, D. A.; Mouesca, J.-M. *Coord. Chem. Rev.* **1995**, *144*, 199.

(45) Noodleman, L.; Davidson, E. R. *Chem. Phys.* **1986**, *109*, 131.

(46) Bencini, A.; Totti, F.; Daul, C. A.; Doclo, K.; Fantucci, P.; Barone, V. *Inorg. Chem.* **1997**, *36*, 5022.

(47) Bencini, A.; Gatteschi, D.; Totti, F.; Sanz, D. N.; McClevrty, J. A.; Ward, M. D. *J. Phys.Chem. A* **1998**, *102*, 10545.

(48) Ruiz, E.; Cano, J.; Alvarez, S.; Alemany, P. *J. Comput. Chem.* **1999**, *20*, 1391.

(49) Caballol, R.; Castell, O.; Illas, F.; Moreira, I. de P. R.; Malrieu, J. P. *J. Phys. Chem. A* **1997**, *101*, 7860.

(50) Moreira, I. de P. R.; Illas, F. *Phys. Chem. Chem. Phys.* **2006**, *8*, 1645.

(51) Illas, F.; Moreira, I. de P. R.; Bofill, J. M.; Filatov, M. *Phys. Rev. B* **2004**, *70*, 132414.

(52) Moreira, I. de P. R.; Costa, R.; Filatov, M.; Illas, F. *J. Chem. Theor. Comput.* **2007**, *3*, 764.

(53) Illas, F.; Moreira, I. de P. R.; Bofill J. M.; Filatov M. *Theor. Chem. Acc.* **2006**, *116*, 587.

(54) Yamaguchi, K.; Takahara, Y.; Fueno, T.; Nasu, K. *Jpn. J. Appl. Phys* **1987**, *26*, L1362.

(55) Yamaguchi, K; Tsunekawa, T.; Toyoda, Y.; Fueno, T. *Chem. Phys. Lett.* **1988**, *143*, 371.

(56) Yamaguchi, K.; Jensen, F.; Dorigo, A.; Houk, K. N. *Chem. Phys. Lett.* **1988**, *149*, 537.

(57) Yamaguchi, K.; Takahara, Y.; Fueno, T.; Houk, K. N. *Theor. Chim. Acta.* **1988**, *73*, 337.

(58) Ruiz, E.; Alvarez, S.; Cano, J.; Polo, V. *J. Chem. Phys.* **2005**, *123*, 164110.

(59) Adamo, C.; Barone, V.; Bencini, A.; Broer, R.; Filatov, M.; Harrison, N. M.; Illas, F.; Malrieu, J. P.; Moreira, I. de P. R. *J. Chem. Phys.* **2006**, *124*, 107101.

(60) Polo, V.; Gräfenstein, J.; Kraka, E.; Cremer, D. *Theor. Chem. Acc.* **2003**, *109*, 22.

(61) Gräfenstein, J.; Kraka, E.; Filatov, M.; Cremer, D. *Int. J. Mol. Sci.* **2002**, *3*, 360.

(62) Martin, R. L.; Illas, F. *Phys. Rev. Lett.* **1997**, *79*, 1539.

(63) Becke, A. D. *Phys. Rev. A* **1988**, *38*, 3098.

(64) Lee, C. T.; Yang, W. T.; Parr, R. G. *Phys. Rev. B* **1988**, *37*, 785.

(65) Becke, A. D. *J. Chem. Phys.* **1993**, *98*, 5648.

(66) Hehre, W. J.; Ditchfield, R.; Pople, J. A. *J. Chem. Phys.* **1972**, *56*, 2257.

(67) Hariharan, P. C.; Pople, J. A. *Theor. Chim. Acta* **1973**, *28*, 213.

(68) Francl, M. M.; Pietro, W. J.; Hehre, W. J.; Binkley, J. S.; Gordon, M. S.; Defrees, D. J.; Pople, J. A. *J. Chem. Phys.* **1982**, *77*, 3654.

(69) Frisch, M. J.; Trucks, G. W.; Schlegel, H. B.; Scuseria, G. E.; Robb, M. A.; Cheeseman, J. R.; Montgomery, J. A. Jr.; Vreven, T.; Kudin, K. N.; Burant, J. C.; Millam, J. M.; Iyengar, S. S.; Tomasi, J. J.; Barone, V.; Mennucci, B.; Cossi, M.; Scalmani, G.; Rega, N.; Petersson, G. A.; Nakatsuji, H.; Hada, M.; Ehara, M.; Toyota, K.; Fukuda, R.; Hasegawa, J ; Ishida, M.; Nakajima, T.; Honda, Y.; Kitao, O.; Nakai, H.; Klene, M.; Li, X.; Knox, J. E.; Hratchian, H. P.; Cross, J. B.; Bakken, V.; Adamo, C.; Jaramillo, J.; Gomperts, R.; Stratmann, R. E.; Yazyev, O.; Austin, A. J.; Cammi, R.; Pomelli, C.; Ochterski, J.; Ayala, P. Y.; Morokuma, K.; Voth, A.; Salvador, P.; Dannenberg, J. J.; Zakrzewski, V. G.; Dapprich, S.; Daniels, A. D.; Strain, M. C.; Farkas, O.; Malick, D. K.; Rabuck, A. D.; Raghavachari, K.; Foresman, J. B.; Ortiz, J. V.; Cui, Q.; Baboul, A. G.; Clifford. S.; Cioslowski, J.; Stefanov, B. B.; Liu, G.; Liashenko, A.; Piskorz, P.; Komaromi, I.; Martin, R. L.; Fox, D. J.; Keith, T.; Al-Laham, M. A.; Peng, C. Y.; Nanayakkara, A.; Challacombe, M.; Gill, P. M. W.; Johnson, B.; Chen, W.; Wong, M. W.; Gonzalez, C.; Pople, J. A. GAUSSIAN 03W (Revision D.01), Gaussian, Inc.: Wallingford, CT, (2004).

(70) Hyperchem Professional Release 7.5 for Windows; Hypercube Inc., Gainesville, 2002.

(71) Flükiger, P.; Lüthi, H. P.; Portmann, S.; Weber, J. MOLEKEL 4.0, J. Swiss Center for Scientific Computing, Manno, Switzerland, 2000.

(72) Brook, D. J. R.; Yee, G. T. *J. Org. Chem.* **2006**, *71*, 4889.

(73) Trindle, C.; Datta, S. N. *Int. J. Quantum Chem.* **1996**, *57*, 781.

(74) Trindle, C.; Datta, S. N.; Mallik, B. *J. Am. Chem. Soc.* **1997**, *119*, 12947.

(75) Wiberg, K. B. *Tetrahedron* **1968**, *24*, 1083.

(76) Lieb, E. H.; Mattis, D. C. *J. Math. Phys.* **1962**, *3*, 749.

(77) Ovchinnikov, A. A. *Theor. Chim. Acta* **1978**, *47*, 297.

(78) Klein, D. J.; Nelin, C.; Alexander, S.; Matsen, F. A. *J. Chem. Phys.* **1982**, *77*, 3101.

(79) Klein, D. J.; Alexander, S. A. *In Graph Theory and Topology in Chemistry*; King, R. B., Rouvay, D. H., Eds.; Elsevier: Amsterdam, The Netherlands, 1987; vol. 51, p 404. (80) Hoffmann, R.; Zeiss, G. D.; Van Dine, G. W. *J. Am. Chem. Soc.* **1968**, *90*, 1485.

(81) Borden, W. T.; Davidson, E. R. *Acc. Chem. Res.* **1981**, *14*, 69.

(82) Constantinides, C. P.; Koutentis, P. A.; Schatz, J. *J. Am. Chem. Soc.* **2004**, *126*, 16232.

(83) Hay, P. J.; Thibeault, C. J.; Hoffmann, R. *J. Am. Chem. Soc.* **1975**, *97*, 4884.

(84) Malloci, G.; Mulas, G.; Cappellini, G.; Joblin, C. *Chem. Phys.* **2007**, *340*, 43.

(85) Reddy, A. R.; Fridman-Marueli, G.; Benidikov, M. *J. Org. Chem.* **2007**, *72*, 51.

(86) Clar, E. *The Aromatic Sextet*, John Wiley and Sons, New York, 1970.

(87) Misra, A.; Klein, D. J.; Morikawa, T. *J. Phys. Chem. A* **2009**, *113*, 1151.

(88) Misra, A.; Schmalz, T. G.; Klein, D. J. *J. Chem. Inf. Model.* **2009**, *49*, 2670.

(89) Katrizky, A.; Barczymski, P.; Musumarra, G.; Pisano, D.; Szafran, M. *J. Am. Chem. Soc.* **1989**, *111*, 7.

(90) Schleyer, P. v. R.; Maerker, C.; Dransfeld, A.; Jiao, H.; Hommes, N. J. R. v. E. *J. Am. Chem. Soc.* **1996**, *118*, 6317.

(91) Schleyer, P. v. R.; Manoharan, M.; Jiao, H.; Stahl, F. *Org. Lett.* **2001**, *3*, 3643.

(92) Chen, Z.; Wannere, C. S.; Corminboeuf, C.; Puchta, R.; Schleyer, P. v. R. *Chem. Rev.* **2005**, *105*, 3842.

(93) Klein, D. J. *J. Chem. Edu.* **1992**, *69*, 691.

(94) Klein, D. J.; Babic, D. *J. Chem. Inf. Comp. Sci.* **1997**, *37*, 656.

(95) Poater, J.; García-Cruz, I.; Illas, F.; Solà, M. *Phys. Chem. Chem. Phys.* **2004**, *6*, 314.

(96) Feixas, F.; Matito, E.; Poater, J.; Solà, M. *J. Comp. Chem.* **2008**, *29*, 1543.

(97) Plater, M. J.; Kemp, S.; Coronado, E.; Gómez-García, C. J.; Harrington, R. W.; Clegg, W. *Polyhedron* **2006**, *25*, 2433.

(98) Neugebauer, F. A.; Fischer, H. *Angew. Chem. Int. Ed. Engl.* **1980**, *19*, 724.

(99) Valero, R.; Costa, R.; Moreira, I. de P. R.; Truhlar, D. G.; Illas, F. *J. Chem. Phys.* **2008**, *128*, 114103.

(100) Rivero, P.; Moreira, I. de P. R.; Illas, F.; Scuseria, G. E. *J. Chem. Phys.* **2008**, *129*, 184110.

(101) Ali, Md. E.; Datta, S. N. *J. Mol. Struct. (THEOCHEM)* **2006**, *775*, 1.

(102) Bhattacharya, D.; Shil, S.; Misra, A.; Klein, D. J. *Theor. Chem. Acc.* **2010**, *127*, 57.

Chapter 5

Influence of Aromaticity on the Magneto Structural Property of Heteroverdazyl Diradicals

This chapter describes theoretical design of 5 different meta phenylene coupled high spin bis-heteroverdazyl diradicals and their analogous para phenylene coupled low spin positional isomers. The geometry based aromaticity index, harmonic oscillator model of aromaticity (HOMA) values for both the couplers (local HOMA) and the whole diradicals (global HOMA) have been calculated for all diradicals. We also qualitatively relate these HOMA values with the intramolecular magnetic exchange coupling constants (J) which is calculated using broken symmetry approach within unrestricted density functional theory framework. Structural aromaticity index HOMA of linkage specific benzene rings in our designed diradical systems shows that the aromatic character depends on the planarity of the molecule and it controls the sign and magnitude of J. The effect of the spin leakage phenomenon on J and HOMA values of certain phosphaverdazyl systems has been explicitly discussed. We also estimate another aromaticity index, nucleus independent chemical shift (NICS) values for the phenylene coupler in each diradical and compare these values with that of HOMA.

5.1. Introduction

The term aromaticity is primarily used in a chemical sense in early 19th century to portray a special class of organic substances.[1,2] However, it remains a mystery to the scientific community even today as there is no unique definition of aromaticity and it is multidimensional in nature. Nevertheless, the aromaticity can be characterized through the properties like (a) planarity (b) total $(4n+2)\pi$ electrons (c) stabilization energie,[3,4] (d) bond length,[5] (e) magnetic exaltation,[6] (f) retention of π–electron delocalization after typical reactions[7] and so on. If any system has all the characteristics mentioned above then it is fully aromatic. The lack of proper definition leads one to assign different indices to quantify aromaticity; these include different structural indices such as HOMA which can reliably give the differences in aromaticity in more complicated systems.[8] HOMA quantifies the decrease in aromaticity with an increase in the bond length alternation and bond elongation.[9] Aromaticity can not only be illustrated by geometry based indices, but also a specified π–electron part in some greater π–electron structure may be affected by its structural environment.[8–10] Beside structural HOMA index nucleus independent chemical shift (NICS) is another widely used index of aromaticity because of its simplicity and efficiency.[11-13] It is well known that, the extent of aromaticity can be established experimentally by the ^{1}H NMR shift of aromatic and anti-aromatic compounds. This effect is a manifestation of the π-electron ring current of aromatic systems under the influence of external magnetic field. NICS can be widely used to identify aromaticity, non-aromaticity and anti-aromaticity of a single ring system and individual ring in polycyclic systems (local aromaticity).

The design and synthesis of high spin magnetic molecules of organic origin have attracted wide attention during last three decades.[14,15] The magnetic properties of a crystalline material are known to be controlled by the intermolecular interaction which depends on the structure and the nature of the crystal. Similarly, for diradical based magnets, magnetic properties are dependent on the intramolecular magnetic exchange interaction which in turn depends on the structure and topology of the molecule.[14] Stable organic radicals in pure state are the most suitable precursor for diradical based magnets. More specifically, stable diradical species based organic ferromagnets are of primary interest in the study of molecular

magnetism.[16] The first reported species of the stable magnetically active radical was β-crystal phase of *p*-nitrophenyl nitronyl nitroxide.[17] After its discovery by Kinosita and co-workers in 1991 nitronyl nitroxide based diradicals with different couplers have been extensively investigated and characterized by many group of researchers.[18-20] There were many investigations to synthesize other radical species such as verdazyl, imino nitroxide, tetrathiafulvalene which are stable at high temperature and are suitable candidates for preparing organic diradical based ferromagnets,[21-25] at relatively higher temperature.

Verdazyl radical has a prolonged history of magnetism as it is very stable and fulfills almost all the necessary requirements for being used as stable diradical based magnets.[26-30] In general, verdazyl based diradicals are known to have the structure as shown in Scheme 5.1. In recent years, lots of effort is given to synthesize and characterize the "so-called" heteroverdazyl radicals incorporating different hetero atoms in place of nitrogen and carbon ring atoms at X or Y position or the both.[31] The most common heteroverdazyls are oxoverdazyls, thioverdazyls and phosphaverdazyls which are in general considered as the inorganic analogue of verdazyl radical.

Oxoverdazyls have C=O substitution at the Y position which interacts with the heterocyclic π-system through the π^* orbital of C=O and in turn gives the observed stability and planarity of the radical.[16] 1,3,5-triphenyl-verdazyl and 1,3,5-triphenyl-oxoverdazyl radicals have been isolated and characterized.[32] It has been found that bis-oxoverdazyl diradical has singlet ground state. However, insertion of suitable coupler between the two radical centers results in the formation of diradical with triplet ground state.

Substitution of the oxygen atom of oxoverdazyl moiety with less electronegative sulfur atom gives thioverdazyl radical moiety with a notable variation of electron density from its oxo-analogue. Like other verdazyl derivatives, suitable choice of coupler gives stable thioverdazyl diradical with triplet ground state.[32,33]

In the case of phosphaverdazyls, one of the skeleton carbon atoms of verdazyl radical is replaced by phosphorus atom. There are two positions in verdazyl radical where carbon atom can be replaced by phosphorus atom. Hence, the two structurally different

phosphaverdazyls have been reported.[16] *Firstly*, the C=O group can be replaced by P=O group resulting a non planar phosphaverdazyl. *Secondly*, the carbon atom at the X position is replaced by P atom (Scheme 5.1). The second one has σ- and π-systems which mix with each other leading to the spin leakage from the P-atom.[31] Due to spin leakage the spin density of a particular atom at a particular site becomes lower than the expected spin density value of that particular site. The spin leakage has a profound effect on magnetic behavior of the concerned diradical. This phenomenon will be discussed later in this article. A number of different phosphaverdazyl radicals have been prepared and characterized by Hicks and co-workers. These radicals show characteristic EPR signal. Moreover, the hyperfine parameters of these systems and that of oxoverdazyl radicals are almost similar.[31] They have established that the method of synthesis of phosphaverdazyls is theoretically analogous with that of oxo- and thio-verdazyls.[32]

Scheme 5.1. Schematic diagrams of benzene coupled bis-heteroverdazyl systems, where the spacer is *meta* phenylene ring (S1) for Set-a diradicals (1a, 2a, 3a, 4a and 5a respectively) and *para* phenylene ring (S2) for Set-b diradicals (1b, 2b, 3b, 4b and 5b respectively). Substitution at 'X' and 'Y' positions gives rise to different "so-called" bis-heteroverdazyl diradical species. Here $\varphi_1$and φ_2 denotes the dihedral angle between the plane of spacer and that of the verdazyl radicals.

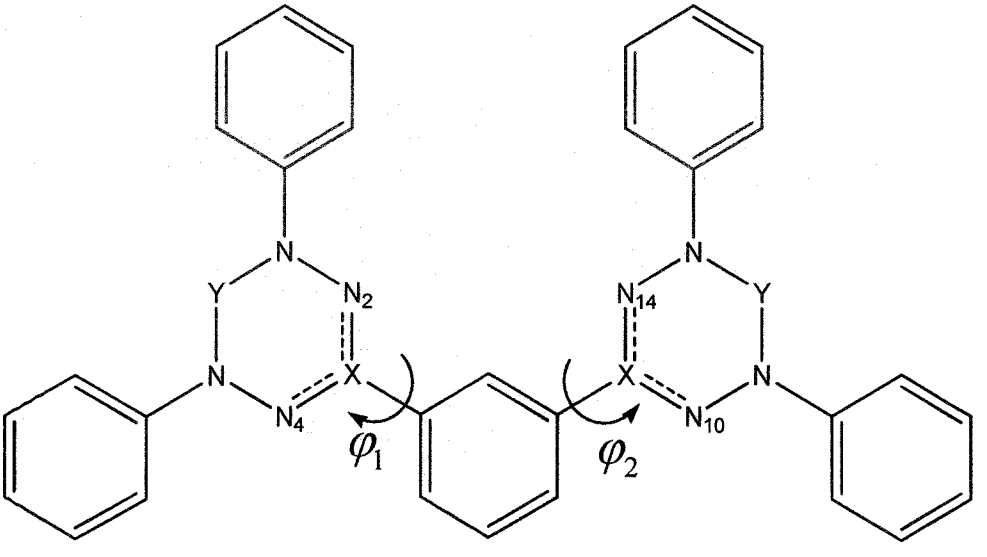

(S1)

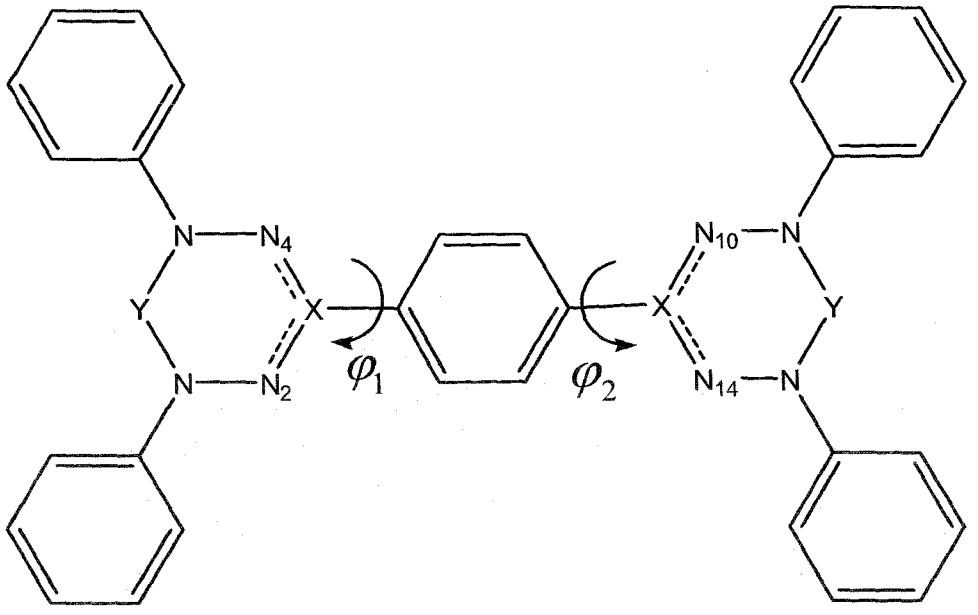

(S2)

In the present chapter, we design and theoretically characterize *meta*-phenylene coupled [Set-a denoted as 1(a), 2(a), 3(a), 4(a), 5(a)) and *para*-phenylene coupled (Set-b denoted as 1(b), 2(b), 3(b), 4(b), 5(b)] diradicals with verdazyl, oxoverdazyl, phosphaverdazyl and thioverdazyl radical centers (Figure 5.1 and also see Scheme 5.2). We design this type of heteroverdazyls based on the fact that very similar types of N-phenyl substituted verdazyl radicals, like 2,4,6-triphenylverdazyl radicals, have already been synthesized and characterized.[34-37] As far as the synthesis of these diradicals is concerned, the synthetic routes of verdazyl radicals with a range of substituents on the nitrogen and carbon atoms are well known. These radicals are air and moisture sustainable and can be easily handled in laboratory. However, magnetic properties of these diradicals have been determined by semi empirical methods.[31] Our primary aim of this chapter is to theoretically investigate the effect of aromaticity of the couplers and that of the molecules as a whole on the magnetic exchange between two monoradical moieties. We report the popular geometry based aromaticity index, Harmonic Oscillator Model of Aromaticity (HOMA)[9,38,39] individually for the couplers and the whole diradicals. We also calculate NICS values for the phenylene coupler in each diradical and compare them with HOMA. A qualitative correlation between the energy differences of two singly occupied molecular orbitals (SOMOs) with the J values has been given.

5.2. Theoretical Background and Methodology

The structural data for calculation of HOMA values of all the diradicals under discussion is taken from the optimized geometries of the diradicals. In this chapter, the molecular geometries of all the molecules (Set-a and Set-b) have been fully optimized with the UB3LYP[40,41] exchange correlation potential using 6-31G(d,p)[42-44] basis set. The optimized geometries are shown in Figure 5.1. The Harmonic Oscillator Model of Aromaticity (HOMA) is an easily accessible geometry based quantitative index of total aromaticity and is defined using the degree of bond length alteration. The advantage of HOMA over other energy based aromaticity index is due to the possibility of using HOMA either for the whole molecule (global HOMA) or for any fragment of the molecule (local HOMA) having π-electron networks. Nonetheless, it can not be limited only for the hydroca-

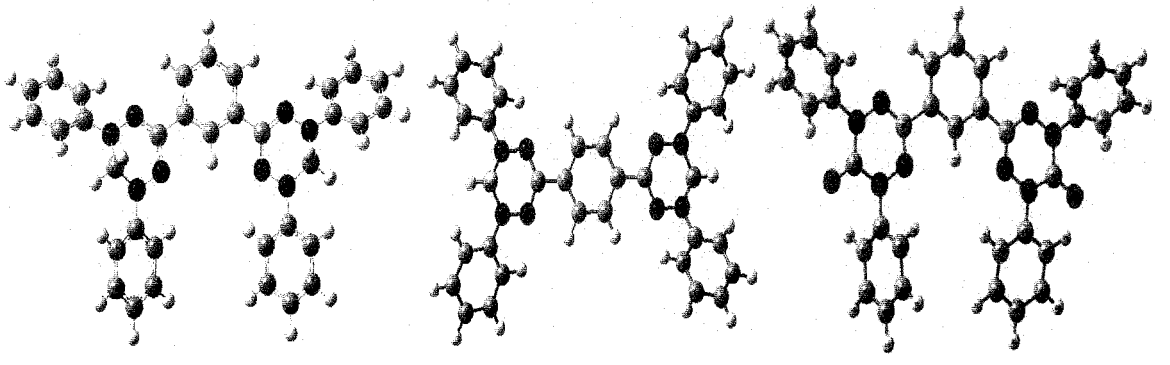

(1a) **(1b)** **2(a)**

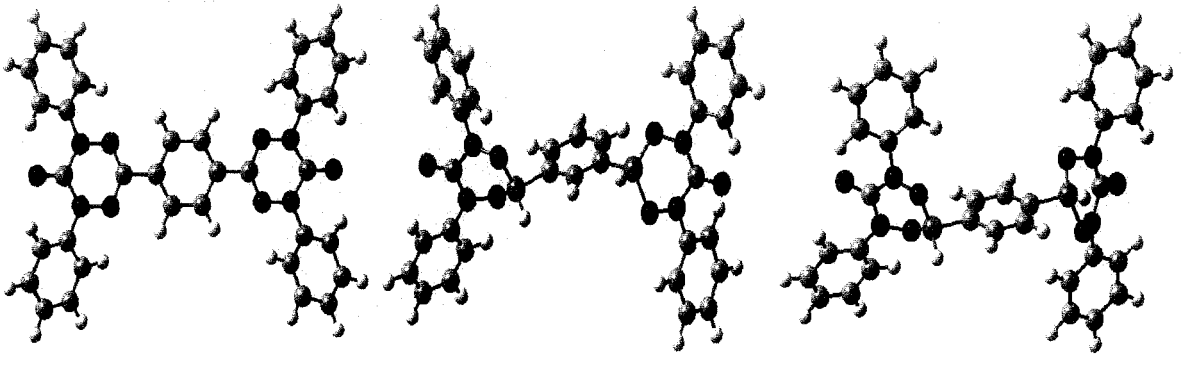

2(b) **(3a)** **(3b)**

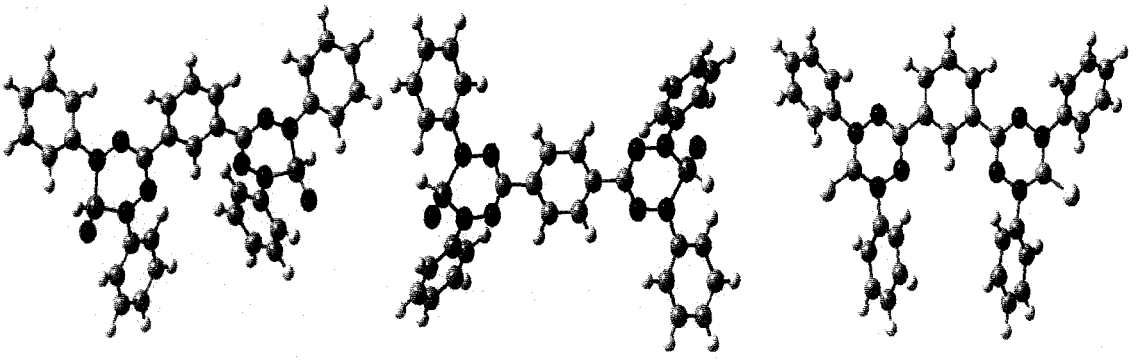

(4a) (4b) (5a)

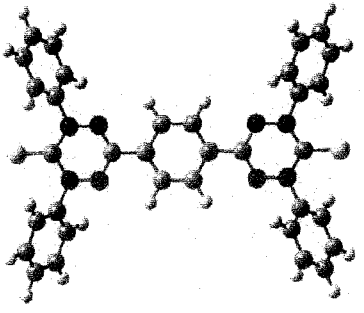

(5b)

Figure 5.1. The optimized geometries of different bis-heteroverdazyl diradical systems with m-phenylene coupler (Set-a: 1a, 2a, 3a, 4a and 5a) and with p-phenylene coupler (Set-b: 1b, 2b, 3b, 4b and 5b) from UB3LYP calculations with the 6-31G(d,p) basis set. The carbon atoms are marked in grey, sulfur in yellow, nitrogen in blue, oxygen in red, phosphorus in orange, and hydrogen in white respectively.

-rbon system. We choose HOMA aromaticity index because of its easy calculation and wide application.[38,39] The HOMA of a species can be calculated as,

$$\text{HOMA} = 1 - \alpha/n \sum (R_{opt} - R_{ij})^2, \quad (5.1)$$

where n is the number of bonds taken into summation, R_{opt} is the optimal bond for fully delocalized π–electron system, R_{ij} is the bond length of the molecule under investigation. HOMA is also a normalized index of aromaticity. It is known that HOMA value closer to the ideal value of 1 indicates the presence of greater aromaticity, whereas, HOMA value equal to

zero indicates non-aromatic system. The parameter α is an empirical constant set to give HOMA to be 0 and 1 for fully non-aromatic and fully aromatic systems respectively. It can also be noted here that, HOMA of bare benzene is 0.969, 0.979 and 0.996 from electron diffraction geometry, from MW (microwave) geometry and from X-ray geometry respectively.[38] In the present chapter, we have determined the HOMA values individually for the couplers and the whole diradicals, the details of which is given in results and discussion section.

In another way, the aromaticity of the couplers has been estimated by NICS index using UB3LYP/GIAO methodology with 6-31G(d,p) basis set for the phenylene coupler in each diradical. The NICS values can be calculated at the centre of the rings [NICS(0)]. The σ framework of C-C and C-H affects the π-electrons and hence NICS is calculated at 1Å above the ring surface [NICS(1)] where the π-electron density is known to be maximum.[11-13]

Using optimized geometries we also calculate the energies of different spin states of the diradical required for estimation of magnetic exchange coupling constant. The magnetic exchange interaction energy between two magnetic sites 1 and 2 is given by the well known Heisenberg-Dirac-van Vleck (HDvV) spin Hamiltonian

$$\hat{H} = -2J\hat{S}_1 \bullet \hat{S}_2, \tag{5.2}$$

where, J is the exchange coupling constant between two magnetic centers, $\hat{S}_i$ is the spin angular momentum operator of ith site. In case of ferromagnetic interaction between two parallel spins, J value is positive, whereas the negative J indicates an antiferromagnetic interaction between two antiparallel spins. The quantity J can be estimated from the energy difference of high spin and low spin states of the magnetically active molecule. As an example, J value of a diradical with single unpaired electron on each site can be written as

$$E_{(S=1)} - E_{(S=0)} = -2J. \tag{5.3}$$

However, pure singlet state of a diradical can not be truly represented by a single determinant (SD) wave function in the unrestricted formalism and this leads to spin contamination in such calculations. One may make use of multiconfigurational methods to describe pure spin states in an appropriate way. However, those methods are computationally expensive and generally not used for large systems. An alternative way is the Broken Symmetry (BS) formalism proposed by Noodleman in DFT framework.[45,46] The BS state is an equal mixture of a singlet and a triplet state and is not an eigenstate of the above Hamiltonian (eq 5.2). Nevertheless, the BS state is a spin contaminated state and one needs spin projection technique for reliable estimation of the magnetic exchange coupling constant. Depending upon the extent of overlap between the magnetic orbitals, J can be estimated in number of ways,[47-62] using unrestricted spin polarized BS solution for lower spin state. However, it has been established[19,20,34,60-64] unambiguously that the following formula by Yamaguchi and co-workers, is the most appropriate one for estimating magnetic exchange coupling constant of diradicals of organic origin. The formula is written as

$$J = \frac{(E_{BS} - E_T)}{\langle S^2 \rangle_T - \langle S^2 \rangle_{BS}}, \tag{5.4}$$

where E_{BS} and E_T denotes the energy of the broken symmetry state and triplet state respectively. The quantities $\langle S^2 \rangle_{BS}$ and $\langle S^2 \rangle_T$ represent square of the total spin for BS and triplet state respectively.

It is well known that commonly used DFT exchange correlation potentials overestimates J values due to the presence of high self interaction error (SIE). To avoid SIE problem, hybrid functionals such as B3LYP are used in BS-UDFT calculations, especially for spin projected techniques that are used to evaluate J.[65,66] Based on these molecular geometries the corresponding J values of each molecule have been estimated from the single point energies of the triplet and BS states. These single point calculations are carried out using UB3LYP method with 6-311++G(d,p) basis set. To obtain open shell BS singlet solution "guess =mix" keyword is used within unrestricted formalism. The BS states for all diradicals are stable. All the calculations have been carried out using GAUSSIAN 03W[67]

quantum chemical package. We also have used Hyperchem 7.5[68] and Molekel 4.0[69] for visualization.

5.3. Results and Discussion

In general, aromaticity depends on the topology of the molecules. Above all, a planar structure favors aromaticity. Here, we observe that the optimized structures of all the heteroverdazyl diradicals are nonplanar. This non planarity of the heteroverdazyls affects the aromaticity as well as the magnetic behavior of the diradical. In determining the sign and magnitude of J of the diradical the geometry of the spacer between two verdazyl moieties is the key factor.

In this present study, the HOMA values are calculated from the data of optimized structures. We have calculated the hitherto undetermined optimal bond lengths (R_{opt}) and the empirical constants α for PO and PN bonds using the experimentally determined single and double bond lengths of the PO and PN bonds. For this purpose we have used eq (6), (7), and (8) of ref. 38. These values are reported in Table 5.1. The experimental data for single and double bond lengths of PO and PN bonds are taken from the work of Hoppe et al.[70] and Markovski et al.[71] respectively.

Table 5.1. Reference single and double bond lengths and approximate optimal bond length, and empirical constant α.

Type of bond	$R_s^{\#}$	R_d^{*}	R_{opt}	α
PO	1.581[a]	1.432[a]	1.482	162.59
PN	1.770[b]	1.530[b]	1.610	62.5

[#]Single bond distance, *Double bond distance, [a]Data from ref. [70], [b]Values from ref. [71].

It has been observed that the HOMA values for phenylene couplers are higher in *meta*-connected diradicals than that in corresponding *para*-connected species (Table 5.2). This is probably due to the fact that π-electron delocalization is lower in *para*-connected diradicals than that of consequent *meta*-connected one. Therefore, one can easily infer that *meta*-connected couplers (Set-a) are more aromatic than the corresponding *para*-connected couplers (Set-b), that is, the delocalization of π–electrons is better among the *meta*-coupler moiety, which favors ferromagnetic interaction between the radical centers attached to the coupler due to itinerant exchange, hence, aromaticity favors the ferromagnetic trend.[19,64]

Table 5.2. Variation of HOMA values for couplers and for the whole diradicals at UB3LYP level of theory with 6-31G(d,p) basis set. Here $\varphi_1$and φ_2 are the dihedral angles (Scheme 5.1) between the two heteroverdazyl moieties with the plane of the coupler.

Set	Diradicals	HOMA for coupler	HOMA for the whole diradical	Dihedral Angle (deg)		
				φ_1	φ_2	Average
Set-a	(1a)	0.96488	0.71024	3.0604	3.0415	3.0510
	(2a)	0.96863	0.72301	6.2164	9.1013	7.6589
	(3a)	0.96822	0.66664	86.1027	86.2033	86.1530
	(4a)	0.96845	0.71712	9.5952	10.0079	9.8016
	(5a)	0.96515	0.74477	–0.3489	0.3824	0.0168
Set-b	(1b)	0.95898	0.70706	2.4790	2.4776	2.4783
	(2b)	0.96209	0.72536	0.5116	0.5116	0.5116
	(3b)	0.96520	0.65616	85.1074	85.1075	85.1075
	(4b)	0.96246	0.73659	0.8646	0.8633	0.8640
	(5b)	0.95807	0.74744	0.7353	0.7354	0.7354

It is established that the unpaired spins of verdazyls are equally distributed among magnetic centers comprising of the specified atoms (N_2, N_4, N_{10} and N_{14}, Scheme 5.1) of the diradicals[32] except the diradicals with phosphaverdazyl radical centers which shows the spin leakage from the phosphorous atom. In case of phosphaverdazyl diradicals, the spin distribution over the specific magnetic centers is unequal. This results in the low J value of the diradical.[24,31] The J values are calculated using eq (5.4). We observe that the more aromatic *meta*-connected molecules (Set-a) are ferromagnetically coupled while the less aromatic *para*-connected molecules (Set-b) are antiferromagnetically coupled. The calculated J values are reported in Table 5.3. These observations follow same trend as found in previous work with different diradicals.[19,20,33,64] A discussion on the magnetic properties of molecule 1(a) and 1(b) is due here. One can easily notice that the molecule (1a) is ferromagnetic whereas the molecule (1b) is antiferromagnetic, which strongly contradicts with the reports claiming that both the molecules possess triplet ground state with exchange energies in excess of 300K.[32,35-37] However, a relatively new experimental study on benzene bridged diradicals of very similar structure reveals that the *para*-connected diradical is antiferromagnetic whereas the *meta*-connected is ferromagnetic one. Our calculation is in good agreement with the later observation. This problem was addressed previously in a review by Koivisto and Hicks lacking a proper theoretical explanation.[32] We unequivocally settle this problem here.

The change in HOMA values with dihedral angle between the spacer plane and that of the radical moieties (Table 5.2) of the whole diradical molecule shows that aromaticity is highly disturbed in (3a) due to high average dihedral angle. This results in the lowest magnetic exchange coupling constant J = 02 cm^{-1} in diradical (3a). It is also evident that diradical (5a) have highest HOMA value with maximum J = 42 cm^{-1} (Table 5.3) among the ferromagnetic series for having low average dihedral angle between the coupler plane and the plane of the radical moieties. In case of diradical (1a) and (2a), as the global HOMA increases the J value also increases. Among the Set-b diradicals low global HOMA is observed for diradical (3b) with very high average dihedral angle. In any case, for all 10 different bis-heteroverdazyl diradicals, the HOMA values are smaller for the benzene acting as a linkage specific coupler between the two radical moieties (Table 5.2) than the HOMA value obtained for bare benzene i.e. $(HOMA)_{\text{coupler benzene}} < (HOMA)_{\text{bare benzene}}$ is observed.

Table 5.3. Calculated absolute energies in atomic unit (*au*), the $\langle S^2 \rangle$ value and intramolecular magnetic exchange coupling constant (J in cm^{-1}) using UB3LYP/6-31G(d,p) and 6-311++G(d,p) for different *meta*-connected (Set-a) and *para*-connected bis-heteroverdazyl diradicals (Set-b).

	At UB3LYP/6-31G(d,p) level			At UB3LYP/6-311++G(d,p) level		
Diradicals	E_{BS} (au)	E_T (au)	J(cm^{-1})	E_{BS} (au)	E_T (au)	J(cm^{-1})
	$\langle S^2 \rangle$	$\langle S^2 \rangle$		$\langle S^2 \rangle$	$\langle S^2 \rangle$	
(1a)	–1750.44633	–1750.44659	57	–1750.78001	–1750.78017	35
	1.049	2.050		1.045	2.047	
(2a)	–1898.47016	–1898.47023	15	–1898.90690	–1898.90708	39
	1.043	2.049		1.042	2.047	
(3a)	–2506.04818	–2506.04834	35	–2506.52823	–2506.52824	02
	1.014	2.014		1.014	2.014	
(4a)	–2506.17215	–2506.17216	02	–2506.64695	–2506.64714	41
	1.046	2.054		1.046	2.051	
(5a)	–2544.35946	–2544.35978	70	–2544.80009	–2544.80028	42
	1.043	2.049		1.043	2.047	
(1b)	–1750.39137	–1750.39105	–71	–1750.44770	–1750.44731	–87
	1.058	2.046		1.055	2.040	
(2b)	–1898.47136	–1898.47084	–115	–1898.90810	–1898.90776	–76
	1.053	2.042		1.051	2.039	
(3b)	–2506.04410	–2506.04405	–11	–2506.52368	–2506.52365	–07
	1.013	2.014		1.013	2.014	
(4b)	–2506.17349	–2506.17324	–55	–2506.64848	–2506.64814	–75
	1.057	2.046		1.055	2.044	
(5b)	–2544.36077	–2544.36063	–31	–2544.41592	–2544.41563	–64
	1.050	2.042		1.051	2.041	

A precise definition of aromaticity is not possible due to its multidimensional nature; hence there is no exact scale to measure it. Therefore, we have also calculated another aromaticity index NICS to comprehend the aromatic character of all the diradicals. Here, NICS(0) and NICS(1) values have been calculated for the phenylene coupler in all 10 bis-heteroverdazyl diradicals. Probes (dummy atoms) are placed at the centre of the ring to compute NICS(0) values and 1Å above the ring surface where π-orbital density is maximum to get NICS(1) values.[11-13] These values are reported in Table 5.4. Here, we also estimate NICS(0) and NICS(1) values for the bare benzene ring at same level of theory. These values are –9.82 and –11.32 respectively. Comparing these NICS values of bare benzene with that of the coupler benzene (Table 5.4), one can very easily surmise that $(NICS)_{coupler\ benzene}$ is less than $(NICS)_{bare\ benzene}$. This is also evident from HOMA values reported in Table 5.2. It is also to be concluded from Table 5.4 that, in every case NICS [NICS(0) and/or NICS(1)] values for the couplers of *meta*-phenylene coupled Set-a diradicals are more negative than their Set-b counterparts, that is, couplers of Set-a diradicals are more aromatic than their corresponding Set-b diradicals. These results are also in good agreement with the HOMA values (Table 5.2), that means HOMA correlates well with NICS.[9,10] From these results one can also conclude that as the couplers of the Set-a diradicals are more aromatic than corresponding Set-b diradicals aromaticity of the coupler favors the ferromagnetic trend which has already been established from the HOMA analysis.

Table 5.4. The calculated NICS(0) and NICS(1) values for the all the ten diradicals at UB3LYP level of theory using 6-31G(d,p) basis set.

Diradicals	NICS(0)	NICS(1)	Diradicals	NICS(0)	NICS(1)
1(a)	−7.60	−9.72	1(a)	−7.59	−9.59
2(a)	−7.90	−9.91	2(a)	−7.89	−9.84
3(a)	−8.54	−11.21	3(a)	−8.42	−11.18
4(a)	−7.87	−9.88	4(a)	−7.86	−9.76
5(a)	−7.98	−10.04	5(a)	−7.95	−10.00

Here we focus on the spin leakage of phosphaverdazyls. As mentioned earlier, Hicks and co-workers[31,32] have shown that due to spin leakage, density of electron spin on linkage phosphorus atom in (3a) and (3b) diradicals decreases in comparison with the spin density found on the linkage carbon atom at the same position of corresponding oxoverdazyls (2a) and (2b). A detail analysis of Mulliken spin densities of (2a) and (3a) diradicals shows a comparatively lower spin density over the P atom (–0.004048) of the phosphaverdazyl (3a) than that over the C atom of corresponding oxoverdazyl (–0.144519) (2a). At the same time, it is found that nitrogen atoms (N_2, N_4, N_{10} and N_{14} in Scheme 5.1) adjacent to P atom at position X in (3a) and (3b) bears more electron spin density than the corresponding nitrogen atoms (N_2, N_4, N_{10} and N_{14} in Scheme 5.1) adjacent to the carbon atom in X position in (2a) and (2b). In case of (3a) and (3b), the electron spin density is about 0.50703 on the nitrogen atoms N_2, N_4, N_{10} and N_{14} (Scheme 5.1) while on the corresponding nitrogen atoms in molecules (2a) and (2b), the electron spin density is about 0.37912. The overall average spin density on N atoms (N_2, N_4, N_{10} and N_{14}) is lower in case of (3a) and (3b) diradicals than that in case of (2a) and (2b) diradicals respectively. We notice that this spin delocalization effect is more clearly observable if one carries out simulations using diffused basis set. Incase of diradical (3a), we get a lower value of J from the calculations carried out using more diffused basis set 6-311++G(d,p) than that obtained from the calculations carried out using 6-31G(d,p) basis set. For the same reason, in case of (3b) the J value obtained from the calculations using 6-311++G(d,p) is higher than that obtained from the calculations using 6-31G(d,p) basis.

So far a quantitative estimation of aromaticity of the diradicals and its effect on magnetic exchange has been discussed. However, we reach at a very similar qualitative conclusion about the state of magnetism of the diradicals using spin alternation rule, which is essentially based on Hund's rule[72,74] The presence of even number of bonds between the two magnetic centers gives rise to ferromagnetic interactions but antiferromagnetism arises in case of odd number of bonds.[19,20] The existence of apparently two different spin polarization paths, presence of heteroatom in the spinning path and non planarity of the system makes the prediction of magnetic characteristics of molecular systems a tricky job.[74] However, Ali and Datta have explicitly shown that

using spin alternation rule qualitative prediction of magnetic characteristics of any diradical system can be given satisfactorily,[19,20] provided one takes into account of the fact that nitrogen, oxygen, sulfur like heteroatom may contribute two π-electrons depending on the bonding pattern, nature and topology of the coupler moiety.[19] In our present chapter, we explicitly show that according to the spin alternation rule molecules of Set-a, which are essentially *m*-phenylene coupled diradicals, give ferromagnetic interaction with positive J value and those of Set-b, that is *p*-phenylene coupled diradicals (Scheme 5.2), shows antiferromagnetic interaction with negative J value. The same can also be established by spin density plots (Figure 5.2). This estimation is supported by the results of our calculations as discussed earlier.

Scheme 5.2. Schematic representation of the ground spin states and the nature of the magnetic exchange coupling on the basis of spin alternation rule for different linkage specific phenylene bridged bis-heteroverdazyl diradicals.

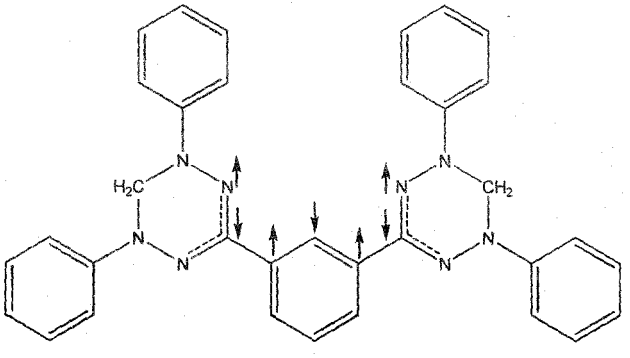

(1a)

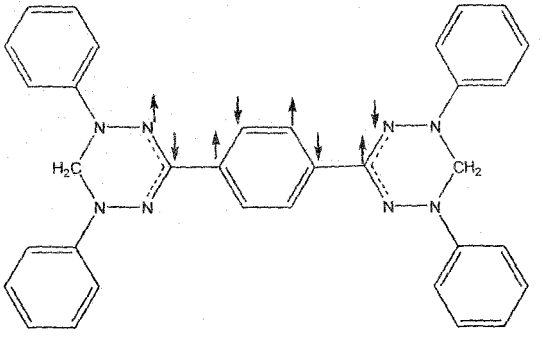

(1b)

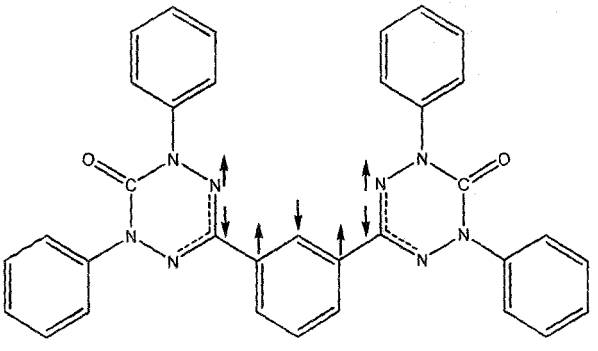

(2a)

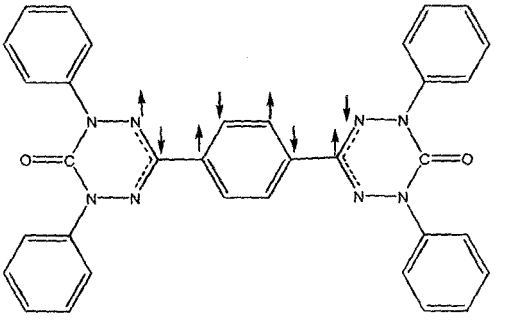

(2b)

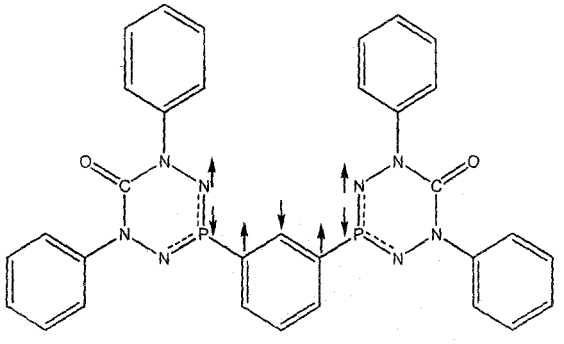

(3a)

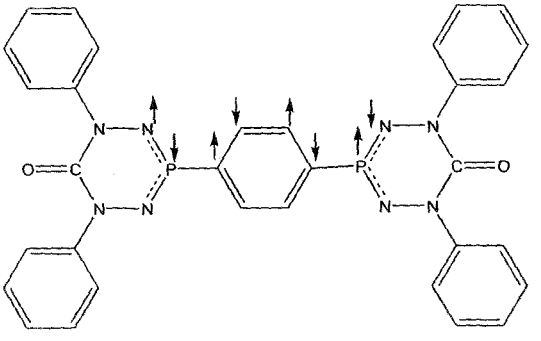

(3b)

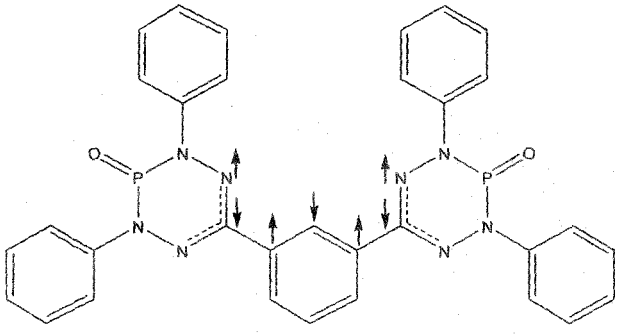

(4a)

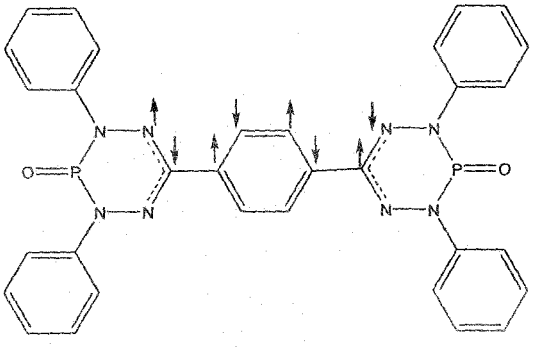

(4b)

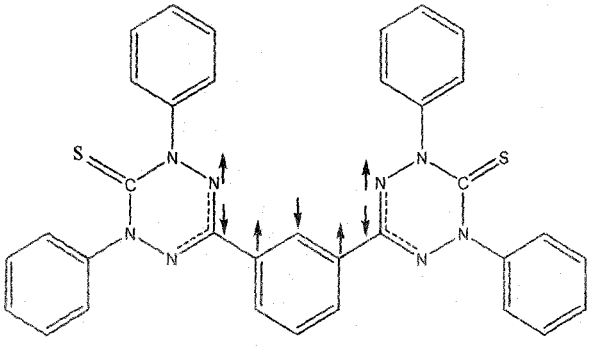

(5a)

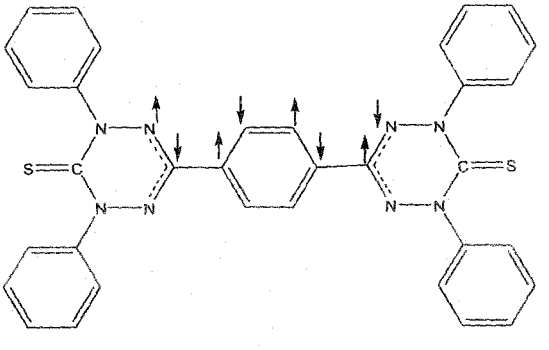

(5b)

On the basis of all valence electron independent particle model on benzyne and diradicals Hoffmann et al. have suggested that if the energy difference between two consecutive SOMOs is less than 1.5 *eV* parallel orientation of spins occur.[75] In another study, Constantinides et al.[76] have showed that for $4n\pi$ antiaromatic linear and angular polyheteroacenes ΔE_{SS} value will be greater than 1.3 *eV*, resulting in antiparallel orientation of spins. Using DFT calculations, however, Zhang et al.[77] have shown that the

magnetic characteristics of a molecule are not explicitly dependent on the critical value of ΔE_{SS} rather it is different in different cases. We find that for the ferromagnetic diradical series (Set-a) the calculated J values decreases as the ΔE_{SS} values increases, where both of the quantities (J and ΔE_{SS}) have been calculated using 6-31G(d,p) basis set at the

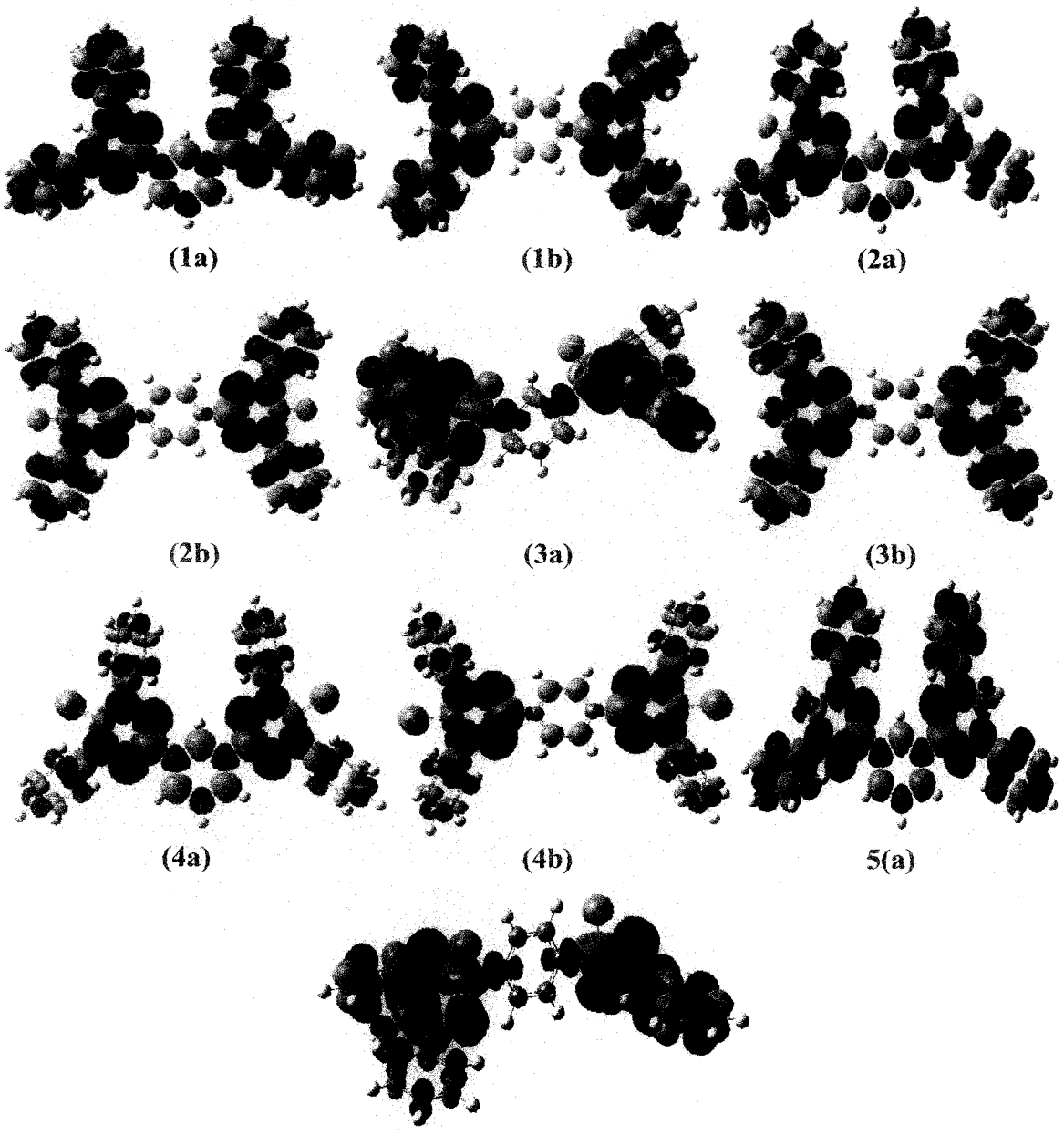

Figure 5.2. Spin density plots for different phenylene bridged bis-heteroverdazyl diradicals (Set-a and Set-b). Purple color indicates α–spin and green color indicates β–spin respectively. The cut off values for this all 10 figures were 0.0004.

UB3LYP level of theory. The highest J value is obtained for diradical (5a) with the lowest value of ΔE_{SS}. On the other hand, the lowest J with highest ΔE_{SS} is obtained in case of diradical (4a). In case of diradical (2a), (3a), and (4a), as ΔE_{SS} value decreases down the series the J value increases (Table 5.5). These observations prove that our calculations agree with the Hay-Thibeault-Hoffmann (HTH) formula[78] for the singlet–triplet energy gap in weakly coupled binuclear metal complexes. This observation is also in accordance with other previous theoretical work.[19,20,34,63,64]

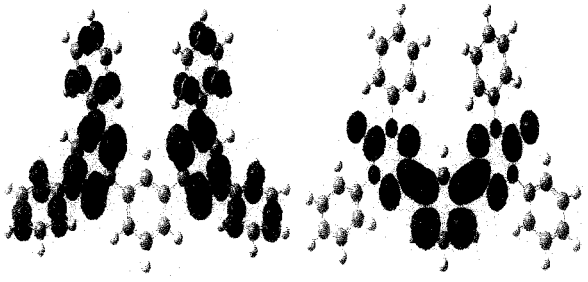

1(a) [Disjoint]

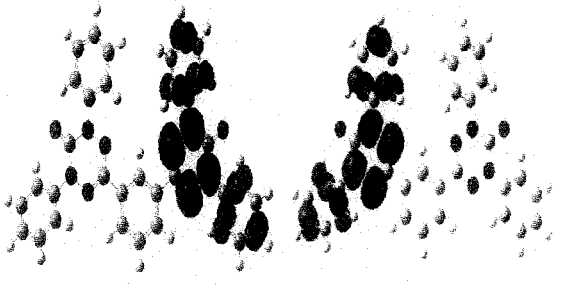

2(a) [Disjoint]

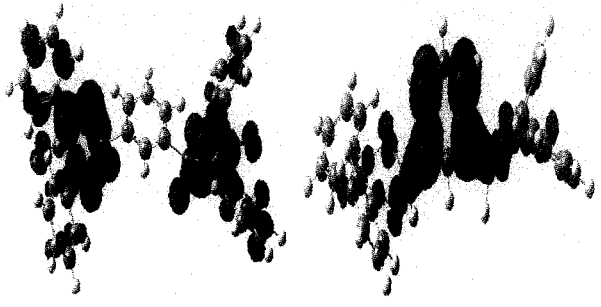

3(a) [Disjoint]

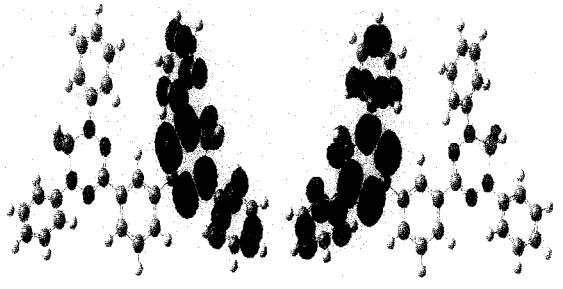

4(a) [Disjoint]

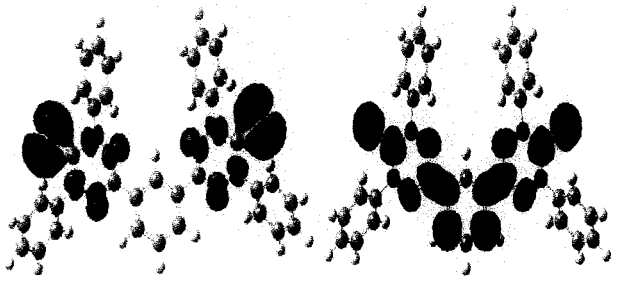

5(a) [Disjoint]

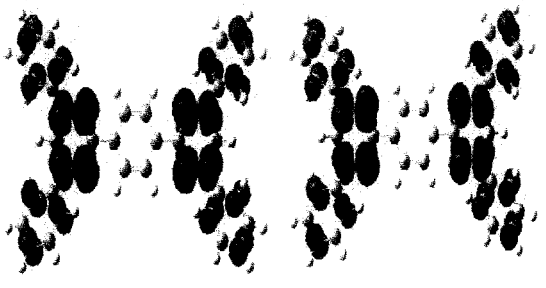

1(b) [Nondisjoint]

2(b) [Nondisjoint] **3(b) [Nondisjoint]**

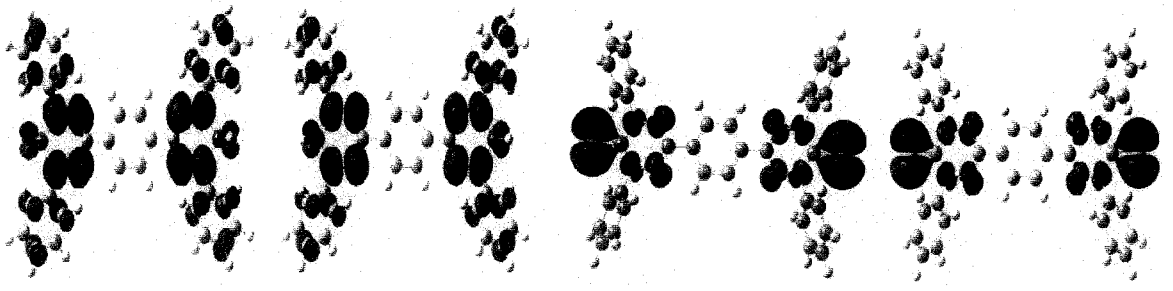

4(b) [Nondisjoint] **5(b) [Nondisjoint]**

Figure 5.3. The triplet disjoint and triplet nondisjoint sets of SOMOs for Set-a [1(a), 2(a), 3(a), 4(a) and 5(a)] and set-b [1(b), 2(b), 3(b), 4(b) and 5(b)] bis-heteroverdazyl diradicals. The diagrams are generated from the results of the calculation carried out using UB3LYP level of theory and 6-31G(d,p) basis set. The cut off values for this all 10 figures were 0.0004.

The shapes of the SOMOs (Figure 5.3) play a major role in determining the magnetic properties of the diradicals. We find that the SOMOs are disjoint (atoms are not common) for Set-a diradicals and nondisjoint (atoms are common) for Set-b diradicals. As a consequence, the diradicals of Set-a are ferromagnetic and that of Set-b are antiferromagnetic. These observations are also in tune with the previous studies[19,64] as well as with our present numerical calculations.

We investigate the energy difference between the highest occupied molecular orbital (HOMO) and lowest unoccupied molecular orbital (LUMO) energy gap of all the 10 molecules (Table 5.6). The HOMO–LUMO energy gap determines the fate of

numerous chemical reactions.[79] Consequently HOMO–LUMO energy gap is used as a simple indicator of kinetic stability. If the energy gap is high, it signifies high kinetic stability as well as low chemical reactivity and hence more aromatic.[80] The energy gap also corresponds to the chemical hardness of the molecule.[81] From Table 5.6, it is evident

Table 5.5. Absolute energies of SOMOs in atomic unit (*au*) and their differences in electron volt (*eV*) along with the *J* values (in cm^{-1}) for different bis-heteroverdazyl diradicals (Set-a and Set-b). All calculations are done using UB3LYP level of theory with 6-31G(d,p) basis set.

Diradicals	$E_S(1)$ *au*	$E_S(2)$ *au*	ΔE_{SS} in *eV*	$J(cm^{-1})$
(1a)	–0.16661	–0.16658	0.00082	57
(2a)	–0.19242	–0.19133	0.02966	15
(3a)	–0.20213	–0.20170	0.01170	35
(4a)	–0.18867	–0.18715	0.04136	02
(5a)	–0.19915	–0.19913	0.00054	70
(1b)	–0.16729	–0.16660	0.01878	–71
(2b)	–0.19262	–0.19161	0.02748	–115
(3b)	–0.20117	–0.20030	0.02367	–11
(4b)	–0.18814	–0.18715	0.02694	–55
(5b)	–0.20003	–0.19891	0.03048	–31

that all the Set-a diradicals have higher HOMO–LUMO energy gap than the corresponding antiferromagnetic Set-b series, which implies that the ferromagnetic Set-a diradicals are kinetically more stable, that is, chemically less reactive and more aromatic in comparison with the corresponding Set-b diradicals. It is also known that the molecules having HOMO–LUMO energy gap of the order of 1.59-3.18 *eV* can be suitable candidates for optoelectronic devices.[82] In that respect, more judicious designing of molecules may come up with good candidates for such applications. We hope to report such molecules in near future.

Table 5.6. The HOMO and LUMO energies in atomic unit (*au*) and their difference in electron volt (*eV*) for different bis-heteroverdazyl diradicals at UB3LYP level of theory with 6-31G(d,p) basis set.

Set	Diradicals	E_{HOMO} in *au*	E_{LUMO} in *au*	$\Delta E_{H\text{-}L}$ in *eV*
Set-a	(1a)	–0.16658	–0.02665	3.80772
	(2a)	–0.19133	–0.05166	3.80064
	(3a)	–0.20170	–0.06673	3.67275
	(4a)	–0.18715	–0.03821	4.05290
	(5a)	–0.19913	–0.06728	3.58785
Set-b	(1b)	–0.16660	–0.03767	3.50839
	(2b)	–0.19161	–0.06389	3.47547
	(3b)	–0.20030	–0.07653	3.36798
	(4b)	–0.18715	–0.05006	3.73044
	(5b)	–0.19891	–0.07854	3.27546

Table 5.7. Ground state energies of heteroverdazyl diradicals determined from the results of single point UB3LYP/6-311++G(d,p) calculations.

Set-a	E_T in *au*	Set-b	Estimated E_s in *au*
(1a)	–1750.78017	(1b)	–1750.44810
(2a)	–1898.90708	(2b)	–1898.90841
(3a)	–2506.52824	(3b)	–2506.52371
(4a)	–2506.64714	(4b)	–2506.64882
(5a)	–2544.80028	(5b)	–2544.41621

We have compared the ground state stability of the two different types of diradicals (Table 5.7). In general, ferromagnetic diradicals show grater stability than their antiferromagnetic counterparts. However, a little bit of over estimation of the energy value of the singlet state (E_S) is observed in two cases. Nonetheless, the estimated E_S values for Set-b diradicals are lower than the respective computed triplet state energy values (E_T), that is, singlet ground states for Set-b diradicals are confirmed.

5.4. Conclusions

This chapter presents a theoretical study of correlation between structural aromaticity index HOMA and intramolecular magnetic exchange coupling in *m*-phenylene and *p*-phenylene coupled bis-heteroverdazyl diradicals. The HOMA index which depends on the structure of the molecules is estimated for the whole diradical molecules and their aromatic coupler fragments to show how intramolecular magnetic interaction is dependent on the aromatic character of the diradical. The HOMA values suggest that increase of aromaticity is associated with the enhancement of ferromagnetism, that is, aromaticity favors ferromagnetic trend in such systems. It can be observed that low HOMA value is observed in case of diradical (3a) and (3b), where spin leakage is prominent. Resembling structural aromaticity index HOMA, the magnetic aromaticity index nucleus independent chemical shift (NICS) also shows that the ferromagnetism is instigated by the aromaticity of the coupler of the diradicals.

In this chapter we find, Set-a diradicals are ferromagnetic where as Set-b diradicals are antiferromagnetic in nature. The exchange-coupling interactions are mainly transmitted through conjugated π-electron system as observed and justified by other authors.[19,20,34,41,42,44] We also show that the low J values for bis-phosphaverdazyl diradicals are due to the spin leakage[27,34] from the phosphorus atom to the spin bearing nitrogen atom of phosphaverdazyl radical center. Here, the effective spin transmission is clearly represented from the strong spin density alternation pattern (Figure 5.2), as obvious from the MO analysis. For each species, a qualitative relation between SOMO–SOMO energy gaps with J values has been made. The shapes of SOMOs also play a

function to predict the state of magnetism (Figure 5.3). One also observes that the variation of average dihedral angles of the radical centers with the coupler plane determines the magnitude of J values. The kinetic stability as well as low chemical reactivity of Set-a diradicals than those of Set-b diradicals has been discussed in light of HOMO–LUMO energy gap. Finally, the ground state stability of these diradicals has also been investigated.

This work has been published in The Journal of Physical Chemistry A (Ref. 83).

5.5. References and Notes

(1) Kekulé, A. *Bull. Soc. Chim. Fr.* **1865**, *3*, 98.

(2) Erlenmeyer, E. *Ann. Chem. Pharm.* **1866**, *137*, 327.

(3) Pauling, L. *The Nature of the Chemical Bond and Structure of Molecules in Crystals*, Cornell University Press: Ithaca, pp 188ff, 1960.

(4) Cyrański, M. K.; Krygowski, T. M.; Katritzky, A. R.; Schleyer, P. v. R. *J. Org. Chem.* **2002**, *67*, 1333.

(5) Bird, C. W. *Tetrahedron* **1985**, *41*, 1409.

(6) Flygare, W. H. *Chem. Rev.* **1974**, *74*, 653.

(7) Breslow, R. *Angew. Chem. Int. Ed. Engl.* **1968**, *80*, 573.

(8) Krygowski, T. M.; Zachara, J. E.; Szatylwicz, H. *J. Org. Chem.* **2004**, *69*, 7038.

(9) Krygowski, T. M.; Cyrański, M. K. *Chem. Rev.* **2001**, *101*, 1385.

(10) Krygowski, T. M.; Cyrański, M. K. *Phys. Chem. Chem. Phys.* **2004**, *6*, 249.

(11) Chen, Z.; Wannere, C. S.; Corminboeuf, C.; Puchta, R.; Schleyer, P. v. R. *Chem. Rev.* **2005**, *105*, 3842.

(12) Schleyer, P. v. R.; Manoharan, M.; Jiao, H.; Stahl, F. *Org. Lett.* **2001**, *3*, 3643.

(13) Schleyer, P. v. R.; Maerker, C.; Dransfeld, A.; Jiao, H.; Hommes, N. J. R. v. E. *J. Am. Chem. Soc.* **1996**, *118*, 6317.

(14) Kahn, O. *Molecular Magnetism*, New York, VCH, 1993.

(15) Coronado, E.; Delhaè, P.; Gatteschi, D.; Miller, J. S. *Molecular Magnetism: From Molecular Assemblies to the Devices*, Eds.; Nato ASI Series E, Applied Sciences, Kluwer Academic Publisher: Dordrecht, Netherland, **1996**; Vol. 321.

(16) Hicks, R. G.; Ohrstrom, L.; Patenaude, G. W. *Inorg. Chem.* **2001**, *40*, 1865.

(17) Tamura, M.; Nakazawa, Y.; Shiomi, D.; Nozawa, K.; Hosokoshi, Y.; Ishikawa, M.; Takahashi, M.; Kinoshita, M. *Chem. Phys. Lett.* **1991**, *186*, 401.

(18) Ziessel, R.; Stroh, C.; Heise, H.; Khler, F. H.; Turek, P.; Claiser, N.; Souhassou, M.; Lecomte, C. *J. Am. Chem. Soc.* **2004**, *126*, 12604.

(19) Ali, Md. E.; Datta, S. N. *J. Phys. Chem. A* **2006**, *110*, 2776.

(20) Ali, Md. E.; Datta, S. N. *J. Phys. Chem. A* **2006**, *110*, 13232.

(21) Kuhn, R.; Trischmann, H. *Angew. Chem. Int. Ed. Engl.* **1963**, *2*, 155.

(22) Nesterenko, A. M.; Polumbrik, O. M.; Markovskii, L. M. *J. Struct. Chem.* **1984**, *25*, 209.

(23) Neugebauer, F. A.; Fischer, H.; Siegel, R. *Chem. Ber.* **1988**, *121*, 815.

(24) Koivisto, B. D.; Ichimura, A. S.; McDonald, R.; Lemaire, M. T.; Thompson, L. K.; Hicks, R. G. *J. Am. Chem. Soc.* **2006**, *128*, 690.

(25) Barclay, T. M.; Hicks, R. G.; Ichimura, A. S.; Patenaude, G. W. *Can. J. Chem.* **2002**, *80*, 1501.

(26) Azuma, N. *Bull. Chem. Soc. Jpn.* **1982**, *55*, 1357.

(27) Takeda, K.; Hamano, T.; Kawae, T.; Hidaka, M.; Takahashi, M.; Kawasaki, S.; Mukai, K. *J. Phys. Soc. Jpn.* **1995**, *64*, 2343.

(28) Mukai, K.; Konishi, K.; Nedachi, K.; Takeda, K. *J. Phys. Chem.* **1996**, *100*, 9658.

(29) Brook, D. J. R.; Fox, H. H.; Lynch, V.; Fox, M. A. *J. Phys. Chem.* **1996**, *100*, 2066.

(30) Serwinski, P. R.; Esat, B.; Lahti, P. M.; Liao, Y.; Walton, R.; Lan, J. *J. Org. Chem.* **2004**, *69*, 5247.

(31) Hicks, R. G.; Hooper, R. *Inorg. Chem.* **1999**, *38*, 284.

(32) Koivisto, B. D.; Hicks, R. G. *Coord. Chem. Rev.* **2005**, *249*, 2612.

(33) Bhattacharya, D.; Shil, S.; Misra, A.; Klein, D. J. *Theor. Chem. Acc.* **2009**, *127*, 57.

(34) Katritzky, A. R.; Belyakov, S. A.; Durst, H. D.; Xu, R.; Dalal, N. S. *Can. J. Chem.* **1994**, *72*, 1849.

(35) Kopf, P.; Morokuma, K.; Kreilick, R. *J. Chem. Phys.* **1971**, *54*, 105.

(36) Azuma, N.; Ishizu, K.; Mukai, K. *J. Chem. Phys.* **1974**, *61*, 2294.

(37) Fico, R. M., Jr.; Hay, M. F.; Reese, S.; Hammond, S.; Lambert, E.; Fox, M. A.; *J. Org. Chem.* **1999**, *64*, 9386.

(38) Krygowski, T. M. *J. Chem. Inf. Comput. Sci.* **1993**, *33*, 70.

(39) Kruszewski, J.; Krygowski, T. M. *Bull. Acad. Pol. Sci. Ser. Sci. Chim.* **1972**, *20*, 907.

(40) Lee, C. T.; Yang, W. T.; Parr, R. G. *Phys. Rev. B* **1988**, *37*, 785.

(41) Becke, A. D. *J. Chem. Phys.* **1993**, *98*, 5648.

(42) Hehre, W. J.; Ditchfield, R.; Pople, J. A. *J. Chem. Phys.* **1972**, *56*, 2257.

(43) Hariharan, P. C.; Pople, J. A. *Theor. Chim. Acta.* **1973**, *28*, 213.

(44) Francl, M. M.; Pietro, W. J.; Hehre, W. J.; Binkley, J. S.; Gordon, M. S.; Defrees, D. J.; Pople, J. A. *J. Chem. Phys.* **1982**, *77*, 3654.

(45) Noodleman, L. *J. Chem. Phys.* **1981**, *74*, 5737.

(46) Noodleman, L.; Baerends, E. J. *J. Am. Chem. Soc.* **1984**, *106*, 2316.

(47) Ginsberg, A. P. *J. Am. Chem. Soc.* **1980**, *102*, 111.

(48) Noodleman, L.; Davidson, E. R. *Chem. Phys.* **1986**, *109*, 131.

(49) Noodleman, L.; Peng, C. Y.; Case, D. A.; Mouesca, J. -M. *Coord. Chem. Rev.* **1995**, *144*, 199.

(50) Bencini, A.; Totti, F.; Daul, C. A.; Doclo, K.; Fantucci, P.; Barone, V. *Inorg. Chem.* **1997**, *36*, 5022.

(51) Bencini, A.; Gatteschi, D.; Totti, F.; Sanz, D. N.; McClevrty, J. A.; Ward, M. D. *J. Phys. Chem. A* **1998**, *102*, 10545.

(52) Ruiz, E.; Cano, J.; Alvarez, S.; Alemany, P. *J. Comput. Chem.* **1999**, *20*, 1391.

(53) Martin, R. L.; Illas, F. *Phys. Rev. Lett.* **1997**, *79*, 1539.

(54) Caballol, R.; Castell, O.; Illas, F.; de Moreira, I. P. R.; Malrieu, J. P. *J. Phys. Chem. A* **1997**, *101*, 7860.

(55) Barone, V.; di Matteo, A.; Mele, F.; de Moreira, I. P. R.; Illas, F. *Chem. Phys. Lett.* **1999**, *302*, 240.

(56) Illas, F.; de Moreira, I. P. R.; de Graaf, C.; Barone, V. *Theor. Chem. Acc.* **2000**, *104*, 265.

(57) de Graaf, C.; Sousa, C.; de Moreira, I. P. R.; Illas, F. *J. Phys. Chem. A* **2001**, *105*, 11371.

(58) Illas, F.; de Moreira, I. P. R.; Bofill, J. M.; Filatov, M. *Phys. Rev. B* **2004**, *70*, 132414.

(59) Ciofini, I.; Daul, C. A. *Coord. Chem. Rev.* **2003**, *238*, 187.

(60) Yamaguchi, K.; Takahara, Y.; Fueno, T.; Nasu, K. *Jpn. J. Appl. Phys.* **1987**, *26*, L1362.

(61) Yamaguchi, K.; Jensen, F.; Dorigo, A.; Houk, K. N. *Chem. Phys. Lett.* **1988**, *149*, 537.

(62) Yamaguchi, K.; Takahara, Y.; Fueno, T.; Houk, K. N. *Theor. Chim. Acta.* **1988**, *73*, 337.

(63) Latif, I. A.; Panda, A.; Datta, S. N. *J. Phys. Chem. A* **2009**, *113*, 1595.

(64) Bhattacharya, D.; Misra, A. *J. Phys. Chem.* A **2009**, *113*, 5470.

(65) Gräfenstein, J.; Kraka, E.; Filatov, M.; Cremer, D. *Int. J. Mol. Sci.* **2002**, *3*, 360.

(66) Ruiz, E.; Alvarez, S.; Cano, J.; Polo, V. *J. Chem. Phys.* **2005**, *123*, 164110.

(67) Frisch, M. J.; Trucks, G. W.; Schlegel, H. B.; Scuseria, G. E.; Robb, M. A.; Cheeseman, J. R.; Montgomery, J. A. Jr.; Vreven, T.; Kudin, K. N.; Burant, J. C.; Millam, J. M.; Iyengar, S. S.; Tomasi, J. J.; Barone, V.; Mennucci, B.; Cossi, M.; Scalmani, G.; Rega, N.; Petersson, G. A.; Nakatsuji, H.; Hada, M.; Ehara, M.; Toyota, K.; Fukuda, R.; Hasegawa, J ; Ishida, M.; Nakajima, T.; Honda, Y.; Kitao, O.; Nakai, H.; Klene, M.; Li, X.; Knox, J. E.; Hratchian, H. P.; Cross, J. B.; Bakken, V.; Adamo, C.; Jaramillo, J.; Gomperts, R.; Stratmann, R. E.; Yazyev, O.; Austin, A J.; Cammi, R.; Pomelli, C.; Ochterski, J.; Ayala, P. Y.; Morokuma, K.; Voth, A.; Salvador, P.; Dannenberg, J. J.; Zakrzewski, V. G.; Dapprich, S.; Daniels, A. D.; Strain, M. C.; Farkas, O.; Malick, D. K.; Rabuck, A. D.; Raghavachari, K.; Foresman, J. B.; Ortiz, J. V.; Cui, Q.; Baboul, A. G.; Clifford. S.; Cioslowski, J.; Stefanov, B. B.; Liu, G.; Liashenko, A.; Piskorz, P.; Komaromi, I.; Martin, R. L.; Fox, D. J.; Keith, T.; Al-Laham, M. A.; Peng, C. Y.; Nanayakkara, A.; Challacombe, M.; Gill, P. M. W.; Johnson, B.; Chen, W.; Wong, M. W.; Gonzalez, C.; Pople, J. A. GAUSSIAN 03W (Revision D.01), Gaussian, Inc.:Wallingford, CT, (2004). Gaussian Inc., Wallingford, CT.

(68) Hyperchem Professional Release 7.5 for Windows, Hypercube Inc.: Gainesville, FL, 2002.

(69) Flükiger, P.; Lüthi, H. P.; Portmann, S.; Weber, J. MOLEKEL 4.0, J. Swiss Center for Scientific Computing, Manno, Switzerland, 2000.

(70) Hoppe, U.; Walter, G.; Barz, A.; Stachel, D.; Hannon, A. C. *J. Phys. Cond. Mat.* **1998**, *10*, 261.

(71) Markovski, L. N.; Romanenko, V. D.; Ruban, A. V. *Pure. Appl. Chem.* **1987**, *59*, 1047.

(72) Trindle, C.; Datta, S. N. *Int. J. Quantum Chem.* **1996**, *57*, 781.

(73) Trindle, C.; Datta, S. N.; Mallik, B. *J. Am. Chem. Soc.* **1997**, *119*, 12947.

(74) Polo, V.; Alberola, A.; Andres, J.; Anthony, J.; Pilkington, M. *Phys. Chem. Chem. Phys.* **2008**, *10*, 857.

(75) Hoffmann, R.; Zeiss, G. D.; Van Dine, G. W. *J. Am. Chem. Soc.* **1968**, *90*, 1485.

(76) Constantinides, C. P.; Koutentis, P. A.; Schatz, J. *J. Am. Chem. Soc.* **2004**, *126*, 16232.

(77) Zhang, G.; Li, S.; Jiang, Y. *J. Phys. Chem. A* **2003**, 107, 5573.

(78) Hay, P. J.; Thibeault, C. J.; Hoffmann, R. *J. Am. Chem. Soc.* **1975**, *97*, 4884.

(79) Fukai, K.; Yonezawa, T.; Shingu, H. *J. Am. Chem. Soc.* **1952**, *93*, 2413.

(80) Aihara, J. *J. Phys. Chem. A* **1999**, *103*, 7487.

(81) Zhou, Z.; Parr, R. G. *J. Am. Chem. Soc.* **1990**, *112*, 5720.

(82) Salcedo, R. *J. Mol. Model.* **2007**, *13*, 1027.

(83) Bhattacharya, D.; Shil, S.; Panda, A.; Misra, A. *J. Phys. Chem. A.* **2010**, *114*, 11833.

Chapter 6

Photoresponsive Magnetic Crossover

In this chapter we present density functional theory based calculations on 6 diradicals in which imino nitroxide (IN) and IN or oxo- or phospha-verdazyl radical centers are linked by fragments of structures called cyan, blue and green fluorescent protein respectively. The photoinduced cis-trans isomerization of these diradical substituted chromophores is accompanied by changes from antiferro- to ferro-magnetic spin coupling on the radical centers. Moreover, upon irradiation with light of appropriate wavelength, the dark trans diradicals turn into their fluorescent cis isomers. Therefore, photoinduced magnetic crossover from antiferromagnetic to ferromagnetic regime associated with the change in color would be noticed in all three cases. This is a novel observation in case of the systems with green fluorescent protein chromophore and its variants. The change in color associated with magnetic crossover for these diradicals increases their suitability as biological taggers.

6.1. Introduction

Photoresponsive green fluorescent protein (GFP) and its various mutants have been extensively used in biotechnology as well as in elemental and applied science research. GFP is stable and fluoresce at least up to 65°C temperature, which was first isolated in 1962 by Shimomura and co-workers from *Aequorea Victoria* jellyfish.[1] It is known to be responsible for the green bioluminescence of the jellyfish.[1,2] *Aequorea* GFP was the first such fluorescent protein for which the gene was cloned.[3] GFP is widely used to study the protein dynamics in living cells, in fluorescence microscopy, as a reporter gene, as a tagger in cellular biology and biotechnology, in transgenic plants, to study fungal biology, for protein localization in bacteria, to study embryos, as a vital marker in mammalian cell, in gene therapy, imaging biochemistry *in vivo*, visualizing chromosome dynamics, lighting up the cell surface, and so on, as have been nicely discussed in the comprehensive review of Zimmer.[4] Different transgenic living fluorescent species have also been developed using GFP.[5] Recently, it has been discovered that the GFP can act as light induced electron donors in photo biochemical reactions with various electron acceptors.[6] There are many other uses of GFP out side the laboratory.[7] Moreover, National Aeronautics and Space Administration (NASA) have developed a GFP Imaging System (GIS), a controlled nondestructive analytical tool to judge the status of a target organism in stellar objects. This device is likely to revolutionize space biological research by eventually eliminating the resource intensive requirement to return biological materials to earth for post flight analysis. This advanced technique can be applied to a host of model organisms engineered with the GFP gene construct including plants, microbes, and nematodes.[8]

The chromophore of GFP is a *p*-hydroxybenzylidene imidazolinone derivative (*p*-HBI) formed by self-catalyzed covalent modification of Ser65-Tyr66-Gly67 residues.[4] Spontaneous rearrangement and oxidation of Ser-Tyr-Gly residue is the source of fluorescence in GFP. The crystal structure study of GFP shows that it contains a unique 11-strand β-barrel fold structure with a central helix containing the fluorophore which plays a significant role in its fluorescence properties. With relatively small molecular mass (27 kDa), the thermostable GFP composed with 238 amino acids can tolerate both N- and C-terminal

protein fusion.[2] When the fluorophore is irradiated with ultra violet (UV) or blue light it emits green light.[2,4] Aequorin, which is a luciferase, contains coelenterazine the luciferin, and GFP are the two proteins which are involved in bioluminescence in wild *Aequorea* jellyfish. Aequorin binds with three calcium ions to oxidize coelenterazine to form Ca_3-apo-aequorin-coelenteramide complex which *in vitro* emits blue light. Instead of giving blue bioluminescence the aequorin complex *in vivo* undergoes radiationless energy transfer to GFP which then gives off green fluorescence.[4] Once excited by light of 488-nm wavelength, it undergoes repeated cycle of fluorescent emission i.e., "blinking" for several seconds. This behavior indicates that it can act as an optical storage material, molecular photonic switch or fluorescent marker.[9] To change the photophysical features, several mutants of GFP have been designed by genetic engineering and some of them are already synthesized and characterized. Three different isomers of dimethyl derivative of GFP chromophore *o*-HBDI, *p*-HBDI and *m*-HBDI have been synthesized and characterized.[10,11] Chromophores of GFP (Ser65-Tyr66-Gly67) analogue are obtained from similar chemical modification with the only difference is that they are formed with other tripeptide chains. Replacing Tyr66 with Trp-, His-, Phe-residues (i.e., triptophan, histidine or phenylalanine) one can get different blue shifted variants of GFP such as, cyan fluorescent protein (analogue of Y66W GFP i.e., CFP), blue fluorescent protein (analogue of Y66H of GFP i.e., BFP), and BFPF (analogue of Y66F GFP) respectively. Thus, when indolyl or imidazolyl or phenyl ring replaces the phenol of GFP moiety, a blue shifted fluorescence is observed; in spite of low quantum yield these mutants perform multidimensional biological applications. All these above mentioned synthetic chromophores undergo photochromic cis/trans isomerization upon irradiation. However, it is to be noted here that Matsuda and co-workers[12] have also isolated and characterized various photochromic spin couplers. Theoretically, Ali and Datta have investigated the photomagnetic behaviour of nitronyl nitroxide, imino nitroxide and verdazyl derivatives of substituted pyrene and found that magnetic coupling constants changed their magnitude when exposed to electromagnetic radiation of right frequency.[13] In a recent work, it has been shown that photochromic antiferromagnetic to ferromagnetic crossover occurs in organic magnetic entity when exposed to light of suitable wavelength.[14] This leads us to focus on the design and investigation of magnetic systems with synthetic analogue of GFP and its different photochromic variants, where photoresponsive antiferromagnetic to ferromagnetic crossover occurs. These prospective biocompatible diradicals undergo magnetic crossover

along with change in color, as a result they are likely to be more useful in different *in vivo* treatments as already discussed. As substituted dark nonfluorescing trans GFP chromophore converts into its bright fluorescing cis isomer when exposed to light,[15] GFP coupler can be suitably crafted between two radical centers so as to produce a photochromic and photoactive reversible diradical which can undergo magnetic crossover with irradiation of light of appropriate wavelength.

Scheme 6.1. Photoinduced conversion of diradicals from trans isomer to cis isomer, where GFP chromophore and its variants are used as couplers. Here, τ and φ are the two stereochemically relevant dihedral angles.

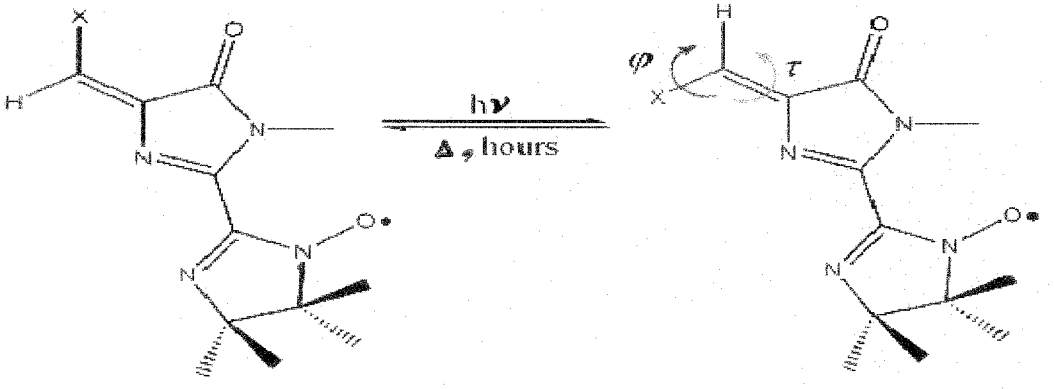

Trans (*E*) (a) Cis (*Z*) (b)

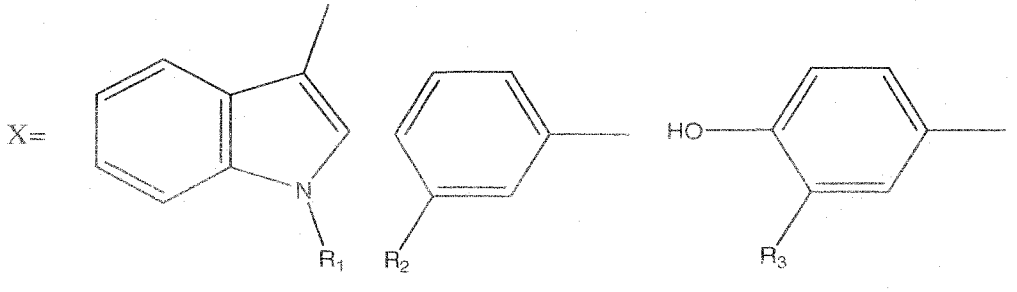

1 2 3

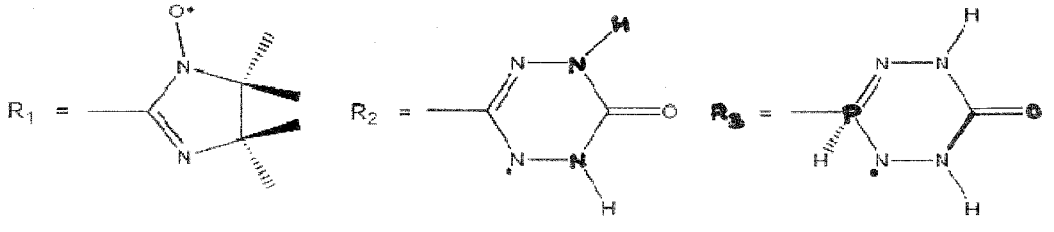

Iminonitroxide Oxoverdazyl Phosphaverdazyl

In GFP like chromophores, generally the cis isomer possesses lower energy than the corresponding trans form.[16] The cis and trans isomers of synthetic analogues of GFP and BFPF are characterized by the rotation of symmetrical phenol and phenyl rings around φ, but in case of CFP, the presence of asymmetric indolyl ring disrupts this symmetry of rotation (Scheme 6.1). Both the cis CFP and trans CFP chromophores are characterized by two energy minima.[15] Here, in this study we take more stable trans CFP configuration as well as its cis form. Radicals of imino nitroxide (IN) family are known to be stable and they are also used to design molecular magnets.[17] Nearly planar or planar verdazyl molecules are attractive alternative to nitroxides as through space interactive building blocks.[18] In this chapter, we design six diradicals with GFP chromophore and its variants (i) CFP as a coupler with two IN moieties act as radical centres in diradicals 1a and 1b; (ii) BFPF as a coupler with oxoverdazyl and IN moieties are the two different radical centres as in diradicals 2a and 2b; and (iii) dimethyl substituted synthetic GFP chromophore (*p*-HBDI) as a coupler with phosphaverdazyl and IN moieties are two different radical centres as in diradicals 3a and 3b (Scheme 6.1), and predict the photoinduced magnetic behaviour therein. Among these molecules 1a, 2a and 3a are the trans isomers, whereas 1b, 2b and 3b are their corresponding cis forms respectively.

6.2. Theoretical Background and Methodology

The interaction between two magnetic sites 1 and 2, is generally expressed by the Heisenberg spin Hamiltonian

$$\hat{H} = -2J\hat{S}_1 \cdot \hat{S}_2, \tag{6.1}$$

where $\hat{S}_1$ and $\hat{S}_2$ are the respective spin angular momentum operators and J is the exchange coupling constant. The positive sign of J signifies the ferromagnetic interaction while the negative value indicates the antiferromagnetic interaction. For a diradical containing one unpaired electron on each site, J can be represented as

$$E_{(S=1)} - E_{(S=0)} = -2J\,. \tag{6.2}$$

Due to spin contamination, the single determinantal wave function cannot satisfactorily represent a singlet state of a diradical in the unrestricted formalism. To overcome this problem one may prefer multiconfigurational approaches to obtain pure spin states. However, these methods are resource intensive and not being used in this chapter. Broken symmetry (BS) approach given by Noodleman[19] in DFT framework is an alternative route to evaluate *J*, which is more effective due to less computational effort. BS state is an artificial state of mixed spin symmetry and lower space symmetry. The BS solution is often found to be spin contaminated, and using spin projection technique one can overcome this problem. Depending on the extent of magnetic interaction between two magnetic sites, many researchers have developed diverse formalisms to assess *J* using unrestricted spin polarized BS solution.[19-25] The equation for evaluating *J* proposed by Ginsberg,[20] Noodleman[21] and Davidson[22] is applicable when interaction between two magnetic sites is small. On the other hand, the expression given by Bencini [23] and co workers and Ruiz et al., [24] is applicable for large interaction. Nevertheless, the eminent expression given by Yamaguchi[25] is relevant for both strong and weak overlap limits. Following the well established and widely applied method,[13,26] we use the Yamaguchi[25] formula for evaluation of *J* value in this chapter, which is given by

$$J = \frac{(E_{BS} - E_{HS})}{\langle S^2 \rangle_{HS} - \langle S^2 \rangle_{BS}}, \tag{6.3}$$

where, E_{BS}, E_{HS} and $\langle S^2 \rangle_{BS}$, $\langle S^2 \rangle_{HS}$ are the energy and average spin square values for corresponding BS and high spin states.

It is necessary to say that, in this chapter, we have used a simple and widely employed approximation to estimate the spin state preference. An estimate of the open shell singlet energy is obtained by broken symmetry wave functions using unrestricted formalism. It is widely accepted that this produces an equal mixture of singlet and triplet states. However, Neese[27] has advocated over the fact that these states are not equally mixed as it thought to be. Moreover, projection of the triplet leaves a singlet component. For diradicals, $\langle S^2 \rangle$ = 1

represents pure BS state. The singlet states are spin contaminated in DFT formalism, and the MOs are not optimized for an open shell singlet. The MOs are optimized for the triplet and these are used to estimate the BS state, as a result, this calculation tends to be biased in favor of the triplet. Here, we estimate the singlet and triplet weightage in the computed BS solutions for each diradical. Another point needs to be noted here that, in molecular level a quantitative calculation of first and second energy derivatives, which are influenced by spin contamination is of significant interest. Recently Yamaguchi and co-workers[28] have used a new method to avoid such spin contamination from geometry optimization using approximate spin projection (AP) procedure, but this procedure is resource intensive and not being employed in the chapter.

Generally, in any photoinduced process it is necessary to know the excitation energy. In GFP chromophores and its variants, the excitation would take place from bonding to antibonding π orbitals. Here, we calculate electronic excitation energies with time-dependent density functional theory (TDDFT) which is essentially a DFT analogue of time dependent Hartee–Fock (TDHF) approach using B3LYP functional with 6-31G(d,p) basis set. In TDDFT the fundamental variable is time dependent density and exchange correlation potential describes many body interactions.[29] TDDFT in early days is considered only for the closed shell molecules by describing singlet–singlet or singlet–triplet excitation dominated by single electron excitation. Recently it has been shown that TDDFT is also useful to estimate excitation energies of open shell molecules.[30] However, in any photoinduced process, $\pi \rightarrow \pi^*$ transition energy can be calculated through time dependent perturbative technique. It is known that there arise inherent errors due to "near triplet instability" in prediction of transition energy through time dependent Hartree–Fock method (TDHF).[31] Hartee–Fock (HF) based single excitation theories, configuration interaction singles (CIS) method, have many similarities with TDHF method. CIS avoids the problem of "near triplet instability" error as it is not a response theory method, even though its results are not precise enough as evident in numerous applications. Many post Hartree Fock *ab initio* methods are free from such errors; however, being computationally expensive not been employed in this chapter. On the other hand, TDDFT is more robust than TDHF and CIS, and known to produce minimal "near triplet instability" error,[32] hence, the TDDFT method is used in this

chapter to calculate excitation energies. The TDDFT method is based on the dynamic polarizability $\bar{\alpha}(\omega)$ of a system which has poles at frequencies analogous to its transition energies. Obtaining the frequency dependent polarizability from TDDFT calculations and substituting it in the relation

$$\bar{\alpha}(\omega) = \sum_I \frac{f_I}{\omega_I^2 - \omega^2}, \tag{6.4}$$

one can get oscillator strength (f_I) and excitation frequency (ω_I) respectively.[31] In this chapter, we calculate $\pi \rightarrow \pi^*$ transition energies for all substituted trans fluorescent protein chromophores following the method mentioned above.

6.3. Results and Discussion

In this chapter, the molecular geometries of all six molecules have been fully optimized by hybrid exchange-correlation functional B3LYP using 6-31G(d,p) basis set within the unrestricted formalism. The optimized geometries are shown in Figure 6.1. Based on these molecular geometries the corresponding J values for each molecule have been estimated from the energies of the triplet and BS states at same level of theory. To obtain open shell BS singlet solution "guess =mix" keyword is used within unrestricted formalism. The BS states for all six diradicals are stable. To confirm the stability of BS solution, we follow the procedure developed by Bauernschmitt and Ahlrichs,[33] which is an extension of the SCF stability analysis given by Čížek and Paldus.[34] This has been implemented in this chapter by using "stable" keyword. All the calculations have been carried out using GAUSSIAN 03W[35] quantum chemical package.

The cis isomers of these chromophores are known to possess lower energy than corresponding trans isomers or zwitterionic species either in gas phase or in solution.[4,15] In the optimized structures (Figure 6.1) of the trans diradicals (1a, 2a, 3a), the atoms containing the unpaired spins and the couplers are in the same plane. The trans diradicals have singlet ground state, so the polarization of spin in the high spin state of these molecules through the

fluoro protein couplers is blocked and hence antiferromagnetic behaviour is observed in such cases (Figure 6.2), this is also in good agreement with spin alternation rule.[36] On the other hand, in cis diradicals (1b, 2b, 3b), the radical centres are slightly out of plane with a very low dihedral angle (φ = 1.07°, −2.76° and −2.71° and τ = 0.27°, −0.74°, −0.63° for diradicals

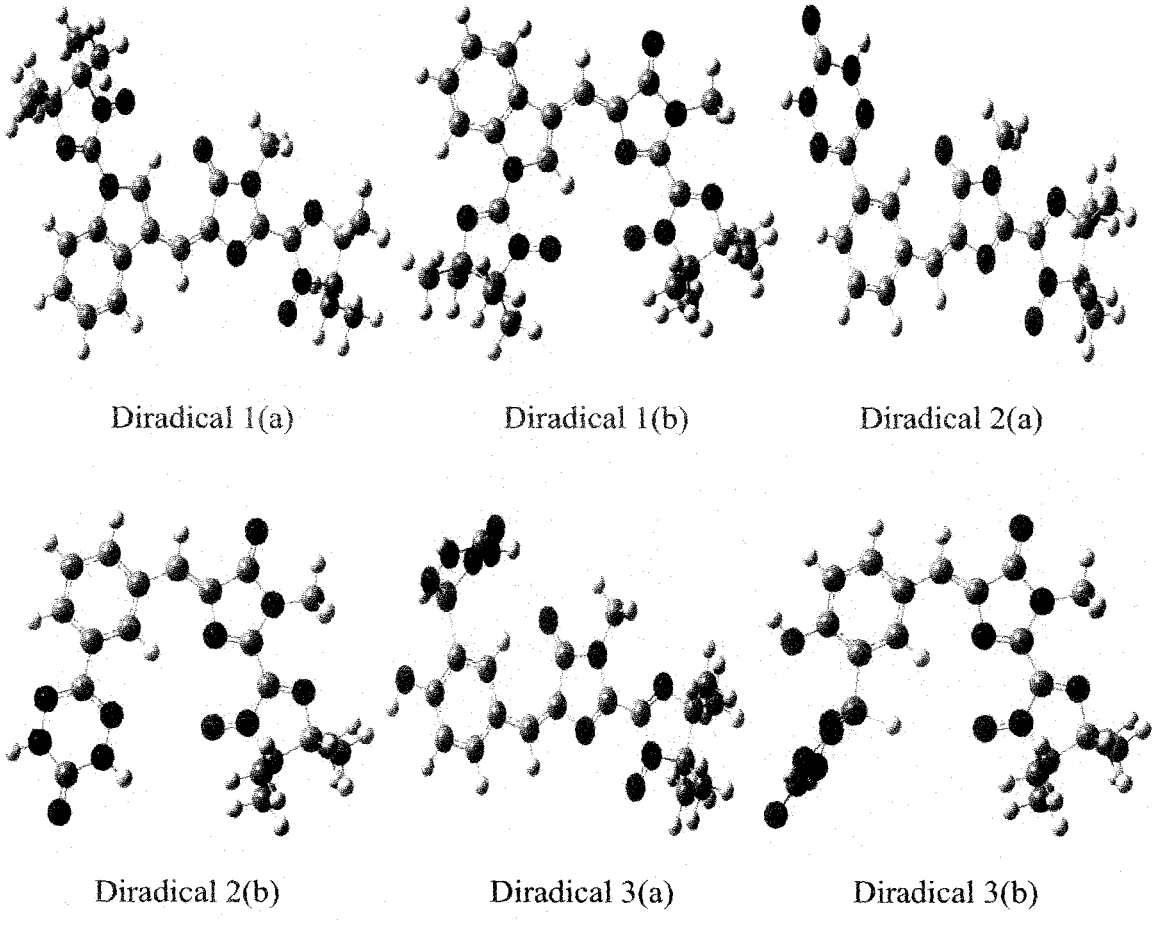

Figure 6.1. The optimized geometries of three trans (1a, 2a, 3a) diradicals and their corresponding cis forms (1b, 2b, 3b) with different GFP variants (CFP, BFPF and *p*-HBDI respectively) as coupler from UB3LYP/6-31G(d,p) calculations. The carbon atoms are represented in grey, nitrogen in blue, oxygen in red, phosphorus in orange, and hydrogen in white respectively.

1b, 2b, 3b correspondingly). The dihedral angles φ and τ are shown in Scheme 6.1. Moreover, in the cis forms radical centres are also closer in space compared to that in the trans diradicals. Proximity of the radical centres in cis isomers facilitates direct exchange,

which usually favours the ferromagnetic coupling.[14] As a result, cis diradicals show ferromagnetic behaviour with the triplet ground state. The spin alternation rule is less pronounced in these cases where the radical sites are close to each other,[14] which is also obvious from spin density plots (Figure 6.2).

We have calculated the value of J for all three systems in the cis and trans forms. The energy and $\langle S^2 \rangle$ values for both triplet and BS states are reported in Table 6.1. Here, the J values of all three species in the trans forms are negative, but in the case of cis forms, J values are positive. Thereby from the point of view of basic principles of magnetism one may note that all trans forms have spins with opposite orientations in two spin sites and similarly all cis forms have spins with same alignments in two radical centers, i.e., antiferromagnetic and ferromagnetic situations in respective cases being observed. This is also obvious from

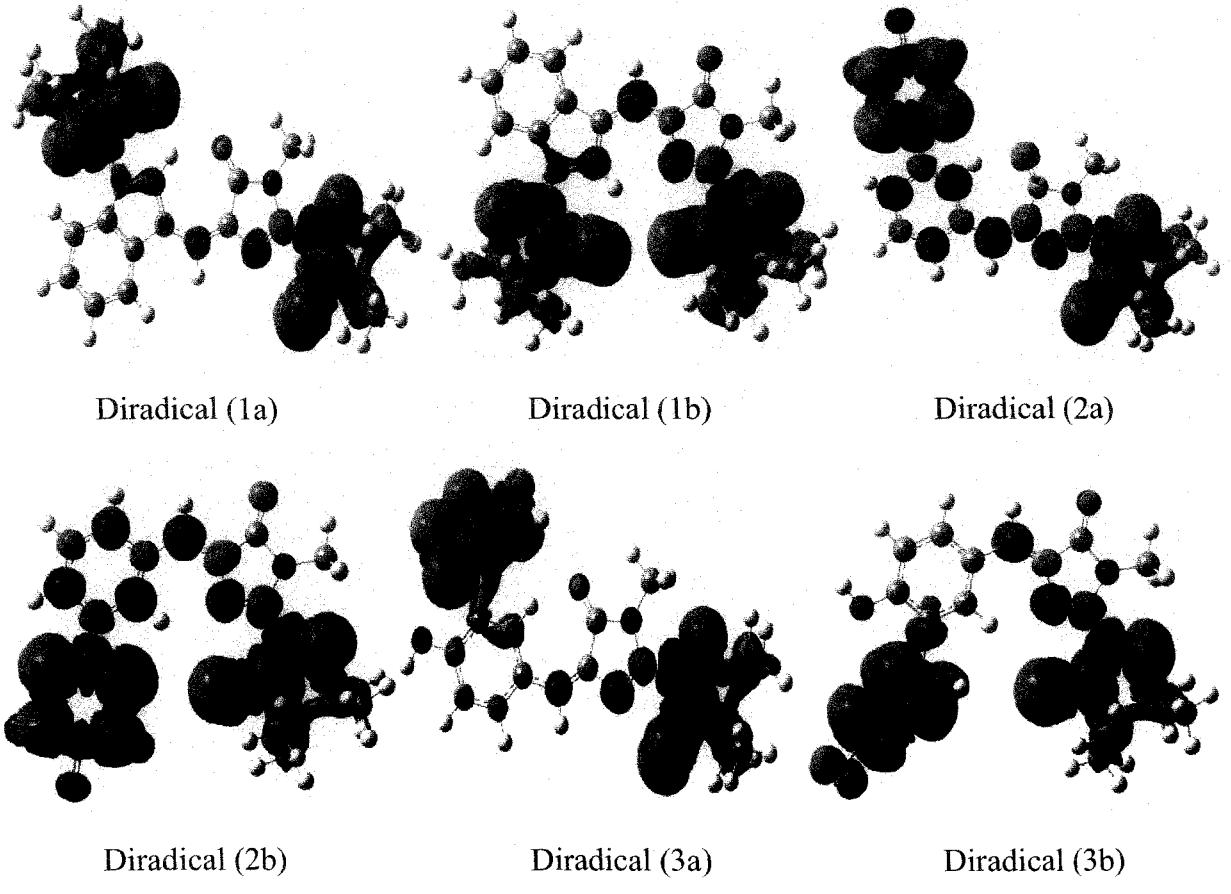

Figure 6.2. Spin density plots for the diradicals in their triplet states; green color indicates up spin and red color indicates down spin.

spin density maps in Figure 6.2. As a result, a magnetic crossover from antiferro to ferro would be noted in all three cases when the trans isomers are subjected to photoisomerization. It is also to be noted that, potential energy of a diradical system has two wells corresponding to the two stable orientations of the magnetism. In case of conventional magnetic reversal by applying magnetic field one of the two wells become metastable when small field is applied. At a particular field, whose frequency matches the precision frequency of the magnetization called the switching field, the energy can be pumped into the system and the energy barrier between the two wells vanishes, as a result magnetization reverses. This magnetic field induced magnetization reversal in magnetically active materials is a fundamental issue in many applications and it is difficult to implement as it requires very high field gradient.[37] On the other hand, photoinduced magnetic crossover is easy to implement and expected to find wide applications. The cis and trans forms of GFP chromophore and its variants have different absorption spectra and these two forms can be converted to each other i.e., their structures and physical properties can change when exposed to proper electromagnetic radiation. Since the trans form of all the diradicals are dark, upon irradiation of light of suitable wavelength on the dark trans isomers corresponding bright fluorescing cis forms (cyan, blue and green colors for diradicals 1b, 2b and 3b respectively) are obtained.[2,15] As a result, here we observe different states of magnetism with different colors, that is, it is easy to understand the magnetic property of these six diradicals by visual inspection even without evaluating coupling constants.

The photoisomerization from diradical (a) to diradical (b) [in every case (1-3)] is initiated by $\pi \rightarrow \pi^*$ transition energy, hence, we calculate the transition energies for trans isomers of each diradical. The experimentally observed excitation peaks for neutral bare couplers in 1a, 2a and 3a diradicals are 436 nm, 360 nm, and 399 nm respectively.[2] Transition energies obtained by TDDFT method are known to be less dependable due to spin contamination.[38] However, many authors have found good agreement between calculated transition energies and experimental values using TDDFT methods.[39,40] Thus, it has been prudently surmised that TDDFT calculations for open shell molecules are very reliable to explain experimental results even it lacks a solid theoretical background.[39] In our TDDFT calculations for diradicals 1-3 (Table 6.2), we get reasonable agreement with previous

experimental results for the respective chromophores.[2] Hence, upon irradiation with light of 360-390 nm wavelengths the trans isomers would be converted into their corresponding cis forms, as a consequence structural isomerization with magnetization reversal from antiferro to ferro associated with change in colors would be observed. It is apparent from other works[2,4] that electronic transition in the GFP like chromophores leads to fluorescence decay. Therefore, it may be argued that in the present case even if a part of the excited molecules fluoresce through $S_1 \rightarrow S_0$ transition, a sizable amount may undergo intersystem crossing (ISC) to the triplet T_1 state which eventually decays energy via nonradiative pathways. A general schematic representation of the photoresponse for all of our designed diradicals is given in Scheme 6.2.

Table 6.1. UB3LYP level absolute energies in *au*, $\langle S^2 \rangle$, and exchange coupling constants (J in cm^{-1}), using 6-31G(d,p) basis set for trans and cis forms of all diradicals.

Diradicals		At UB3LYP/6-31G(d,p) level		
		Energy(*au*)	$\langle S^2 \rangle$	$J(cm^{-1})$
1a	Triplet	–1657.61021	2.032	–20
	BS	–1657.61030	1.034	
1b	Triplet	–1657.61180	2.032	9
	BS	–1657.61176	1.032	
2a	Triplet	–1438.97996	2.050	–2
	BS	–1438.97997	1.046	
2b	Triplet	–1438.98505	2.052	35
	BS	–1438.98489	1.046	
3a	Triplet	–1817.99078	2.025	–15
	BS	–1817.99085	1.025	
3b	Triplet	–1817.99461	2.027	13
	BS	–1817.99455	1.028	

Table 6.2. The $\pi \rightarrow \pi^*$ transition energy values, estimated wave length $^{a}\lambda_{exc}$ in trans diradicals at UB3LYP (TDDFT) level using 6-31G(d,p) basis set, $^{b}\lambda_{exc}$ is the experimental value for bare coupler from ref. 15(a).

Diradicals	E_{π} in *au*	E_{π^*} in *au*	Transition energy in *eV*	Estimated $^{a}\lambda_{exc}$ for diradicals in nm	Experimental $^{b}\lambda_{exc}$ for bare couplers in nm
1a	–0.19374	–0.07620	3.1985	387	436
2a	–0.21580	–0.09002	3.4227	361	360
3a	–0.21349	–0.08939	3.3770	366	399

Scheme 6.2. A general schematic representation of the photoresponse for all of our designed diradicals, where S_0, S_1, and T_1 are the singlet electronic ground state, singlet electronic excited state and triplet electronic excited state respectively. ISC represents intersystem crossing.

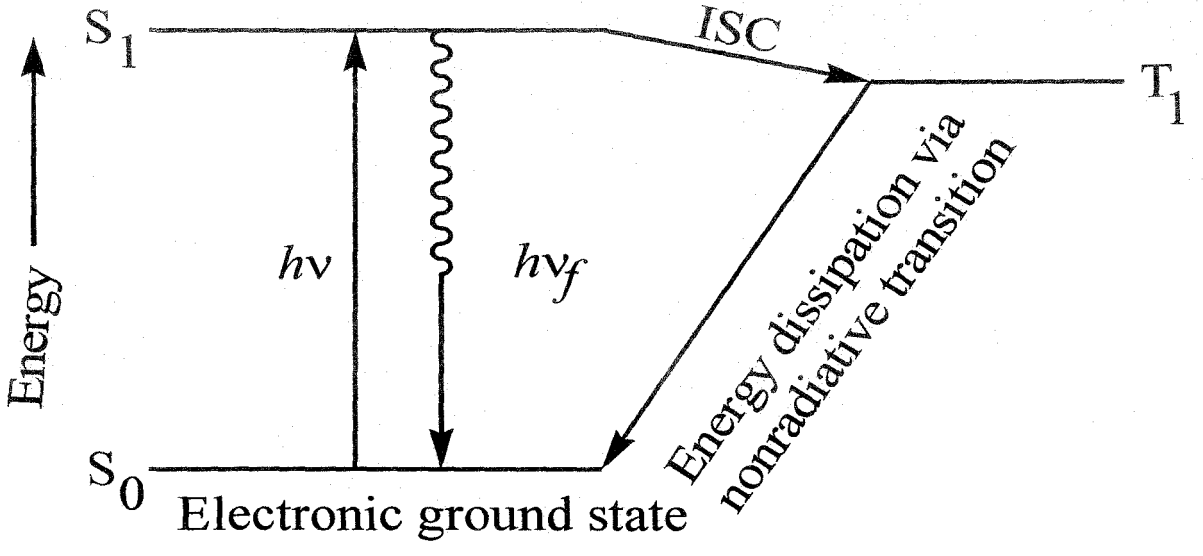

The up-spin density on both radical sites is intense as obvious from spin density plots (Figure 6.2), hence spin-up electrons will go through the molecules from one magnetic sites to another when bias is applied, whereas the propagation of spin-down electrons are

blocked.[41] Using GaussSum v. 2.1 software,[42] the density of states (DOS) plots (Figure 6.3) are evaluated from the output file of population analysis obtained using Gaussian 03W.[35] From DOS plots one can find very easily that the spins are highly polarized at Fermi level in bright ferromagnetic cis diradicals, whereas in case of dark trans diradicals no such polarization is observed. Thus ferromagnetic cis diradicals can show spin valve effect, that is, the majority spins are conveyed only in one direction when bias is applied.[41] It is also noted that in case of diradicals 1b and 3b, the β-HOMO is located above the Fermi level. This observation is due to non-Aufbau occupation of molecular orbitals (MOs) in these cases. Non-Aufbau behavior is experimentally and theoretically supported by Westcott et al.[43] Aufbau principle can also be violated due to delicate balance between promotion energies, coulomb repulsions and exchange interactions.

Diradical 1(a)

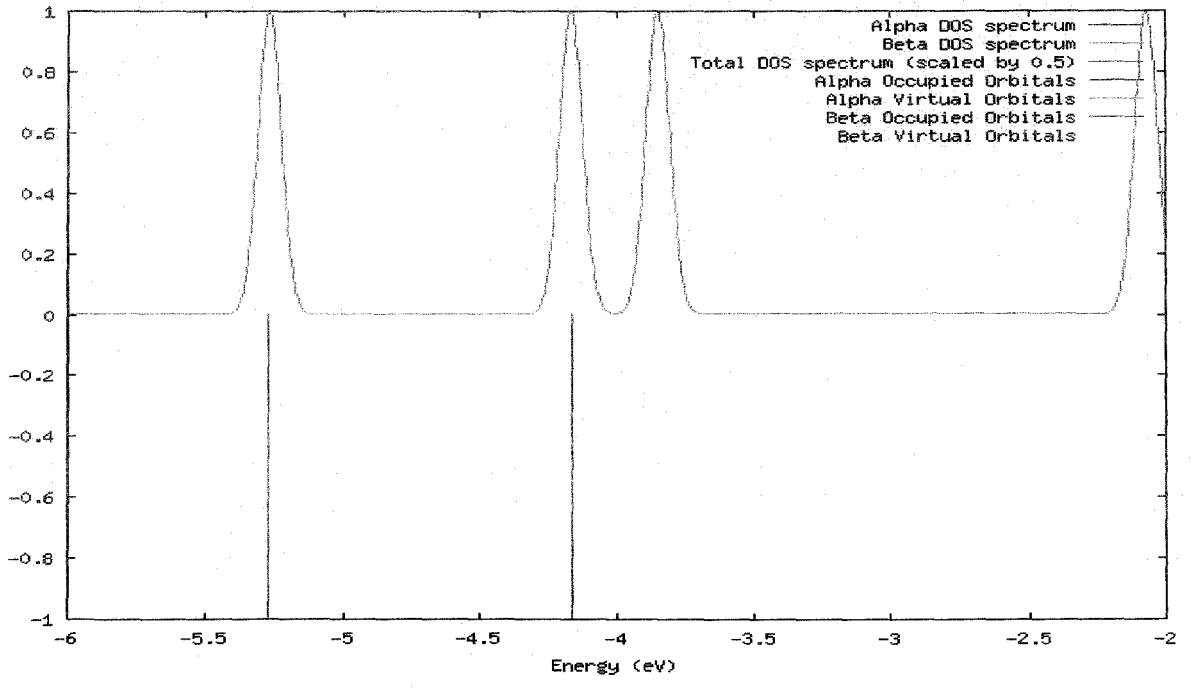

Diradical 1(b)

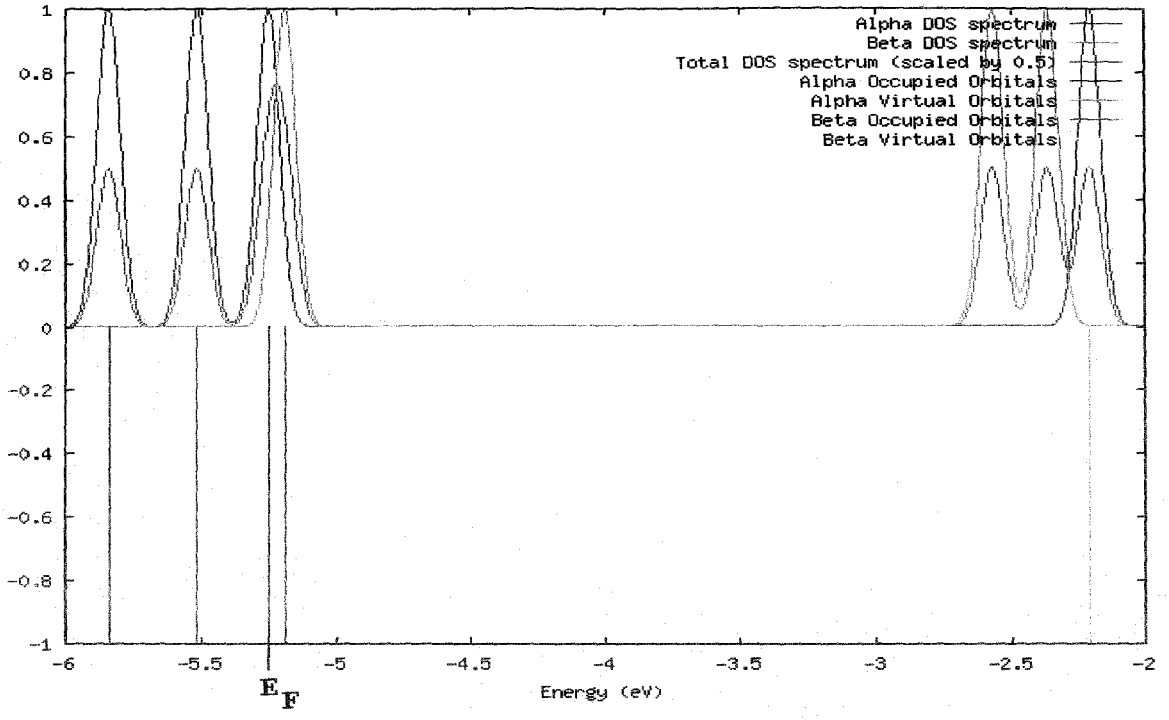

Diradical 2(a)

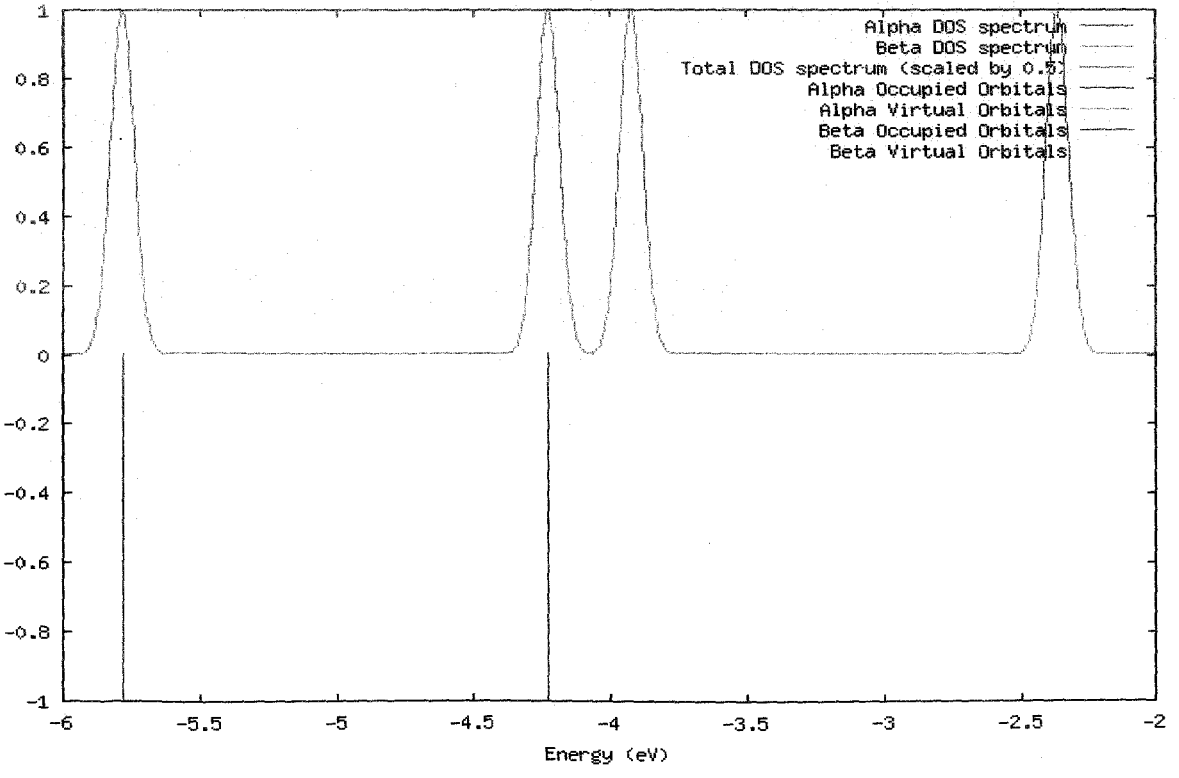

Diradical 2(b)

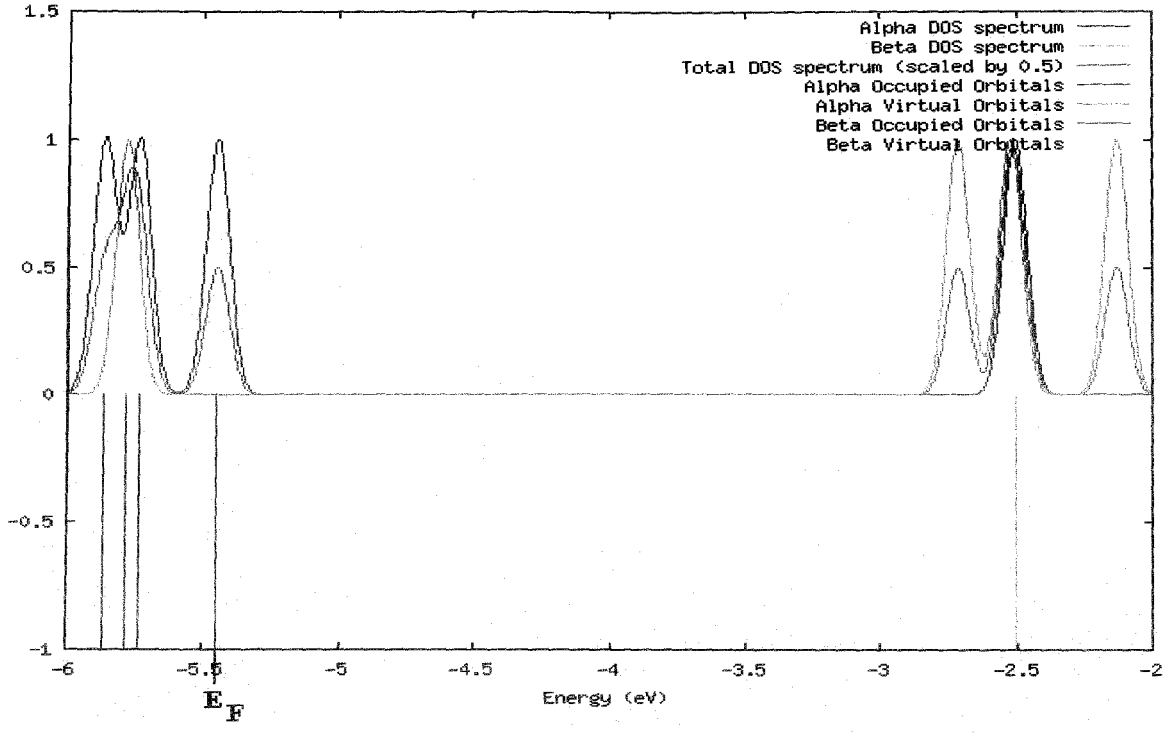

Diradical 3(a)

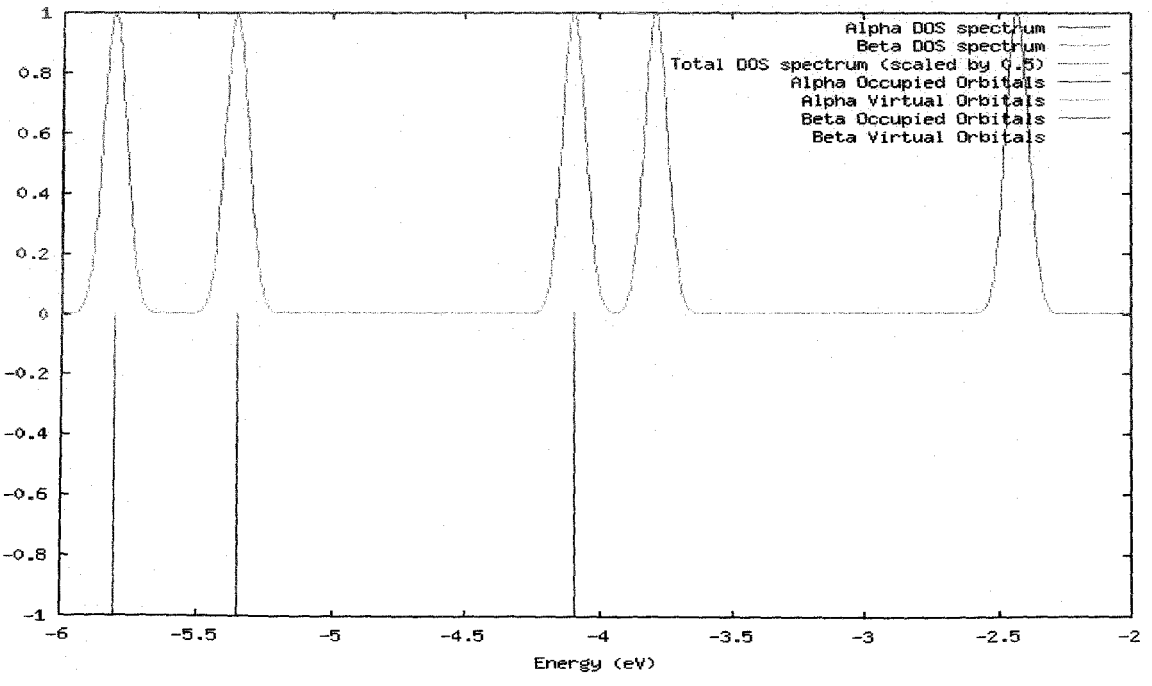

Diradical 3(b)

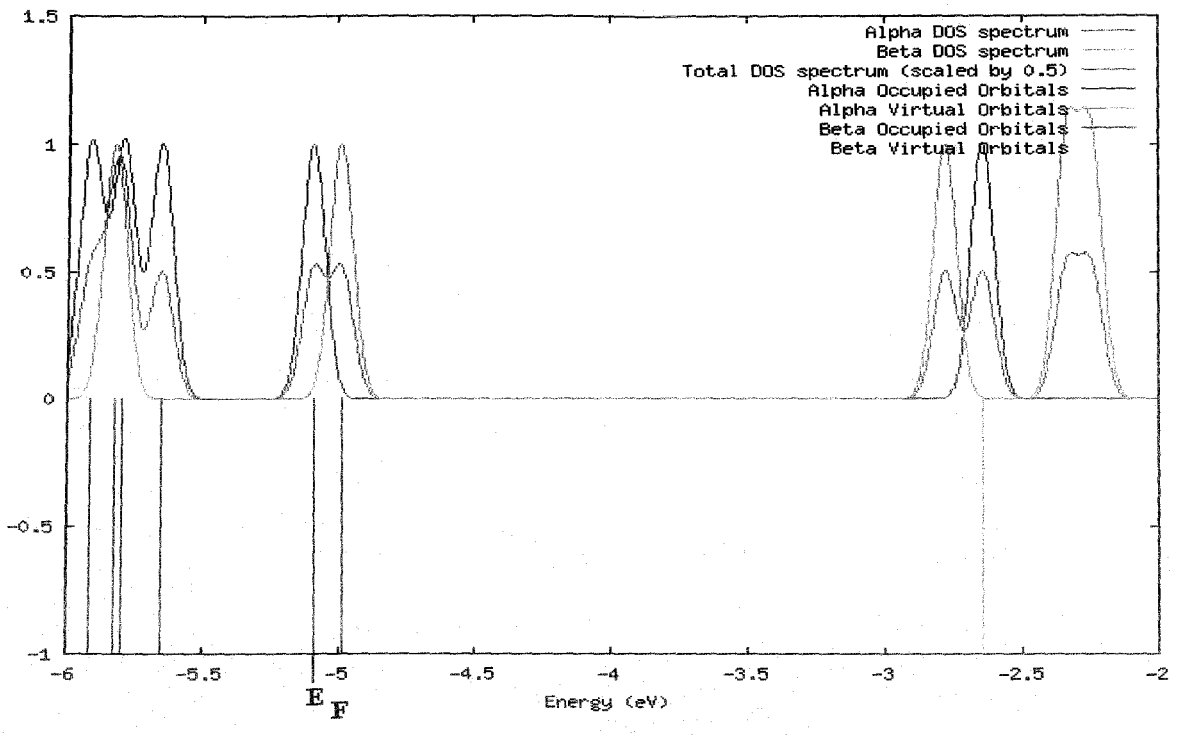

Figure 6.3. DOS vs energy plots for antiferromagnetic trans (1a, 2a and 3a) and their respective ferromagnetic cis (1b, 2b and 3b) isomers, consequent Fermi levels are indicated as E_F.

A discussion on estimated singlet and triplet weightage for each diradicals is due here. These estimated values are given in Table 6.3. For this calculations, in pure state, we take the broken symmetry wave function, $\psi_{BS} = m\ \psi_S^{BS} + n\ \psi_T^{BS}$, where ψ_S^{BS} and ψ_T^{BS} singlet and triplet component functions, and $m^2 \approx n^2 = \frac{1}{2}$, that is, $m^2 + n^2 = 1$. Also $n^2 = \frac{1}{2}\langle S^2 \rangle_{BS}$, so that, $m^2 = 1 - \frac{1}{2}\langle S^2 \rangle_{BS}$. It is obvious from Table 6.3 that for both ferromagnetic and antiferromagnetic species the triplet weightage is greater in every case as also obvious from the work of Datta and co-workers.[45]

Table 6.3. Percent net weight of singlet and triplet components in the computed BS Solution, using $50\langle S^2\rangle_{BS}$ and Singlet weightage = 100 – Triplet weightage.

Diradicals	Singlet % Weightage ($100m^2$)	Triplet % Weightage ($100n^2$)
1a	48.30	51.70
1b	48.40	51.60
2a	47.70	52.30
2b	47.70	52.30
3a	48.75	51.25
3b	48.60	51.40

We have compared the ground state stability of the cis and trans forms of these fluoro proteins coupled diradicals. Commonly, ferromagnetic diradicals show greater stability than their antiferromagnetic counterparts,[45] as also apparent from Table 6.4. Nonetheless, the estimated singlet state energy (E_S) values for trans diradicals are lower than the respective computed triplet state energy values (E_T) (Table 6.1 and Table 6.4), i.e., singlet ground states for trans diradicals are confirmed.

Table 6.4. Ground state energies of six diradicals from single point UB3LYP/6-31G(d,p) calculations.

Diradicals	Estimated E_s in *au*	Diradicals	E_T in *au*
1a	–1657.61039	1b	–1657.61180
2a	–1438.97998	2b	–1438.98505
3a	–1817.99092	3b	–1817.99461

The energy differences between the α–highest occupied molecular orbital (α–HOMO) and α–lowest unoccupied molecular orbital (α–LUMO) for all 6 molecules (Table 6.5) have been evaluated. The energy gap also corresponds to the chemical hardness of the molecule. Chemical hardness is calculated from the formula, $\eta = (E_{LUMO}-E_{HOMO})/2$, where η is the molecular hardness, E_{LUMO} and E_{HOMO} are the energy of the LUMO and HOMO respectively. From Table 6.5, it is evident that all the cis diradicals have lower HOMO–LUMO energy gap than the corresponding antiferromagnetic trans isomer, which implies that lower molecular hardness and the higher molecular polarizability is observed for ferromagnetic cis diradicals.

Table 6.5. Energy of HOMO and LUMO in au and their differences in *eV* and molecular hardness (η) at the UB3LYP/6-31G(d,p) level for diradicals.

Diradicals	E_{HOMO} in *au*	E_{LUMO} in *au*	$\Delta E_{HOMO-LUMO}$ in *eV*	Molecular Hardness(η)
1a	–0.19503	–0.07942	3.1459	1.5730
1b	–0.19318	–0.08107	3.0507	1.5254
2a	–0.21286	–0.09474	3.2142	1.6071
2b	–0.21256	–0.10218	3.0036	1.5018
3a	–0.18638	–0.09803	2.4042	1.2021
3b	–0.18323	–0.09983	2.2695	1.1347

However, Chattaraj and co-workers[46] have advocated over the fact that for open shell spin polarized triplet state the relationship between HOMO–LUMO gap and the stability of the molecules is not as simple as widely assumed. This is because LUMO may come below the HOMO giving a negative contribution to the hardness, as in some cases LUMO is not well defined. It is also known that the molecules having HOMO–LUMO energy gap of the order of 1.59–3.18 *eV* can be used in optoelectronic devices, and in non-linear optical (NLO) imaging.[47] On the other hand, the fluorophores similar to GFP have their uses as optoelectronic devices.[48] In this case all the diradicals have HOMO–LUMO energy gap

2.44–3.14 *eV* (Table 6.5) and can be used for preparing organic light emitting diode (OLED), and in the development of high-density optical memories and switches.[49] The acidic –OH group in GFP makes it less useful as OLED material; nevertheless, efforts are being put to develop oxazolone and imidazolidinone derivatives related to GFP chromophore to overcome this problem.[48]

6.4. Conclusions

Magnetic nano- and micro-particles are judiciously used in various biomedical applications.[50] On the other hand, GFP and its different variants also earned substantial attention in the field of molecular biology.[9] The reversible photochromic cis/trans isomerization, which is independent of the nature of the solvents, is displayed by GFP and its different analogous chromophores.[15] In this chapter, six GFP based photoswitchable diradicals are theoretically designed and characterized. These molecules undergo magnetization reversal associated with change in color, which are likely to receive attention in the field of biomedical applications. A general schematic representation (Scheme 6.3) shows such magnetic reversal in all our designed GFP based diradicals from bright fluorescent cis form to their dark trans form. The extent of magnetic interactions in all six molecules have been quantified in terms of the coupling constant through unrestricted broken symmetry approach in the framework of density functional theory. In our investigated systems, antiferromagnetic dark trans isomers turn into bright fluorescing ferromagnetic cis forms when exposed to light in the wavelength range 360-390 nm. Thus, one can observe cyan, blue and green colours for systems 1, 2 and 3 respectively, when magnetic crossover takes place. From DOS plots it is clear that at Fermi level the spins are highly polarized for ferromagnetic cis diradicals, which indicates such molecules will show a spin valve effect. We have also compared the ground state stabilities of these diradicals and find that the ferromagnetic cis isomer is more stable than respective antiferromagnetic one. The HOMO–LUMO energy gap indicates that the diradicals can be used in NLO imaging. It can also be used to prepare OLED devices, high-density optical memories and switches.[48,49]

Scheme 6.3. A general schematic representation of magnetic reversal of GFP based diradicals from bright fluorescent cis form to their dark trans form.

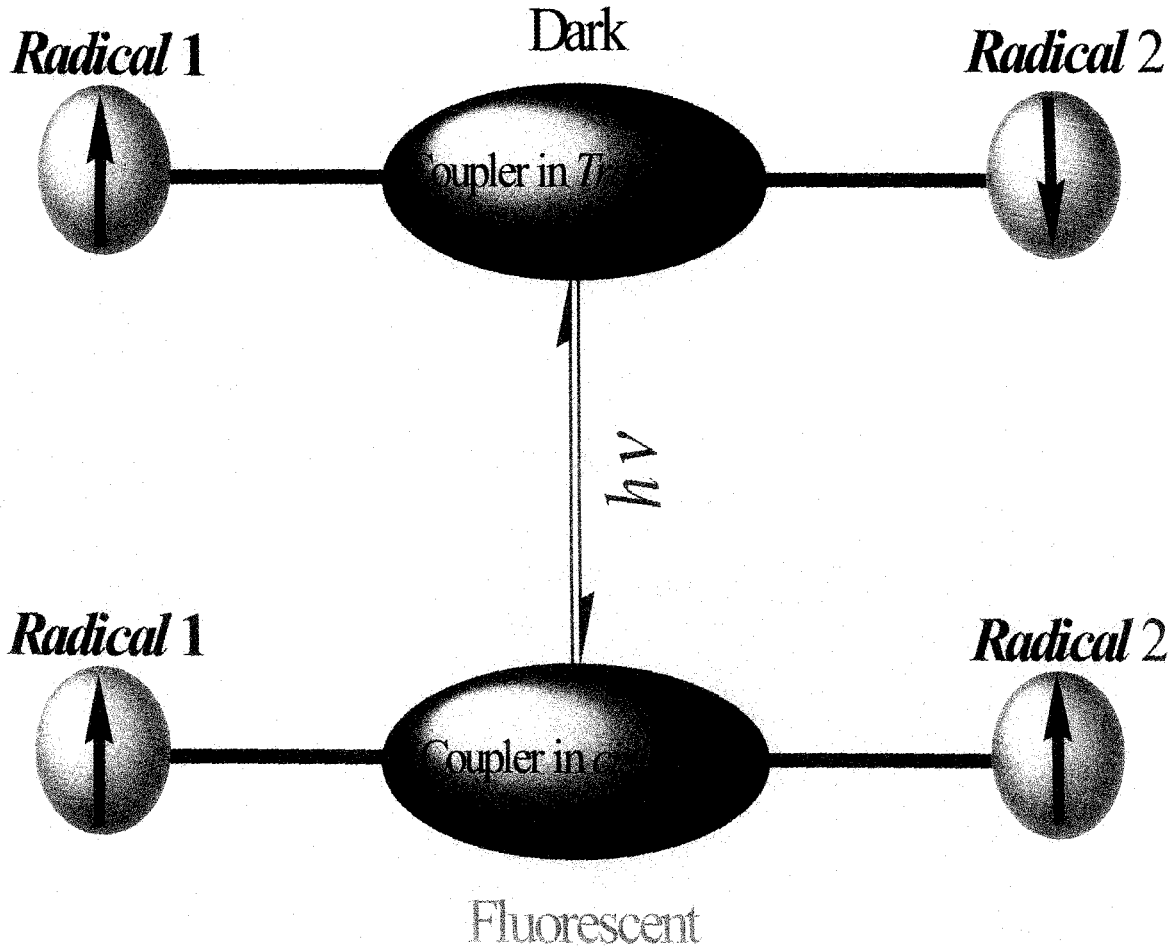

Recently, in an interesting work, Weber et al. have addressed the use of magnet guided transduction of enhanced GFP encoded lentiviral particles coupled with three layers carbon coated cobalt based nanoparticle in targeted delivery of therapeutic transgene to the pathologic tissue.[51] The capacity of magnetic folate conjugate nanoparticle towards its tagging ability in the cancerous cell with the reduction of unwanted side effects and toxicity has been shown by Pramanik and co-workers.[52] However, GFP functions as magnetic drug carrier without any biocompatible coating; moreover, GFP based multifunctional magnetic drug carrier can also act as a biological magnetic tagger which can be traced with the change in color associated with magnetization reversal. In the first step, GFP based magnetic drug

carriers can label the living cells *in vivo* and then magnetic separation of desired biological entity is possible. GFP based diradicals attached with multifunctional drugs can congregate at the required pathological site by local or external control. In the next step, it can discharge the specific drug at precise target or one can treat it by hyperthermia. GFP based fluorescent magnetic particles can be utilized as a multidimensional tool to molecular biologists; i.e., it can assist to test drug effectiveness or can help to act as a drug carrier in controlled drug delivery *in vivo*. Contrast agents, such as nitroxyls or aminoxyls, are used in magnetic resonance imaging (MRI) to enhance the image quality.[53] Here we have imino nitroxide moieties in the diradicals; hence, such multifunctional diradicals might also be used as a contrast agent in MRI. Last but not the least; it is needless to say photocontrol of magnetic crossover in GFP based diradicals make them suitable for next generation biomedical research.

This work has been published in Photochemistry photobiology A: Chemistry (Ref. 54).

6.5. References and Notes

(1) Shimomura, O.; Johnson, F. H.; Saiga, Y. *J. Cell. Comp. Physiol.* **1962**, *59*, 223.

(2) Tsien, R. Y. *Annu. Rev. Biochem.* **1998**, *67*, 509.

(3) Prasher, D. C.; Eckenrode, V. K.; Ward, W. W.; Pendergast, F. G.; Cormier, M. J. *Gene* **1992**, *111*, 229.

(4) Zimmer, M. *Chem. Rev.* **2002**, *102*, 759.

(5) Chan, A. W. S.; Chong, K. Y.; Martinovich, C.; Simerly, C.; Schatten, G. *Science* **2001**, *29*, 309.

(6) Bogdanov, A. M.; Mishin, A. S.; Yampolsky, I. V.; Belousov, V. V.; Chudakov, D. M.; Subach, F. V.; Verkhusha, V. V.; Lukyanov, S.; Lukyanov, K. A. *Nat. Chem. Biol.* **2009**, *5*, 459.

(7) Gory, L.; Montel, M. C.; Zagorec, M. *FEMS Microbiol. Lett.* **2001**, *194*, 127.

(8) See link: http://www.nasa.gov/mission_pages/station/science/experiments/TAGES.html

(9) Dickson, R. M.; Cubitt, A. B.; Tsien, R. Y.; Moerner, W. E. *Nature* **1997**, *388*, 355.

(10) Dong, J.; Solntsev, K. M.; Poizat, O.; Tolbert, L. M. *J. Am. Chem. Soc.* **2007**, *129*, 10084.

(11) Chen, K. Y.; Cheng, Y. M.; Lai, C. H.; Hsu, C. C.; Ho, M. L.; Lee, G. H.; Chou, P. T. *J. Am. Chem. Soc.* **2007**, *129*, 4534.

(12) Matsuda, K.; Irie, M. *J. Am. Chem. Soc.* **2000**, *122*, 7195.

(13) Ali, Md. E.; Datta, S. N. *J. Phys. Chem. A* **2006**, *110*, 10525.

(14) Shil, S.; Misra, A. *J. Phys. Chem. A* **2010**, *114*, 2022.

(15) Voliani, V.; Bizzarri, R.; Nifosí, R.; Abbruzzetti, S.; Grandi, E.; Viappiani, C.; Beltram, F. *J. Phys. Chem. B* **2008**, *112*, 10714.

(16) Grigorenko, B.; Savitsky, A.; Topol, I.; Burt, S.; Nemukhin, A. *Chem. Phys. Lett.* **2006**, *424*, 184.

(17) Ullman, E. F.; Boocock, D. G. B. *J. Chem. Soc. D: Chem. Commun.* **1969**, 1161.

(18) Koivisto, B. D.; Hicks, R. G. *Coord. Chem. Rev.* **2005**, *249*, 2612.

(19) Noodleman, L. *J. Chem. Phys.* **1981**, *74*, 5737.

(20) Ginsberg, A. P. *J. Am. Chem. Soc.* **1980**, *102*, 111.

(21) Noodleman, L.; Peng, C. Y.; Case, D. A.; Mouesca, J. M. *Coord. Chem. Rev.* **1995**, *144*, 199.

(22) Noodleman, L.; Davidson, E. R. *Chem. Phys.* **1986**, *109*, 131.

(23) Bencini, A.; Totti, F.; Daul, C. A.; Doclo, K.; Fantucci, P.; Barone, V. *Inorg. Chem.* **1997**, *36*, 5022.

(24) Ruiz, E.; Cano, J.; Alvarez, S.; Alemany, P. *J. Comput. Chem.* **1999**, *20*, 1391.

(25) Yamaguchi, K.; Takahara, Y.; Fueno, T.; Nasu, K. *Jpn. J. Appl. Phys.* **1987**, *26*, L1362.

(26) (a) Polo, V.; Alberola, A.; Andres, J.; Anthony, J.; Pilkington, M. *Phys. Chem. Chem. Phys.* **2008**, *10*, 857. (b) Bhattacharya, D.; Misra, A. *J. Phys. Chem.* A **2009**, *113*, 5470. (c) Bhattacharya, D.; Shil, S.; Misra, A.; Klein, D. J. *Theor. Chem. Acc.* **2009**, *127*, 57.

(27) Neese, F. *J. Phys. Chem. Solids* **2004**, *65*, 781.

(28) Kitagawa, Y.; Saito, T.; Nakanishi, Y.; Kataoka, Y.; Matsui, T.; Kawakami, T.; Okumura, M.; Yamaguchi, K. *J. Phys. Chem. A* **2009**, *113*, 15041.

(29) Scalmani, G.; Frisch, M. J.; Mennucci, B.; Tomasi, J.; Cammi, R.; Barrone, V. *J. Chem. Phys.* **2006**, *124*, 094107.

(30) Seth, M.; Ziegler, T. *J. Chem. Phys.* **2005**, *123*, 144105.

(31) Casida, M. E.; Jamorski, C.; Casida, K. C.; Salahub, D. R. *J. Chem. Phys.* **1998**, *108*, 4439.

(32) Bauernschmitt, R.; Ahlrichs, R. *Chem. Phys. Lett.* **1996**, *256*, 454.

(33) Bauernschmitt, R.; Ahlrichs, R. *J. Chem. Phys.* **1996**, *104*, 9047.

(34) Čížek, J.; Paldus, J. *J. Chem. Phys.* **1967**, *47*, 3976.

(35) Frisch, M. J.; Trucks, G. W.; Schlegel, H. B.; Scuseria, G. E.; Robb, M. A.; Cheeseman, J. R.; Montgomery, J. A. Jr.; Vreven, T.; Kudin, K. N.; Burant, J. C.; Millam, J. M.; Iyengar, S. S.; Tomasi, J. J.; Barone, V.; Mennucci, B.; Cossi, M.; Scalmani, G.; Rega, N.; Petersson, G. A.; Nakatsuji, H.; Hada, M.; Ehara, M.; Toyota, K.; Fukuda, R.; Hasegawa, J ; Ishida, M.; Nakajima, T.; Honda, Y.; Kitao, O.; Nakai, H.; Klene, M.; Li, X.; Knox, J. E.; Hratchian, H. P.; Cross, J. B.; Bakken, V.; Adamo, C.; Jaramillo, J.; Gomperts, R.; Stratmann, R. E.; Yazyev, O.; Austin, A. J.; Cammi, R.; Pomelli, C.; Ochterski, J.; Ayala, P. Y.; Morokuma, K.; Voth, A.; Salvador, P.; Dannenberg, J. J.; Zakrzewski, V. G.; Dapprich, S.; Daniels, A. D.; Strain, M. C.; Farkas, O.; Malick, D. K.; Rabuck, A. D.; Raghavachari, K.; Foresman, J. B.; Ortiz, J. V.; Cui, Q.; Baboul, A. G.; Clifford. S.; Cioslowski, J.; Stefanov, B. B.; Liu, G.;

Liashenko, A.; Piskorz, P.; Komaromi, I.; Martin, R. L.; Fox, D. J.; Keith, T.; Al-Laham, M. A.; Peng, C. Y.; Nanayakkara, A.; Challacombe, M.; Gill, P. M. W.; Johnson, B.; Chen, W.; Wong, M. W.; Gonzalez, C.; Pople, J. A. GAUSSIAN 03W (Revision D.01), Gaussian, Inc.: Wallingford, CT, (2004).

(36) Trindle, C.; Datta, S. N. *Int. J. Quantum Chem.* **1996**, *57*, 781.

(37) Thirion, C.; Wernsdorfer, W.; Mailly, D. *Nat. Mater.* **2003**, *2*, 524.

(38) Rinkevicius, Z.; Tunell, I.; Salek, P.; Vahtras, O.; Agren, H. *J. Chem. Phys.* **2003**, *119*, 34.

(39) Radziszewski, J. G.; Gil, M.; Gorski, A.; Larsen, J. S.; Waluk, J.; Mroz, B. J. *J. Chem. Phys.* **2001**, *115*, 9733.

(40) Hirata, S.; Lee, T. J.; Gordon, M. H. *J. Chem. Phys.* **1999**, *111*, 8904.

(41) Liu, R.; Ke, S. H.; Baranger, H. U.; Yang, W. *Nano Lett.* **2005**, *5*, 1959.

(42) O'Boyle, N. M.; Tenderholt, A. L.; Langner, K. M. *J. Comput. Chem.* **2008**, *29*, 839.

(43) Westcott, B. L.; Gruhn, N. E.; Michelsen, L. J.; Lichtenberger, D. L. *J. Am. Chem. Soc.* **2000**, *122*, 8083.

(44) Franceschetti, A.; Zunger, A. *Europhys. Lett.* **2000**, *50*, 243.

(45) Latif, I. A.; Panda, A.; Datta, S. N. *J. Phys. Chem. A* **2009**, *113*, 1595.

(46) Fuentealba, P.; Simon-Manso, Y.; Chattaraj, P. K. *J. Phys. Chem. A* **2000**, *104*, 3185.

(47) Khatchatouriants, A.; Lewis, A.; Rothman, Z.; Loew, L.; Treinin, M. *Biophy. J.* **2000**, *79*, 2345.

(48) You, Y.; Yingke, H.; Burrows, P. E.; Forrest, S. R.; Petasis, N. A.; Thompson, M. E. *Adv. Mater.* **2000**, *12*, 1678.

(49) Cinelli, R. A. G.; Pellegrini, V.; Ferrari, A.; Faraci, P.; Nifosí, R.; Tyagi, M.; Giacca, M.; Beltram, F. *Appl. Phys. Lett.* **2001**, *79*, 3353.

(50) Pankhurst, Q. A.; Connolly, J.; Jones, S. K.; Dobson, J. *J. Phys. D: Appl. Phys.* **2003**, *36*, R167.

(51) Weber, W.; Lienhart, C.; Baba, M. D.; Grass, R. N.; Kohler, T.; Müller, R.; Stark, W. J.; Fussenegger, M. *J. Biotechnol.* **2009**, *141*, 118.

(52) Mohapatra, S.; Mallick, S. K.; Maiti, T. K.; Ghosh, S. K.; Pramanik, P. *Nanotechnology* **2007**, *18*, 385102.

(53) Sosnovsky, G.; Rao, N. U. M.; Li, S. W.; Swartz, H. M. *J. Org. Chem.* **1989**, *54*, 3667.

(54) Bhattacharya, D.; Shil, S.; Misra, A. *J. Photochem. Photobiol. A: Chem.* **2011**, *217*, 402.

Chapter 7

Possible Applications of Fluoro Protein Chromophore Coupled Photomagnetic Diradicals

The design, characterisation and application of three different pairs of imino nitroxide based green fluorescent protein chromophore and its different homologue coupled diradicals have been theoretically studied in this chapter. To begin with, the geometries of all these diradicals have been optimized at high spin state in gas phase, in water medium and in blood plasma medium. For calculations in water medium, we have adopted the 2-layer our own N-layer integrated molecular orbital and molecular mechanics (ONIOM) method. Similarly for blood phase calculations, the polarized continuum model (PCM) method has been adopted. With these optimized geometries the magnetic exchange coupling constant (J) values are estimated for these diradicals in different medium using broken symmetry (BS) approach in unrestricted DFT framework. We have found that these diradicals have an ability to change their magnetic nature from antiferromagnetic in trans form to ferromagnetic in cis form upon irradiation with light of appropriate wavelength. Using time dependent DFT (TDDFT) technique the required wavelengths of light by which non-fluorescent dark trans diradicals turn into their corresponding bright fluorescent cis isomers, are determined for each pair of diradicals for gas and water medium. This color change which can be observed in bare eyes is indeed a signature of the change in magnetic state of the diradicals concerned. Moreover, we have also calculated the zero field splitting (ZFS) parameter (D), rhombic ZFS parameter (E) and ZFS magnitude (a_2). From our calculations we ambitiously expect that if these diradicals are synthesized then they can be used as successful, non-hazardous magnetic resonance imaging contrast agent (MRICA) in place of other metal based contrast agents.

7.1. Introduction

Materials science research has gained notable importance in the field of biomedical research through design, preparation and appliance of effective multifunctional biomaterials.[1-3] Some of these multifunctional systems are useful because they exhibit magnetic behavior in reduced dimension. The fundamental requirement for developing multifunctional nano-magnetic material is to design ferromagnetic molecules with diverse functional characteristics such as photosensitivity, fluorescence activity, water solubility etc. These types of multifunctional molecules have earned huge interest in the lurking field of materials science research.[4] Following this trend, attention has been given on designing photomagnetic molecules which change their magnetic behavior when exposed to suitable external radiation.[5] Thus, these systems can be activated or deactivated by appropriate irradiation as required for effective use of their magnetic property. Nevertheless, magnetic field induced magnetization reversal procedure for magnetically active molecules is well known and used for diverse technological applications.[6] However, this process is difficult to implement as it requires very high field gradient. On the other hand, compared to the field induced process, photoinduced magnetic crossover is easier to accomplish and more suitable for functional uses.[7]

Photochromic molecules undergo photon induced reversible chemical change involving two different wavelengths of electromagnetic radiation and instantaneously modulate their geometries and physical properties. If two monoradical moieties are connected with such photochromic coupler of particular structural form the resulting diradical switch to another structural form of the coupler by a definite external electromagnetic radiation.[8] As a result, change in magnetic property due to this structural change is observed. The photomagnetic behavior of substituted pyrene molecules has been nicely studied by Ali and Datta.[9] Photoinduced antiferromagnetic to ferromagnetic crossover in case of organic diradicals has also been reported and widely studied very recently.[5]

Fluorescent proteins, with photochromic property have revolutionized the study of living cells. The first such protein utilized in cell biology was green fluorescent protein

(GFP) which was obtained from jellyfish *Aequorea Victoria.*[10] The GFP has found its use in cellular and molecular biology, genetics, medicines and chemistry over the past several years.[10,11] This has also initiated several studies on different natural and artificial homologues of GFP.[12,13] The structural aspects and uses of GFP and its various homologues are nicely illustrated in the detailed review of Zimmer.[13]

Photomagnetic molecules with GFP chromophore and its homologues based diradicals have recently been designed and studied by Bhattacharya et al.[5(b)] There is certainly a possibility of developing multifunctional photochromic ferromagnetic molecules with GFP and its different derivatives as couplers which are expected to show fluorescence properties in addition to the ferromagnetic properties. Existence of both magnetic and fluorescence properties in same molecule will certainly make them a potent candidate for different biomedical applications particularly in the field of magnetic resonance imaging (MRI). The site specific MRI contrast agent (MRICA) with increased rate of relaxation of water protons in the targeted tissues, makes MRI fascinating in the field of *in vivo* bimolecular imaging. Most widely used MRICAs are various Gd-chelate compounds. However, Gd ion being poisonous in nature, toxic effect of Gd ion due to accidental *in vivo* dissociation of the Gd-chelate can not be avoided causing renal failure of patient after MRI investigation.[14] An alternative way is to use radical based organic MRICAs like nitroxide-leveled anti-cancer drug lomustine.[15] The point to be noted here is that a successful MRICA should be anti toxic, water soluble, biocompatible, easily renal excreable, and most importantly *in vivo* stable. Moreover, it should have greater volume distribution and better cell permeability. So far, among the synthesized stable radicals, nitroxyl radicals possess these qualities making themselves suitable for designing of MRICA.[16] Moreover, pyrrolidine and piperidine type nitroxyl radicals have the ability to cross the blood brain barrier (BBB) which is the primary requirement for a MRICA to be suitable for brain MRI scan.[15]

In this chapter, we have used (1) *p*-HBDI, (2) *m*-HBDI and (3) BFPF as fluorescent couplers with imino nitroxide (IN) as magnetic center to construct the diradicals. In every case trans-isomers of diradicals are designated as (a) and its corresponding cis-isomers are indicated as (b). Diradicals attached to the trans and cis states of GFP type coupler absorb

Scheme 7.1. Pictographic representation of reversible trans-cis photoisomerization of green fluorescent protein chromophore based diradicals (1-3). Where, X is imino nitroxide (IN) moiety and Y represents the fragment of the particular chromophore. Here, τ and φ stands for the dihedral angles as shown.

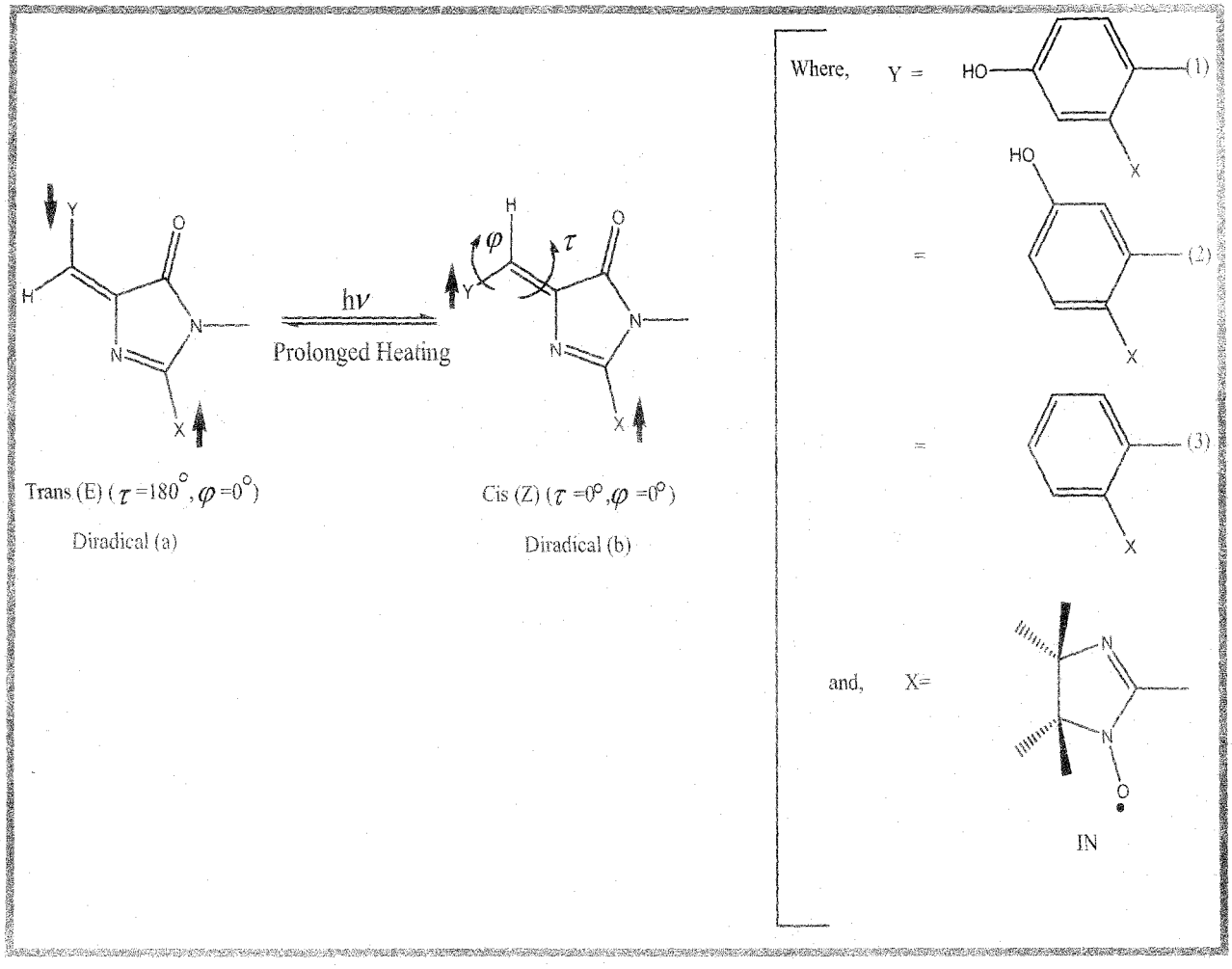

two different wavelengths and interchange their states as well as the nature of magnetism depending upon the state of GFP coupler to which it is attached. We choose the imino nitroxide radical because of its stability, non-toxicity and solubility in water medium.[17] These designed diradicals are useful in making water soluble photoswitchable magnetic molecules with fluorescence properties observable in naked eye. The whole process is shown in Scheme 7.1. We have estimated the magnetic exchange coupling constant values (J) for two different forms of every diradical in gas phase. We have also evaluated their J values in water and

blood plasma medium to understand their *in vivo* suitability. By writing *blood plasma* in italics we really mean that we have taken an average condition of a very complicated physiological fluid, blood. Throughout this article the same has been referred as "blood" in several occasions. The relative stability of the designed diradicals in different medium with respect to the total energy value is discussed. In every medium we have observed a magnetic crossover from antiferro- to ferro-magnetic states when the trans forms of each diradical is exposed to suitable wavelength of light. The required wavelength of external radiation is estimated through time dependent density functional theory (TDDFT) based calculations both in gas phase and in water medium. To know the suitability of our designed diradicals as MRICAs, we have evaluated their zero field splitting (ZFS) parameters and compared with other synthesized molecular systems which are already in use as MRICAs.

7.2. Theoretical Background and Methodology

The exchange interaction between two magnetic sites 1 and 2, is in general expressed by the Heisenberg spin Hamiltonian, $\hat{H} = -2J\hat{S}_1 \cdot \hat{S}_2$, where $\hat{S}_1$ and $\hat{S}_2$ are the spin angular momentum operators of site 1 and 2 respectively and J is the exchange coupling constant. A positive J value indicates ferromagnetic interaction whereas the negative value of J signifies antiferromagnetic interaction. To evaluate the exchange coupling constant with reasonably less computational effort, Noodleman[18] has proposed an unrestricted spin polarized broken symmetry (BS) formalism in DFT framework. The BS state is not a pure spin state but a state of mixed spin symmetry with lower spatial symmetry. Depending on the extent of magnetic interaction between two magnetic sites, many scientists have developed different formulae to estimate J using the BS approach.[18-20] Ideally, for diradicals the computed average $<S^2>$ values for triplet and BS states should be exactly 2.00 or 1.00 respectively. However in reality, their difference is not exactly unity showing a clear indication of spin contamination problem. In order to neutralize the spin contamination error associated with the BS state, one can use spin projection technique. For estimating the J values of diradicals of organic origin, the following expression by Yamaguchi et al.[19] is the most widely applied[5,9,21] and has been used by us in this chapter. This expression is given by

$$J = \frac{(E_{BS} - E_{HS})}{\langle S^2 \rangle_{HS} - \langle S^2 \rangle_{BS}}, \tag{7.1}$$

where E_{BS}, $\langle S^2 \rangle_{BS}$ and E_{HS}, $\langle S^2 \rangle_{HS}$ are the energy and average spin square values for corresponding BS and high spin states respectively.

As far as the biomedical applications are concerned, gas phase calculations of molecular energies are unlikely to produce a reliable picture. A more realistic approach is to consider the molecule-medium interaction. To achieve this end, one can employ the Our own N-layer Integrated molecular Orbital molecular Mechanics (ONIOM) method. In this method the whole system is divided into several onion-like layers. Out of which the inner active centre is treated with highest level *ab initio* QM method while the outer layer is treated with low-level QM or MM method. In a two layer hybrid ONIOM (high: low) method the extrapolated energy of the real system at high level is given by

$$E_{total}^{ONIOM} = E_{core}^{high} + E_{total}^{low} - E_{core}^{low}, \tag{7.2}$$

where 'high' and 'low' refers to high- and low-level theoretical methods. The subscripts 'core' and 'total' indicate the active site and the whole system respectively. Explicit solvation effect on the triplet geometry and triplet energy can be obtained from the ONIOM optimized geometry of the diradical molecule. A similar calculation using BS state of the inner high level layer will give the solvation effect on the energy of BS state. The method is named as ONIOM-BS method.[22]

Another way of considering the effect of medium on molecule is to apply polarized continuum model (PCM) method. This method, proposed by Newton,[23] evaluates the solute charge density distribution in dielectric continuum by solving the Schrödinger equation self consistently. The method considers that a molecule has a definite shape and effective volume and it is rarely spherical. Moreover, half the diameter of the solvent molecule is added with the constructed boundary of the solute molecule. In most cases the solvent is water unless specified and in general 0.5Å is added leading to slight error. As this method relies on self

consistency, it is valid for any order and one can perform PCM calculations for various quantum chemical methods like DFT, perturbation theory etc. Using PCM one can also optimize molecular geometry. The PCM method actually considers medium as a dielectric continuum and any averaging is included in the dielectric constant. As a matter of fact, PCM does not explicitly consider any fluctuation effect from average solvent polarization.[24] For all three diradical pairs PCM optimization calculations have been carried out taking *blood plasma* (ε = 58) as medium. With the PCM optimized geometry of these diradicals in high spin state, the BS treatment has been performed to know the magnetic nature of these molecules in *blood plasma* medium. This method is named as PCM-BS method.

It is known that the spectroscopic and photochemical properties of any photoactive molecule can be well comprehended by knowing the ground and excited state energies of the molecule. For any photoinduced chemical process involving chromophore, it is necessary to know the transition energy barrier between the two photo reactive forms of the species. It has been observed that the transition energy barrier has close correspondence with the excitation energy of the chromophoric molecule. To be more specific, in the different variants of GFP chromophores the excitation would take place from bonding (π) to antibonding (π^*) orbitals. It is already known that, the post Hartree Fock methods are suitable to estimate the wave length of external radiation for electronic transition in molecular systems.[25] However, they are also computationally expensive and following our recent works,[5(a),5(b)] we have employed time dependent density functional theory (TDDFT)[26] based calculations, which is a way out to obtain electronic excitation energies with less computational efforts.[27] The TDDFT method, relies on the frequency dependent polarizability of a system, and produces more reliable results than other methods.[28] On the other hand, TDDFT is almost free from "near triplet instability"[29] error and in addition the excited state energies from filled to unfilled orbitals can be obtained by performing only ground state Kohn-Sham calculations.[30,31]

The TDDFT method is based on the dynamic polarizability $\overline{\alpha}(\omega)$ of a system which has poles at frequencies analogous to its transition energies. Obtaining the frequency dependent polarizability from TDDFT calculations and substituting it in the sum-over-states relation

$$\bar{\alpha}(\omega) = \sum_I \frac{f_I}{\omega_I^2 - \omega^2}, \tag{7.3}$$

one can get oscillator strength (f_I) and excitation frequency (ω_I) respectively.[29] We calculate $\pi \rightarrow \pi^*$ transition energies for all designed trans fluorescent protein chromophores following the above method. All these above mentioned computations are implemented through Gaussian 09W quantum chemical package.[32]

Rajca and coworkers have established that the diradical and polyradical systems with organic origin can be successfully used as MRI contrast agent.[33] For the rational designing of MRICA one needs to know the extent of zero field splitting (ZFS) in addition to the solubility criterion. The ZFS, associated with magnetic anisotropy, is one of the important parameters to investigate the geometric and electronic properties of a radical with $S > ½$.[34] Having known the ZFS, one can easily estimate the electron spin correlation time which is one of the governing factors for clearer MRI scans with enhanced contrast.[35]

The ZFS arises from two contributions, namely the direct electron-electron magnetic dipole spin-spin (SS) interaction and the spin-orbit coupling (SOC) of the electronically excited state with the ground state.[34] It has also been established from the earlier work that the SS coupling happens to be the main source of ZFS in case of organic diradicals.[36] The ZFS value arising from the SS interactions can be estimated through effective spin Hamiltonian

$$\hat{H}_{ZFS} = \sum_{ij} \boldsymbol{D}_{ij} \hat{S}_i \hat{S}_j, \tag{7.4}$$

where $\boldsymbol{D}_{ij}$ is the ZFS tensor, $\hat{S}_k$ is the k'th Cartesian component of the total electron spin operator. For a diagonalized $\boldsymbol{D}_{ij}$ one can write the Hamiltonian as

$$\hat{H}_{ZFS} = D\left(\hat{S}_z^2 - \frac{1}{3}\hat{S}^2\right) + E\left(\hat{S}_x^2 - \hat{S}_y^2\right), \tag{7.5}$$

where D and E are the axial and rhombic ZFS parameters respectively.[37]

The first order contribution to the ZFS energy using the single ground state Kohn-Sham determinant is the SS coupling part of the ZFS and it can be calculated by applying the following formula[38]

$$D_{kl}^{(SS)} = \frac{g_e}{4}\frac{\alpha^2}{S(2S-1)}\left\langle 0SM_S \left| \sum_i \sum_{j\neq i} \frac{r_{ij}^2\delta_{kl} - 3(r_{ij})_k(r_{ij})_l}{r_{ij}^5} \times \left\{ 2\hat{S}_{iz}\hat{S}_{jz} - \hat{S}_{ix}\hat{S}_{jx} - \hat{S}_{iy}\hat{S}_{jy} \right\} \right| 0SM_S \right\rangle, \tag{7.6}$$

where α is the fine structure constant, g_e is the gyromagnetic ratio. The operators $\hat{S}_{mn}$ signify n'th component of m'th spin vector and r_{ij} is the magnitude of the distance vector between spins i and j. The equation can be safely approximated as[39]

$$D_{kl}^{(SS)} = \frac{g_e}{4}\frac{\alpha^2}{S(2S-1)}\sum_{\mu\nu}\sum_{\kappa\lambda}\left\{ P_{\mu\nu}^{\alpha-\beta}P_{\kappa\lambda}^{\alpha-\beta} - P_{\mu\kappa}^{\alpha-\beta}P_{\nu\lambda}^{\alpha-\beta} \right\} \times \left\langle \mu\nu \left| r_{12}^{-5} \left\{ \left\{ 3r_{12,k}r_{12,l} \right\} - \delta_{kl}r_{12}^2 \right\} \right| \kappa\lambda \right\rangle, \tag{7.7}$$

where $P^{\alpha-\beta} = P^{\alpha} - P^{\beta}$ the spin density matrix in the atomic orbital basis, and μ, ν, κ and λ are the basis functions.[36] These tensor elements can be used to evaluate the ZFS parameters D and E.[40] The D and E values are utilized to determine the static ZFS magnitude (a_2) using the formula

$$a_2 = \sqrt{\left(\frac{2}{3}D^2 + 2E^2 \right)}. \tag{7.8}$$

From this a_2 longitudinal electron spin relaxation rate $\frac{1}{T_{1e}}$ can be estimated following the expression[41]

$$\frac{1}{T_{1e}(B_0)} = \frac{2}{5}a_2^2\tau_R\left[\frac{1}{1+\omega_0^2\tau_2^2} + \frac{4}{1+4\omega_0^2\tau_2^2} \right] + \frac{12}{5}a_{2T}^2\tau'\left[\frac{1}{1+\omega_0^2\tau'^2} + \frac{4}{1+4\omega_0^2\tau'^2} \right], \tag{7.9}$$

where B_0 is the external magnetic field, ω_0 is the Larmor frequency, τ_2 and τ' are the reduced spectral densities and a_{2T} is the transient ZFS magnitude.[42] Larger a_2 corresponds to

a faster relaxation rate $\frac{1}{T_{1e}}$.[41] Here B3LYP correlation functional along with 6-31G(d,p) basis set has been used in the unrestricted formalism for the calculation of D and a_2.

7.3. Results and Discussion

The gas phase molecular geometries of all three cis-trans pairs have been fully optimized with the unrestricted B3LYP exchange correlation functional using 6-31G(d,p)

Table 7.1. The gas phase single molecule optimized energies (in *au*) for trans and their corresponding cis forms of all 3 sets of diradicals. The $\langle S^2 \rangle$ values and corresponding exchange coupling constants (J in cm^{-1}) are also reported. The calculations are done using UB3LYP level of theory with 6-311++G(d,p) basis set.

Diradical		At UB3LYP/6-311++G(d,p) level		
		Energy(*au*)	$\langle S^2 \rangle$	$J(cm^{-1})$
1a	Triplet	– 1601.62893	2.037	–8.8
	BS	– 1601.62897	1.038	
1b	Triplet	– 1601.63404	2.038	2.2
	BS	– 1601.63403	1.036	
2a	Triplet	– 1601.62905	2.035	–8.8
	BS	– 1601.62909	1.040	
2b	Triplet	– 1601.63386	2.037	8.8
	BS	– 1601.63382	1.034	
3a	Triplet	–1526.38116	2.036	–8.8
	BS	–1526.38120	1.038	
3b	Triplet	–1526.38590	2.037	7.4
	BS	–1526.38589	1.741	

Scheme 7.2. Schematic representation of geometrical and exchange pattern of different photoconvertable GFP based antiferromagnetic (itinerant exchange) dark trans (1a, 2a and 3a) and their corresponding ferromagnetic (direct exchange) fluorescent cis (1b, 2b and 3b) diradicals taking imino nitroxide (IN) as radical centers. The red colored up and down arrows represent α and β spin respectively.

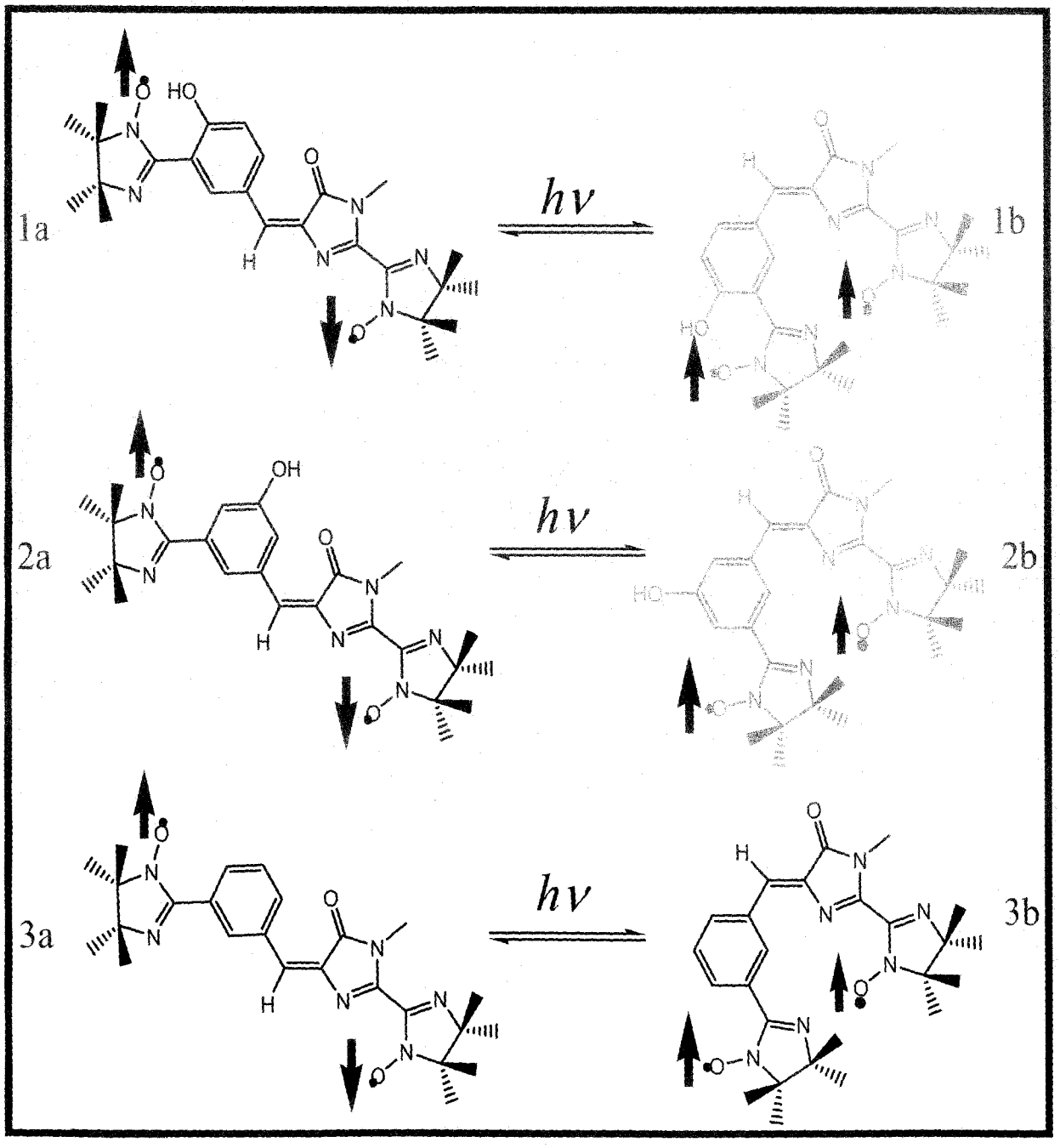

basis set. Scheme 7.2 shows the actual structure, exchange pattern and colors of all the ferromagnetic cis form and their corresponding dark antiferromagnetic trans form. The Figure 7.1 shows the gas phase optimized geometries. Based on these molecular geometries, the corresponding *J* values for each pair have been estimated from single point energies of the triplet and BS states at UB3LYP/6-311++G(d,p) level (eq 7.1). All the gas phase *J* values are shown in Table 7.1. Hence, antiferro- to ferro-magnetic crossover in all chosen diradical systems are observed when the trans isomers are exposed with proper electromagnetic radiation. It is also to be noted that, this type of magnetic crossover is associated with fluorescence color change, which can be viewed in naked eye. It is clear from Figure 7.1 that the trans form of all the diradicals are planar. They possess singlet ground state with opposite spin orientation in two different spin sites. In these isomers spin polarization is blocked through the coupler resulting in a manifestation of antiferromagnetic behavior. However, in the corresponding cis states of the respective diradicals the monoradical centers are out of plane in a manner that their close proximity facilitates direct exchange which results in ferromagnetism. The spin density plots admit the fact that although the spin density is less pronounced through the coupler, the direct exchange makes them magnetically active.[5(a-b)] The spin density distribution in gas phase optimization and in PCM optimization are depicted in Figure 7.2 and Figure 7.3 respectively.

To account for the solvent effect in the designed diradicals, we have performed ONIOM optimization (Figure 7.4) for each pair at UB3LYP/6-31G(d,p):UFF level treating the diradical as higher level and water as lower level in two level ONIOM. We take approximately 65 to 75 water molecules in low layer of ONIOM. The optimized geometries have been used for single point calculation of ONIOM-triplet and corresponding ONIOM-BS energies in UB3LYP/6-31G(d,p):UB3LYP/3-21G level of theory. The corresponding magnetic exchange coupling constant values obtained from the difference of ONIOM-triplet and ONIOM-BS energies using Yamaguchi formula are compiled in Table 7.2. Like that in gas phase here also we observe the antiferro- to ferro-magnetic crossover when explicit solvation model ONIOM method is considered. We have also taken into account the implicit solvation model using PCM technique. All the diradical pairs are optimized (Figure 7.5) at blood dielectric constant ($\varepsilon = 58$). We calculate the *J* values for all the diradicals through the

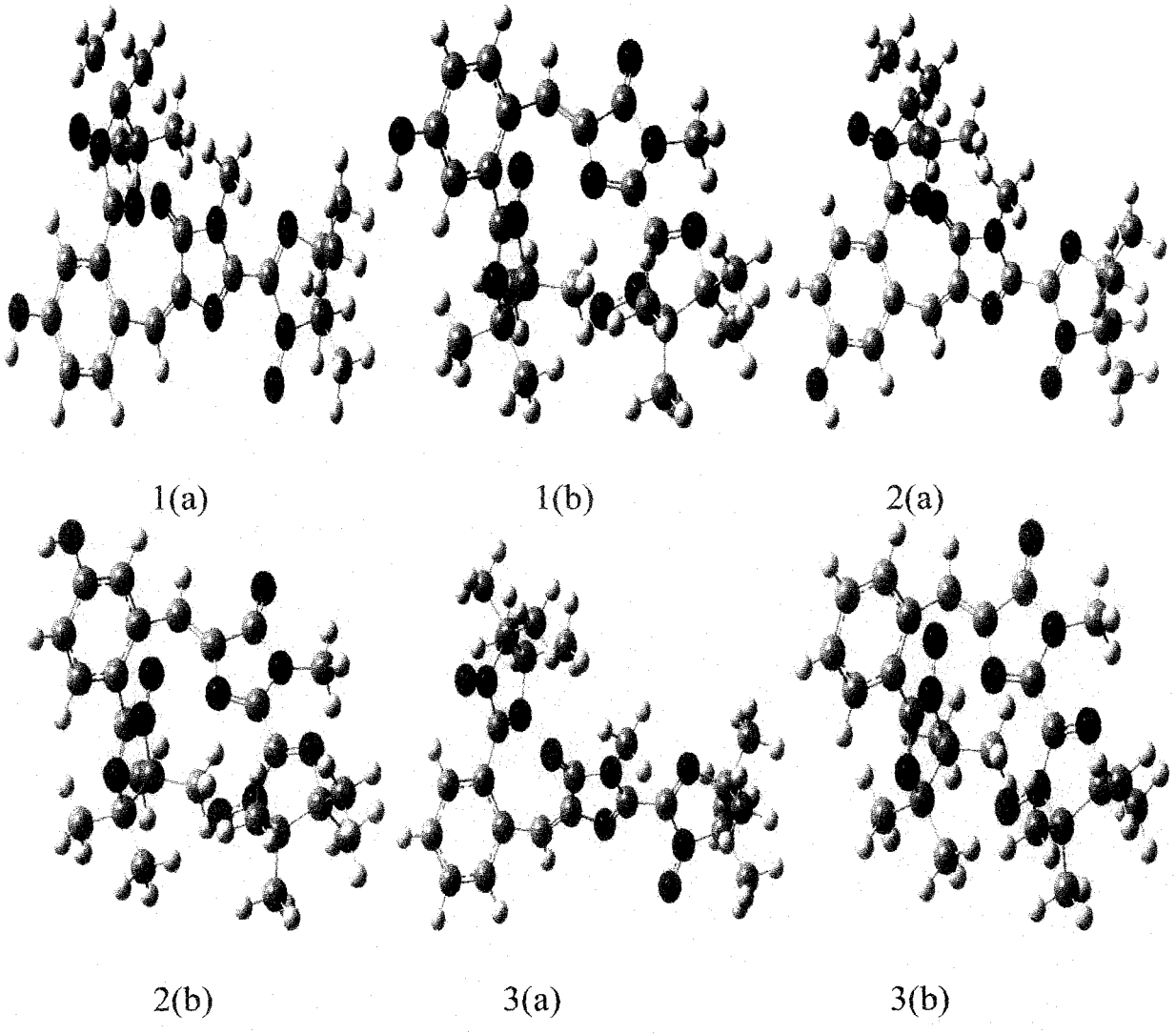

Figure 7.1. The gas phase optimized geometries of three trans (1a, 2a, 3a) diradicals and their corresponding cis forms (1b, 2b, 3b) with different GFP variants (*p*-HBDI, *m*-HBDI and BFPF respectively) as coupler. The geometries are optimized using UB3LYP method at 6-31G (d,p) level. The carbon atoms are represented in grey, nitrogen in blue, oxygen in red and hydrogen in white respectively.

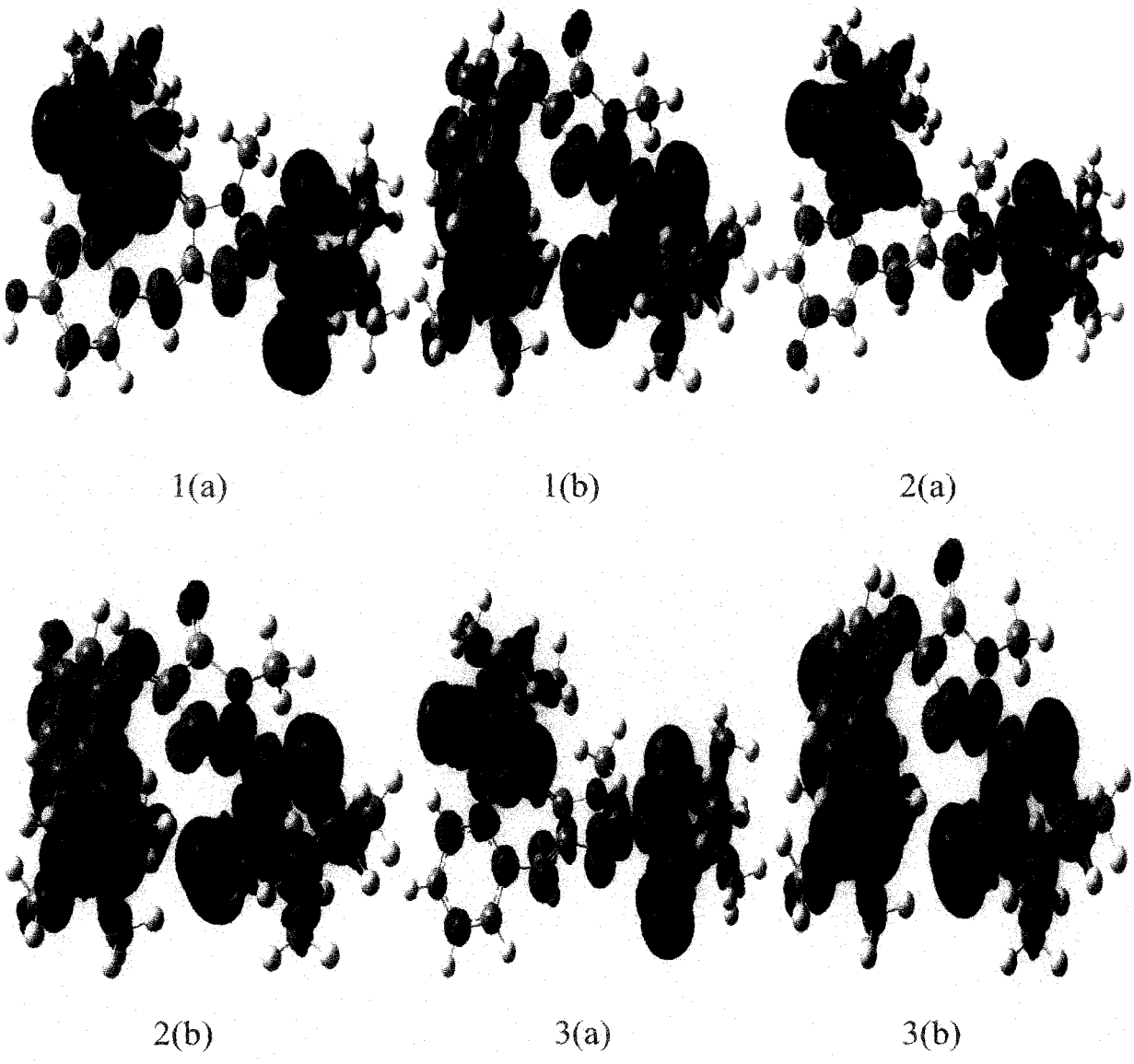

Figure 7.2. Gas phase spin-density plots for the diradicals in their triplet optimized states. Different color schemes are used for two different spins.

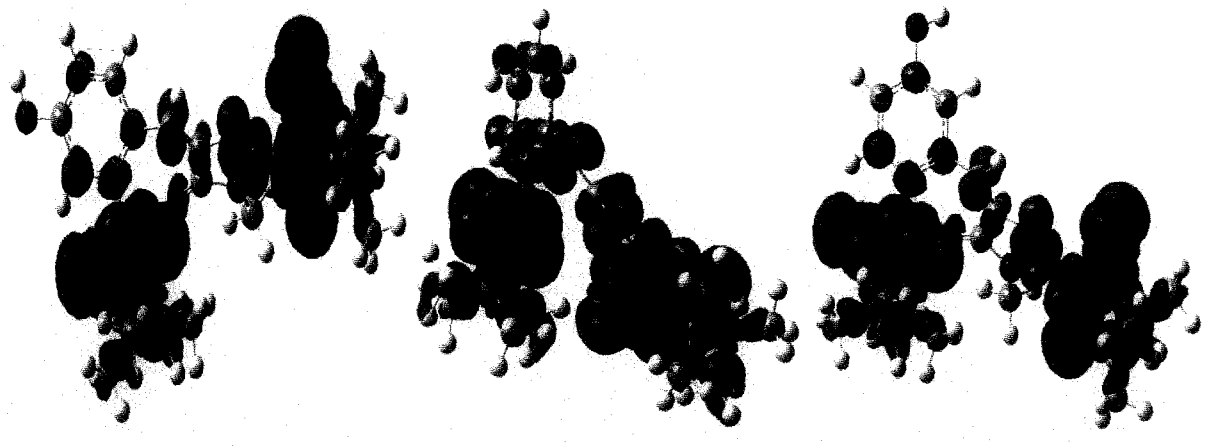

1(a) 1(b) 2(a)

2(b) 3(a) 3(b)

Figure 7.3. The spin-density plots for the triplet diradicals optimized using PCM method with $\varepsilon = 58$. Red and green color schemes are used for the representation of α and β spin respectively.

1(a) 1(b)

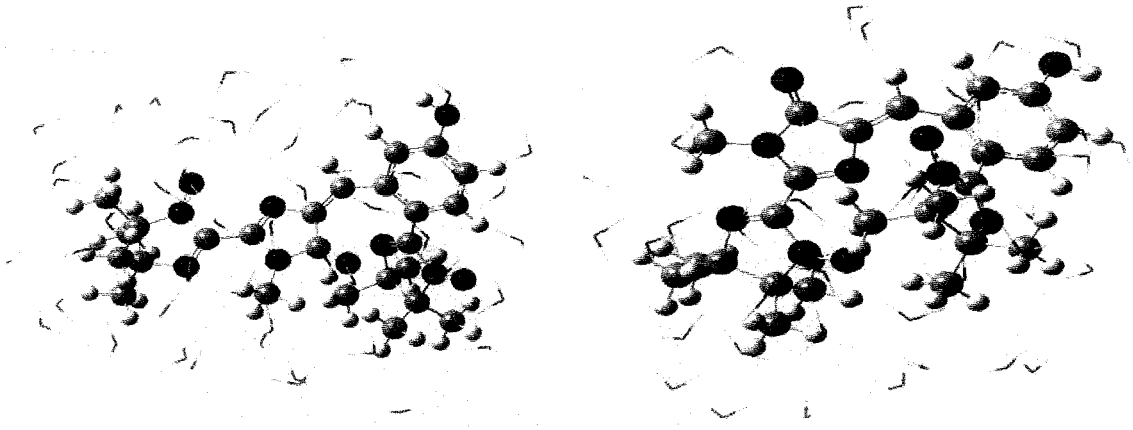

2(a) 2(b)

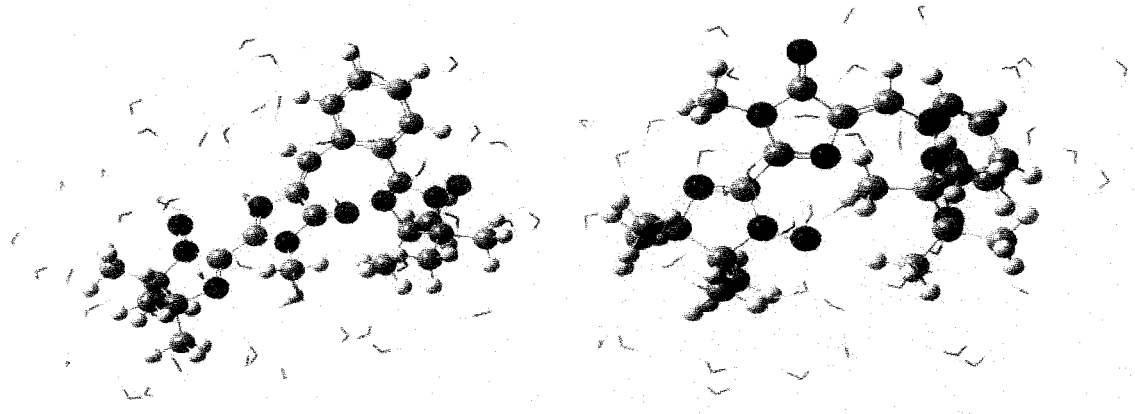

3(a) 3(b)

Figure 7.4. The ONIOM optimized geometries of water solvated 3 trans (1a, 2a, 3a) diradicals and their corresponding cis forms (1b, 2b, 3b) with different GFP variants (*p*-HBDI, *m*-HBDI and BFPF respectively) as coupler. The QM and MM levels are represented by ball and stick and only ball model respectively. The two layer ONIOM optimization for each diradical pairs are performed at UB3LYP/6-31G(d,p):UFF level; where the diradicals are treated as higher level (QM) and water molecules at lower level (MM). The carbon atoms are represented in grey, nitrogen in blue, oxygen in red and hydrogen in white respectively.

PCM-BS approach. The results of the PCM calculations are shown in Table 7.3. Even in this implicit solvent model we observe antiferro- to ferro-magnetic crossover. It has been noticed that there is a difference between the computed crossover values ($\Delta J = J_{cis} - J_{trans}$) in PCM and ONIOM methods. The ONIOM being explicit in nature shows greater crossover (ΔJ) values. This is because of the fact that, instantaneous interaction of water molecule with that –OH group has an effect on the total energy values (for both singlet and triplet) of the trans

isomer. On the other hand, in PCM method all the diradicals of each and every pair are in same dielectric environment. It is evident from the PCM optimized spin density plots (Figure 7.3) that for the cis-diradicals the direct exchange interaction between the spin centers is predominant. However, for planer trans-isomers antiferromagnetic interaction is observed which is also in accordance with spin density alternation rules (Figure 7.3).[43]

Table 7.2. The ONIOM energies (in *au*) of all three different sets of diradicals and their corresponding $\langle S^2 \rangle$ values at UB3LYP/6-31G(d,p):UB3LYP/3-21G level of theory for inner core diradical and outer water layer respectively. All exchange coupling constants have been estimated in the unit of cm^{-1}.

Diradical		At (UB3LYP/6-31G(d,p):UB3LYP/3-21G) level		
		Energy(*au*)	$\langle S^2 \rangle$	$J(cm^{-1})$
1a	Triplet	−1592.37843	2.033	−6.6
	BS	−1592.37846	1.036	
1b	Triplet	−1592.38692	2.035	2.2
	BS	−1592.38691	1.036	
2a	Triplet	−1592.38116	2.037	−11
	BS	−1592.38121	1.040	
2b	Triplet	−1592.38587	2.034	4.4
	BS	−1592.38585	1.034	
3a	Triplet	−1517.58297	2.037	−8.8
	BS	−1517.58301	1.040	
3b	Triplet	−1517.58784	2.035	2.2
	BS	−1517.58783	1.035	

Table 7.3. The PCM optimization results for different trans and their respective cis forms of all studied diradicals in *blood plasma* (taking ε = 58) medium using UB3LYP/6-31G(d,p) level of theory. The $\langle S^2 \rangle$ values of each diradical are reported separately. The absolute energies are expressed in au, exchange coupling constants (J) in cm^{-1}.

Diradical		At UB3LYP/6-31G(d,p) level		
		Energy(*au*)	$\langle S^2 \rangle$	$J(cm^{-1})$
1a	Triplet	−1601.26522	2.037	−8.8
	BS	−1601.26526	1.040	
1b	Triplet	−1601.26938	2.039	2.2
	BS	−1601.26937	1.039	
2a	Triplet	−1601.26465	2.037	−6.6
	BS	−1601.26468	1.039	
2b	Triplet	−1601.26937	2.037	4.4
	BS	−1601.26935	1.037	
3a	Triplet	−1526.04072	2.037	−6.6
	BS	−1526.04075	1.040	
3b	Triplet	−1526.04523	2.038	2.2
	BS	−1526.04522	1.038	

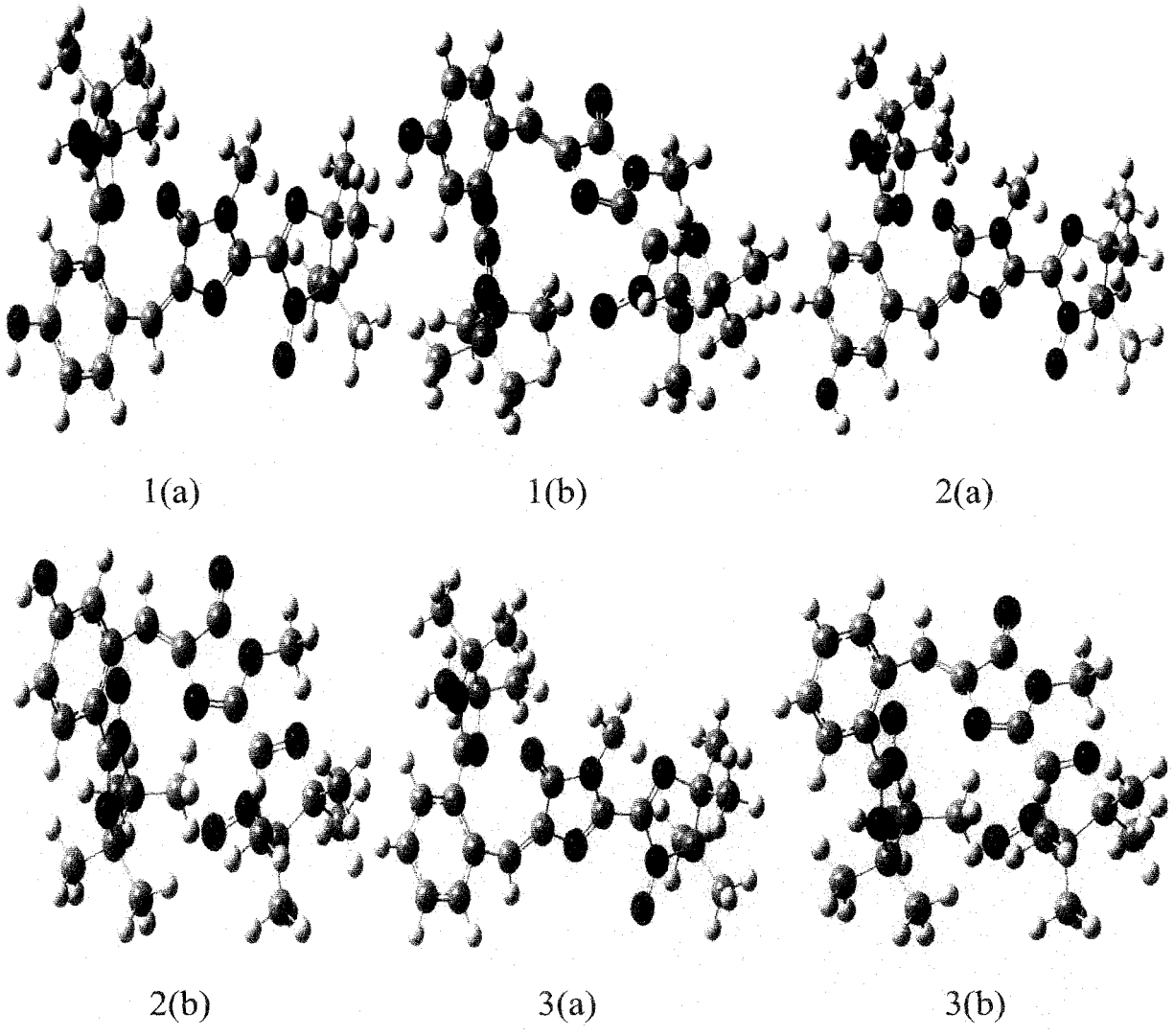

Figure 7.5. The PCM optimized geometries of three trans (1a, 2a, 3a) diradicals and their corresponding cis forms (1b, 2b, 3b) with different GFP variants (*p*-HBDI, *m*-HBDI and BFPF respectively) as coupler. The geometries are optimized using PCM method with ε = 58, at UB3LYP/6-31G(d,p) level of theory. The carbon atoms are represented in grey, nitrogen in blue, oxygen in red and hydrogen in white respectively.

7.3.1. Time Dependent Density Functional Study

As discussed earlier, the transition energies for the cis-trans conversion on irradiation of appropriate wave length of light can be estimated using TDDFT technique. The

experimentally found excitation peaks for different variants of neutral bare GFP used in the trans form of diradicals 1 and 3 are 399 nm and 355 nm respectively. By cautiously applying TDDFT technique we found a reasonably good match between the experimental findings[10(b),12(a)] and our calculated data. From the gas phase TDDFT results (Table 7.4), we conclude that with the application of 360-390 nm wave length of light the antiferromagnetic trans diradicals convert into their corresponding ferromagnetic cis forms. The transition brings out magnetic crossover along with a visual change from non-fluorescent dark to fluorescent green or blue form of GFP-diradicals. Similar types of calculations using water as solvent (Table 7.5) have been carried out for each pair of diradicals. A reasonable agreement between the experimental data[12(a)] and our calculated data for absorption wavelength of GFP at water medium at least for one example (1a) inspires about the authenticity of our calculation for rest of the molecules for which such experimental data are absent. For a visual effect, as all the trans forms of these diradicals are dark, upon irradiation of light of suitable wavelength the trans isomers change to corresponding bright fluorescent cis forms (green for *p*-HBDI and *m*-HBDI, blue for BFPF).[11,12] As a result, even without evaluating coupling constants, one can easily identify the magnetic status of the molecules, by visual inspection alone.

Table 7.4. The $\pi \rightarrow \pi^*$ transition energy values in gas phase, estimated wave length ${}^{a}\lambda_{exc}$ in trans diradicals at UB3LYP (TDDFT) level using 6-31G(d,p) basis set, ${}^{b}\lambda_{exc}$ is the experimental value for bare couple [ref. 12(a)].

Diradicals	E_{π} in *au*	E_{π^*} in *au*	Transition energy in *eV*	Estimated ${}^{a}\lambda_{exc}$ for diradicals in nm	Experimental ${}^{b}\lambda_{exc}$ for bare couplers in nm
1a	–0.20780	–0.08309	3.39353	364	392
2a	–0.21606	–0.08664	3.52170	351	–
3a	–0.21675	–0.08634	3.54864	349	355

Table 7.5. The estimated $\pi \rightarrow \pi^*$ transition energy values of all trans diradicals with wave length ${}^{a}\lambda_{exc}$ in water medium. Calculations are done at UB3LYP (TDDFT)/6-31G(d,p) level of theory, ${}^{b}\lambda_{exc}$ is the experimental value for bare coupler in water medium taken from ref. 12(a).

Diradicals	E_π in *au*	E_{π^*} in *au*	Transition energy in *eV*	Estimated ${}^{a}\lambda_{exc}$ for diradicals in nm	Experimental ${}^{b}\lambda_{exc}$ for bare couplers in nm
1a	–0.21875	–0.09473	3.37476	366	368
2a	–0.22717	–0.09679	3.54782	349	–
3a	–0.22843	–0.09715	3.57231	346	–

7.3.2. Applicability of the Designed Diradicals as Magnetic Resonance Imaging Contrast Agent (MRICA)

In this chapter, the ZFS parameter D and static ZFS magnitude (a_2) have been numerically estimated in gas phase, in water medium (with dielectric constant ε =80 and refractive index μ_{ri} = 1.33) and also in *blood plasma* medium (ε =58 and μ_{ri} = 1.1315),[44] (Table 7.6) for diradicals with S=1 states using ORCA program package[45] in DFT formalism. One point to be noted here is that, all the ferromagnetic diradicals possess the primary criterion to be a MRICA as discussed in the introduction section. Another point to be noted here is that, compared to nitroxide monoradical, nitroxide based di- or poly-radicals have the ability to increase the longitudinal relaxation rate ($1/T_{1e}$).[33(b)] A discussion about the D, a_2 and $1/T_{1e}$ is due here. The calculated D values and a_2 are reported in Table 7.6. It is apparent from the eq (7.9) that the static ZFS magnitude (a_2) is directly proportional to the longitudinal relaxation rate, (reciprocal of time taken for protons to realign with the external magnetic field, $1/T_{1e}$), which can be controlled in molecular level.[33(b)] Nonetheless, with the increase of $1/T_{1e}$ the observed MRI signal is enhanced.[46] From Table 7.6 it is evident that our computed $|D|$ values for cis diradicals are in the range of 1.62×10^{-2} to 1.69×10^{-2} cm^{-1} in

three different mediums. In an experimental work, Rajca and co-workers have synthesized nitroxide based high spin ($S = 1$) diradicals, which have been already established as standard MRICA of organic origin. In water ethanol mixture these synthesized diradicals have furnished the $|D|$ values in the range of 1.2×10^{-2} to 1.7×10^{-2} cm^{-1}.[33(a)] In another recent communication, we have noticed that, a stable diarylnitroxide triplet diradical is capable to be used as MRICA with $|D|$ and $|E|$ values 1.223×10^{-2} and 1.44×10^{-3} cm^{-1} correspondingly.[47] As a result, the calculated a_2 value for that diradical comes around 1.02×10^{-2} in the unit of cm^{-1}. In our designed GFP chromophore based diradicals, the calculated a_2 values are in the range of 1.33×10^{-2} to 1.39×10^{-2} cm^{-1} as depicted in Table 7.6. From these two experimental findings,[33(a),46] it is clear that, our designed diradicals are able to perform well as MRICA of organic origin, capable of producing clearer MRI image.[33(b),35] Moreover, each fragment of the diradicals i.e., the radical moieties[15,16] and the GFP fragments[11,13] both can cross the BBB. As a result, the constructed diradicals are also expected to cross the BBB and hence suitable as brain MRICAs.

Table 7.6. Spin-spin ZFS parameter $D^{(SS)}$ in cm^{-1}, static ZFS magnitude a_2 in cm^{-1} and rhombic ZFS parameter (E) values in cm^{-1} are given for all different ferromagnetic cis diradicals in three different mediums using UB3LYP/6-31G(d,p) basis set.

Diradicals	Medium	$D^{(SS)}$ in cm^{-1}	E in cm^{-1}	a_2 in cm^{-1}
	Gas	−0.01696	−0.00054	0.01387
1b	Water	−0.01682	−0.00053	0.01375
	Blood plasma	−0.01683	−0.00053	0.01376
	Gas	−0.01644	−0.00052	0.01344
2b	Water	−0.01628	−0.00051	0.01331
	Blood plasma	−0.01629	−0.00051	0.01332
	Gas	−0.01651	−0.00052	0.01350
3b	Water	−0.01636	−0.00051	0.01338
	Blood plasma	−0.01636	−0.00051	0.01338

7.4. Conclusions

In this chapter, we have designed and investigated three different pairs of photoswitchable antiferromagnetic trans and their corresponding ferromagnetic cis diradicals where GFP chromophore and its different fluorescent homologue are used as couplers with Imino Nitroxide (IN) as radical centers. The basis of choosing Imino Nitroxide (IN) as radical moiety lies on a report by Rajca et al., that the water soluble nitroxides can be used as very effective spin level, magnetic resonance imaging contrast agent, antioxidant etc.[47]

From our calculations we infer that all the designed diradicals are not only stable in different solvents but they also show antiferromagnetic to ferromagnetic crossover in different mediums like water (dielectric constant, $\varepsilon = 80$ and refractive index, $\mu_{ri} = 1.33$) and blood (dielectric constant, $\varepsilon = 58$ and $\mu_{ri} = 1.1315$),[44] when exposed to appropriate electromagnetic radiation. The calculations are done employing both ONIOM and PCM techniques. All the high spin geometries are optimized using UB3LYP/6-31G(d,p) method in ONIOM and PCM. The low spin states of these diradicals are described by ONIOM-BS and PCM-BS states. The photochemical properties of the diradicals in gas phase and in solvent phases have been investigated using TDDFT method.

We have investigated the possibility of using our designed diradicals as successful magnetic resonance imaging contrast agent. As of now, most of the widely used Gd-based MRICAs show adverse side effects due to Gd ions.[14] The designed diradicals, if synthesized, is expected to be free from such hazards. Rajca and co-workers[33(a)] have reported diradicals ($S = 1$) in water-ethanol mixture which can be used as MRICA. We found that our designed nitroxide based diradicals have static ZFS parameters D in the same range (1.2×10^{-2} to 1.7×10^{-2} cm^{-1}).[33(a)] The ZFS parameter is indicative of the efficiency of MRICA as already discussed. Moreover, the GFP chromophore is stable even at 65°C.[13] Thereby, these GFP based nano-magnetic moieties can be used in hyperthermia treatment where the therapeutic threshold is of 42°C.[1(a), 48] The GFP is also known to have good tagging ability,[13] thus magnetic separation of different GFP-tagged biological entity is possible with suitable use of these diradicals.

The concluding point to be discussed here has an ambitious note. The GFP encoded lentiviral particles paired with carbon coated Co-nanoparticle are used for therapeutic uses, particularly in the field of targeted gene delivery.[49] On the other hand, folate leveled magnetic nano-particles are used for their tagging ability in malignant cell without any side effects and toxicity.[50] As a matter of fact, one may combine these two ideas and converge to the point that if GFP based ferromagnetic diradicals tagged with folate moiety is injected without any biocompatible coating in a living organism, it can serve both these purposes. Nevertheless, this area is relatively young, rapidly developing, and multidisciplinary and can find a huge application in various fields if these diradicals are synthesized. The whole idea is represented in simple schematic manner by Scheme 7.3.

Scheme 7.3. The Schematic representation of bio-applicability of these six diradicals.

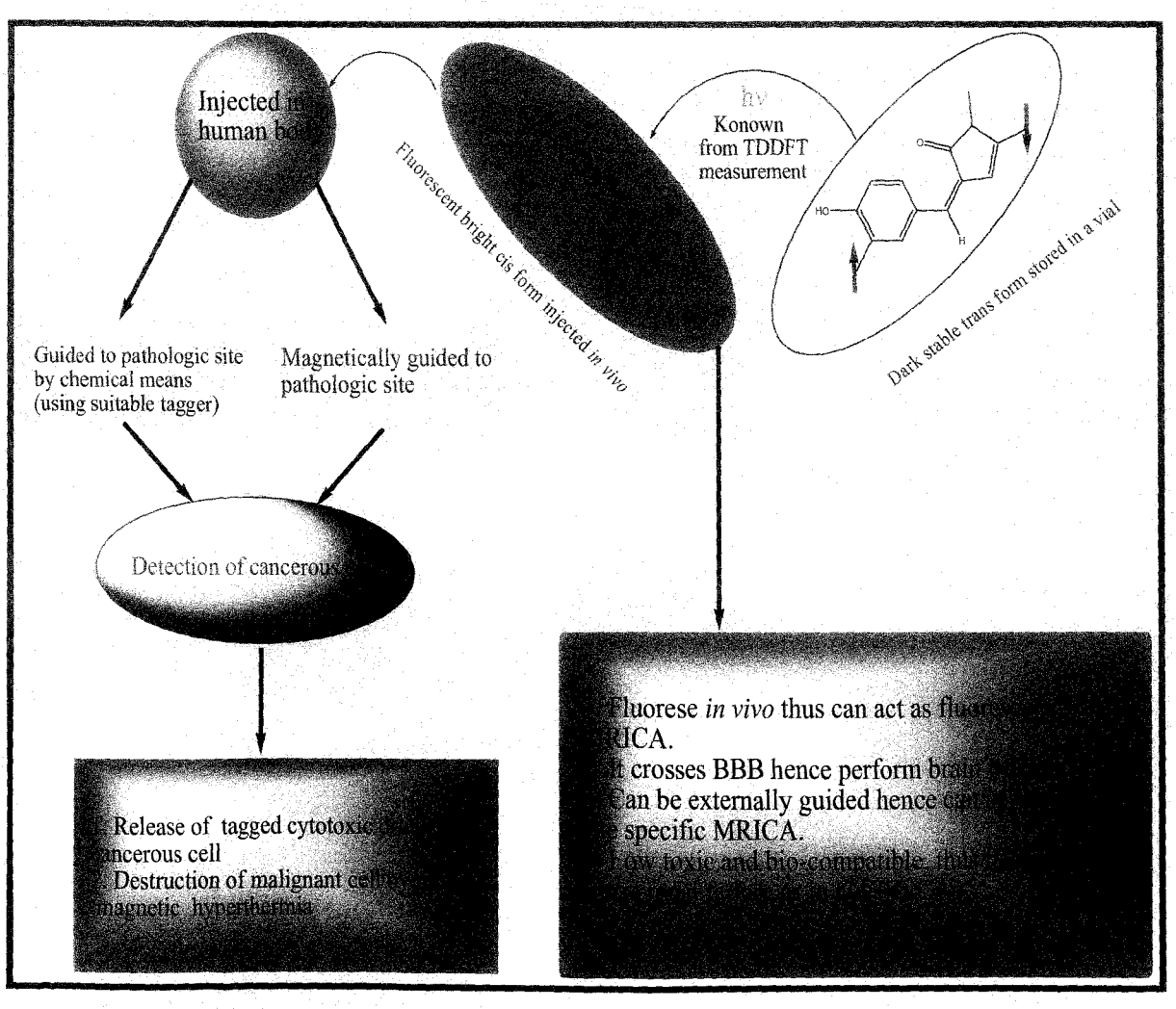

This work has been published in Physical Chemistry Chemical Physics (Ref. 51).

7.5. References and Notes

(1) (a) Pankhurst, Q. A.; Connolly, J.; Jones, S. K.; Dobson, J. *J. Phys. D: Appl. Phys.* **2003**, *36*, R167. (b) Tartaj, P.; Morales, M. P.; Veintemillas-Verdaguer, S.; González-Carreño, T.; Serna, C. J. *J. Phys. D: Appl. Phys.* **2003**, *36*, R182. (c) Pankhurst, Q. A.; Thanh, N. K. T.; Jones, S. K.; Dobson, J. *J. Phys. D: Appl. Phys.* **2009**, *42*, 224001.

(2) Salata, O. V. *J. Nanobiotechnol.* **2004**, *2*, 3.

(3) Jun, J.-W.; Seo, J.-W.; Cheon, J. *Acc. Chem. Res.* **2008**, *41*, 179.

(4) Palacio, F.; Miller, J. S. *Nature* **2000**, *408*, 421.

(5) (a) Shil, S.; Misra, A. *J. Phys. Chem. A* **2010**, *114*, 2022. (b) Bhattacharya, D.; Shil, S.; Misra, A. *J. Photochem. Photobiol. A: Chem.* **2011**, *217*, 402. (c) Saha, A.; Latif, I. A.; Datta, S. N. *Phys. Chem. A* **2011**, *115*, 1371.

(6) Thirion, C.; Wernsdorfer, W.; Mailly, D. *Nat. Mater.* **2003**, *2*, 524.

(7) Sato, O.; Iyoda, T.; Fujishima, A.; Hashimoto, K. *Science* **1996**, *272*, 704.

(8) (a) Tanifuji, N.; Matsuda, K.; Irie, M. *Polyhedron* **2005**, *24*, 2484. (b) Matsuda, K.; Irie, M. *Polyhedron* **200**^{5}, *24*, 2477. (c) Matsuda, K. *Bull. Chem. Soc. Jpn.* **2005**, *78*, 383. (d) Tanifuji, N.; Irie, M.; Matsuda, K. *J. Am. Chem. Soc.* **2005**, *127*, 13344. (e) Tanifuji, N.; Matsuda, K.; Irie, M. *Org. Lett.* **2005**, *7*, 3777.

(9) Ali, Md. E.; Datta, S. N. *J. Phys. Chem. A* **2006**, *110*, 10525.

(10) (a) Prasher, D. C.; Eckenrode, V. K.; Ward, W. W.; Pendergast, F. G.; Cormier, M. J. *Gene* **1992**, *111*, 229. (b) Tsien, R. Y. *Annu. Rev. Biochem.* **1998**, *67*, 509.

(11) (a) Tsien, R. Y. *FEBS Lett.* **2005**, *579*, 927. (b) Zimmer, M. *Glowing Genes: A Revolution in Biotechnology*; Prometheus Books: Amherst, NY, 2005. (c) Megley, C. M.; Dickson, L. A.; Maddalo, S. L.; Chandler, G. J.; Zimmer, M. *J. Phys. Chem. B* **2009**, *113*, 302.

(12) (a) Nifosí, R.; Amat, P.; Tozzini V. *J. Comput. Chem.* **2007**, *28*, 2366 and references therein. (b) Voliani, V.; Bizzarri, R.; Nifosí, R.; Abbruzzetti, S.; Grandi, E.; Viappiani, C.; Beltram, F. *J. Phys. Chem. B* **2008**, *118*, 10714.

(13) Zimmer, M. *Chem. Rev.* **2002**, *102*, 759, and references therein.

(14) Yerram, P.; Saab, G.; Karuparthi, P. R.; Hayden, M. R.; Khanna, R. *Clin. J. Am. Soc. Nephrol.* **2007**, *2*, 258.

(15) (a) Zhelev, Z.; Bakalova, R.; Aoki, I.; Matsumoto, K.; Gadjeva, V.; Anzai, K.; Kanno, I. *Mol. Pharmaceutics* **2009**, *6*, 504. (b) Zhelev, Z.; Bakalova, R.; Aoki, I.; Matsumoto, K.; Gadjeva, V.; Anzai, K.; Kanno, I. *Chem. Commun.* **2009**, 53.

(16) Konorev, E. A.; Tarpey, M. M.; Joseph, J.; Baker, J. E.; Kalyanaraman, B. *Free Rad. Bio. Med.* **1995**, *18*, 169.

(17) Lescope, C.; Luneau, D.; Rey, P.; Bussiere, G.; Reber, C. *Inorg. Chem.* **2002**, *41*, 5566.

(18) (a) Noodleman, L. *J. Chem. Phys.* **1981**, *74*, 5737. (b) Noodleman, L.; Baerends, E. J. *J. Am. Chem.* Soc. **1984**, *106*, 2316. (c) Noodleman, L.; Davidson, E. R. *Chem. Phys.* **1986**, *109*, 131. (d) Noodleman, L.; Peng, C. Y.; Case, D. A.; Mouesca, J.-M. *Coord. Chem. Rev.* **1995**, *144*, 199.

(19) (a) Yamaguchi, K.; Takahara, Y.; Fueno, T.; Nasu, K. *Jpn. J. Appl. Phys.* **1987**, *26*, L1362. (b) Yamaguchi, K.; Jensen, F.; Dorigo, A.; Houk, K. N. *Chem. Phys. Lett.* **1988**, *149*, 537. (c) Yamaguchi, K.; Takahara, Y.; Fueno, T.; Houk, K. N. *Theo. Chim. Acta.* **1988**, *73*, 337.

(20) (a) Martin, R. L.; Illas, F. *Phys. Rev. Lett.* **1997**, *79*, 1539. (b) Caballol, R.; Castell, O.; Illas, F.; Moreira, I. de P. R.; Malrieu, J. P. *J. Phys. Chem. A* **1997**, *101*, 7860. (c) Barone, V.; di Matteo, A.; Mele, F.; Moreira, I. de P. R.; Illas, F. *Chem. Phys. Lett.* **1999**, *302*, 240. (d) Illas, F.; Moreira, I. de P. R.; de Graaf, C.; Barone, V. *Theor. Chem. Acc.* **2000**, *104*, 265. (e) Illas, F.; Moreira, I. de P. R.; Bofill, J. M.; Filatov, M. *Phys. Rev. B* **2004**, *70*, 132414.

(21) (a) Polo, V.; Alberola, A.; Andres, J.; Anthony, J.; Pilkington, M. *Phys. Chem. Chem. Phys.* **2008**, *10*, 857. (b) Bhattacharya, D.; Misra, A. *J. Phys. Chem. A* **2009**, *113*, 5470. (c) Bhattacharya, D.; Shil, S.; Misra, A.; Klein, D. J. *Theor. Chem. Acc.* **2010**, *127*, 57. (d) Bhattacharya, D.; Shil, S.; Panda, A.; Misra, A. *J. Phys. Chem. A* **2010**, *114*, 11833.

(22) Ali, E. Md.; Oppeneer, P. M.; Datta, S. N. *J. Phys. Chem. B* **2009**, *113*, 5545.

(23) (a) Newton, M. D. *J. Chem. Phys.* **1973**, *58*, 5833. (b) Newton, M. D. *Annual Rev. Phys. Chem.* **1984**, *35*, 437.

(24) Mehta, N.; Datta, S. N. *J. Chem. Sci.* **2007**, *119*, 501.

(25) Parac, M.; Grimme, S. *J. Phys. Chem. A* **2002**, *106*, 6844.

(26) Stratmann, R. E.; Scuseria, G. E. *J. Chem. Phys.* **1998**, *109*, 8218.

(27) Slaughter, B. D.; Allen, M. W.; Lushington, G. H.; Johnson, C. K. *J. Phys. Chem. A* **2003**, *107*, 5670.

(28) Harbola, M. K. *Phys. Rev. B* **2002**, *65*, 052504.

(29) Casida, M. E.; Jamorski, C.; Casida, K. C.; Salahub, D. R. *J. Chem. Phys.* **1998**, *108*, 4439.

(30) Bauernschmitt, R.; Ahlrichs, R. *Chem. Phys. Lett.* **1996**, *256*, 454.

(31) Bauernschmitt, R.; Ahlrichs, R. *J. Chem. Phys.* **1996**, 104, 9047.

(32) Frisch, M. J.; Trucks, G. W.; Schlegel, H. B.; Scuseria, G. E.; Robb, M. A.; Cheeseman, J. R.; Scalmani, G.; Barone, V.; Mennucci, B.; Petersson, G. A.; Nakatsuji, H.; Caricato, M.; Li, X.; Hratchian, H. P.; Izmaylov, A. F.; Bloino, J.; Zheng, G.; Sonnenberg, J. L.; Hada, M.; Ehara, M.; Toyota, K.; Fukuda, R.; Hasegawa, J.; Ishida, M.; Nakajima, T.; Honda, Y.; Kitao, O.; Nakai, H.; Vreven, T.; Montgomery, J. A.; Jr., Peralta, J. E.; Ogliaro, F.; Bearpark, M.; Heyd, J. J.; Brothers, E.; Kudin, K. N.; Staroverov, V. N.; Keith, T.; Kobayashi, R.; Normand, J.; Raghavachari, K.; Rendell, A.; Burant, J. C.; Iyengar, S. S.; Tomasi, J.; Cossi, M.; Rega, N.; Millam, J. M.; Klene, M.; Knox, J. E.; Cross, J. B.; Bakken, V.; Adamo, C.; Jaramillo, J.; Gomperts, R.; Stratmann, R. E.; Yazyev, O.; Austin, A. J.; Cammi, R.; Pomelli, C.; Ochterski, J. W.; Martin, R. L.; Morokuma, K.; Zakrzewski, V. G.; Voth, G. A.; Salvador, P.; Dannenberg, J. J.; Dapprich, S.; Daniels, A. D.; Farkas, O.; Foresman, J. B.; Ortiz, J. V.; Cioslowski, J.; Fox, D. J. Gaussian 09 W, revision B.01; Gaussian, Inc.: Wallingford CT, 2010.

(33) (a) Spagnol, G.; Shiraishi, K.; Rajca, S.; Rajca, A. *Chem. Commun.* **2005**, 5047. (b) Olankitwanit, A.; Kathirvelu, V.; Rajca, S.; Eaton, G. R.; Eaton, S. S.; Rajca, A. *Chem. Commun.* **2011**, *47*, 6443.

(34) Duboc, C.; Ganyushin, D.; Sivalingam, K.; Collomb, M.; Neese, F. *J. Phys. Chem. A* **2010**, *114*, 10750.

(35) Tucker, B. J. *Dissertation in Chemistry in the Graduate College of the University of Illinois at Urbana-Champaign*, 2010.

(36) Zein, S.; Duboc, C.; Lubitz, W.; Neese, F. *Inorg. Chem.* **2008**, *47*, 134.

(37) Loboda, O.; Minaev, B.; Vahtras, O.; Schimmelpfennig, B.; Ågren, H.; Ruud, K.; Jonsson, D. *Chem. Phys.* **2003**, *286*, 127.

(38) Harriman, J. E. *Theoretical Foundations of Electron Spin Resonance*, Academic Press, New York, 1987.

(39) McWeeny, R.; Mizuno, Y. *Proc. R. Soc.*, London, **1961**, *A259*, 554.

(40) Boča, R. *Theoretical Foundations on Molecular Magnetism*, Elsevier, 1999.

(41) Benmelouka, M.; Borel, A.; Moriggi, L.; Helm, L.; Merbach, A. E. *J. Phys. Chem. B* **2007**, *111*, 832.

(42) Belorizkya, E.; Fries, P. H. *Phys. Chem. Chem. Phys.* **2004**, *6*, 2341.

(43) (a) Klein, D. J.; Nelin, C. J.; Alexander, S.; Matsen, F. A. *J. Chem. Phys.* **1982**, *77*, 3101. (b) Trindle, C.; Datta, S. N. *Int. J. Quantum Chem.* **1996**, *57*, 781. (c) Trindle, C.; Datta, S. N.; Mallik, B. *J. Am. Chem. Soc.* **1997**, *119*, 12947.

(44) Jin, Y. L.; Chen, J . Y.; Xu, L.; Wang, P. N. *Phys. Med. Biol.* **2006**, *51*, N371.

(45) Neese, F. *ORCA – an ab-initio density functional and semiempirical program package*, Version 2.8-20; Max-Planck institute for bioinorganic chemistry, Mulheim an der Ruhr, Germany, 2010.

(46) (a) Bottrill, M.; Kwok, L.; Long, N. J. *Chem. Soc. Rev.* **2006**, *35*, 557. (b) Hanaoka, K.; Kikuchi, K.; Terai, T.; Komatsu, T.; Nagano, T. *Chem. Eur. J.* **2008**, *14*, 987.

(47) Rajca, A.; Shiraishi, K.; Rajca, S. *Chem. Commun.* **2009**, 4372.

(48) (a) Kar, R.; Misra, A. *J. Magn. Magn. Mater.* **2010**, *322*, 671. (b) Kar, R.; Misra, A. *Nanosci. Nanotechnol. Lett.* **2010**, *2*, 253.

(49) Weber, W.; Lienhart, C.; Baba, M. D.; Grass, R.N.; Kohler, T.; Muller, R.; Stark, W. J.; Fussenegger, M. *J. Biotechnol.* **2009**, *141*, 118.

(50) Mohapatra, S.; Mallick, S. K.; Maiti, T. K.; Ghosh, S. K.; Pramanik, P. *Nanotechnology* **2007**, *18*, 385102.

(51) Bhattacharya, D.; Panda, A.; Shil, S.; Goswami, T.; Misra, A. *Phys. Chem. Chem. Phys.* **2012**, *14*, 6509.

Chapter 8

Conclusions

A comprehensive conclusion on all the chapters of the thesis is given here.

Conclusions

This part of the thesis deals with the concluding remarks among different aspects of design, characterisation and application of molecular magnetic systems particularly on the diradicals of organic origin, albeit theoretically. The origin of magnetism in an organic diradical arises due to the presence of unpaired electrons in the nonbonding molecular orbitals (NBMOs). Generally, designing of molecular magnetic entities means a strategy of constructing new tailor made molecules having essential desired characteristics. The bioactivity, insulation, transparency, photoactivity, spintronic properties and so on are such divergent areas of research which make organic diradical based magnetic molecules a promising field.

In Chapter 1 (**Chapter 1: Molecules Manifesting Magnetic Behavior**) we have discussed the general introduction of the thesis comprising about the molecules with magnetic characters. The background of the thesis work including the stable building blocks for the organic magnetic molecules, qualitative predictions of the ground state of organic diradicals is embodied in this chapter. The biological and technological applications of different relevant molecular magnetic systems are clearly stated. The objectives of the thesis are also categorically mentioned in this chapter.

The Chapter 2 (**Chapter 2: Theoretical Background**) portrays the theoretical background of magnetic exchange coupling constant (J) in diradical species applying broken symmetry (BS) approach. The difference in energies between singlet and triplet state is related to the value of J. The magnetic molecules considered in this thesis are characterised by the sign and magnitude of J values. Positive and negative values of J indicate ferro- and antiferro-magnetic interactions respectively. Starting from the expression of Heisenberg effective spin Hamiltonian the popular Giensberg, Noodlemann and Davidson (GND) formula for the evaluation of J value is given. However, the GND equation is applicable where the overlap between the two magnetic orbitals is small. Another formula for the estimation of J proposed by Bencini, Ruiz and further justified by Illas is applied for a

system where the overlap between the orbitals is large enough. However, Yamaguchi formula is used for the calculation of J throughout my entire thesis work because of its suitability and wide applicability in all cases. The utility of zero field splitting (ZFS) parameters for the quantification of different applications especially related to the organic diradical based magnets are discussed. It is mentioned that, the ZFS parameters are associated with the magnetic anisotropy. The different electronic and geometric properties of radicals with S higher than ½, are properly investigated through ZFS data. Although the spin-spin interaction and spin-orbit coupling of the ground state and the excited state are responsible for ZFS, however, the spin-spin coupling is the main source of ZFS in case of organic radicals. The ZFS value arising from the spin-spin interactions can be anticipated through effective spin Hamiltonian. The conventional methodologies for the determination of axial ZFS parameter (D) and rhombic ZFS parameter (E) are discussed. The formula for evaluating the static ZFS magnitude (a_2) from the values of D and E is also mentioned.

In Chapter 3 (**Chapter 3: Magnetism in Bis-Oxoverdazyl Diradicals Coupled with Different Linkage Specific Aromatic Ring Spacers**), we have predicted intramolecular magnetic exchange coupling constants for 11 different linkage specific bis-oxoverdazyl diradicals divided into two groups (*meta* and *para*) with different aromatic ring couplers. All the molecules have been optimized at UB3LYP/6-311+G(d,p) level of theory and the J values are calculated using BS approach under DFT framework at the optimized level along with 6-311++G(d,p) basis set using the same methodology by single point calculations. The general observation shows that *meta* connected molecules are ferromagnetic, whereas the *para* connected ones are antiferromagnetic. The magnetic interactions are conveyed via π-conjugated path of the aromatic couplers as established by the spin density alternation rule. The figures of singly occupied molecular orbitals (SOMOs) are in good agreement with our predicted results. We also estimate hyperfine coupling constant (HFCC) values.

The Chapter 4 (**Chapter 4: Role of Linear Polyacene Spacers in Intramolecular Magnetic Exchange Coupling**) describes the theoretical investigation on 10 bis-oxo- and bis-thioxo-verdazyl diradicals with linear *meta* connected polyacenes (benzene to pentacene) of varying length as couplers. All the molecules are essentially ferromagnetic according to

the spin density alternation rule, as we have deliberately used *meta*-connected ring couplers. The evaluated magnetic exchange coupling constants (J) decrease regularly when benzene, naphthalene and anthracene are used as couplers with the increase of coupler chain length, whereas for tetracene and pentacene couplers the J values are decreasing although the chain length is increased. This observation is explained in the light of open shell radicaloid character of the higher polyacenes. Nonetheless, the observed J values are in good agreement with the experimental findings. Magnetic aromaticity index, nuclear independent chemical shift (NICS) values for the each benzenoid ring at the ring plane [NICS(0)] and 1 Å above the plane of the ring surface [NICS(1)] of every coupler for all diradicals are evaluated. It is found that the central benzenoid rings of each coupler have higher NICS values compared to the terminal rings of the coupler. That is, a loss of benzenoid character is observed for the terminal rings. A relation between ΔNICS (1) with that of J values is made. One should note that, the difference between average $NICS(1)_{coupler}$ and $NICS(1)_{acene}$ is represented by ΔNICS(1).

The Chapter 5 (**Chapter 5: Influence of Aromaticity on the Magneto Structural Property of Heteroverdazyl Diradicals**) finds a theoretical correlation between the structural aromaticity index, harmonic oscillator model of aromaticity (HOMA) and magnetic aromaticity index NICS. These two indices are separately compared with the J values evaluated for the *meta*-phenylene and their corresponding *para*-phenylene coupled bis-heteroverdazyl diradicals as designed for this chapter. The HOMA index is estimated for the whole diradicals as well as for the aromatic six membered coupler fragments. On the other hand, the NICS index is evaluated only for the six membered coupler fragments of the diradicals. The HOMA and NICS values suggest that the increase of aromaticity is associated with the rise of ferromagnetism, that is, aromaticity favors ferromagnetic trend in such diradical systems. In this chapter, the low J values for bis-phosphaverdazyl diradicals are attributed due to the spin leakage phenomena associated with the phosphorus atom. A quantitative relation between SOMO–SOMO energy gaps with J values has been made for all molecules. The shapes of SOMOs also play a role to envisage the state of magnetism. The ground state stability of these diradicals has also been investigated and found that the ferromagnetic diradicals are more stable than their respective antiferromagnetic counterparts.

In Chapter 6 (**Chapter 6: Photoresponsive Magnetic Crossover**), the green fluorescent protein (GFP) chromophore based photoswitchable diradicals in two different structural isomeric forms (cis and trans) are theoretically designed and characterized. The cyan, blue and green variants of GFP chromophores are used as couplers to form the photomagnetic diradicals. These photochromic diradicals undergo antiferromagnetic (trans) to ferromagnetic (cis) crossover upon irradiation of appropriate wavelength of light associated with alteration in color, which are likely to be useful in the field of biomedical applications. From the time dependent density functional theory (TDDFT) measurement it is found that if the dark trans diradicals are exposed to the light of wavelength range 360 to 390 nm, the transformation to their puckered fluorescent cis form is observed. As far as the technological applications of these diradicals are concerned, we have made the density of states (DOS) plots and found that at the Fermi level the spins are highly polarized for ferromagnetic cis diradical indicating to show the spin valve effect. The HOMO-LUMO energy gap qualitatively indicates that these diradicals can be used in non linear optical (NLO) imaging, in organic light emitting diode (OLED) devices, high-density optical memories and switches. The efficiency of these diradicals to be used as magnetic resonance imaging contrast agents (MRICAs) and in many other biomedical cases are qualitatively justified. The ground state stability with the two different structural forms of all these diradicals are made and have shown that the cis fluorescent ferromagnetic molecules are more stable than their dark trans counterparts.

The quantification of the different variants of the fluoroprotein chromophore coupled diradicals which can be used as MRICAs are furnished in Chapter 7 (**Chapter 7: Possible Applications of Fluoro Protein Chromophore Coupled Photomagnetic Diradicals**). Here, the GFP chromophore based 6 photoswitchable diradicals are theoretically designed with bis-imino nitroxide (IN) as magnetic sites and a magnetic crossover is observed when irradiated with appropriate wave length of light. The extent of magnetic interactions in all these molecules has been quantified in terms of *J*. The choice of IN as radical sites in these diradicals is due to its water solubility, the ability to act as very effective spin levels and most importantly capacity to perform as MRICAs. The *in vivo* suitability of these diradicals has been tested by calculating these diradicals with 2-layer Our own N-layer Integrated

molecular Orbital molecular Mechanics (ONIOM) and Polarized Continuum Model (PCM) methods. Along with gas phase optimization, the ONIOM optimization for all diradicals is performed where the diradicals are treated as high level layer and the surrounding water molecules are selected as low level layer. However, for PCM optimization in *blood plasma medium* the dielectric constant, $\varepsilon = 58$ and reflective index, $\mu_{ri} = 1.1315$ have been chosen. Like gas phase calculation a magnetic crossover from antiferromagnetic (trans, dark) state to ferromagnetic (cis, fluorescent) state is also observed for ONIOM and PCM methods. As a matter of fact, only visual inspection is required to understand the nature of magnetism; however, the extent of magnetism can be theoretically determined by applying the above methodologies. The photochemical properties of the diradicals in gas phase and in water solvated phases have been investigated using TDDFT method. The novel property of these diradicals is about their *in vivo* utilities as MRICAs. From our calculations it is found that all these designed fluoro protein chromophore coupled nitroxide based diradicals have axial zero field splitting (ZFS) parameter $|D|$ in the range from 1.2×10^{-2} to 1.7×10^{-2} cm^{-1}, which is essential to act as contrast agents in MRI. Moreover, the GFP chromophore is stable even at 65°C. Thereby, these fluorescent nano-magnetic moieties can have the utilities in magnetic hyperthermia treatment as 42°C temperature is required to destroy the required malignant sites. Being a good tagger, the magnetic separation of different biological entity with external magnetic field control is possible by the judicious use of these GFP based diradicals.

ACKNOWLEDGMENT

It would never have been known to me that 'work is joy' if I had not started my journey of Ph.D. under the guidance of Dr. Anirban Misra. His constant vigilance over his disciples' works, great enthusiasm for multifarious probabilities and possibilities of scientific problems, moral support, valuable suggestions, and worthy criticism helped me to carry on with my project. I feel greatly honored to honor this man of gigantic energy, colossal patience and friendliness. I could have hardly completed my work without his positive outlook and keen interest on my freedom of thought. I express humble gratitude and respect to 'Baudidi' (Mrs. Amrita Misra) and affection to little Mithi.

I am indebted to Prof. D. J. Klein, Dr. Anirban Panda my co-authors with whom I conversed for hours on various problems related to my work. Those discourses helped me a lot in the gradual development of the work. I express my gratitude from the core of my heart to Suranjan Shil and Tamal Goswami my co-authors and lab-mates for their strenuous effort and incessant abetment to my work.

I am also grateful to my other lab-mates Satadal Paul, Rakesh Kar, Manoj Majumder, Sonali Sarkar, Banita Sinha for their constant help and assistance during my research period. It will be very ungrateful if I can not recognize the hospitality made by Suranjan. Discussions on different technical problems with Satadal are also acknowledged.

I am especially thankful to Prof. Swapan Kumar Saha, my respected teacher, who primarily sent me to Dr. Anirban Misra for doing the research work. He continuously encouraged me and helped me for various papers during my Ph.D. programme. He had always been concerned for me during the entire time of my M.Sc. to Ph.D. I can never forget this man of great disposition. Dr. Amiya Kumar Panda also deserves special thanks from me for his precious technical suggestions in the process of preparation of my thesis. I also show my deep respect and gratitude to all other faculty members, Department of Chemistry, University of North Bengal, for their help in different ways in my journey.

I thankfully acknowledge Santanu Sinha (Pishemoshai) and Santana Sinha (Pisi) for their constant encouragement, good wishes and blessings in my journey of Ph.D. I am

grateful to our family friends Debabrata and Jayeta Bhattacharya for their good wishes. I am also indebted to the Head Master, Anwarul Islam of Matikunda High School for his support from the beginning of my teaching life and good wishes for doing my Ph.D. work.

I reminisce my father, Biswajit Bhattacharya, who always wanted me to perform some research work in the field of chemistry. He became very concerned when once I discontinued my research work after getting a service. Now with his blessings I have started the same again though after his sad untimely demise. My mother's blessings enforced me to complete my Ph.D. programme. I am also thankful to my brother, sister, father in law and mother in law for their good wishes.

My little 'Ninja', my cup of elixir, has been a constant source of energy and delight. Last but not the least, Ilora, my wife has always kept kindled the urge of doing better works within me during our period of struggle and hardship.

Debojit Bhattacharya

Debojit Bhattacharya 17.09.2012